CHEMIA

This issue contains papers based on the communications presented at "Journées d'Electrochimie 2009, Sinaia, Romania, 6-10 July 2009". We thank again to all participants for their valuable contributions and particularly those who agreed to publish their results in this journal.

Cluj-Napoca, January 15, 2010

On behalf of the conference organizers
Ionel Catalin Popescu

S T U D I A

UNIVERSITATIS BABEŞ-BOLYAI

CHEMIA

SPECIAL ISSUE

1

14ème Édition des Journées d'Électrochimie, 6-10 Juillet 2009, Sinaia, Roumanie

CUPRINS – CONTENT – SOMMAIRE – INHALT

Message de Mme Liliane RAMAROSOA, Directeur régional Agence Universitaire de la Francophonie (AUF), présenté par Mme Roxana TURCANU, chargée des relations extérieures pour l'Europe Centrale et Orientale

Madame et Monsieur les Présidents du Comité d'organisation,
Monsieur le représentant du Comité Scientifique,
Madame la Secrétaire Nationale de la Société Roumaine de l'Electrochimie,
Monsieur l'Attaché de coopération universitaire et scientifique,

Chers collègues participants,

Je tiens d'abord à exprimer mon regret de ne pas pouvoir être des vôtres lors de cette 14ème édition des Journées d'Electrochimie, du fait d'autres engagements pris de longue date.

D'une manière générale, les mobilités des étudiants et enseignants entre les universités francophones du monde entier, l'organisation de manifestations scientifiques francophones, des projets de coopération entre universités sont autant de preuves de l'engagement pris par l'AUF dans la promotion de la francophonie universitaire. Mais de manière particulière, je suis ravie que cette grande manifestation francophone soit organisée pour la première fois en Europe centrale et orientale, après 13 éditions dans des pays et villes avec une forte tradition francophone.

A tous les participants venus d'ailleurs, je souhaite, de concert avec les collègues roumains, la bienvenue dans une région qui, n'étant pas nativement francophone, prouve toutefois un attachement particulier aux valeurs de la francophonie.

L'Agence universitaire de la Francophonie – à travers son bureau régional - offre un appui constant aux manifestations vivantes de la Francophonie en Roumanie et en Europe centrale et orientale.

Par ailleurs, je suis particulièrement fière de constater que cet événement rassemblant plus de 350 chercheurs autour d'un thème essentiel pour le développement et le progrès de notre monde contemporain, est directement lié à un projet de l'Agence universitaire et de l'Université « Babès-Bolyai » - le Pôle d'excellence régional « Laboratoire associé francophone » mis en place au sein de la Faculté de Chimie et Génie Chimique.
La richesse des thématiques que vous allez aborder à travers les communications comme les posters, la variété des cultures dont vous provenez, la diversité de vos partenaires issus du monde académique et économique, témoignent de la qualité scientifique et académique de cette 14ème édition des Journées d'Electrochimie et augure surtout de sa contribution significative à l'essor d'un espace universitaire sous le signe de l'ouverture à la société, de l'interculturel, du multilatéral et du partage des expériences.

Je salue également la vision de l'avenir que les institutions dans le domaine de l'électrochimie apportent par l'association à cet événement de la remise des prix du **« Jeune Chercheur en Électrochimie »** et de la **Société d'Électrochimie de Roumanie**.
Félicitations aux heureux lauréats, succès et fructueux travaux aux participants. Et je ne saurais terminer sans féliciter tout particulièrement les organisateurs de cette manifestation.

Sinaia, le 7 juillet 2009
à l'ouverture des JE'09

THE ELECTROCHEMICAL BEHAVIOR OF SOME BERRIES EXTRACTS

MARIANA NELA ŞTEFĂNUŢ[a], ADINA CĂTA[a], IOANA IENAŞCU[a], CRISTIAN TĂNASIE[a], RALUCA POP[a]

ABSTRACT. In this paper, cyclic voltammetry was used as method to estimate the antioxidant activity of anthocyanins extracts from frozen fruits of some berries. Extraction in methanol for four types of indigene berries, *Ribes nigrum* L., *Ribes rubrum* L., *Vaccinium myrtillus* L., *Prunus spinosa* L. and *Rubus fruticosus* L., have been made. The voltammograms were recorded at room temperature. Some information on the electrochemical properties of the extracts could be provided by comparing the oxidation potentials at different pH values. The antioxidant capacities of the extracts were also evaluated by DPPH (1,1-diphenyl-2-picrylhydrazyl) radical scavenging method and correlated with their oxidation potentials.

Keywords: anthocyanins, antioxidant activity, cyclic voltammetry, DPPH

INTRODUCTION

Anthocyanins are natural pigments widely distributed in flowers, fruits (especially in berries) and vegetables, being responsible for their bright colors. Interest for anthocyanins has intensified due to their biological activities [1,2,3], the most important being the strong antioxidant activity in metabolic reaction, and their possible health benefits [4,5,6].

The aglycon forms, anthocyanidins, are the basic structure of anthocyanins (Figure 1) [7]. The most common anthocyanidins are cyanidin, delphinidin, pelargonidin, peonidin, petunidin and malvidin. In plants, anthocyanidins occur in their glycosidic form (bonded to a sugar moiety), anthocyanins.

Anthocyanins may exist in a variety of protonated, deprotonated, hydrated, and isomeric forms. The relative proportion of these forms is strongly dependent on pH (Figure 2) [3,8]. At very low pH values (pH 1-3), the red flaviulium cation is the predominant species. At pH 4-5, a colorless carbinol pseudo-base is generated, which can further undergo to pale yellow chalcones (Figure 2, C_E and C_Z). At pH 6-7, the flavylium cation can alternatively be transformed to quinoidal-base isomers through deprotonation and proton-transfer reactions and can be further converted to the blue-purple quinonoid anions [3,8]. The possible pH effect on the antioxidant properties of anthocyanins is of great interest due to the presence of different pH values in different human body fluids.

---

[a] *National Institute of Research-Development for Electrochemistry and Condensed Matter, Str. Dr. A. P. Podeanu 144, 300569 Timişoara, Romania, mariana_stefanut@yahoo.com*

Anthocyanidin	R_1	R_2	R_3
Pelargonidin	H	H	H
Cyanidin	OH	H	H
Delphinidin	OH	OH	H
Peonidin	OCH_3	H	H
Petunidin	OCH_3	OH	H
Malvidin	OCH_3	OCH_3	H
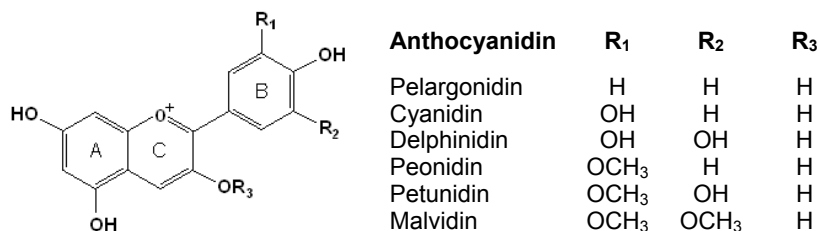
Figure 1. Structures of common anthocyanidins
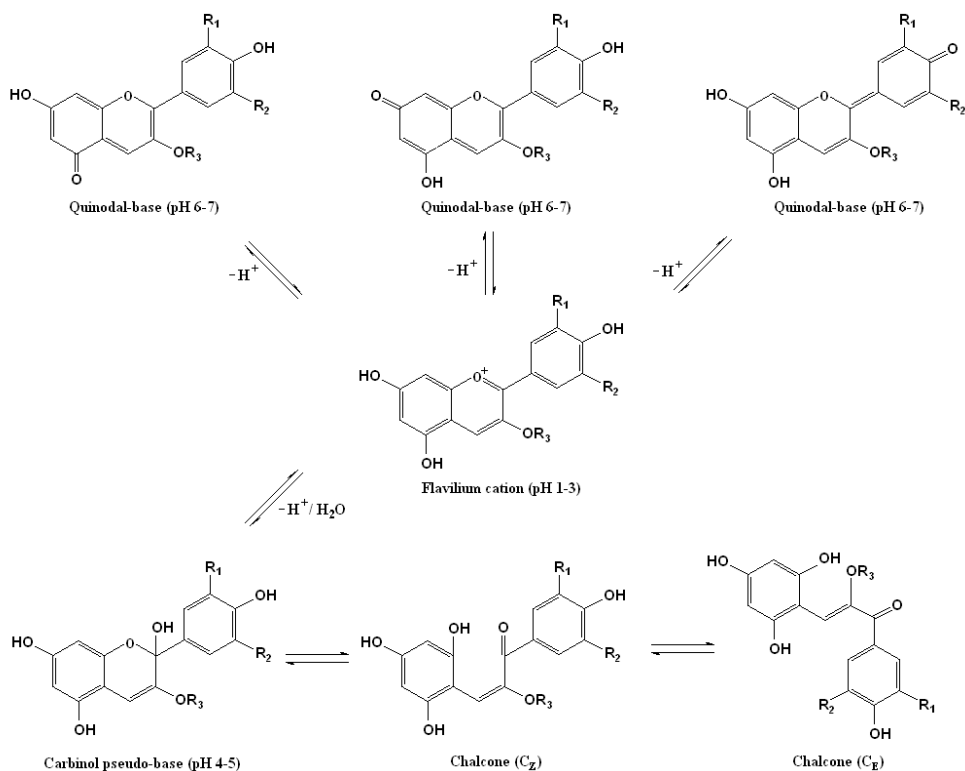
Figure 2. Structural changes of anthocyanins in aqueous solution at different pH

The antioxidant potential of anthocyanins occurs due to phenolic hydroxyl groups attached to their three-ring flavonoid structure and can change with the hydroxyl substituents and the sugar moieties bonded to the molecule [3,9].

There are several methods for in vitro determination of antioxidant capacity, mainly based on reaction between an antioxidant and a chromogen compound [10]. Among these methods, the electrochemical methods are simple, rapid and economic. Cyclic voltammetry is the most used electrochemical

technique for evaluation of the overall reducing capacity of low molecular weight antioxidants from biological samples (blood plasma, body fluids) and plant extracts [11,12,13,14].

In this work, cyclic voltammetry was used to evaluate antioxidant activity of the methanolic extracts of some indigene fruits rich in anthocyanins: black currants (*Ribes nigrum* L.), red currants (*Ribes rubrum* L.), bilberries (*Vaccinium myrtillus* L.), blackthorns (*Prunus spinosa* L.) and blackberry (*Rubus fruticosus* L.). For all the extracts, the oxidation profile in several background electrolytes at different pH values was investigated. The antioxidant capacity of the studied extracts was also determined using the 1,1-diphenyl-2-picrylhydrazyl (DPPH) radical-scavenging method [15]. In this assay, the purple chromogen radical DPPH is reduced by antioxidant compounds to the corresponding pale yellow hydrazine [16]. The reduction of DPPH was followed by a spectrophotometric method and the antioxidant capacities of the extracts evaluated by this assay were correlated with their oxidation potentials and anthocyanins content.

RESULTS AND DISCUSSION

Anthocyanins content of the extracts

The anthocyanins content in studied extract were determined by a pH differential method. Anthocyanins present a maximum absorbance at a wavelength of around 520 nm at pH 1.0. At pH 1.0, the flavylium cation is the predominant species and has a red color, in aqueous media at pH 4.5 hydration reaction generates the colorless carbinol pseudo-base (Figure 2).

The total monomeric anthocyanins are calculated based on the molecular weight and extinction coefficient of the predominant anthocyanin in the sample. If the ε value of the major pigment is not available or if the sample composition is unknown, anthocyanins content is calculate as cyinidin-3-glucoside [17] which is the most abundant in nature.

The composition of fruits extracts analyzed in this paper is not completely determined. We tried to establish the qualitative composition of the extracts through HPLC analysis. For all fruits extracts, chromatograms revealed the presence of a large number of anthocyanins: bilberries – 15 compounds, black currants – 18 compounds, red currants – 13 compounds, blackberries – 2 compounds and blackthorns – 7 compounds. We have succeeded to identify all anthocyanins only in bilberries extract [19]. We had no available commercial pure standards for all compounds. For this reason, the anthocyanins content is calculate as cyaniding-3-glucoside (MW = 449.2 and ε = 26900) and the obtained values are presented in Table 1.

It was found that bilberries extract provided the highest content of anthocyanins pigments from analyzed species of fruits. Smaller amounts of anthocyanins were found in the other fruits extracts, in the following order: black currants > blackthorns > blackberries > red currants.

Cyclic voltammetry

The electrochemical behavior of the fruits extracts was investigated with two different working electrodes: a platinum electrode (Pt) and a glassy carbon electrode (GCE).

Platinum electrode had no relevant response in the three supporting electrolytes chosen in this study. As example, in figure 3, are presented the cyclic voltammograms obtained on Pt electrode for black currants extract.

Figure 3. Cyclic voltammograms (Pt) of black currants extract at w=500 mV/s, supporting electrolyte: (**A**) NaClO4 0.1M in methanol; (**B**) acetate buffer (pH=3); (**C**) phosphate buffer (pH=7.6)

Unlike the results obtained using the platinum electrode, the voltammetric curves obtained with glassy carbon electrode present well defined oxidation peaks.

The electrochemical behavior of all the extracts on glassy carbon electrode was studied at different scan rates in the three support electrolytes.

Cyclic voltammograms were recorded from 0 to 1400 mV for NaClO4 0.1M in methanol and from -200 to 1300 mV for the other two supporting electrolytes at scan rates ranging from 100 to 500 mV/s. The best defined peaks were obtained at 500 mV/s and are exemplified for black currants extract using as supporting electrolyte NaClO4 0.1M in methanol (Figure 4). The following measurements were recorded at 500 mV/s.
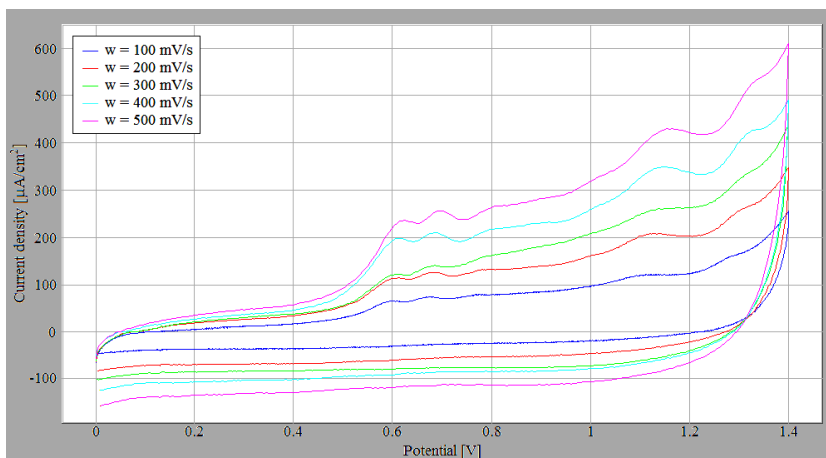
Figure 4. Cyclic voltammograms (GCE) of black currants extract at different scan rates, supporting electrolyte: NaClO4 0.1M in methanol

Also, it can be observed that the oxidation peak potentials shift to more positive values and the anodic peak currents become more accentuated with the increase of scan rate. These scan rate-dependent processes indicates that EC reaction mechanisms take place [20].

The electrochemical behavior in time of the anthocyanins extracts it has been also studied (Figure 5). In this type of experiments, the electrode remained immersed in the solution on entire duration of an experiment.

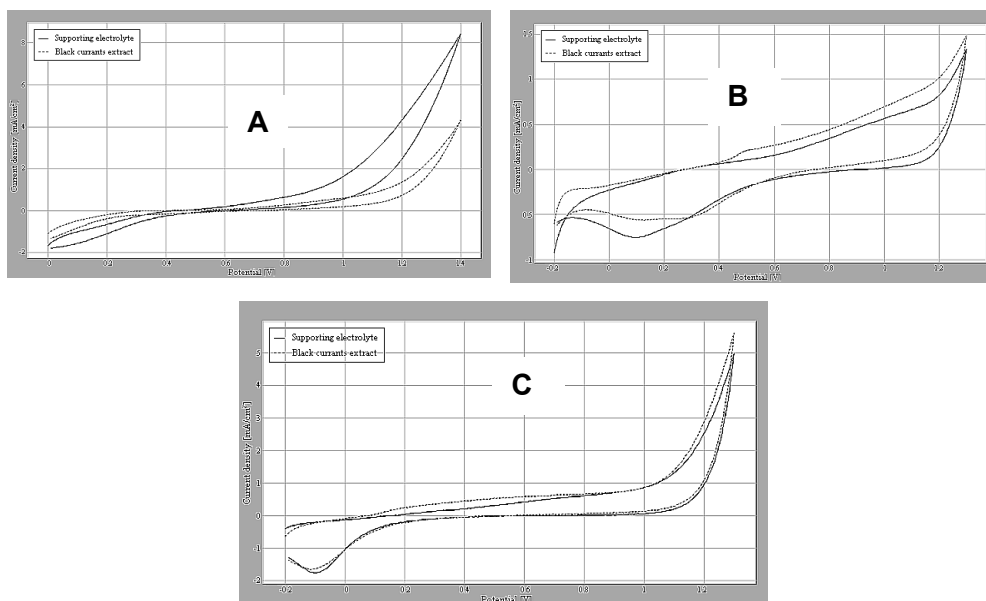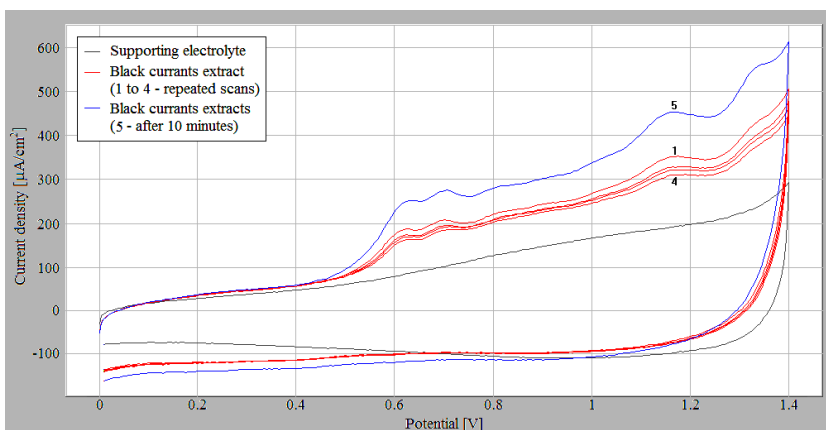**Figure 5.** Cyclic voltammograms (GCE) of black currants extract at w=500 mV/s, supporting electrolyte: NaClO4 0.1M in methanol

After several repeated scans (Figure 5, the curves from 1 to 4), it has been observed the decrease of the current density for all oxidation peaks,

due to a decrease of species concentration at electrolyte-electrode interface. After 10 minutes, we expected that the electrode surface will be coated by the anthocyanins or their oxidation products which may be adhering to the electrode surface, lowering the efficiency with which a new quantity of anthocyanins are oxidized and significantly altering the current response of the electrode [12]. However, after 10 minutes, the anodic peaks increased (Figure 5, curve 5), probably due to the concentration restoration by diffusion of anthocyanins molecules at electrolyte-electrode interface.

The influence of supporting electrolyte is illustrated in Figures 6, 7, and 8. For testing were chosen three supporting electrolytes: $NaClO_4$ 0.1M in methanol (pH=2.35) because the most phenolic antioxidants are soluble in methanolic medium, and two buffer solution, one at acidic pH (acetate buffer pH=3) and the other one at alkaline pH (phosphate buffer pH=7.6).

Significant results were obtained with $NaClO_4$ 0.1M in MeOH (Figure 6). Cyclic voltammograms of the all studied extracts display more than one oxidation peaks in the range 400-1400 mV and practically no reverse reduction peak, indicating the irreversibility of the electrode processes, except for the blackthorns extract. The position of anodic peaks in the voltammograms suggests the antioxidant ability; peaks at lower potential mean a higher antioxidant capacity [11]. The lowest potential for the first distinct peak in this supporting electrolyte belongs to blackthorns extract. On the basis of electrochemical data, the order of antioxidant activity of analyzed fruits extracts is: blackthorns > black currants > bilberries > blackberries > red currants.
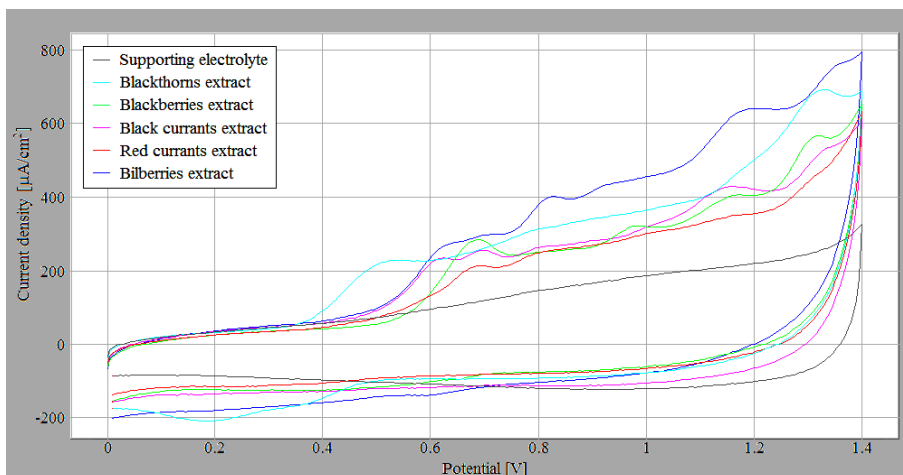
Figure 6. Cyclic voltammograms of of the extracts at w=500 mV/s,
supporting electrolyte: NaClO4 0.1M in methanol
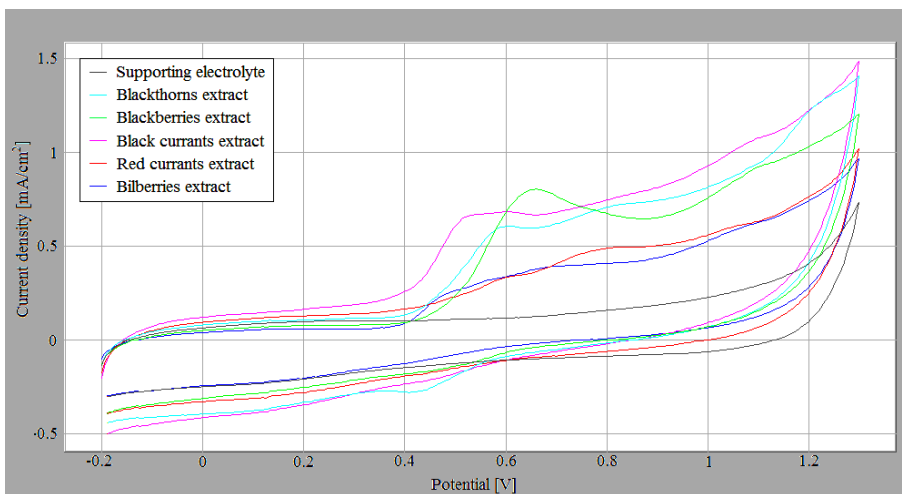
Figure 7. Cyclic voltammograms of the extracts at w=500 mV/s, supporting electrolyte: acetate buffer pH=3

In buffer solutions, the electrochemical behavior of the extracts is changed. The cyclic voltammograms shapes for the fruits extracts, in the two buffer solution, is quite similar, but different from those obtained with $NaClO_4$ 0.1M in MeOH, even if the acetate buffer solution and the methanolic solution have close values of pH. In the two buffer solution (Figure 7 and Figure 8), the less positive potential peak corresponds to black currants extract.
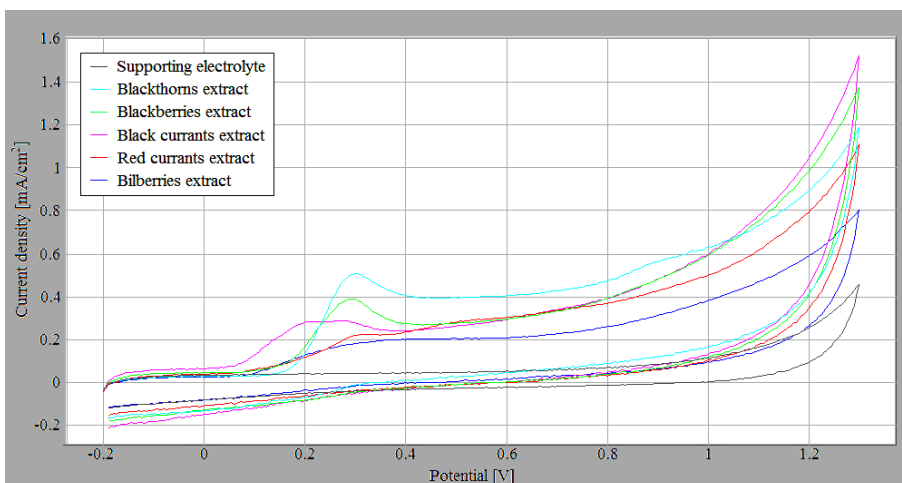
Figure 8. Cyclic voltammograms of of the extracts at w=500 mV/s, supporting electrolyte: phosphate buffer pH=7.6

Some information about the mechanism of anthocyanins oxidation could be provided by comparing oxidation potential at different pH values. In this case, is difficult to present an oxidation mechanism because the studied extracts are mixtures of anthocyanins with one or more hydroxyl groups attached in various positions to their three-ring flavonoid structure. However, it can be observed that, for all studies extracts, oxidation potentials shift to lower values at higher pH, indicating that the compounds are easier oxidized, so their antioxidant activity is increasing. These results are in agreement with data obtained by other authors for pure compounds [21].

Free radical scavenging activity

The antioxidant activity of the extracts was estimated by the ability to scavenging the DPPH radical. The DPPH concentration in the reaction medium was calculated from the calibration curve with the following equation determined by linear regression:

$$A_{515} = 11048 \cdot c_{DPPH} + 3.6828 \cdot 10^{-3} \quad (R^2 = 0.99987) \tag{3}$$

For each extract, the amount of the remaining DPPH expressed as a percentage was calculated as:

$$\text{Remaining DPPH [\%]} = (c_{DDPH})_t / (c_{DPPH})_{t=0} \cdot 100 \tag{4}$$

where $(c_{DDPH})_t$ is the value of DPPH concentration in the presence of extracts at time t.

The percentage of remaining DPPH concentration against reaction time for the five extracts is illustrated in Figure 9. In Table 1 is presented the percentage of remaining DPPH concentration after 4 hours. The lower this value, the higher is antiradical efficiency.
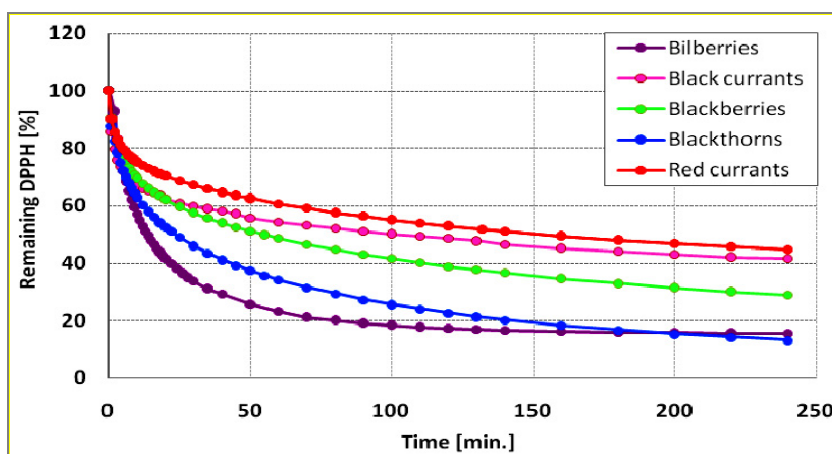
Figure 9. Kinetic behavior of DPPH scavenging

Table 1. Comparison between anthocyanins content, voltammetric behavior and DPPH radical scavenging activity of analysed extracts

Fruits extract	Anthocyanins content [mg/l]	Oxidation potentials [mV]						Remaining DPPH at the time $t = 4h$ [%]
		E_{pa1}	E_{pa2}	E_{pa3}	E_{pa4}	E_{pa5}	E_{pa6}	
Bilberries	3888	637	708	830	927	1205	1357	15.38
Black currants	860	624	695	799	1160	1334	-	41.53
Blackberries	458	685	981	1172	1317	-	-	28.88
Blackthorns	709	529	unread	1328	-	-	-	13.16
Red currants	127	693	805	unread	unread	-	-	44.73

The scavenging of the free radical by the studied extract show similar pattern curves of remaining DPPH versus time. The reaction between samples and DPPH show a biphasic kinetic behaviour, the reaction occurs rapidly in the first minutes and then slowed. This behaviour type has been reported also by some authors [22,23]. The lower step can be due to the antioxidant properties of the slow reacting components originally present in the sample and/or due to the reaction products formed during rapid phase [23].

The DPPH radical scavenging activities reveal the following order for antioxidant activities of the extracts: blackthorns > bilberries > blackberries > blackcurrants > red currants.

Comparing the experimental results obtained by the two methods, it is observed that the order of antioxidant activities for studied fruits extracts established on the basis of oxidation potentials is confirmed by the DPPH assay with only one exception, the black currants extracts, which show a weak radical scavenging effect.

Considering the anthocyanins content, we expected a higher antioxidant activity for bilberries extract which has the highest concentration in anthocyanins. It is an interesting fact that the blackthorns extract presents the strongest antioxidant activity even if the anthocyanins content is much smaller than for bilberries. This phenomenon can be explained by the possible presence of other antioxidant compounds in methanolic extract which can amplify the antioxidant effect.

CONCLUSIONS

Cyclic voltammetry can be considered a rapid and simple technique to evaluate the antioxidant properties of natural extracts. Between the two tested electrodes, glassy carbon is an excellent electrode material to study the electrochemistry of natural antioxidants.

The obtained results show that the electrochemical behavior of studied berries extracts is dependent on supporting electrolyte and solutions pH. The blackthorns extracts present the less positive potential peak, so the higher antioxidant activity in NaClO$_4$ 0.1M in MeOH and black currants extract present the less positive potential peak in the two buffer solution. Depending on pH all extracts have the same behavior, oxidation potentials shift to lower values at higher pH.

The data obtained by the cyclic voltammetry were substantially confirmed by the DPPH method. The antioxidant activities of analyzed extracts decrease in the following order: blackthorns > bilberries > blackberries > red currants. Black currants extracts presents a different behavior. No correlation between antioxidant activity and anthocyanins content has been observed for unpurified studied indigene extracts.

The further objectives regard: separation, identification and quantitative determination of anthocyanins and anthocyanidins from different fruits like bilberry, black currant, red currant, raspberry, strawberry, mulberry, grapes, blackberry etc., and determination of their "in vitro" antioxidant activity and "in vivo" testing of extracts on rats with experimentally induced diabetic disease.

EXPERIMENTAL SECTION

Extraction of Anthocyanins

The ultrasonication method in methanol acidified with 0.1% HCl, at 25°C, 59 kHz, 60 min. (ultrasonic bath FALC Instruments - Italy) has been used. 25 g of black currants, red currants, bilberries, blackthorns and blackberries frozen fruits (without seed) were treated with 100 ml extracting material for each experiment (solid to solvent ratio 1:4 w/v). After filtration through a Whatman no. 1 filter paper, the methanolic extracts were concentrated in a rotary evaporator at 40°C under vacuum (40-45 mbar) until complete solvent evaporation. For an accurate comparative analysis of extracts, they were brought to the same volume (25 ml) with methanol. The samples were kept in the freezer until analysis.

Anthocyanins content of the extracts

Anthocyanins content were quantified using the pH differential method described by Giusti and Wrolstad [17]. This method, based on reversible structural transformations of anthocyanin pigments in different pH solutions [18], permits a rapid and accurate measurement of the total anthocyanins even in the presence of polymerized degraded pigments and other interfering compounds.

A Jasco V 530 UV-Vis spectrophotometer was used for measurements. Samples were diluted in buffer solutions of pH 1.0 (0.025 M potassium chloride buffer) and pH 4.5 (0.4 M sodium acetate buffer) and then it has been made the measurements of absorbance for each solution at maximum wavelength (λ_{max}) and 700 nm (to correct for haze). The absorbance (A) was calculated using the following relation:

$$A = (A_{\lambda_{max}} - A_{700})_{pH1.0} - (A_{\lambda_{max}} - A_{700})_{pH4.5} \tag{1}$$

The monomeric anthocyanin pigment concentration was calculated using the following formula:

$$C[mg/l] = \frac{A \times MW \times DF \times 1000}{\varepsilon \times l} \tag{2}$$

where *MW* is the molecular weight, *DF* is the dilution factor, ε is the molar absorptivity and *l* is the pathlength (1 cm). Each sample was analyzed in duplicate and the results were expressed as the averages of the two measurements.

Cyclic voltammetry

Electrochemical experiments were carried out with a Voltalab 80 PGZ 402 apparatus from Radiometer Copenhagen, equipped with VoltaMaster 4 software, version 7.0 using a three-electrode electrochemical cell equipped with a working electrode, a platinum wire auxiliary electrode and Ag/AgCl, KCl sat. reference electrode. The potentials were recorded at room temperature.

Prior to each run, the electrode surface was cleaned by polishing with alumina powder and ultrasonified 10 minutes in HCl 5% solution. In order to minimize the adsorption of the compounds and their oxidation products onto the electrode surface, the voltammograms were recorded immediately after the immersing of the working electrode in the solution.

The following support electrolytes were tested: $NaClO_4$ 0.1M in methanol (pH=2.35), acetate buffer CH_3COONa/HCl (pH=3) and phosphate buffer Na_2HPO_4/NaH_2PO_4 (pH=7.6). 300 µl of extracts was diluted in 25 ml background electrolyte for electrochemical tests.

Free radical scavenging activity

The free radical scavenging activity of the studied fruits extracts was perform by using the 1,1-diphenyl-2-picrylhydrazyl (DPPH) assay according to the procedure described by Brand-Williams et al. [15] with some modifications. This assay is based on the spectrophotometric measurements of the loss of DPPH colour caused by consumption of DPPH radical by antioxidant species present in the sample.

In order to evaluate antioxidant activities, each extract has been diluted 1:25 v/v with methanol. Antioxidant solution in methanol (0,1 ml) was added to 2,9 ml of a solution $6 \cdot 10^{-5}$ mol/l DPPH in methanol. The reduction of DPPH was followed by monitoring the decrease of absorbance at 515 nm during 4 hours. A Jasco V 530 UV-Visible spectrophotometer was used for measurements.

ACKNOWLEDGMENTS

REFERENCES

1. H. Wang, M. G. Nair, G. M. Strasburg, Y. Chang, A. M. Booren, J. I. Gray, D.L. DeWitt, *Journal of Natural Products*, **1999**, *62*, 294.

2. M. Xia, M. Hou, H. Zhu, J. Ma, Z. Tang, Q. Wang, Y. Li, D. Chi, X. Yu, T. Zhao, P. Han, X. Xia, W. Ling, *The Journal of Biological Chemistry*, **2005**, *280*, 36792.

3. M. P. Kähkönen, M. Heinonen, *Journal of Agricultural and Food Chemistry*, **2003**, *51*, 628.

4. I. Konczak, W. Zhang, *Journal of Biomedicine and Biotechnology*, **2004**, *5*, 239.

5. M. A. Lila, *Journal of Biomedicine and Biotechnology*, **2004**, *5*, 306.

6. E. Kowalczyk, P. Krzesiński, M. Kura, B. Szmigiel, J. Błaszczyk, *Polish Journal of Pharmacology*, **2003**, *55*, 699.

7. A. Castañeda-Ovando, Ma. de Lourdes Pacheco-Hernández, Ma. E. Páez-Hernández, J. A. Rodríguez, C.A. Galán-Vidal, *Food Chemistry*, **2009**, *113*, 859.

8. T. Borkowski, H. Szymusiak, A. Gliszczyńska-Świgło, I. M. C. M. Rietjens, B. Tyrakowska, *Journal of Agricultural and Food Chemistry*, **2005**, *53*, 5526.

9. C. A. Rice-Evans, N. J. Miller, G. Paganga, *Free Radical Biology & Medicine*, **1996**, *20*, 933.

10. L. M. Magalhães, M. A. Segundo, S. Reis, J. L. F. C. Lima, *Analytica Chimica Acta*, **2008**, *613*, 1.

11. S. Chevion, M.A. Roberts, M. Chevion, *Free Radical Biology & Medicine*, **2000**, *28*, 860.

12. P. A. Kilmartin, *Antioxidants & Redox Signaling*, **2001**, *3*, 941.

13. M.S . Cosio, S. Buratti, S. Mannino, S. Benedetti, *Food Chemistry*, **2006**, *97*, 725.

14. D. Zielińska, L. Nagels, M. K. Piskuła, *Analytica Chimica Acta*, **2008**, *617*, 22.

15. W. Brand-Williams, M. E. Cuvelier, C. Berset, *LWT - Food Science and Technology*, **1995**, *28*, 25.

16. P. Molyneux, *Songklanakarin Journal of Science and Technology*, **2004**, *26*, 211.

17. M. M. Giusti, R. E. Wrolstad, "Unit F1.2. Anthocyanins. Characterization and Measurement of Anthocyanins by UV-Visible Spectroscopy", *Current Protocols in Food Analytical Chemistry* **2001**, F1.2.1-F1.2.13., John Wiley & Sons, Inc.

18. R. E. Wrolstad, R. W. Durst, J. Lee, *Trends in Food Science & Technology,* **2005**, *16*, 423.

19. I. David, M. N. Ştefănuţ, A. Căta, I. Ienaşcu, R. Pop, C. Tănasie, I. Balcu, *Journal of Agroalimentary Processes and Technologies,* **2009**, *15*, 348.

20. A. J. Bard, L. R. Faulkner, "Electrochemical Methods. Fundamentals and Applications" (2nd Edition), John Wiley & Sons Publisher, New York, **2001**, chapter 12.

21. A. A. De Lima, E. M. Sussuchi, W. F. De Giovani, *Croatica Chemica Acta*, **2007**, *80*, 29.

22. L. M. Magalhães, M. A. Segundo, S. Reis, J. L. F. C. Lima, *Analytica Chimica Acta*, **2006**, *558*, 310.

23. D. I. Tsimogiannis, V. Oreopoulou, *Innovative Food Science and Emerging Technologies*, **2006**, *7*, 140.

OBTAINING PYRAZINE-2,3-DICARBOXYLIC ACID THROUGH ELECTROCHEMICAL OXIDATION OF QUINOXALINE ON COPPER ELECTRODE

MARIUS DOBRESCU[a], NANDINA VLĂTĂNESCU[a], IULIANA POPA[a], BOGDAN ȚĂRANU[a], ANA DRAGOȘ[a], IOAN ȚĂRANU[a]

ABSTRACT. In order to improve current knowledge and to expand the variety of electrodes used for the pyrazine-2,3-dicarboxylic acid (PDCA) production process, we investigated the behaviour of the copper anode. A laboratory electrolyser for PDCA synthesis with copper anode using electrochemically regenerated $KMNO_4$ as chemical reagent was manufactured based on results from cyclic voltammetry studies performed on copper electrode. The best performances of this electrolyser are current efficiencies of ~55% and substance efficiencies up to 72% - achieved at a current density of 3,5 A/dm^2. Maximum conversion was 90%.

Keywords: quinoxaline, pyrazine-2,3-dicarboxylic acid, electrolyser, copper electrode, potassium permanganate

INTRODUCTION

The synthesis of pyrazinamide – efficient in tuberculosis treatment – in an advantageous way is of maximum interest [1-3]. The raw material for pyrazinamide manufacture is dipotassium-pyrazine-2,3-dicarboxylic acid (K_2PDCA) which must be obtained by chemical oxidation of quinoxaline (Q) [4-6] with KMnO4 in alkaline medium [7-9].
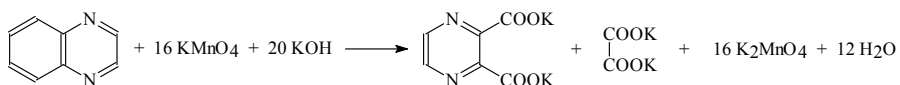
K_2MnO_4 formed in this reaction is decomposed immediately, form MnO_2 precipitate, which is released and leads to a $KMnO_4$ consumption about 16 kg for each kg of K_2PDCA [10].

Previous studies have shown that the pyrazine-2,3-dicarboxilic acid (PDCA) production process is possible, through quinoxaline chemical oxidation on platinum [11] and nickel [12] electrodes with electrochemically regenerated potassium permanganate ($KMNO_4$). Unlike the platinum electrode – known for

---

[a] *National Institute of Research-Development for Electrochemistry and Condensed Matter, Str. Dr. A.P Podeanu, No.144, RO-300569, Timişoara, Romania, dmciprian@yahoo.com*

its stability in strong oxidation and reduction conditions – the copper electrode undergoes a series of chemical transformations when immersed in electrolyte solutions. Thus, in alkaline medium, a layer of $Cu(OH)_2$ is formed on its surface influencing electrode processes. This is why we studied through cyclic voltammetry the behaviour of the copper electrode in electrolyte alkaline solutions with potassium manganate and quinoxaline. Based on study results, a laboratory electrolyser was made for PDCA synthesis on perforated copper plate anode, using electrochemically regenerated potassium permanganate as chemical reagent.

RESULTS AND DISCUSSION

The curves obtained through cyclic voltammetry at 20°C and $0.4 \cdot 10^{-3}$M Mn(VI) concentrations, on copper anode, for different support-electrolyte concentrations, are shown in figure 1.
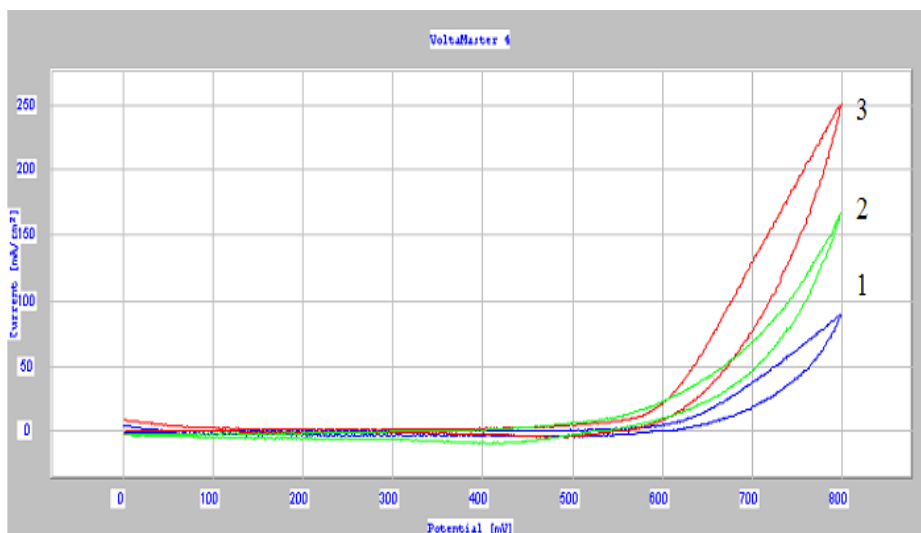
Figure 1. Cyclic voltammograms recorded on the copper electrode, v = 100 V/s, T = 20°C; $0.4 \cdot 10^{-3}$M Mn(VI); KOH solution: 1) – 2M; 2) - 4M; 3) – 8M.

Increase of KOH concentration in the electrolyte solution in the presence of Mn(VI), leads to a significant depolarisation of electrode reactions.

Current density variation at a constant electrochemical potential with temperature and KOH concentration is shown, with and without potassium manganate addition, on the copper electrode, in tables 1 and 2.

22

Table 1. Current density variation at constant electrochemical potential (700 mV) with electrolyte concentration and work temperature, on the copper electrode, in the absence of Mn(VI).

	Temperature (°C)	KOH 2N	KOH 4N	KOH 8N
$i_{[E=700mV]}$ [mA/cm²]	20	17,514	60,635	52,639
	45	18,686	81,341	87,936
	55	59,352	126,36	139,76

Table 2. Current density variation at constant electrochemical potential (700 mV) with electrolyte concentration and work temperature, constant concentration of Mn(VI) ($0.4 \cdot 10^{-3}$ M), on the copper electrode.

	Temperature (°C)	KOH 2N	KOH 4N	KOH 8N
$i_{[E=700mV]}$ [mA/cm²]	20	18,597	65,455	68,777
	45	31,44	92,26	119,3
	55	54,989	126,89	183,3

An increase in temperature and KOH concentration leads to an increase in current density at a constant electrochemical potential and to oxygen release depolarisation. By comparing this depolarisation with the one observed in the absence of potassium manganate one can see a 30% increase in current at constant electrochemical potential (700 mV). This increase shows that there is another process taking place on the electrode at electrochemical potentials close to oxygen release.
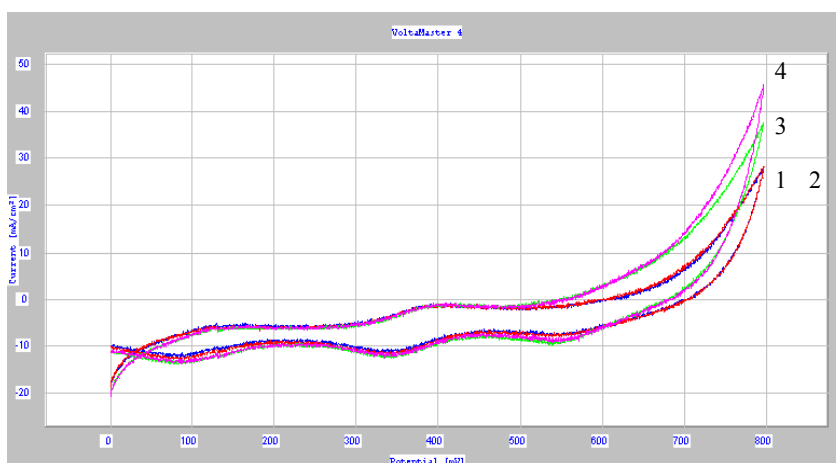
Figure 2. Cyclic voltammograms at different concentration (M) of Q: 0(1); $1.18 \cdot 10^{-2}$ (2); $2.04 \cdot 10^{-2}$ (3); $2.61 \cdot 10^{-2}$ (4) M; [KOH] = 5%; $6 \cdot 10^{-2}$ M Mn(VII); 25°C.

Increasing the concentration of Q does not affect the peaks observed in curve 1 (in figure 2), in the absence of Q, but leads to oxygen release depolarisation. The depolarisation increase is greater with the concentration value of Q. This behaviour is different from the one observed on the nickel and platinum electrode where the effect of Q in the electrolyte solution was similar to the addition of Mn(VII) in the system [11,13]. This behaviour could be explained by the fact that the oxidation of Q takes place simultaneously with the O_2 release.

The temperature effect in the presence of Q is shown in figure 3.
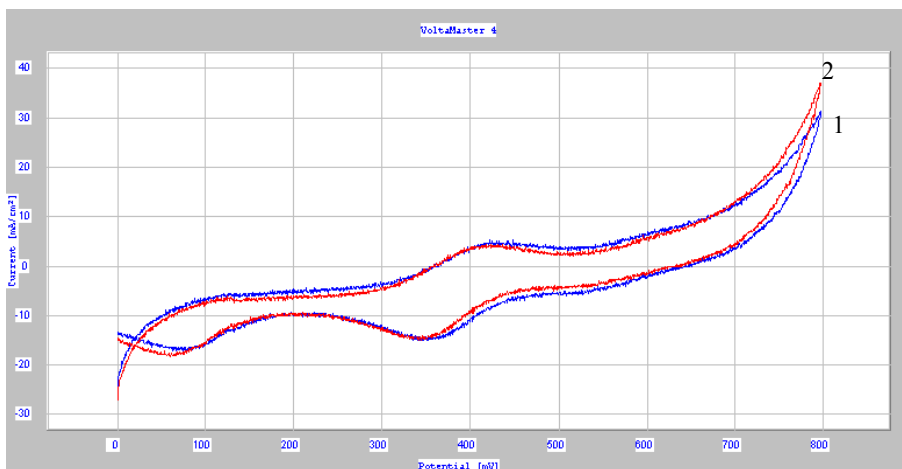
Figure 3. Cyclic voltammograms on the copper electrode at $3.8 \cdot 10^{-2}$M $KMnO_4$; 10% KOH solution; $2.61 \cdot 10^{-2}$M Q; temperature: 1)- 25°C, 2)- 40°C.

The effect of temperature increase on the peaks is insignificant (very low). On the other hand the oxygen release is slightly moved towards more negative potentials (figure 3).

Based on the results from cyclic voltammograms we made a laboratory electrolyser with perforated copper plate anode, used for the electrochemical regeneration of potassium permanganate.

Results obtained on this electrolyser are shown in table 3, where: *Q – electricity quantity; U_{med} - cell tension; m_{Qi} – initial quantity of quinoxaline; m_{Qf} – final quantity of quinoxaline; Conv.- conversion of quinoxaline and m_{K2PDCA} - K_2PDCA quantity.*

One can deduce, from table 3, that quinoxaline oxidation leads to K_2PDCA formation. Current efficiencies have values between 37 and 80% and substance efficiencies between 43 and 72%. In these conditions specific energy consumptions are between 4.8 and 17 KWh/kg K_2PDCA.

24

Table 3. Results from Mn(VII) regeneration process on the copper anode.

Nr. crt.	I [A]	i [A/m²]	Q [C]	U_{med} [V]	T [°C]	m_{Qi} [g]	m_{Qf} [g]	Conv [%]	m_{K_2PDCA} [g]	η_s [%]	η_c [%]	C. En. Kwh/kg
1.	2	3.5	32400	2.9	45	2	0.2	90	2.7	71.9	52.73	9.67
2.	1	1.7	30000	2.5	35	2	0.34	83	2	53.3	42.19	10.42
3.	2	3.5	15000	3.1	35	1	0.4	60	1.3	69.3	54.84	9.94
4.	1	1.7	15000	2.2	45	2	1	50	1.88	50.1	79.31	4.88

- KOH concentration, % - 16.6
- Quinoxaline concentration, % – 1.4 – 2.8
- Mn(VII) concentration, % - 1.4.

The best performances – current efficiencies of ~55% and substance efficiencies up to 72% - are achieved at a current density of 3.5 A/dm² and maximum 90% conversions. Doubling the current density value leads to a significant decrease in current efficiency – down to 37%.

This behaviour could be explained by the simultaneous oxygen release and Mn(VII) regeneration, favoured by the high anodic potential and leading to current consumption for a secondary product – oxygen generation.

CONCLUSIONS

Mn(VII) regeneration, from Mn(VI) resulted after the Q oxidation chemical process, takes place on the copper electrode. We did not identify any investigation of such a process in the scientific literature. The best results – maximum current and substance efficiency and minimum specific energy consumption – are achieved at a current density of 3,5 A/dm² and the temperature interval 35 - 45°C.

High current efficiencies are achieved at small Q conversions.

High conversions and substance efficiencies are achieved at small current efficiencies. Instead, the extraction and separation of unreacted Q is no longer necessary.

Temperature has no significant effect in the studied interval.

EXPERIMENTAL SECTION

Cyclic voltammetry method

For the cyclic voltammetry studies we used a PGZ 301 Dynamic-EIS Voltammetry potentiostat with VoltaMaster 4 software manufactured by Radiometer Copenhagen and an electrolysis cell equipped with three electrodes:
- the working electrode – copper wire (0.031 cm²)
- the counter electrode – platinum (0.25 cm²)
- the reference electrode – Saturated Calomel Electrode.

All electrochemical potentials from this paper are related to the SCE electrode unless otherwise specified.

Electrolyte

The Mn(VII) regeneration process was studied by cyclic voltammetry at various concentrations of KOH (2 and 4M), K_2MnO_4 (0.4-$16 \cdot 10^{-3}$M) and quinoxaline (1.18-$3.62 \cdot 10^{-2}$M). Studies were carried out at three temperatures: 20, 45 and 55°C.

The KOH was delivered by Lach-Ner, quinoxaline was taken from Merck, $KMnO_4$ was a Riedel-de Haen product and K_2MnO_4 was synthesised in our laboratory.

The method for synthesizing potassium manganate is as follows: an alkaline aqueous solution of 8N KOH containing 10g of potassium permanganate was heated at a temperature of 120 °C. After the colour changed from violet (Mn(VII)) to intense green (Mn(VI)) the supersaturated solution of Mn(VI) was obtained. K_2MnO_4 crystals were filtered from this solution on a *S4* frit, washed with $CHCl_3$, dried and weighed, and then directly dissolved in 8N KOH solution (25 ml gauge flask) and used in cyclic voltammetry tests.

Laboratory electrolyser

In order to establish the current and substance efficiencies as well as the specific energy consumption for the pyrazine-2,3-dicarboxilic acid potassium salt (K_2PDCA), experiments were performed using the perforated copper plate anode.

The amount of electric current used in synthesis was correlated with the amount of quinoxaline in the electrolyte solution and the KOH concentration was properly chosen to ensure the required quantity for K_2PDCA formation as well as the alkaline environment for the Mn(VII) regeneration reaction in optimum conditions. The anode was manufactured from a 0.5 mm thick perforated copper plate – for ensuring the easy access of the solution on the two faces of the electrode (figure 4). Before the experiments the electrode was pickled in nitric acid and after each synthesis was treated in a mixture of sulphuric and oxalic acid.

Figure 4. Copper anode.

The **_general characteristics_** of the electrolyser are the following:
- Anodic surface, dm^2 – 0.56
- Cathodic surface, dm^2 – 0.034
- Sa/Sc ratio – 16.6
- Electrolyte volume, ml – 90
- Total volume of the electrolyser, ml – 150
- Current density, A/dm^2 – 3.5
- Working temperature, ^oC – 35-45
- Anodic material – perforated copper plate
- Cathodic material – stainless steel.

REFERENCES

1. *U.S. Pattent* 6124298/**2000**.
2. K. E. Bergmann, M. H. Cynamon, J. T. Welch, *Journal of Medicinal Chemistry,* **1996**, *39*, 3394.
3. M. H. Cynamon, S. P. Klemens, T. S. Chou, R. H. Gimi, J. T. Welch, *Journal of Medicinal Chemistry*, **1992**, *35,* 1212.
4. *** - Organic Syntheses, Coll. Vol. 4, **1963**, 824.
5. A. Diether, "Manganese Compounds as Oxidizing Agents in Organic Chemistry", **1981**, 254.
6. J. March, "Advanced Organic Chemistry – Reactions, Mechanisms and Structure", Third Edition, Wiley, N. York, **1984**, 1048-1100.
7. C. A. Obafemi, W. Pfleiderer, *Helvetica Chimica Acta,* **2004**, *77*, 1549.
8. L. Henning, *Journal of the Electrochemical Society*, **2002**, *149*, S21- S33.
9. S.A. Kotharkar; D. B. Shinde, *Journal of the Iranian Chemical Society*, **2006**, *3*, 267.
10. C. A. Obafemi, W. Pfleiderer*, Helvetica Chimica Acta*, **1994**, *72*, 1549.
11. A. Dragos, I. Popa, I. Taranu, Electrochemical Syntessis of Pyrazine-2,3-Dicarboxylic Acid. II. Electrochemically kinetic studies on platinum electrode in quinoxaline presence, Symposium "New Trends and Strategies in the Chemistry of Advanced Materials with Relevance in Biological Systems, Technique and Environmental Protection", Timişoara, 8-9 November **2007**, 28.

12. I. Țăranu, I. Popa, A. Dragos, N. Vlătănescu, D. Buzatu, *Scientific Bulletin of UPT, Series of Chemistry and Environmental Engineering*, **2008**, *53 (67)*, 192.

13. I. Taranu, A. Dragos, I. Popa, Electrochemical synthesis of the pirazine-2,3-dicarboxilic acid. III. Electrochemical kinetic studies on nickel electrode in quinoxaline presence, Symposium "New Trends and Strategies in the Chemistry of Advanced Materials with Relevance in Biological Systems Technique and Environmental Protection", Timişoara, 8-9 November **2007**, 29.

STUDY OF THE EFFECTS OF MINOR ELEMENTS ON THE ELECTROCHEMICAL BEHAVIOUR OF CAST LOW ALLOY STEELS IN A MOLAR SOLUTION OF SULFURIC ACID

JULIEN HERNAIRE[a], PATRICE BERTHOD[a,b]

ABSTRACT. Fifteen low alloys steels were synthesized by induction foundry under argon atmosphere, with varied chemical compositions. In their as-cast states they were immersed in a H_2SO_4 1M solution and subjected to electrochemical measurements: polarization resistance and cyclic intensity-potential curves. All steels were logically in an active state, with low polarization resistances, low open circuit potentials and high corrosion currents. However they were all able to reach passivation for applied potentials high enough, but they fell again in the active state in the potential-decreasing part of cyclic polarization. Nevertheless, some differences were seen between the corrosion characteristics of some of these steels. The presence of niobium, tantalum and vanadium tend to lower the corrosion rate in the active state as well as they facilitate passivation. Niobium seems having a particularly strong beneficial effect on the corrosion rate of such steels both in the active state and in the passive state.

Keywords: low alloy steels, molar sulphuric acid, electrochemical behaviour, minor alloying elements

INTRODUCTION

In contrast with the stainless steels which contain at least ten percents of chromium [1], the low alloy steels, with significantly smaller contents in elements other than iron, are not resistant against corrosion, notably in acid solutions. The corrosion behaviour of stainless steels in acid solutions was extensively studied since several tens of years, for instance in aqueous solutions with more [2] or less [3] high concentrations of sulphuric acid. In contrast, works concerning corrosion of low alloy steels in such solutions, dilute [4] or concentrated [5], seem to be less frequent.

The purpose of this work is to characterize the corrosion behaviour, in a molar sulfuric acid solution, of several cast low alloy steels with various chemical compositions, by applying some of the classical electrochemical methods:

---

[a] *Faculty of Sciences and Techniques, UHP Nancy 1, Nancy – University, Postal Box 70239, 54506 Vandoeuvre-lès-Nancy, France*
[b] *Institut Jean Lamour (UMR 7198), Department of Chemistry and Physics of Solids and Surfaces, Faculty of Sciences and Techniques, Postal Box 70239, 54506 Vandoeuvre-lès-Nancy, France, Patrice.Berthod@lcsm.uhp-nancy.fr*

- measurement of polarization resistance (according to the Stern Geary method) which gives first indications about the corrosion rates

- and cyclic polarization to get first estimations of the potential and current of corrosion (according to the Tafel method) but also to know the conditions of passivation and of passivation loss, as well as the level of corrosion intensity in the passive state, and to analyze the influence of each minor element on these corrosion characteristics.

RESULTS AND DISCUSSION

The obtained chemical compositions were analyzed by microprobe on mounted samples prepared from parts cut in each ingots. The results are presented in Table 1. Generally the alloys contain as least 95 wt.% Fe and the other elements are all present with low or very low contents: 0 to 0.1 of Si, 0 to 1.2 of Mn, 0 to 1.4 of Cr, 0 to 1.7 of Mo, 0 to 1.1 of W, 0 to 0.9 of V, 0 to 1.7 of Nb and 0 to 1.2 of Ta (all contents in weight percents).

Nital-etching followed by optical microscopy observation allowed evidencing the microstructures of all steels. They are generally similar to one another, and characterized by the presence of small dispersed precipitates which seem being carbides formed from carbon and the present carbides-former elements (Cr, Mo, ...). Figure 1 shows an example of the obtained microstructures.
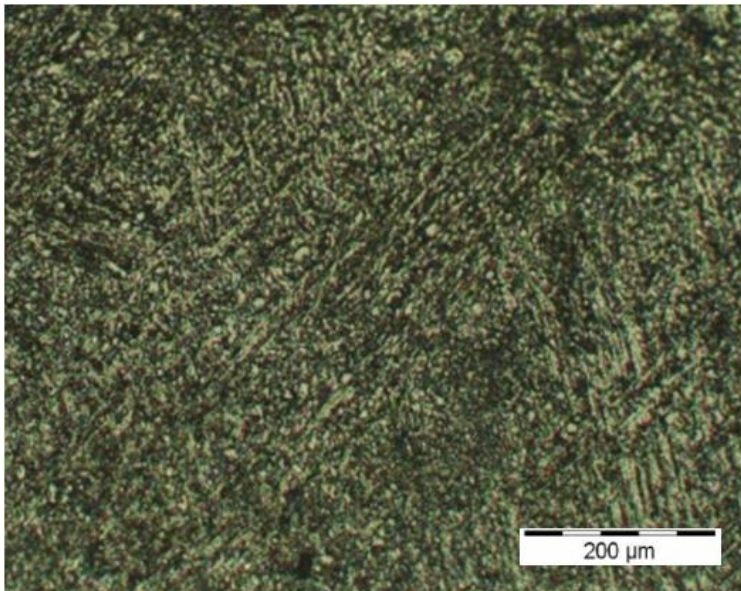
Figure 1. Example of obtained microstructure
(here: the S01r steel after Nital etching, optical microscope)

Table 1. Chemical compositions of the obtained steels (WDS, microprobe)

Steels	Fe	Si	Mn	Cr	Mo	W	V	Nb	Ta
S01r	95.8 ±0.7	0.07 ±0.02	0.40 ±0.04	1.02 ±0.04	0.19 ±0.09	/	/	/	/
S02	95.6 ±1.1	0.09 ±0.02	1.22 ±0.08	1.05 ±0.04	0.29 ±0.06	/	/	/	/
S03	98.5 ±0.64	0.10 ±0.02	0.44 ±0.03	/	0.08 ±0.09	/	/	/	/
S04	97.8 ±0.2	0.09 ±0.02	0.37 ±0.04	0.96 ±0.05	/	/	/	/	/
S05	92.2 ±1.2	0.11 ±0.01	0.37 ±0.05	1.02 ±0.02	1.59 ±0.2	/	/	/	/
S06	97.2 ±0.64	0.09 ±0.01	0.11 ±0.02	1.04 ±0.06	1.66 ±0.19	/	/	/	/
S07	94.4 ±4.4	0.11 ±0.03	0.41 ±0.04	1.10 ±0.04	0.23 ±0.14	1.08 ±0.15	/	/	/
S08	95.5 ±0.5	0.09 ±0.02	0.38 ±0.06	1.03 ±0.05	0.18 ±0.09	/	/	1.73 ±0.23	/
S09	92.9 ±0.2	0.08 ±0.01	0.40 ±0.05	1.41 ±0.07	0.27 ±0.07	/	0.89 ±0.05	/	/
S10	95.5 ±0.6	0.05 ±0.03	0.41 ±0.05	1.06 ±0.06	0.17 ±0.12	/	/	/	1.19 ±0.14
S11	96.6 ±0.45	0.08 ±0.02	0.43 ±0.04	1.07 ±0.02	0.43 ±0.07	0.28 ±0.07	/	/	/
S12	96.7 ±0.7	0.10 ±0.02	0.45 ±0.07	1.08 ±0.04	0.43 ±0.07	0.12 ±0.12	0.07 ±0.02	/	/
S13	97.7 ±0.49	0.09 ±0.02	/	1.06 ±0.04	0.24 ±0.08	/	/	/	/
S14	97.6 ±0.5	/	0.43 ±0.05	1.03 ±0.05	0.24 ±0.07	/	/	/	/
S15	96.8 ±0.3	0.08 ±0.03	0.39 ±0.05	0.99 ±0.04	0.36 ±0.16	0.29 ±0.10	/	0.01 ±0.01	/

Just after immersion in the molar H_2SO_4 solution, the Stern-Geary method was used to measure successively three times the polarization resistance by applying an increase of potential from E_{ocp} – 20 mV to E_{ocp} + 20 mV at +10 mV/min, over a whole duration of about 30 minutes (E_{ocp} : open circuit potential, measured just before each Stern-Geary run). Thereafter a cyclic polarization was performed from E_{ocp} – 250 mV to 1.9 V at 5 mV/s and from 1.9 V down to E_{ocp} – 250 mV at -5 mV/s, with E_{ocp} measured just before the cyclic polarization start. The part of the obtained log(I)=f(E) curve corresponding to the [E_{ocp} – 250 mV, E_{ocp} + 250 mV] range was considered for applying the Tafel method in order to estimate both potential and current of corrosion E_{corr} and I_{corr}.

The obtained values all show that the steels were all in the active state. All these first results, which thus concern the corrosion parameters for the active state, are presented in Table 2 (successive polarization resistances Rp1, Rp2 and Rp3, potentials and currents of corrosion E_{corr} and I_{corr}, anodic and cathodic Tafel coefficients b_a and b_c).

Table 2. Effect of the minor elements on the corrosion parameters in the active state (Stern-Geary + Tafel in the E-increasing part of the cyclic polarization curves)

steels	Stern-Geary	Tafel (cyclic polarization curve, part E ↑)			
	Rp1–Rp2–Rp3 $((\Omega \times cm^2)$	E_{corr}/NHE (mV)	I_{corr} (mA/cm²)	b_a (mV/dec)	b_c (mV/dec)
S01r (reference steel)					
S01r	25.6 – 25.0 – 23.2	-228	0.95	66	148
Effect of Cr (comparison with **S01r: 1.02 wt.% Cr**)					
S03: 0.00Cr	24.3 – 23.6 – 21.6	-228	1.19	72	145
Effect of Si (comparison with **S01r: 0.07 wt.% Si**)					
S14: 0.00Si	31.0 – 30.8 – 28.8	-231	1.00	76	185
Effect of Mo (comparison with **S01r: 0.19 wt.% Mo**)					
S04: 0.00Mo	24.4 – 23.1 – 21.9	-243	0.90	67	157
S05: 1.59Mo	25.1 – 22.3 – 21.1	-205	0.88	55	159
Effect of Nb (comparison with **S01r: 0.00 wt.% Nb**)					
S08: 1.73Nb	30.7 – 62.2 – 71.5	-265	0.21	50	177
Effect of Ta (comparison with **S01r: 0.00 wt.% Ta**)					
S10: 1.19Ta	29.2 – 25.6 – 25.6	-232	0.68	66	169
Effect of V (comparison with **S01r: 0.00 wt.% V**)					
S09: 0.89V	24.6 – 24.7 – 24.0	-239	0.82	80	172
Effect of Mn (comparison with **S01r: 0.40 wt.% Mn**)					
S13: 0.00Mn	28.3 – 26.4 – 25.0	-232	1.17	74	177
S02: 1.22Mn	17.4 – 19.2 – 17.7	-236	1.47	79	189
Effect of Mn (comparison between the alloys bellow only)					
S06: 0.11Mn	24.3 – 22.1 – 20.1	-204	1.02	56	165
S05: 0.37Mn	25.1 – 22.3 – 21.1	-205	0.88	55	159
Effect of W (comparison with **S01r: 0.00 wt.% W**)					
S07: 1.08W	20.2 – 19.0 – 17.7	-215	1.70	81	214
Effect of W (comparison between the alloys bellow only)					
S12: 0.12W	23.0 – 19.9 – 19.5	-219	0.70	67	144
S11: 0.28W	24.6 – 22.9 – 17.2	-215	0.84	64	146
S15: 0.29W	23.0 – 21.4 – 19.5	-220	1.25	68	180

By comparing directly the steels with the S01r steel (which plays the role of reference steel in many cases) which significantly differ from the latter one concerning only one element, or simply some of the steels to each other when only one element is significantly different between them, it appears that:

* the Rp values tend to increase and the I_{corr} values tend to decrease when the following elements are present or when their contents are higher: Cr, Nb (effect especially strong), Ta and V
* the Rp values tend to decrease and the I_{corr} values to increase when W and even Si are present or when their content are higher,
* while no systematic evolution of Rp and I_{corr} can be noted for the changes in the contents of Mo and Mn.

One can remark the absence of real correlation between the corrosion rate and the E_{corr} values. The latter are all between -0.3 V and -0.2 V, as is to say between the standard potentials of the Fe^{2+}/Fe^0 and H^+/H_2 systems. The anodic and cathodic Tafel coefficients b_a and b_c are also generally consistent with the reactions $Fe^0 \rightarrow Fe^{2+} + 2e$ and $H^+ \rightarrow \frac{1}{2} H_2 + e$ since they are more or less close to 59 mV/decade and 118 mV/decade, respectively.

The parameters corresponding to the passive state were measured on the cyclic polarization curves, an example of which is given in Figure 2.
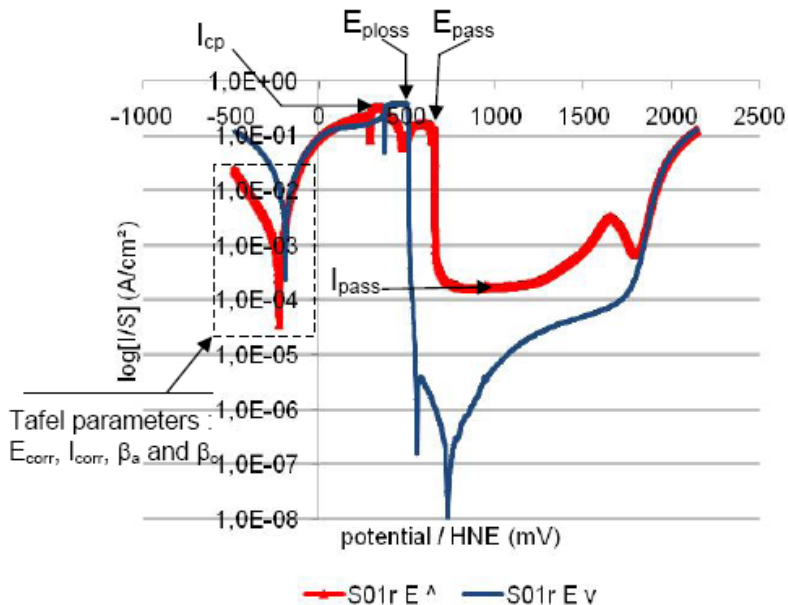

Figure 2. The whole cyclic polarization curve for the reference steel S01r, with visualization of the parameters of interest

The corrosion parameters which were of interest are:

- for the potential-increasing part of the cyclic polarization curve: the critical current of passivation I_{cp} and the potential of passivation E_{pass} (which both characterize the level of difficulty to reach the passive state) and the average corrosion current in the passivation plateau I_{pass} (corrosion rate in the passive state),
- for the potential-decreasing part of the curve: the potential of passivation loss E_{ploss} (characterizing the stability of the passive state when the potential is lowering).

All the measured values are given in Table 3, which also allows either comparing directly the steels with the reference S01r steel when they differ from this one about only one element, or directly steels to each other when one element is different between them (cases of Mn and W again).

Concerning the conditions for reaching the passive state it appears that:

* the I_{cp} and E_{pass} values tend to decrease when the following elements are present or when their contents are higher: Nb, Ta and W; in contrast it is not so clear for vanadium,
* the I_{cp} and E_{pass} values tend to increase when Cr, Si and Mo is present or when their contents are higher; Mn seems also to have the same effect.

Concerning the corrosion rates in the passive state one can notice that:

* unsurprisingly the corrosion current is significantly lowered by passivation (about ten times lower than in the active state) but most of the alloying elements led to higher values of critical current of passivation Icp (Si, Mn, W but also Ta and V),
* three elements (Cr, Mo and Nb) lower I_{cp}.

The protective layer formed by passivation is unfortunately lost in all cases when the applied potential decreases. However this generally occurs at lower potentials when the alloying elements are added or when their contents are higher. Indeed, Cr, Nb, Ta, V and W all led to lower E_{ploss} values while no systematic effect was observed in the case of Mo and Mn. Si is the single element which appeared to deteriorate the stability of the passive state.

The differences discussed before between steels about the corrosion potential and current, and the characteristics of passivation, can be graphically illustrated by Figure 3 and Figure 4, in which the potential-increasing parts of the cyclic polarization of some of the studied steels are superposed with the S01r reference steel one.

Table 3. Effect of the minor elements on the corrosion parameters concerning the passive state (in the E-increasing part of the polarization curve: critical current of passivation I_{cp}, potential of passivation E_{pass} and average corrosion current in the passive state I_{pass}; in the E-decreasing part of the cyclic polarization curve: potential of passivation loss E_{ploss})

steels	E-increasing part of the cyclic polarization curve			E-decreas. part
	I_{cp} (mA/cm²)	E_{pass}/NHE (mV)	I_{pass} (µA/cm²)	E_{ploss}/NHE (mV)
S01r (reference steel)				
S01r	339	+666	177	+546
Effect of Cr (comparison with **S01r: 1.02 wt.% Cr**)				
S03: 0.00Cr	223	+640	192	+570
Effect of Si (comparison with **S01r: 0.07 wt.% Si**)				
S14: 0.00Si	280	+577	147	+511
Effect of Mo (comparison with **S01r: 0.19 wt.% Mo**)				
S04: 0.00Mo	281	+572	215	+510
S05: 1.59Mo	> 285	+939	413	+507
Effect of Nb (comparison with **S01r: 0.00 wt.% Nb**)				
S08: 1.73Nb	277	+551	133	+509
Effect of Ta (comparison with **S01r: 0.00 wt.% Ta**)				
S10: 1.19Ta	271	+587	193	+511
Effect of V (comparison with **S01r: 0.00 wt.% V**)				
S09: 0.89V	378	+600	270	+520
Effect of Mn (comparison with **S01r: 0.40 wt.% Mn**)				
S13: 0.00Mn	266	+578	176	+508
S02: 1.22Mn	181	+762	390	+538
Effect of Mn (comparison between the alloys bellow only)				
S06: 0.11Mn	386	+570	166	+526
S05: 0.37Mn	> 285	+939	413	+507
Effect of W (comparison with **S01r: 0.00 wt.% W**)				
S07: 1.08W	244	+641	214	+517
Effect of W (comparison between the alloys bellow only)				
S12: 0.12W	373	+664	169	+516
S11: 0.28W	276	+574	187	+530
S15: 0.29W	399	+558	188	+512

For example in Figure 3 one find again the increase in passivation potential (1) due to silicon or the increase in anodic current in the passive state (2) due to tungsten. But one see also, for the alloys containing Cr while it

is absent for the Cr-free S03 steel) the enlargement of the peak (3) preceding the solvent's oxidation due to the small quantity of chromium which previously led to a $Cr^{III}(OH)_3$ layer partly covering the steel surface and which thereafter suffers new oxidation in $Cr^{VI}O_7{}^{2-}$ species by transpassivation.
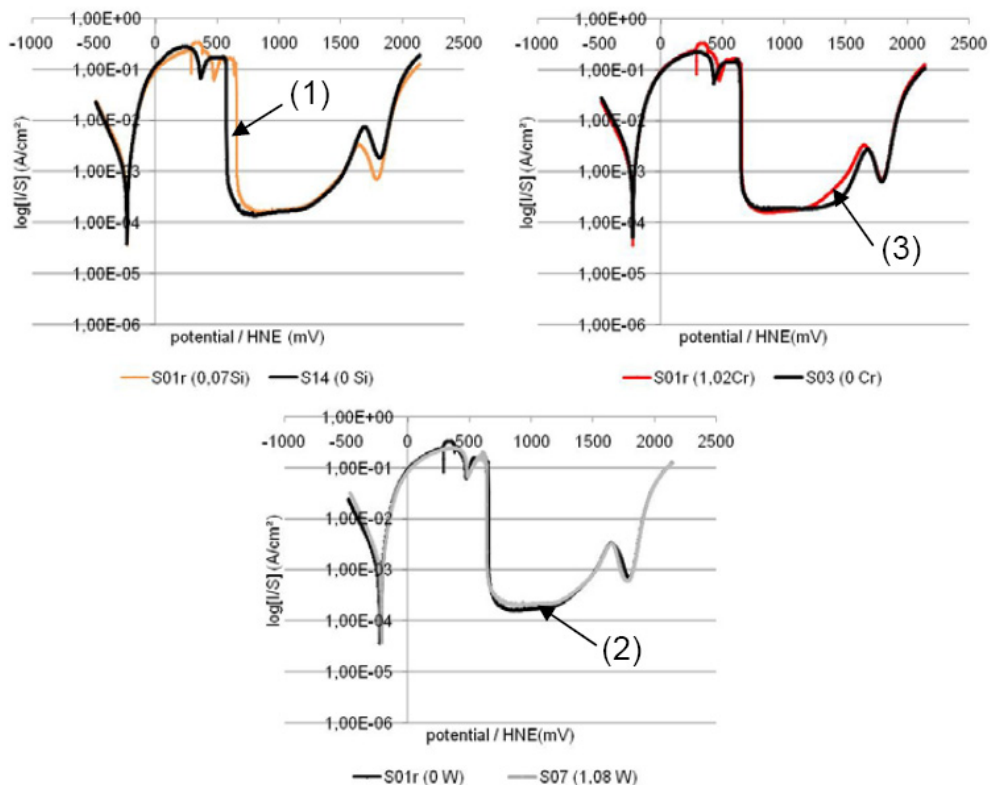
Figure 3. Effects of silicon, tungsten and chromium on the E-increasing parts of the polarization curves (steels S14, S03 and S07 compared to the reference steel S01r)

In Figure 4, one find again the tendency of tantalum (4), vanadium (5) and niobium (6) to decrease the passivation potential, but a new observation is the progressive second decrease in anodic current (following the first sudden part of decrease) which delays over several hundreds mV the reaching of the minimum passivation current (7). In the curve corresponding to the S09 steel, there is an additional small peak near 1000 mV (8) which may correspond to the re-oxidation of $V^{IV}O^{++}$ (coming from the vanadium initially present in the steel) in $V^{V}O_2{}^{+}$ in the solution [6].
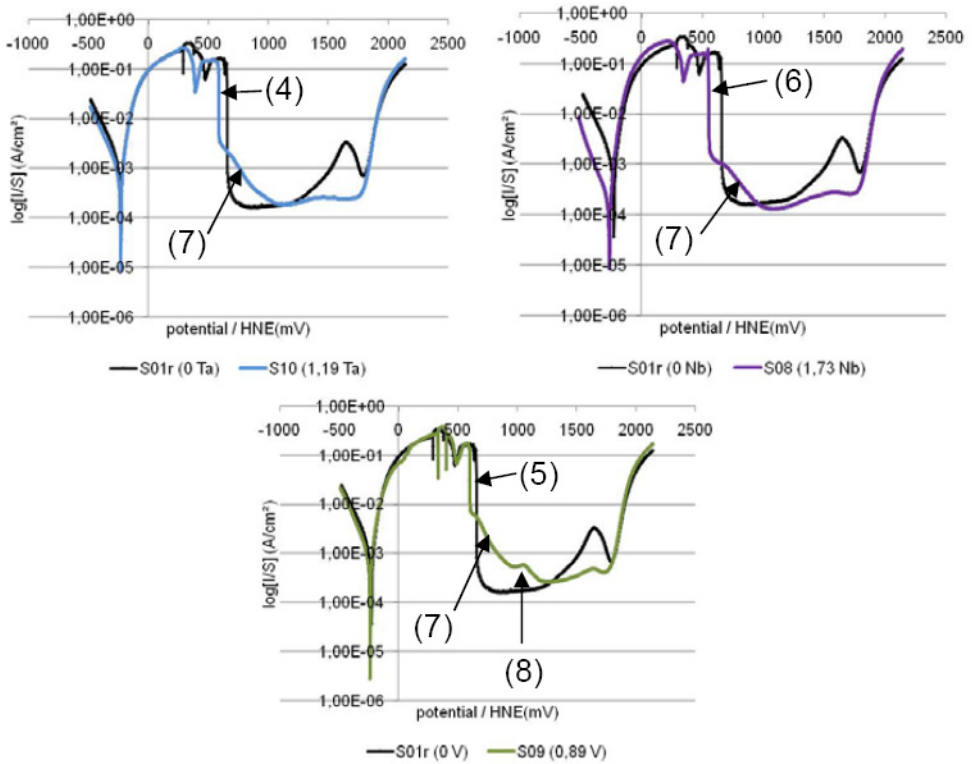
Figure 4. Effect of tantalum, niobium and vanadium on the E-increasing parts of the polarization curves (steels S10, S08 and S09 compared to the reference S01r)

The effects of minor elements on the corrosion behaviour of steels in such acid solutions were previously studied in numerous works when these alloys were stainless steels, but more rarely when they were low alloy steels. Indeed, the latter were more studied in other aqueous solutions, such as sea water (e.g. [7]) or underground water (e.g. [8]). Therefore comparisons with earlier results are difficult to do. Nevertheless one can remind that it was previously found that niobium and tungsten were beneficial (as found here for Nb but not for W) to the corrosion resistance in dilute sulphuric acid solutions [4], but in the case of an austenitic stainless steel. It was also reported that sufficiently high amounts in molybdenum or chromium led to improvements in corrosion resistance for some Cr-rich steels and nickel-base alloys in sulphuric acid solutions with various concentrations [9,10] (this was the case only for Cr here). Contrarily to what was observed here, it was formerly found that silicon favors corrosion resistance, but again in the case of stainless steel able to passivate [11] for which Si decreased the passive current density.

37

CONCLUSIONS

The low alloy steels studied here are unsurprisingly not resistant against corrosion in a molar sulphuric solution since they logically remain in the active state if simply immersed. However they are able to passivate if a sufficiently high potential is applied. Nevertheless the presence of minor elements may slightly modify (and even significantly in the case of niobium) their corrosion potential and intensity, as well as the easiness of their passivation, their corrosion rate in the passive state and the stability in potential of the latter. To finish, one may underline the beneficial effect of niobium on all corrosion characteristics in the active state as in the passive state.

EXPERIMENTAL SECTION

All the alloys were cast using a high frequency induction furnace (CELES), by melting pure elements (Alfa Aesar, >99.9 wt.%) together under 300 mbars). Fusion and solidification were achieved in the water-cooled copper crucible of the furnace. The obtained ingots, which weighed about 100 g, were cut, tin-soldered to a plastic-isolated copper wire, and embedded in a cold resin before polishing with 1200-grit paper. The areas of steel in contact with the electrolyte were comprised between about 1 and 2 cm².

The microstructures of the steels were observed by optical microscopy after etching by Nital 4% (96% ethanol + 4% HNO_3 and their chemical compositions controlled by Wavelength Dispersion Spectrometry using a Cameca SX50 or SX100 microprobe.

The electrochemical experiments were performed using a classical three-electrodes cell containing the H_2SO_4 1M solution and a Princeton Applied Research potensiostat (model 263A) driven by the software M352 of EGG/Princeton. The electrolyte was replaced after each {3 × Rp + 1 × cyclic polarization} whole experiment.

The electrochemical experiments performed were composed of:

* the measurement of three successive polarization resistances (Rp) from E_{ocp} – 20 mV to E_{ocp} + 20 mV at 10 mV/min,

* a cyclic polarization run, from E_{ocp} – 250 mV to 1.9 V at 10 mV/min, then from 1.9 V down to E_{ocp} – 250 mV at -10 mV/min.

REFERENCES

1. G. Murry, "Aide-mémoire Métallurgie", Dunod, Paris, **2004**, chapter 12.
2. B.T. Ellison, W.R. Schmeal, *Journal of the Electrochemical Society*, **1978**, *125*, 524.
3. U. Quaranta Cabral, L. Sathler, *Metal ABM*, **1973**, *29*, 91.
4. K. Osozawa, Y. Fukase, K. Yokota, *Corrosion Eng.*, **1971**, *20*, 11.

5. M.B. Ives, J.R. Kish, J.R. Rodda, *Materials Science Forum*, **1995**, *185-188*, 887.

6. D.F. Shriver, P.W. Atkins, C.H. Langford, "Inorganic Chemistry", Oxford University Press, Oxford, **1990**.

7. E. Dajoux, S. Malard, Y. Lefèvre, D. Kervadec, O. Gil, *Matériaux et Techniques*, **2005**, *93*, 69.

8. C. Bataillon, C. Musy, M. Roy, *J. Phys. IV France*, **2001**, 11, Pr1-267.

9. M. A. A. Tullmin, F. P. A. Robinson, *Corrosion*, **1988**, *44*, 664.

10. N. Sridhar, *Materials Performance*, **1988**, *27*, 40.

11. K. Hio, Y. Hosoi, M. Tsutsui, M. Okabe, *Journal of the Japan Institute of Metals*, **1999**, *63*, 1248.

CARBON STEEL CORROSION INHIBITION BY PLANT EXTRACT BASED GREEN INHIBITORS

ANCA COJOCARU[a], IOANA MAIOR[a], IOSIF LINGVAY[b], CARMEN LINGVAY[b], SIMONA CAPRARESCU[a], DANUT-IONEL VAIREANU[a]

ABSTRACT. The inhibition effect of several plant extracts on the corrosion of carbon steel in 0.5 M H_2SO_4 has been investigated by potentiodynamic polarization and electrochemical impedance spectroscopy (EIS). One has attempted to determine the corrosion characteristics in the absence and in the presence of natural plant extracts obtained from *Allium Sativum and Juglans Regia* using VoltaLab 40 potentiostat.

Potentiodynamic polarization curves were plotted at a scan rate of 20 mV/min. The EIS investigations have measured the response of the electrochemical system using a 10 mV a.c. potential excitation within a frequency zone ranging from 100 kHz to 50 mHz. Equivalent circuit model was proposed based on fitting the impedance data and hence the main parameters of the corrosion system were obtained.

The potentiodynamic polarization curves were employed to represent the Tafel lines and to evaluate the corrosion potential E_{corr} and the kinetic parameters namely the corrosion current density i_{corr} and the anodic, b_a and cathodic b_c Tafel slopes. The corrosion current densities have lower values in the presence of plant extracts. The inhibition efficiency calculated from the potentiodynamic polarization parameters and from EIS measurements were in agreement, the best results were obtained for the mixtures containing 400 ppm *AS* for all *AS*/*JR* concentration ratios.

Keywords: Inhibitors, Electrochemical impedance spectroscopy, Corrosion, Sulphuric acid, Steel

INTRODUCTION

Nowadays intensive researches are accomplished to find new natural environmental friendly products, the so-called "green products". These may be able to substitute, up to a certain limit, the synthetic products, considered harmful for the environment, and no longer acceptable taking into account the environmental impact and also the true cost of using the synthetic products with serious side effects. Natural plant extracts may show inhibiting effects,

[a] University Politehnica of Bucharest, Faculty of Applied Chemistry and Materials Science, 1-7 Polizu St, 011061, Bucharest, Romania, *a_cojocaru@chim.upb.r*o

[b] National Institute for Advanced Researches and Development in Electrical Engineering INIDIE ICPE-CA, 313 Splaiul Unirii, 030138, Bucharest, Romania

these products presenting the advantage of biodegradability, being able to replace synthetic inhibitors phased out due to increased enforced stringent environmental legislation.

The cost of corrosion is very high for any country. Corrosion never stops but its damages can be decreased. The use of inhibitors is one of the best-known methods of corrosion protection [1, 2]. The importance of inhibitive protection in acidic solutions is increased by the facts that steels, that are more susceptible to be attacked in aggressive media, are the commonly exposed metals in industrial environments. Numerous works have been dedicated to corrosion inhibiting effects of different plant extracts in acidic aqueous solutions on metallic materials [3-6]. Their choice is based on their low-cost and stability as corrosion inhibitors for metallic materials in acidic media and because these compounds are environmental friendly.

Among other methods of corrosion investigation, the application of electrochemical impedance spectroscopy technique (EIS) as a new tool for the study of corrosion research has resulted in information concerning the methods of corrosion protection [7], which were difficult to study with traditional dc techniques; EIS has provided useful information concerning corrosion protection by anodic films and by inhibitors [8-13]. In addition to specification of the physical properties of the system, the technique leads to important mechanistic and kinetic information [14-16]. Some advantages of ac impedance techniques are the use of only very small signals which do not disturb the electrode properties to be measured, the possibility of studying corrosion reactions and measuring corrosion rates in media where traditional dc methods fail, and the fact that polarization resistance as well as double layer capacitance data can be obtained in the same measurements.

The authors have previously investigated [17] the effect of the addition of single plant extract as inhibitor for steel corrosion in sulphuric acid. This paper shows the results obtained on the corrosion inhibition of steel in 0.5 M sulphuric acid by combining the studied plant extracts at different ratios. It was analyzed the interaction between the plant extracts by calculating the synergism parameter, and also the authors have proposed an electrical equivalent circuit model by using EIS results.

RESULTS AND DISCUSSION

Polarization measurements

The potentiodynamic curves were recorded in the absence (blank test solution) and in the presence of various plants extract concentration. Figure 1 shows some of the potentiodynamic polarization curves carried out at 25^0 after 30 minutes of immersion time in 0.5 M H_2SO_4 in the presence and absence of *Allium Sativum* (*AS*) and *Juglans Regia* (*JR*). By using the

experimental data important parameters were extracted: corrosion current density, i_{corr}, corrosion potential, E_{corr}, anodic b_a and cathodic b_c Tafel slopes, which are listed in Table1. These values were calculated from the intersection of the anodic and cathodic Tafel lines of the polarization curve at E_{corr}. The inhibition efficiencies were calculated by the following expression:

$$IE = \left(1 - \frac{i_{corr}}{i_{corr}^0}\right) \times 100 \ , \ \%$$

(1)

were i_{corr}^0 and i_{corr} are respectively, the corrosion current densities without and with addition of plant extracts in 0.5 M H_2SO_4 solution.
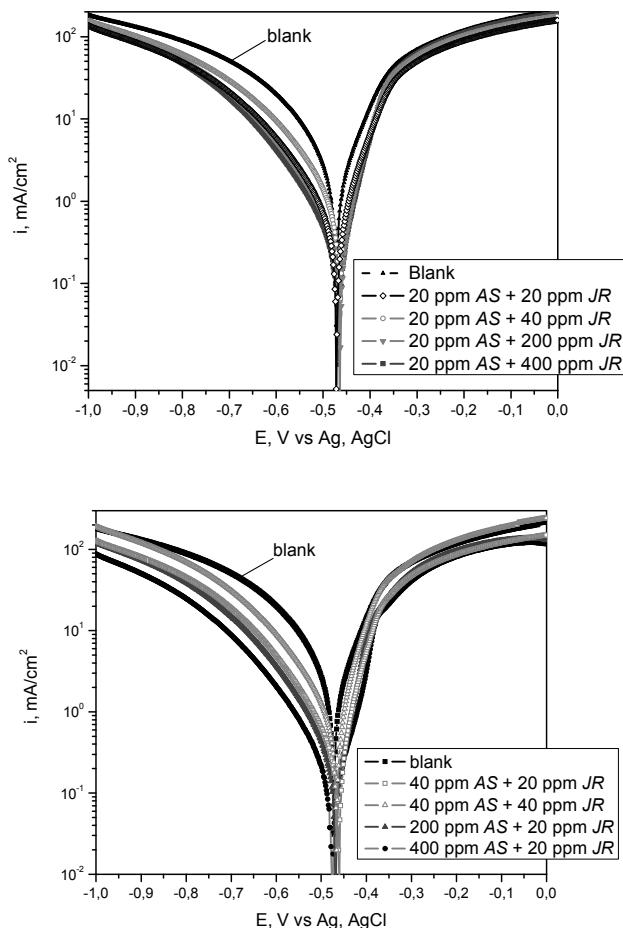

Figure 1. Polarization curves for steel in 0.5 M H_2SO_4 with mixtures of different concentrations of *Allium Sativum* and *Juglans Regia*

Although the addition of *AS* and *JR* does not affect the general shape of the curves, it can be seen (Figure 1) that both cathodic and anodic curves are affected by the inhibitor presence. The results presented in Table 1 indicate that the presence of *AS* and *JR* inhibit the corrosion process by reducing the corrosion current densities to lower values.

Tafel plots in 0.5 M H_2SO_4 revealed that the presence of the plant extracts generally shifted the corrosion potential towards positive values with reference to the blank 0.5 M H_2SO_4. This signifies that the addition of *AS* and *JR* has an inhibitor effect on the corrosion process. The presence of plant extracts lead to a decrease of anodic Tafel slopes, indicating that the inhibitor acts mainly on the anodic reaction. Based on these results *AS* and *JR* are considered as mixed-type inhibitor, meaning that it reduces the anodic dissolution of steel and also retards the cathodic reaction.

Table 1. Tafel polarization parameters for steel corrosion in 0.5 M H_2SO_4 in the presence of different concentrations of *Allium Sativum* and/or *Juglans Regia*

AS conc. (ppm)	*JR* conc. (ppm)	i_{corr} (mA/cm^2)	E_{corr} (mV)	b_c (mV/ dec)	b_a (mV/dec)	IE%
0	0	0,738	-483	110	74	-
0	20	0.611	-470	115	69	17.22
20	0	0.424	-465	111	53	42.58
20	20	0.387	-477	111	58	47.62
40	20	0.331	-463	114	50	55.09
200	20	0.265	-470	109	46	64.09
400	20	0.158	-478	103	51	78.60
40	0	0.549	-480	107	54	25.69
0	40	0.500	-463	120	59	32.22
20	40	0.651	-469	98	63	11.87
40	40	0.625	-471	99	50	15.39
200	40	0.268	-469	109	43	63.66
400	40	0.114	-472	113	44	84.63
200	0	0,211	-462	115	47	71.42
0	200	0.376	-457	119	54	49.03
20	200	0.369	-466	113	51	50.02
40	200	0.587	-465	115	57	20.49
200	200	0.301	-469	115	40	59.30
400	200	0.177	-477	104	53	76.01
400	0	0.216	-459	101	45	70.79
0	400	0.438	-452	119	57	40.69
20	400	0.300	-469	110	51	59.33
40	400	0.617	-465	116	55	16.47
200	400	0.207	-473	111	44	72.02
400	400	0.134	-486	109	51	81.90

The inhibition efficiencies from Table 1 are calculated with equation (1), and show highest values for 400 ppm *AS*, the highest efficiency value being obtained for the mixture 400 ppm *AS* + 40 ppm *JR*. For the same concentration of *JR* the inhibition efficiency is generally increasing with the increase of *AS* concentration.

Electrochemical Impedance Spectroscopy

The impedance diagrams are given in the Nyquist (Figure 2) and Bode (Figure 3) representations.

The data processing was based on a non-linear least squares fitting procedure. In this case inhibition efficiencies IE% were calculated through the following expression:

$$IE = \left(1 - \frac{R_p^0}{R_p} \right) \times 100 \ , \ \% \tag{2}$$

where R_p^0 and R_p are the polarization resistance values observed in absence and presence of inhibitor, respectively.

The polarization resistance (R_p) values are calculated from the difference in impedance at lower and higher frequencies [12].

To obtain the double layer capacitance (C_{dl}) one must found the frequency at which the imaginary component of the impedance is maximum (Z_{max}) and the capacitance is represented by the equation

$$C_{dl} = \frac{1}{\omega \cdot R_p} \tag{3}$$

were $\omega = 2 \cdot \pi \cdot f_{max}$, is the angular frequency.

All Nyquist diagrams of steel exposed for 30 min at free corrosion potential in inhibited and uninhibited acidic solution containing different concentrations of *AS* and *JR* plant extracts consist of a depressed capacitive semicircle at high frequencies and a small inductive one at low frequencies (Figure 2). The low frequency inductive loop may be attributed to the relaxation process of the adsorbed species.

The intersection of the capacitive loop with the real axes at the highest values of frequencies gives the value for the resistance of the solution (R_s) enclosed between the working electrode and the counter electrode. The point of intersection between the inductive loop and the real axis represents the sum ($R_s + R_p$) where R_p is the polarization resistance defined as the dc limit of the impedance.

The highest values of polarization resistances were generally obtained for the mixtures containing 200 and 400 ppm *AS*.
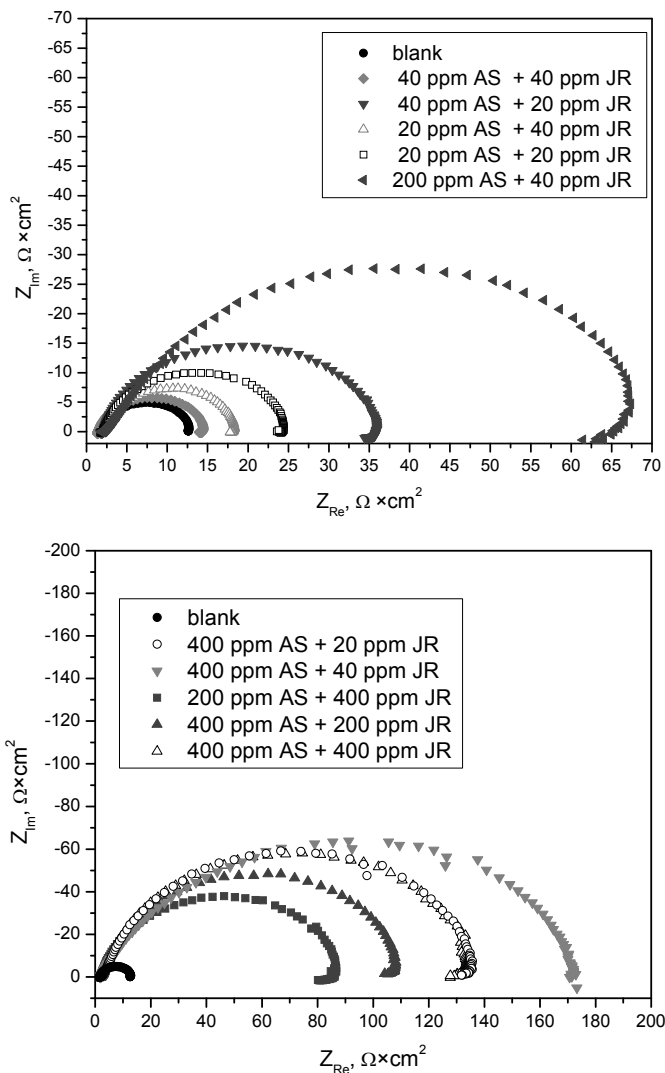
Figure 2. Nyquist plots for steel corrosion in 0.5 M H_2SO_4 with different concentrations of *Allium Sativum* and *Juglans Regia*

It is essential to develop the appropriate model for the impedance, which then can be used to fit the experimental data and to evaluate the parameters that characterize the corrosion process.

The Nyquist plots in Figure 2 are not perfect semicircles, and in the Bode plots, in Figure 3, the slopes of the log IZI against log f curves are lower than -1. This kind of deviations can be attributed to the non-homogeneity of the electrode surface arising from surface roughness or interfacial phenomena.

The impedance parameters obtained from electrochemical spectroscopy investigations are mentioned in Table 2.

The presence of *AS* and *JR* compounds (Table 2) enhances the value of R_p in acidic solution indicating that a charge transfer process is mainly controlling the corrosion of steel, also the increase of R_p is generally interpreted by the adsorption of inhibitor molecules [18].

The decrease of the double layer capacitance C_{dl} is due to the adsorption of plant extract on the metal surface leading to the formation of film from acidic solution [19]. More the inhibitor is adsorbed, more the thickness of the deposited film is increased according to the expression of the layer capacitance presented in the Helmholtz model [20].

Figure 3. Bode plots of impedance spectra for steel in 0.5 M H_2SO_4 at 25^0C with various concentrations of *Allium Sativum* and *Juglans Regia*
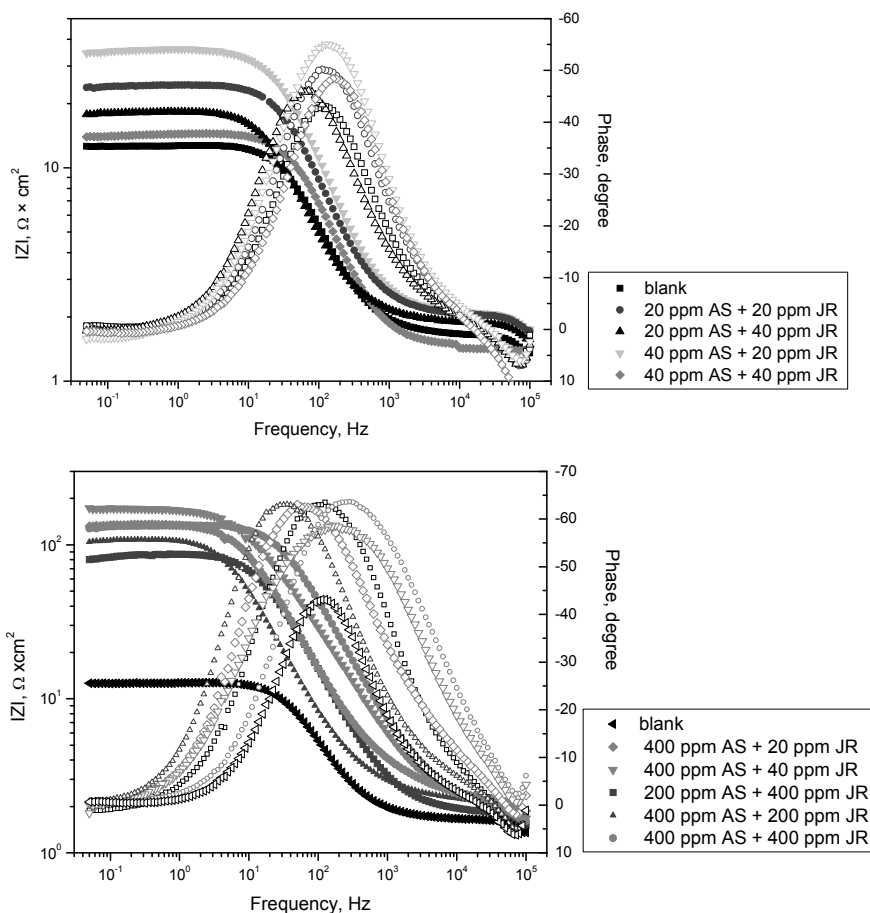
Table 2. Electrochemical parameters of impedance for the corrosion of steel in 0.5 M H_2SO_4 in the presence of different concentrations of *Allium Sativum* and/or *Juglans Regia*

AS conc. (ppm)	JR conc. (ppm)	R_p, $\Omega \times cm^2$	C_{dl}, $\mu F \times cm^{-2}$	φ_{max}, degree	IE%
0	0	11.35	350.4	-43	-
0	20	27.82	326.1	-47	59.20
20	0	31.76	220.0	-55	64.26
20	20	22,80	195.4	-50	50.22
40	20	34.13	165.9	-55	66.74
200	20	66.86	266.5	-62	83.02
400	20	134.10	149.4	-63	91.54
0	40	60.23	797.7	-55	81.15
40	0	44.75	157.3	-54	74.64
20	40	16.22	490.5	-46	30.02
40	40	13.12	242.5	-48	13.49
200	40	64.55	345.1	-53	82.42
400	40	172.70	92.1	-59	93.43
0	200	25.28	588.8	-55	55.10
200	0	90.11	228.2	-62	87.40
20	200	20.66	308.1	-52	45.06
40	200	20.19	441.2	-52	43.78
200	200	57.56	221.1	-60	80.28
400	200	107.00	296.6	-63	89.41
0	400	23.68	521.8	-53	52.07
400	0	71.46	291.9	-62	84.12
20	400	25.92	245.6	-54	56.21
40	400	13.82	230.2	-48	17.87
200	400	86.70	130.6	-64	86.91
400	400	136.90	36.7	-64	91.71

Figure 3 shows the influence of concentrations on modulus spectra of steel and on phase angle in absence and presence of the inhibitor. In all cases the figures show that the IZI against f logarithmic curves exhibit three distinctive segments. In the higher frequency region, the IZI tends to become 1 with the phase angle values falling rapidly towards 0 with increasing frequency. This is a typical response of resistive behavior and corresponds to the solution resistance [21]. In the medium frequency region, a linear relationship between IZI against f, with a slope lower than -1 and the phase angle being in the range -43 in blank acidic solution to -64 degree in the presence of plant extracts, can be observed (Table 2). This response is characteristic for a capacitive behavior. An ideal capacitive response would result in a slope of -1 and a phase angle of -90 degree. In the low-frequency region, the resistive behavior of the electrode increases.

The phase angle for the double layer in the presence of *AS* and *JR* inhibitors were shifted toward higher degrees comparing to the case of acidic solution, because these extracts may have effects on the frequency dispersion of the double layer capacitance.

The equivalent circuit used to fit the experimental data, in the absence and in the presence of inhibitor, is shown in Fig. 4. The components of the circuit are R_s, the electrolyte resistance ($\Omega \times cm^2$), R_p the polarization resistance ($\Omega \times cm^2$) and CPE, a constant phase element. As mentioned before, the presence of CPE in the electrical circuit instead of a capacitance is due to the non-homogeneity of the electrode surface.
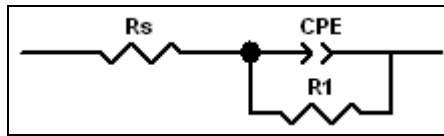

Figure 4. The equivalent electrical circuit of the impedance spectra obtained for steel in the absence and presence of the investigated mixtures of inhibitor

With this proposed model a very good fit was obtained with our experimental data, the fitted data matching the experimental, with an average error of about 2.5%.

For studying the joint effect of *Allium Sativum* and *Juglans Regia*, the synergism parameter, *s* was calculated, as proposed by Hosseini et al [22] which is describing the combined inhibition behavior of the studied extracts. Generally, for the interaction of two inhibitors A and B, the synergism parameter is defined as [23]:

$$s = \left(\frac{1 - IE_A - IE_B + IE_A \times IE_B}{1 - IE_{AB}} \right) \tag{4}$$

where IE_A and IE_B are the inhibition efficiencies evaluated for compound A and B respectively acting alone, and IE_{AB} is the experimentally observed inhibition efficiency for the mixture AB, the concentration of the compounds A and B in the mixture being the same as in the corresponding separate situations. The expression compares the theoretically expected corrosion rate based on the condition where either A or B are present or on the condition that they do not interact, with the experimentally observed rate in the presence of the inhibitor mixtures [23]. In the case where inhibitors A and B have no effect on each other and adsorb at the metal/solution interface independently, s = 1 as in that case the predicted behavior is experimentally confirmed. Alternatively, the effect would be synergistic if s > 1 or antagonistic if s < 1.
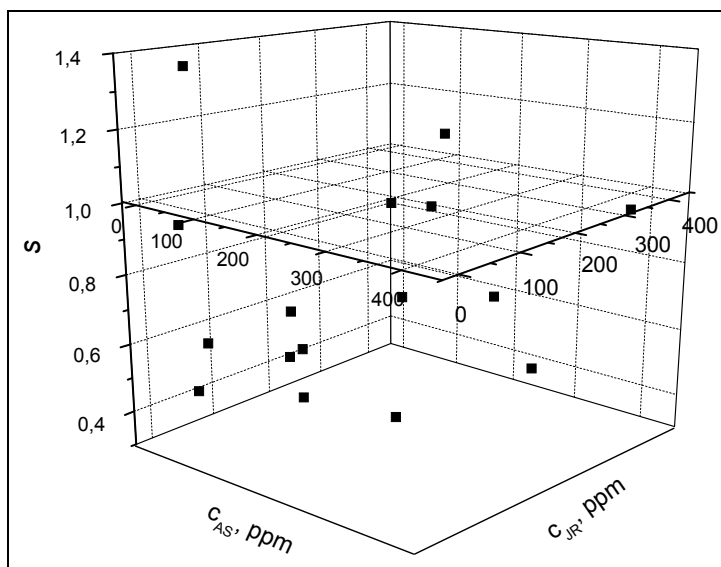
Figure 5. Synergism parameter s for the combined effect of *AS* and *JR* on the corrosion of steel in 0.5 M H_2SO_4

In Figure 5 the values of synergism parameter, s, for the investigated concentrations of *AS* and *JR* are presented. This 3D graph shows that antagonism occurs in many of the studied mixtures. It can be observed that the mixture 200 ppm *AS* + 20 ppm *JR* is characterized by a very moderate synergism (1< s <1.2) whereas for the mixtures 40 ppm *AS*+ 20ppm *JR* and 200ppm *AS* + 40ppm *JR* a more pronounced synergistic effect is found.

The antagonistic and synergetic effects observed can be due to the electrostatic interaction between the oppositely charged ions that prevents their co-adsorption on the metal surface. The forces involved in that case enable interfacial adsorption to occur at a higher extent (resulting in a higher value of surface adsorption for the same concentration) than in the case if only one inhibitor is present.

CONCLUSIONS

Tafel polarization and EIS measurements were accomplished in the present study to increase the possibility of using plant extracts as green type inhibitors for the corrosion of steel in 0.5 M H_2SO_4. The inhibitive and the combining effect of *Allium Sativum* (*AS*) and *Juglans Regia* (*JR*) were studied.

Tafel measurements showed that the presence of *AS* and *JR* mixtures lowered the corrosion current densities and shifted the corrosion potential towards positive values. This fact signifies that the addition of *AS* and *JR*

inhibitive mixture has an inhibitor effect on the corrosion of steel in 0.5 M sulphuric acid solution. The anodic Tafel slopes decrease in the presence of plant extracts and the cathodic Tafel slopes has a generally increasing tendency.

The electrochemical impedance spectroscopy studies have shown that the impedance response consists of large capacitive depressed semicircles for high frequencies values and small inductive loops for the low frequency values. The presence of *AS* and *JR* compounds increases the polarization resistance values indicating that a charge transfer process is mainly controlling the corrosion of steel. The decrease of the double layer capacitance is due to the adsorption of plant extracts on the metal surface. A Randles type equivalent circuit was proposed for the studied system and the fitting data matched the experiment with an average error of about 2.5%.

The best inhibition efficiencies were obtained for the mixtures containing 400 ppm *AS* and also for the mixture 200 ppm *AS* + 400 ppm *JR*.

For studying the joint effect of *Allium Sativum* and *Juglans Regia*, the synergism parameter, s was calculated, and the mixture 200 ppm *AS* + 20 ppm *JR* was found to be characterized by a weak synergism (1< s <1.2) whereas the mixtures 40 ppm *AS*+ 20ppm *JR* and 200ppm *AS* + 40ppm *JR* has a more pronounced synergistic effect. For the other studied mixtures the data showed that antagonism occurs.

The study showed that *Allium Sativum* and *Juglans Regia* can act as corrosion inhibitor for steel in sulphuric acid media.

EXPERIMENTAL SECTION

Working electrodes consist of steel sheets with the following chemical composition, wt.%, C: 0.21, Mn: 2.5, S: 0.04, P: 0.04, Si: 0.35, Fe: to balance. H_2SO_4 reagent used was of analytical grade without previous purification. Double distilled water was used for solution preparations. The plant extracts are commercially available, being purchased from different manufacturers: *Allium Sativum* (*AS*) supplied by HOFIGAL S.A. Romania (50% vol in ethylic alcohol), reference no. 93 GMP and *Juglans Regia* (*JR*) supplied by PlantExtract®, Romania (50% vol in ethylic alcohol), reference no. 05170807A. For the experiments containing plant extracts, the appropriate quantity was added to blank solutions to reach final concentrations of 20, 40, 200 and 400 ppm.

The methodologies used to investigate steel corrosion inhibition of *Allium Sativum* and *Juglans Regia* in aerated 0.5 M H_2SO_4 included potentiodynamic polarization (Tafel polarization) and electrochemical impedance spectroscopy techniques. Thermostated double-walled (50 mL) Metrohm glass cell was used for all the electrochemical tests.

Prior to all measurements, the steel samples were polished with different emery paper grades up to 1000, washed with bidistilled water and dried. The base solution (0.5 M H_2SO_4) was prepared by dilution of analytical grade (Merck) 98% H_2SO_4, used without further purification, with bidistilled water.

Impedance spectroscopy measurements were carried out in the same three electrodes glass cell, with a square steel sheet with the exposed area 0.5 cm^2 as the working electrode. A silver/silver chloride immersed directly into the solution and a platinum disc with the surface of 1.13 cm^2 Radiometer Analytical electrodes are used, as reference and auxiliary electrodes, respectively. All potentials in the text are referred to this reference electrode (Ag, AgCl). The temperature was thermostatically controlled and set up at 25±1^{0}C and the electrolyte solutions were in equilibrium with the atmosphere (i.e., aerated solutions).

All the measurements were carried out using a Voltalab 40, Radiometer Analytical potentiostat/galvanostat interfaced with a computer using VoltaMaster 4.0 software. Experiments were performed in duplicate; data reported are the average.

Before polarization and EIS measurements, the working electrode was introduced in the test solution and left for 30 min to attain the open circuit potential. Polarization curve measurements were made at a scan rate of 20 mV/min starting from cathodic potential towards anodic direction. Electrochemical impedance spectroscopy was carried out at the open-circuit potentials in the frequency range 100 kHz– 50 mHz with a sinusoidal potential perturbation of 10mV amplitude. The data of impedance spectra results were fitted on equivalent circuits, a Randles type circuit, using ZView software.

REFERENCES

1. R. Javaherdashti, *Anti-Corrosion Methods and Materials*, **2000**, *47*, 30.
2. M. Elachouri, M.R. Infante, F. Izquierdo, S. Kertit, H.M. Gouttaya, B. Nciri, *Corrosion Science*, **2001**, *43*, 19.
3. K. Anuradha, R. Vimala, B. Narayanasamy, J. Arockia Selvi, Susai Rajendran, *Chemical Engineering Communication*, **2008**,195, *3*, 352.
4. Y. Abboud, A. Abourriche, T. Ainane, M. Charrouf, A. Bennamara, O. Tanane, B. Hammouti, *Chemical Engineering Communication*, **2009**,196, *7*, 788.
5. H. Ashassi-Sorkhabi, E. Asghari, *Electrochimica Acta*, **2008**, *54,* 162.

6. P.C. Okafor, U.J. Ekpe, E.E. Ebenso, E.M. Umoren, K.E. Leizou, *Bulletin of Electrochemistry*, 21, 8, **2005**, 347.

7. S.S. Abdel Rehim, H.H. Hassaan, M.A. Amin, *Materials Chemistry and Physics,* **2001**, *70*, 64.

8. F. Mansfeld, M.W. Kendig, *Journal of Electrochemical Society*, **1988**, *135*, 828.

9. K.F. Khaled, *Electrochimica Acta,* **2003**, *48*, 2493.

10. S.W. Donne, J.H. Kennedy, *Journal of Applied Electrochemistry,* **2004***, 34*, 159.

11. F. Bentiss, M. Traisnel, H. Vezin, H.F. Hildebrand, M. Lagrenée, *Corrosion Science*, **2004**, *46*, 278.1.

12. M. Bouklah, A. Attayibat, B. Hammouti, A. Ramdani, S. Radi, M. Benkaddour, *Applied Surface Science,* **2005**, *240,* 341.

13. B. El Mehdi, B. Mernari, M. Traisnel, F. Bentiss, M. Lagrenée, *Materials Chemistry and Physics*, **2002**, *77,* 489.

14. F. Mansfeld, M.W. Kendig, W. Lorenz, *Journal of Electrochemical Society*, **1985**, *132*, 290.

15. D.D. Macdonald, *Electrochimica Acta,* **1990**, *35*, 1509.

16. F. Mansfeld, S. Lin, S. Kim, H. Shin, *Corrosion Science*, **1987**, *27*, 997.

17. A. Cojocaru, I. Maior, D.I. Vaireanu, I. Lingvay, C. Lingvay, S. Caprarescu, *Revista de Chimie*, **2009**, *in press.*

18. A. Yurt, A. Balaban, S. Üstün Kandemir, G. Bereket, B. Erk, *Materials Chemistry and Physics*, **2004**, *85*, 420.

19. F. Bentiss, M. Lagrenée, M. Traisnel, J.C. Hornez, *Corrosion Science*, **1999**, *41,* 789.

20. M. Kissi, M. Bouklah, B. Hammouti, M. Benkaddour, *Applied Surface Science*, **2006**, *252*, 4190.

21. Z. Zhang, S. Chen., Y. Li, S. Li, L. Wang, *Corrosion Science,* **2009**, *51*, 291.

22. M. Hosseini, S.F.L. Mertens, M.R. Arshadi, *Corrosion Science*, **2003**, *45*, 1473.

23. L. Larabi, Y. Harek, M. Traisnel, A. Mansri, *Journal of Applied Electrochemistry*, **2004**, *34*: 833.

METHOD OF CLASSIFYING THE DRUGS BY USING THE NYQUIST PLOTS OF A REFERENCE REDOX DIELECTRODE (RRD) AND OF THE MULTIELECTRODE (ME)_D=(RRD) CONTAINING THE DRUG D

NICOLAE BONCIOCAT[a] AND ADINA COTARTA[a]

ABSTRACT. The proposed method uses a *reference redox dielectrode* (RRD) in whose electrical scheme enter: the Faraday impedance $[Z_F(\omega)]_{RRD}$ in parallel with the double layer capacity C_d, and the solution resistance R_{sol}. In $[Z_F(\omega)]_{RRD}$ enter in series: the *charge transfer* $(A_{ct})_{RRD}$ and the *diffusion* $(B_d)_{RRD}$ resistances, and the *Warburg* pseudo-capacitance $C_W(\omega)$, ω being the radial frequency of the current. In the multielectrode $(ME)_D = (RRD)$ containing the drug, C_d and R_{sol} maintain their values. To account for the change of $[Z_F(\omega)]_{RRD}$, we have considered *two theoretical quantities*: a *pseudo-capacitance* and a *pseudo- inductance*, and two possible arrangements of them: *in series*, respective *in parallel*. Consequently, other two Faraday impedances have resulted: $[Z_F^*(\omega)]_{(ME)_D^*}$ containing the series arrangement of $L_s^*(\omega)$, $C_s^*(\omega)$, respective $[Z_F^{**}(\omega)]_{(ME)_D^{**}}$ containing the parallel arrangement of $L_p^{**}(\omega)$, $C_p^{**}(\omega)$:

$$[Z_F^*(\omega)]_{(ME)_D^*} \rightarrow \cdot \!\!-\!\!(A_{ct}^*)_{(ME)_D^*}\!\!-\!\!(B_d^*)_{(ME)_D^*}\!\!-\!\!L_s^*(\omega)\!\!-\!\!C_s^*(\omega)\!\!-\!\!\cdot \qquad \textbf{(I}^{*}\textbf{)}$$

$$[Z_F^{**}(\omega)]_{(ME)_D^{**}} \rightarrow -\!\!(A_{ct}^{**})_{(ME)_D^{**}}\!\!-\!\!(B_d^{**})_{(ME)_D^{**}}\!\!-\!\!\begin{bmatrix} L_p^{**}(\omega) \\ C_p^{**}(\omega) \end{bmatrix}\!\!- \qquad \textbf{(I}^{**}\textbf{)}$$

As criteria of classifying the drug, we have proposed the Thomson radial frequencies $\omega_{Th,s} = [L_s(\omega) \cdot C_s(\omega)]^{-1/2}$, respective $\omega_{Th,p} = [L_p^{**}(\omega) \cdot C_p^{**}(\omega)]^{-1/2}$. Three classes of drugs have resulted: the class(1) of drugs *having no effect*, for which $\omega_{Th,s} = \infty$ and $\omega_{Th,p} = 0$; the class (1*) of drugs *having effect*, for which $\omega_1 \langle \omega_{Th,s} \langle \infty$ and the class (1**) of drugs *having effect*, for which $0 \langle \omega_{Th,p} \langle \omega_1$. By ω_1 is denoted the smallest radial frequency used.

Keywords: multielectrode, electrochemical impedance spectroscopy, Thomson radial frequencies, drugs classification

---

[a] *University Politehnica of Bucharest, Department of Applied Physical Chemistry and Electrochemistry, Computer Aided Electrochemistry Laboratory, 1 Gh. Polizu Street, Bucharest 011061, Romania, PO BOX 12- 112, e-mail: c_adina1@yahoo.fr*
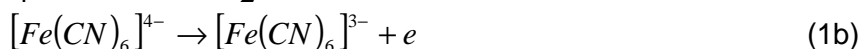
INTRODUCTION

In a series of papers, Bonciocat et al., have shown that the faradaic current density of an electrode redox reaction occuring with combined limitations of charge transfer and nonstationary, linear, semiinfinite diffusion is the solution of an integral equation of Volterra type[1-7]. By solving this integral equation, new methods of direct and cyclic voltammetry, applicable in aqueous electrolytic solutions, or in molten salts, have been developed [8-20]. The above mentioned equation has also led to a new approach to the Electrochemical Impedance Spectroscopy when only the charge transfer and diffusion limitations are present[21-23]. Very recently has been shown that the (E I S) method may have important applications in drug research[24-27].

The proposed (E I S) method of classifying the drugs uses the following *reference redox dielectrode*(RRD):

Pt| [Fe(CN)$_6$]$^{3-}$ / Fe(CN)$_6$]$^{4-}$, KCl (in excess), O$_2$ physically dissolved

(1)
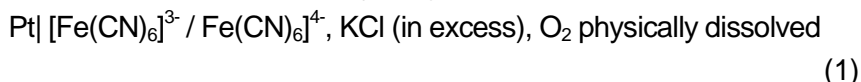
which, e.g., in weak acidic media, has the reactions:

$$\frac{1}{4}O_2 + H^+ + e \rightarrow \frac{1}{2}H_2O \tag{1a}$$

$$[Fe(CN)_6]^{4-} \rightarrow [Fe(CN)_6]^{3-} + e \tag{1b}$$

Concerning the electric scheme of the measuring cell needed to obtain the Nyquist plots, it refers only to the electrode under study, because the impedance of the reference electrode is practically equal to zero. In an oversimplified scheme, but adequate for the aim of this paper, must enter the *Faraday impedance* Z_F in parallel with the double layer capacity C_d and in series with this parallel arrangement the solution resistance R_{sol}.

As for Z_F, it represents the impedance of a series circuit, in which enter: the *charge transfer resistance* A_{ct}, the *Warburg diffusion resistance* $R_W(\omega)$, and the *Warburg pseudo-capacitance* $C_W(\omega)$, ω being the *radial frequency* of the alternating current [see figure 1].
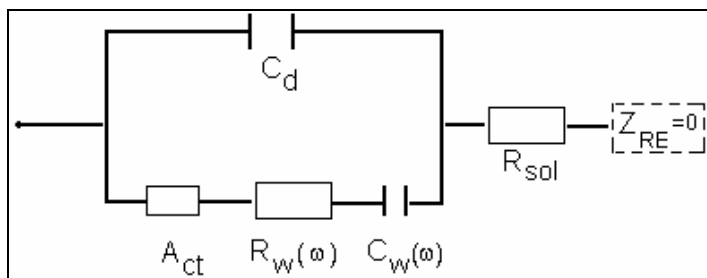

Figure 1. The electric scheme of the measuring cell nedeed to obtain the Nyquist plot of the RRD dielectrode

$C_W(\omega)$ has been introduced by Warburg to explain the phase difference between the current and the tension. A_{ct} and $R_W(\omega)$ are *ohmical terms* which don't introduce a phase difference between the current and the tension, and for this reason, in the complex plane, their values represent the lengths of two segments situated along the *real axes*. $C_W(\omega)$ introduces a *Warburg capacitive reactance* $X_{C_W}(\omega)$, situated along the *imaginary* axes and having the expression:

$$X_{C_W}(\omega) \cong - R_W(\omega)\, j \tag{2}$$

Taking into account the relation that exists between a capacitance C and its capacitive reactance X_C, i.e., $C = 1/\left[\omega |X_C|\right]$, it follows:

$$C_W(\omega) = 1/\left[\omega R_W(\omega)\right] \tag{2'}$$

and thus:

$$\boxed{R_W(\omega) C_W(\omega) = \frac{1}{\omega}} \tag{3}$$

Because the reactions (1a and 1b) occur simultaneously, with *their individual contributions,* it follows that the quantities A_{ct}, $R_W(\omega)$ and $C_W(\omega)$ may be written in the forms:

$$\frac{1}{A_{ct}} = \frac{1}{A_{ct1}} + \frac{1}{A_{ct2}}\,; \qquad \frac{1}{R_W(\omega)} = \frac{1}{R_{W_1}(\omega)} + \frac{1}{R_{W_2}(\omega)}\,;$$
$$C_W(\omega) = C_{W_1}(\omega) + C_{W_2}(\omega) \tag{4}$$

taking into account the fact that the corresponding resistances and pseudo-capacitances are arranged in parallel.

The figure1 has been considered adequate for the *reference redox dielectrode* (RRD), because the expressions of the Nyquist plots in the domain of very small values of ω, obtained on its basis, have proved to be in good agreement with the experimental data.

THEORETICAL SECTION

The theoretical development given in this paper is based on the following idea: to explain the phase difference between the current and the tension, we shall use instead of *one theoretical quantity* (as the *Warburg pseudo-capacitance* $C_W(\omega)$, *two theoretical quantities*, namely a *pseudo-capacitance*, and a *pseudo-inductance*. Because the phase differences introduced by these physical quantities are different, and depend on their arrangement, i.e., in *series* or in *parallel*, we must analyse separately these two possibilities.

Consequently, to propose criteria of classifying the drugs, we have considered other two electric schemes of the measuring cells, because the drug D, introduced in the electrolytic solution of the (RRD) *dielectrode*, changes the figure1, either in figure1*, corresponding to a *multielectrode* $(ME)_D^*$, or in figure1**, corresponding to a *multielectrode* $(ME)_D^{**}$:
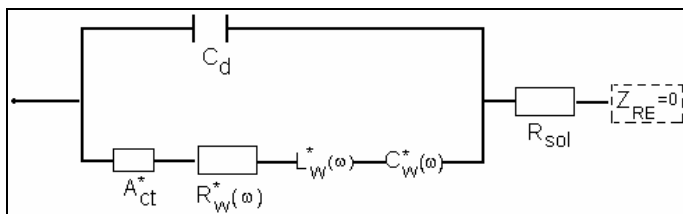
Figure 1*. The electric scheme of the measuring cell nedeed to obtain the Nyquist plot of the $(ME)_D^*$ multielectrode

respective:
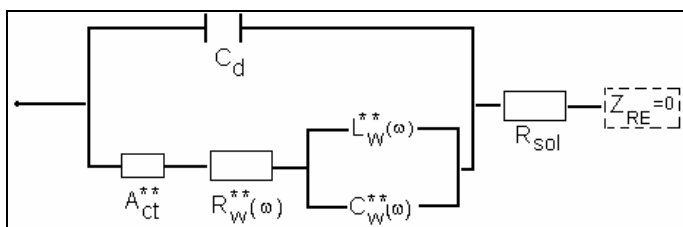
Figure 1**. The electric scheme of the measuring cell nedeed to obtain the Nyquist plot of the $(ME)_D^{**}$ mutielectrode.

Because KCl is in excess, the double layer capacity C_d and the solution resistance R_{sol}, maintain their values in all these schemes. Of course, a drug that *has no effect*, doesn't change the figure 1. Therefore, there are three classes of drugs, corresponding to these three electric schemes: (1), (1*) and (1**). To estimate the effects of drugs, we have decide to establish first the equations expressing in what conditions the electric schemes (1*), respective (1**), come back to the scheme (1), i.e., the effects of the respective drugs are *theoretically annihilated.*

**Equations expressing the coming back of the figure(1*)
to the figure(1)**

As one knows, in the complex plane, the impedance of an inductance L is $\omega L j$, and of a capacitance C is $-\dfrac{1}{\omega C} j$. Then, the impedance of the

series arrangement Z^*_{series} must be equal to the impedance of the *Warburg pseudo-capacitance* $C_W(\omega)$, i.e.,

$$Z^*_{series}(\omega) = Z_{C_W}(\omega) \tag{5}$$

which, explicitly, writes:

$$\left(\omega L^*_W(\omega) - \frac{1}{\omega C^*_W(\omega)} \right) j = -\frac{1}{\omega C_W(\omega)} j \tag{6}$$

Eq.(6) represents the *first equation*, and expresses the equality between the values on the imaginary axes of the complex plane. From eq.(6) results:

$$\omega L^*_W(\omega) = \frac{1}{\omega C^*_W(\omega)} - \frac{1}{\omega C_W(\omega)} \tag{6'}$$

Because $\omega L^*_W(\omega)$ is a positive quantity, it follows:

$$\boxed{\begin{array}{l} C^*_W(\omega) = \alpha^*_D(\omega) C_W(\omega); \qquad \omega L^*_W(\omega) = \frac{1 - \alpha^*_D(\omega)}{\alpha^*_D(\omega)} \cdot \frac{1}{\omega C_W(\omega)}; \\[4mm] \alpha^*_D(\omega) \langle 1 \end{array}}$$

$$\tag{7}$$

Eqs.(7) represent the consequences of eq.(6), and give the relations that must exist between *the theoretical quantities* $C^*_W(\omega)$, respective $L^*_W(\omega)$, and the *Warburg pseudo-capacitance* $C_W(\omega)$. As one sees, there are an infinity of possibilities, because there are an infinity of values $\alpha^*_D(\omega)$ less than unity.

Coming back to eq.(3), one sees that the product $R_W(\omega) C_W(\omega)$ depends only on the *radial frequency* ω. Consequently, *a second equation* will be the equality:

$$R^*_W(\omega) C^*_W(\omega) = R_W(\omega) C_W(\omega) \tag{8}$$

Taking into account the first equation(7), it results:

$$\boxed{R_W(\omega) = \alpha^*_D(\omega) R^*_W(\omega); \qquad \alpha^*_D(\omega) \langle 1} \tag{9}$$

i.e., there are again an infinity of possibilities (because of $\alpha_D^*(\omega)\langle 1$) relating the *Warburg diffusion resistances* of the two electric schemes (1) and (1*).

The *third equation* gives the equality of the *total ohmical resistances* in the two schemes (i.e., of the values on the real axes the complex plane):

$$A_{ct}^* + R_W^*(\omega) = A_{ct} + R_W(\omega) \tag{10}$$

Using eq.(9), results:

$$\boxed{R_{sol} + A_{ct} = [1 - \alpha_D^*(\omega)]\, R_W^*(\omega) + R_{sol} + A_{ct}^*} \tag{11}$$

if one introduce the solution resistance too.

Equations expressing the coming back of the figure(1**) to the figure(1)

Now the impedance of the parallel arrangement $Z_{parallel}^{**}$ must be equal to the impedance of the *Warburg pseudo-capacitance* $C_W(\omega)$:

$$Z_{parallel}^{**}(\omega) = Z_{C_W}(\omega),\ \text{i.e.,}\quad 1/\,Z_{parallel}^{**}(\omega) = 1/Z_{C_W}(\omega) \tag{12}$$

which, explicity, writes:

$$\frac{1}{\omega L_W^{**}(\omega)\, j} + \omega C_W^{**}(\omega)\, j = \omega C_W(\omega)\, j \tag{13}$$

Eq.(13) represents the *first equation*, and expresses the equality between the values on the imaginary axes of the complex plane. From eq.(13) results:

$$1/\,\omega L_W^{**}(\omega) = \omega C_W^{**}(\omega) - \omega C_W(\omega) \tag{13'}$$

$1/\,\omega L_W^{**}(\omega)$ being a positive quantity, it follows:

$$\boxed{\begin{aligned} &C_W^{**}(\omega) = \frac{1}{\alpha_D^{**}(\omega)} C_W(\omega);\qquad \omega L_W^{**}(\omega) = \frac{\alpha_D^{**}(\omega)}{1 - \alpha_D^{**}(\omega)} \cdot \frac{1}{\omega C_W(\omega)}; \\ &\alpha_D^{**}(\omega)\langle 1 \end{aligned}}$$

$$\tag{14}$$

Eqs.(14) give the relations that must exist between the *theoretical quantities* $C_W^{**}(\omega)$, respective $L_W^{**}(\omega)$, and the *Warburg pseudo-capacitance* $C_W(\omega)$.

The *second equation* is similar to eq.(8), i.e.,

$$R_W^{**}(\omega)\, C_W^{**}(\omega) = R_W(\omega)\, C_W(\omega) \tag{15}$$

and taking into account the first equation(14), results:

$$\boxed{R_W(\omega) = \frac{1}{\alpha_D^{**}(\omega)} \cdot R_W^{**}(\omega); \quad \alpha_D^{**}(\omega) \langle\, 1} \tag{16}$$

The *third equation* gives the equality of the *total ohmical resistances* in the two schemes (i.e., of the values on the real axes of the complex plane):

$$A_{ct}^{**} + R_W^{**}(\omega) = A_{ct} + R_W(\omega) \tag{17}$$

which, using eq.(16), writes:

$$\boxed{R_{sol} + A_{ct} = \left[1 - \frac{1}{\alpha_D^{**}(\omega)}\right] R_W^{**}(\omega) + R_{sol} + A_{ct}^{**}} \tag{18}$$

if one introduces the solution resistance too.

Finally, from eqs.(7, 9 and 11) one sees that for $\alpha_D^* < 1$, the *pseudo-inductance* $L_W^*(\omega)$ is different of zero, and $C_W^*(\omega)$, $R_W^*(\omega)$ and A_{ct}^* are different of $C_W(\omega)$, $R_W(\omega)$ and A_{ct}. In other words, for $\alpha_D^*(\omega) < 1$, the drug D belongs to the class (1*). The same equations show that for $\alpha_D^*(\omega)=1$, $L_W^*(\omega)=0$, and $C_W^*(\omega)$, $R_W^*(\omega)$ and A_{ct}^* are equal to $C_W(\omega)$, $R_W(\omega)$ and A_{ct}. This means that for $\alpha_D^*(\omega)=1$, the drug D *has no effect*, i.e., belongs to the class(1). Similarly, eqs.(14, 16 and 18) show that for $\alpha_D^{**}(\omega) < 1$, the drug D belongs to the class (1**), and for $\alpha_D^{**}(\omega)=1$, the drug D *has no effect*, i.e., belongs to the class (1). Generally, $\alpha_D^*(\omega) \neq \alpha_D^{**}(\omega)$, because there are an infinity of drugs belonging to the class(1*), as well as an infinity of drugs belonging to the class(1**). Unfortunately, the use of the pair $\alpha_D^*(\omega)$, $\alpha_D^{**}(\omega)$, *as a criterion of classifying the drugs*, has an important disadvantage, namely, the fact that their values are both less than unity, i.e., they are *on the same side of the unity*. It is necessary to find a pair of quantities, one for the class(1*), the other for the class(1**), whose values are *on the left, respective right, side of a reference value.*

The Thomson radial frequency $\omega_{Th,s} = \left[L_W^*(\omega) \, C_W^*(\omega) \right]^{-\frac{1}{2}}$ **of the series circuit considered instead of Warburg pseudo-capacitance** $C_W(\omega)$

From eqs.(7), one gets:

$$\omega_{Th,s} = \left[L_W^*(\omega) \, C_W^*(\omega) \right]^{-\frac{1}{2}} = \left[\frac{1 - \alpha_D^*(\omega)}{\omega^2} \right]^{-\frac{1}{2}} = \frac{\omega}{\sqrt{1 - \alpha_D^*(\omega)}} \qquad (19)$$

which, for $\omega = \omega_1$, i.e., the smallest radial frequency used (say 0.2Hz = 1.256s^{-1}), becomes:

$$\omega_{Th,s}\left[\alpha_D^*(\omega_1) \right] = \frac{\omega_1}{\sqrt{1 - \alpha_D^*(\omega_1)}} \qquad (19')$$

Eq.(19') shows that for $\alpha_D^*(\omega_1) = 0$, the *Thomson radial frequency* is equal to ω_1, i.e., ω_1 represents the *resonance Thomson radial frequency* of the series circuit $\text{—}\, L_W^*(\omega)\text{—}\, C_W^*(\omega)\text{—}$ of the scheme (I*). Because $0 \le \alpha_D^*(\omega_1) \langle\, 1$, it folows that:

$$\omega_1 \le \omega_{Th,s}[0 \le \alpha_D^*(\omega_1) \langle\, 1] \langle\, \infty \qquad (20)$$

i.e., the values of the *Thomson radial frequencies* $\omega_{Th,s}[\alpha_D^*(\omega_1)]$ are greater than the *resonance Thomson radial frequency* $\omega_{Th,s}[\alpha_D^*(\omega_1) = 0] = \omega_1$, i.e., on the real axes, they are situated on the right hand side of the *reference value* ω_1.

The Thomson radial frequency $\omega_{Th,s} = \left[L_W^{**}(\omega) \, C_W^{**}(\omega) \right]^{-\frac{1}{2}}$ **of the parallel circuit considered instead of the Warburg pseudo-capacitance** $C_W(\omega)$

From eqs.(14) one gets:

$$\omega_{Th,p} = [L_W^{**}(\omega) \, C_W^{**}(\omega)]^{-\frac{1}{2}} = \left[\frac{1}{\omega^2 \left[1 - \alpha_D^{**}(\omega) \right]} \right]^{-\frac{1}{2}} = \omega \sqrt{1 - \alpha_D^{**}(\omega)} \qquad (21)$$

which, for $\omega = \omega_1$, becomes:

$$\omega_{Th,p}\left[\alpha_D^{**}(\omega_1) \right] = \omega_1 \sqrt{1 - \alpha_D^{**}(\omega_1)} \qquad (21')$$

Eq.(21') shows that for $\alpha_D^{**}(\omega_1)=0$, ω_1 represence also the *resonance Thomson radial frequency* of the parallel circuit of the scheme (I^{**}). Because $0 \le \alpha_D^{**}(\omega_1) \le 1$, it follows that:

$$\omega_1 \ge \omega_{Th,p}\,[\alpha_D^{**}(\omega_1)] \ge 0 \tag{22}$$

i.e, the values of the *Thomson radial frequencies* $\omega_{Th,p}[\alpha_D^{**}(\omega_1)]$ are less than the *resonance Thomson radial frequency* $\omega_{Th,p}[\alpha_D^{**}(\omega_1)=0]=\omega_1$, i.e., on the real axes, they are situated on the left hand side of the *reference value ω_1*.

From the inequalities (15 and 17), results that *the pair* $\omega_{Th,s}[\alpha_D^*(\omega_1)]$, $\omega_{Th,p}[\alpha_D^{**}(\omega_1)]$ *satisfies the necessary conditions for being used as criterion of classifying the drugs.*

Indeed, for a drug belonging to the class(1), i.e, *having no effect*, because both $\alpha_D^*(\omega_1)$ and $\alpha_D^{**}(\omega_1)$, tend to unity, the *Thomson radial frequency* $\omega_{Th,s}[\alpha_D^*(\omega_1)]$ will tend to infinity, while the *Thomson radical frequency* $\omega_{Th,p}[\alpha_P^{**}(\omega_1)]$ will tend to zero. For the drugs belonging to the class (1*), the classifying criterion will be the *Thomson radial frequency* $\omega_{Th,s}[\alpha_D^*(\omega_1)]$, while for the drugs belonging to the class(1**), the classifying criterion will be the *Thomson radial frequency* $\omega_{Th,p}[\alpha_D^{**}(\omega_1)]$.

From a series of drugs belonging to the class(1*), the most efficient is that corresponding to the smallest value $\omega_{Th,s}[\alpha_D^*(\omega_1)]$. From a series of drugs belonging to the class (1**), the most efficient is that corresponding to the greatest value $\omega_{Th,p}[\alpha_D^{**}(\omega_1)]$.

The expression of $\omega_{Th,s}[\alpha_D^*(\omega_1)]$ in terms of A_{ct}, A_{ct}^* and $R_W^*(\omega_1)$

From eq.(11) results:

$$1-\alpha_D^*(\omega_1) = \frac{R_{sol}+A_{ct}-\left(R_{sol}+A_{ct}^*\right)}{R_W^*(\omega_1)} \tag{23}$$

To go further, we remind that the parametric equation giving the real part of a Nyquist plot in the domain of very small frequencies (round $\upsilon = \omega/2\pi = =0.2Hz$), is (see[22, 23]):

$$\text{Re}(\omega) \cong R_{sol} + A_{ct} + \frac{J}{\sqrt{2\pi}} B_d\, \omega^{-1/2} = R_{sol} + A_{ct} + \frac{B_d}{2\omega^{1/2}} \quad (24)$$

where J represents the Fresnel integral:

$$J = \int_0^\infty \frac{\cos x}{x^{1/2}} dx = \sqrt{\frac{\pi}{2}} \quad (24')$$

The last term on the right hand side of eq.(24), represents the *Warburg diffusive* resistance $R_W(\omega)$, and thus (for $\omega_1 = 1.256 s^{-1}$):

$$1 - \alpha_D^*(\omega_1) = \frac{R_{sol} + A_{ct} - \left(R_{sol} + A_{ct}^*\right)}{0.446\, B_d^*} \quad (25)$$

Introducing the expression of $1 - \alpha_D^*(\omega_1)$ in eq.(19'), one gets:

$$\omega_{Th,s}\left[\alpha_D^*(\omega_1)\right] = \left[\frac{R_{sol} + A_{ct} - \left(R_{sol} + A_{ct}^*\right)}{0.446\, B_d^*}\right]^{-1/2} \omega_1 \quad (26)$$

(R_{sol} is maintained in eqs. (23-26), because we shall give equations for determining the sum of the solution and charge transfer resistances).

The expression of $\omega_{Th,p}[\alpha_D^{**}(\omega_1)]$ in terms of A_{ct}, A_{ct}^{**} and $R_W^{**}(\omega_1)$

From eq.(18) results:

$$\left[1 - \frac{1}{\alpha_D^{**}(\omega_1)}\right] = \frac{R_{sol} + A_{ct} - \left(R_{sol} + A_{ct}^{**}\right)}{R^{**}(\omega_1)} \quad (27)$$

and explicitating the *Warburg diffusion resistance* $R^{**}(\omega_1)$ (see eqs. (24, 24')):

$$\left[1 - \frac{1}{\alpha_D^{**}(\omega_1)}\right] = \frac{R_{sol} + A_{ct} - \left(R_{sol} + A_{ct}^{**}\right)}{0.446\, B_d^{**}} \quad (27')$$

Further, after some trivial operations, eqs. (27' and 21') lead to:

$$\omega_{Th,p}\left[\alpha_D^{**}(\omega_1)\right] = \left\{\frac{R_{sol} + A_{ct}^{**} - \left(R_{sol} + A_{ct}\right)}{0.446\, B_d^{**} - \left[R_{sol} + A_{ct} - \left(R_{sol} + A_{ct}^{**}\right)\right]}\right\}^{1/2} \omega_1 \quad (28)$$

Estimation of $R_{sol} + A_{ct}$ and B_d, in terms of the abscissae, $Re(\omega_1)$ and $Re(\omega_2)$, of the Nyquist plot of the RRD dielectrode; ω_1= 1.256s^{-1}, ω_2= 1.582s^{-1}

In figure 2, is given the shape of a Nyquist plot obtained by points, e.g., 10 points per decade (i.e., corresponding to a unitary distance on the logaritmic scale).

From eq.(24), it follows:

$$\frac{Re(P_1) - X}{Re(P_2) - X} \cong \left(\frac{\omega_1}{\omega_2}\right)^{-1/2} \quad ; \qquad X = R_{sol} + A_{ct} \tag{29}$$

i.e.,

$$R_{sol} + A_{ct} \cong \left[Re(\omega_2) - \frac{Re(\omega_1) - Re(\omega_2)}{0.122}\right] \tag{30}$$

where:

$$\left(\frac{\omega_1}{\omega_2}\right)^{-1/2} - 1 = 0.122 \tag{30'}$$

Further, from eq.(24) written for ω_1, results:

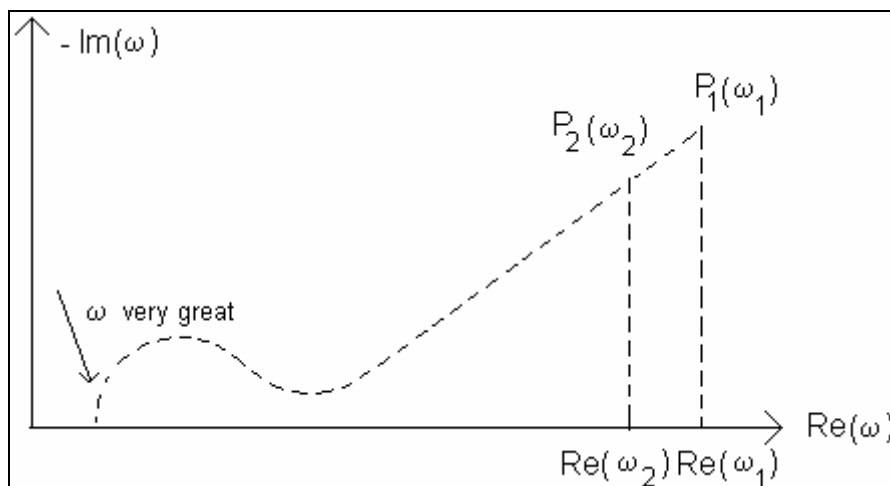$$B_d = 20.6\left[Re(\omega_1) - Re(\omega_2)\right] \tag{31}$$

Figure 2. The shape of a Nyquist plot obtained by 10 points per decade. The first point corresponds to ω_1= 1,256s^{-1}, and the second point to $\omega_2 = \omega_1 \cdot 10^{0.1}$=1.582s^{-1}.

Estimation of $R_{sol} + A_{ct}^*$ **and** B_d^***, in terms of the abscissae,** $\mathrm{Re}^*(\omega_1)$ **and** $\mathrm{Re}^*(\omega_2)$ **of the Nyquist plot of the** $(ME)_D^*$ **multielectrode;** $\omega_1 =$**1.256s**$^{-1}$**,** $\omega_2 =$**1.582s**$^{-1}$

In this case, the Nyquist plot gives the dependence $-\mathrm{Im}^*(\omega)$ vs $\mathrm{Re}^*(\omega)$.

In rest, the procedure of getting the expressions of $R_{sol} + A_{ct}^*$ and B_d^* is the same(see eqs.(29-31)).

Thus:

$$R_{sol} + A_{ct}^* \cong \left[\mathrm{Re}^*(\omega_2) - \frac{\mathrm{Re}^*(\omega_1) - \mathrm{Re}^*(\omega_2)}{0.122} \right] \qquad (32)$$

and:

$$B_d^* \cong 20.6[\mathrm{Re}^*(\omega_1) - \mathrm{Re}^*(\omega_2)] \qquad (33)$$

Estimation of $R_{sol} + A_{ct}^{**}$ **and** B_d^{**} **in terms of the abscissae,** $\mathrm{Re}^{**}(\omega_1)$ **and** $\mathrm{Re}^{**}(\omega_2)$ **of the Nyquist plot of the** $(ME)_D^{**}$ **multielectrode;** $\omega_1 =$**1.256s**$^{-1}$**,** $\omega_2 =$**1.582s**$^{-1}$

In this case, the Nyquist plot gives the dependence $-\mathrm{Im}^{**}(\omega)$ vs. $\mathrm{Re}^{**}(\omega)$, and by applying the same procedure, one gets:

$$R_{sol} + A_{ct}^{**} \cong \left[\mathrm{Re}^{**}(\omega_2) - \frac{\mathrm{Re}^{**}(\omega_1) - \mathrm{Re}^{**}(\omega_2)}{0.122} \right] \qquad (34)$$

respective:

$$B_d^{**} \cong 20.6\,[\mathrm{Re}^{**}(\omega_1) - \mathrm{Re}^{**}(\omega_2)] \qquad (35)$$

The values $\omega_{Th,s}[\alpha_D^*(\omega_1)]$ **may be obtained by using the experimental values** $\mathrm{Re}(\omega_1),\ \mathrm{Re}(\omega_2)$ **and** $\mathrm{Re}^*(\omega_1),\ \mathrm{Re}^*(\omega_2)$

Coming back to eq.(26), and using eqs.(30, 32, 33) one gets:

$$\omega_{Th,s}\left[\alpha_D^*(\omega_1)\right] \cong \left\{ \frac{1.121\left[\mathrm{Re}^*(\omega_1) - \mathrm{Re}^*(\omega_2)\right]}{a^* - b^*} \right\}^{1/2} \omega_1 \qquad (36)$$

where

$$a^* = 1.122\,[\,\mathrm{Re}(\omega_1) - \mathrm{Re}^*(\omega_2)] \qquad (36')$$

and

$$b^* = \text{Re}(\omega_1) - \text{Re}^*(\omega_1) \qquad (36")$$

Because of the inequalities (20), *the criterion $\omega_{Th,s}[\alpha_D^*(\omega_1)]$ may be used to classify the drugs belonging to the class(1*), characterized by the inequality $a^* \rangle b^*$, or to show that a drug has no effect, i.e., belongs to the class(1), characterized by the equality $a^* \cong b^*$ when $\omega_{Th,s}[\alpha_D^*(\omega_1)] \to \infty$.*

The values $\omega_{Th,p}[\alpha_D^{**}(\omega_1)]$ may be obtained by using the experimental values $\text{Re}(\omega_1)$, $\text{Re}(\omega_2)$ and $\text{Re}^{**}(\omega_1)$, $\text{Re}^{**}(\omega_2)$

Coming back to eq.(28), and using eqs.(30, 34, 35), one gets:

$$\omega_{Th,p}\left[\alpha_D^{**}(\omega_1)\right] \cong \left\{ \frac{-a^{**} + b^{**}}{1.121\left[\text{Re}^{**}(\omega_1) - \text{Re}^*(\omega_2)\right] - a^{**} + b^{**}} \right\}^{1/2} \omega_1 \quad (37)$$

where:

$$a^{**} = 1.122\,[\text{Re}(\omega_2) - \text{Re}^{**}(\omega_2)] \qquad (37')$$

and:

$$b^{**} \cong \text{Re}(\omega_1) - \text{Re}^{**}(\omega_1) \qquad (37")$$

Because of the inequalities(22), *the criterion $\omega_{Th,p}[\alpha_D^{**}(\omega_1)]$ may be used to classify the drugs belonging to the class(1**), characterized by the inequality $a^{**} \langle b^{**}$, or to show that a drug has no effect, i.e., belongs to the class(1), characterized by the equality $\alpha^{**} \cong b^{**}$, when $\omega_{Th,p}[\alpha_D^{**}(\omega_1)] \to 0$.*

The necessary steps in applying the procedure of classifying and testing the efficiency of drugs.

1. One records the Nyquist plot of the RRD dielectrode, and one gets the values Re(ω_1) and Re(ω_2).

2. One records the Nyquist plot of the multielectrode = RRD containing the investigated drug D, and one gets the values corresponding to the abscissae of the first two points P$_1$(ω_1), P$_2$(ω_2). These values may be, either $\text{Re}^*(\omega_1)$, $\text{Re}^*(\omega_2)$, or $\text{Re}^{**}(\omega_1)$, $\text{Re}^{**}(\omega_2)$, depending on the type of the multielectrode, i.e., $(ME)_D^*$ or $(ME)_D^{**}$.

One decides by means of the inequalities $a^* \rangle b^*$ or $a^{**} \langle b^{**}$.

3. If $a^* \rangle b^*$ one concludes that *D belongs to the class (1*), and* $(ME)_D = (ME)_D^*$

4. If $a^{**} \langle b^{**}$, one concludes that *D belongs to the class (1**), and* *(ME) = (ME**)$_D$*

5. If $a^* \cong b^*$ (when also $a^{**} \cong b^{**}$), one concludes that *D has no effect, i.e., belongs* to the class(1), and (ME)= RRD.

6. If D$\in$ (1*), one obtains the *radial Thomson frequency* $\omega_{Th,s}[\alpha_D^*(\omega_1)]$, by applying equation(36).

7. If D$\in$ (1**), one obtains the *radial Thomson frequency* $\omega_{Th,p}[\alpha_D^{**}(\omega_1)]$, by applying equation(37).
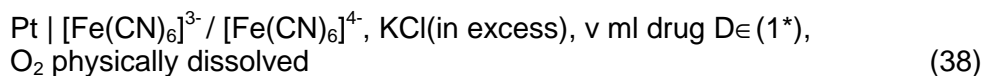
In conclusion, for getting the values $\omega_{Th,s}[\alpha_D^*(\omega_1)]$, **respective** $\omega_{Th,p}[\alpha_D^{**}(\omega_1)]$ **sufice to take, from the corresponding Nyquist Plots, only two values,** $\mathrm{Re}[P_1(\omega_1)]$ **and** $\mathrm{Re}[P_2(\omega_2)]$**, and to apply the formulae (36) and (37).**
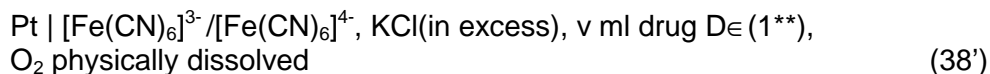
EXPERIMENTAL SECTION

Method of recording the Nyquist plots

As we have already said(see the end of the INTRODUCTION chapiter) the figure(1) of the (RRD)- dielectrode has proved to be adequate for explaining the Nyquist plots in the domain of very small values of ω. In other words, to explain the phase difference between the current and the tension, suffice to use *one single theoretical quantity*, i.e., the *Warburg pseudo-capacitance* $C_W(\omega)$.

In this paper, one analyzes the effect that some drugs have upon the electrochemical properties of the reference redox dielectrode(RRD). These drugs have been introduced in the electrolytic solution of the *reference redox dielectrode*, maintaining the total volume of the solution at V=300ml. In this way, the electrochemical system(eq.(1)) of the *reference redox dielectrode*(1) transforms in the electrochemical systems of the *redox multielectrodes*: $(ME)_D^*$, or $(ME)_D^{**}$, i.e., of:

Pt | $[Fe(CN)_6]^{3-}$ / $[Fe(CN)_6]^{4-}$, KCl(in excess), v ml drug $D \in (1^*)$,
O_2 physically dissolved (38)

or:

Pt | $[Fe(CN)_6]^{3-}$ /$[Fe(CN)_6]^{4-}$, KCl(in excess), v ml drug $D \in (1^{**})$,
O_2 physically dissolved (38')

depending on the type of schemes: (1*) or (1**), of the measuring cells nedeed to obtain the Nyquist plots of the respective multielectrodes $(ME)_D^*$ or $(ME)_D^{**}$. The concentrations of all species, *excepting those of the investigated drugs*, are given with respect to the same total volume V= (V-v)+v = 300ml, and are equal in the three systems: (1), (38) and (38'). Because of this request, one may consider that the drugs that *don't have therapeutic effects*, *maintain the type of scheme(1) for the measuring cell nedeed to obtain their Nyquist plots*, i.e., that they belong to the class(1).

To perform the experiments a SP-150 Potentiostat/ Galvanostat Bio-Logic Science Instruments has been used.

The experiments have been made at equilibrium, i.e., at a *constant overtension* η =0V, and for each drug, four Nyquist plots have been recorded, using an amplitude of 10mV for the alternating overtension $\tilde{\eta}$, and radial frequencies between ω_1 =1.256s^{-1} and ω_N= 6.28x10^{5}s^{-1}.

The Nyquist plots have been recorded by points, using 10 points per decade(i.e., for passing from a value ω' to the value ω'' =10ω'). For this reason, ω_2 =$\omega_1 \cdot 10^{0.1}$=1.582s^{-1}.

Method of classifying the drugs

In Tables 1 and 2 one gives the method used for establishing to what class belongs the investigated drug.

Table 1. Method of establishing to what class of drugs belong
the investigated drugs

Dielectrode	Re(ω_1) (Ω)	Re(ω_2) (Ω)	
RRD	319	291	
	322	291	
V= 300 ml	318	289	
	320	290	

Multielectrode	$\text{Re}^*(\omega_1)$ or $\text{Re}^{**}(\omega_1)$ (Ω)	$\text{Re}^*(\omega_2)$ or $\text{Re}^{**}(\omega_2)$ (Ω)	a^* or a^{**} (Ω)	b^* or b^{**} (Ω)	Conclusions
$(ME)_B$ V= 300ml v= 20ml	10447 10936 11688 12721	9944 10409 11125 12206	-10830 -10761 -12158 -13370	-10128 -10614 -11370 -12401	$a^{**} < b^{**}$ $B \in (I^{**})$ $(ME)_B = (ME)_B^{**}$
$(ME)_{Am}$ V= 300ml v= 30ml	3333 3032 3032 3168	2924 2871 2871 3010	-2954 -2895 -2897 -3052 -2950	-3014 -2710 -2714 -2848 -2822	$a^{**} < b^{**}$ $Am \in (I^{**})$ $(ME)_{Am} = (ME)_{Am}^{**}$
$(ME)_{Cf}$ V= 300ml v= 20ml	7622 6388 7465 9013	7391 6209 7256 8709	-7966 -6640 -7817 -9446	-7303 -6066 -7147 -8693	$a^{**} < b^{**}$ $Cf \in (I^{**})$ $(ME)_{Cf} = (ME)_{Cf}^{**}$
$(ME)_{Cf}$ V= 300ml v= 30ml	18773 21816 21443 22051	17761 20100 20235 21410	-19601 -22226 -22379 -23697	-18454 -21494 -21125 -21731	$a^{**} < b^{**}$ $Cf \in (I^{**})$ $(ME)_{Cf} = (ME)_{Cf}^{**}$

In these Tables:

B= Sweedish Bitter (Original Schweden Tropfen, BANO)
Am= Achillea Millefolium (S C Dacia Plant SRL Romania Sebes-Tincture)
Cf= Calendula flos (S C Hofigal S.A. Romania, Bucuresti- Tincture)
Uh= Urticae herba (S C Hofigal SA Romnaia, Bucuresti- Tincture)

Table 2. Method of establishing to what class of drugs
belong the investigated drugs

Dielectrode	$\text{Re}(\omega_1)$ (Ω)	$\text{Re}(\omega_2)$ (Ω)	
RRD V= 300 ml	319 322 318 320	291 291 289 290	

Multielectrode	$Re^*(\omega_1)$ or $Re^{**}(\omega_1)$ (Ω)	$Re^*(\omega_2)$ or $Re^{**}(\omega_2)$ (Ω)	a^* or a^{**} (Ω)	b^* or b^{**} (Ω)	Conclusions
$(ME)_{Uh}$ V= 300ml v= 20ml	4235 3987 3745 3551	4039 3816 3582 3367	-4205 -3955 -3695 -3452	-3916 -3665 -3427 -3231	$a^{**} < b^{**}$ $U_h \in (I^{**})$ $(ME)_{Uh} = (ME)^{**}_{Uh}$
$(ME)_{Uh}$ V= 300ml v= 30ml	10769 11098 11236 11600	10330 10636 10843 11133	-11264 -11607 -11842 -12166	-10450 -10776 -10915 -11280	$a^{**} < b^{**}$ $Uh \in (I^{**})$ $(ME)_{Uh} = (ME)^{**}_{Uh}$
$(ME)_{Uh+Am}$ V= 300ml v= (20+20)ml	3029 3008 3200 3735	2871 2848 3023 3551	-2895 -2869 -3068 -3659	-2710 -2686 -2882 -3415	$a^{**} < b^{**}$ $(Uh+Am) \in (I^{**})$ $(ME)_{Ud+Am} = (ME)^{**}_{Ud+Am}$
$(ME)_{B+Am+Cf+Uh}$ V= 300ml v = (10+10+ 10+10)ml	3007 3256 3487 3478	2859 3107 3339 3804	-2881 -3160 -3422 -3943	-2688 -2934 -3169 -3658	$a^{**} < b^{**}$ $B+Am+Cf+Uh \in (I^{**})$ $(ME)_{B+Am+Cf+Uh} =$ $(ME)^{**}_{B+Am+Cf+Uh}$

The values (a^* or a^{**}), respective (b^* or b^{**}) have led to the conclusions given in the last columns of these tables, and show that all drugs investigated belong to the class (I**). Concerning the drug Am, the first two values (i.e., -2954Ω, -3014Ω) satisfy the inequality $a^* > b^*$, but the mean values (-2950Ω, -2822Ω) *justify the conclusion given in the last column of Table1.*

Estimation of the Thomson radial frequencies

Once the values of a^{**} and b^{**} known, one may go further and estimate the *Thomson radial frequencies* $\omega_{Th,p}[\alpha_D^{**}(\omega_1)]$ by using eq.(37). The results are given in tables 3 and 4.

As one may observe, in the case of the drug Am, the first value of a^{**} (i.e., -2954Ω has been replaced by the mean value -2950Ω (see Table 1)), and similarly the first value of b^{**} (i.e., -3014Ω) has been replaced by the mean value -2822Ω.

Table 3. The Thomson radial frequencies $\omega_{Th,p}[\alpha_D^{**}(\omega_1)]$
estimated by using equation (37)

Drug	$Re^{**}(\omega_1)$ (Ω)	$Re^{**}(\omega_2)$ (Ω)	a^{**} (Ω)	b^{**} (Ω)	$\omega_{Th,p}[\alpha_D^{**}(\omega_1)]$ (s^{-1})	$\omega_{Th,p}[\alpha_D^{**}(\omega_1)]$ (s^{-1}) **Mean values**
B V=300ml v=20ml	10447 10936 11688 12721	9944 10409 11125 12206	-10830 -10761 -12158 -13370	-10128 -10614 -11370 -12401	0.935 0.561 0.936 0.994	0.857
Am V=300ml v=20ml	3333 3032 3032 3168	2924 2871 2871 3010	-2950 -2895 -2897 -3052	-2822 -2710 -2714 -2848	0.587 0.894 0.891 0.919	0.823
Cf V=300ml v=20ml	7622 6388 7465 9013	7391 6209 7256 8709	-7966 -6640 -7817 -9446	-7303 -6066 -7147 -8633	1.065 1.081 1.081 1.042	1.067
Cf V=300ml v=30ml	18773 21816 21443 22051	17761 20100 20235 21410	-19601 -22226 -22379 -23697	-18454 -21494 -21125 -21731	0.891 0.659 0.871 1.075	0.874

Table 4. The Thomson radial frequencies $\omega_{Th,p}[\alpha_D^{**}(\omega_1)]$ estimated
by using equation (37)

Drug	$Re^{**}(\omega_1)$ (Ω)	$Re^{**}(\omega_2)$ (Ω)	a^{**} (Ω)	b^{**} (Ω)	$\omega_{Th,p}[\alpha_D^{**}(\omega_1)]$ (s^{-1})	$\omega_{Th,p}[\alpha_D^{**}(\omega_1)]$ (s^{-1}) **Mean values**
Uh V=300ml v=20ml	4235 3987 3745 3551	4039 3816 3582 3367	-4205 -3955 -3695 -3452	-3916 -3665 -3427 -3231	0.947 0.965 0.969 0.913	0.949
Uh V=300ml v=30ml	10769 11098 11236 11600	10330 10636 10843 11133	-11264 -11607 -11842 -12166	-10450 -10776 -10915 -11280	0.992 0.986 1.034 0.996	1.002
Uh+Am V=300ml v=(20+20)ml	3029 3008 3200 3735	2871 2848 3023 3551	-2895 -2869 -3068 -3659	-2710 -2686 -2882 -3415	0.898 0.893 0.874 0.925	0.898
B+Am+ Cf+Uh V=300ml v=(10+10+ +10+10)ml	3007 3256 3487 3978	2859 3107 3339 3804	-2881 -3160 -3422 -3943	-2688 -2934 -3169 -3658	0.921 0.952 0.976 0.968	0.954

As one sees from the mean values of the *Thomson radial frequencies*, the *increase* of the concentration of the drug Cf (by passing from v=20ml to v=30ml) leads to a *decrease* of $\omega_{Th,p}[\alpha_{Cf}^{**}(\omega_1)]$, from 1.067 s^{-1}, to 0.874 s^{-1}. This is not *the normal case*, because by *increasing* the concentration, the efficiency of the drug must *increase* too. Consequently, because $\omega_{Th,p}[\alpha_{Cf}^{**}(\omega_1)] = \sqrt{1 - \alpha_{Cf}^{**}(\omega_1)} \cdot \omega_1$, its value must *increase* from zero (when $\alpha_{Cf}^{**} = 1$) towards ω_1 (when α_{Cf}^{**} =0), and *not to decrease* from 1.067s^{-1} to 0.874s^{-1}.

The *normal case* is that of the drug Uh, because by *increasing* its concentration $\omega_{Th,p}[\alpha_{Ud}^{**}(\omega_1)]$ *increases too*, from 0.949s^{-1} to 1.002s^{-1}.

A way of interpreting the obtained Thomson radial frequencies

To explain these two possibilities, one exemplifyed by the drug Cf, the other by the drug Uh, let's write eq.(27') in the form:

$$1 - \frac{1}{\alpha_D^{**}(\omega_1)} = \frac{A_{ct} - A_{ct}^{**}}{0.446 B_d^{**}} \tag{27''}$$

Further, coming back to the first equation(4), one gets:

$$\frac{1}{A_{ct}} = 2\frac{(A/A_{ct1} + A/A_{ct2})}{2} \cdot \frac{1}{A} = 2(\overline{A/A_{ct}}) \cdot \frac{1}{A} \tag{38}$$

and thus:

$$A_{ct} = \frac{1}{2(\overline{A/A_{ct}})} \cdot A \tag{38'}$$

Similarly:

$$\frac{1}{A_{ct}^{**}} = p\frac{\left(A^{**}/A_{ct1}^{**} + ... + A^{**}/A_{ctp}^{**}\right)}{p} \cdot \frac{1}{A^{**}} \tag{39}$$

and therefore:

$$A_{ct}^{**} = \frac{1}{p\left(\overline{A^{**}/A_{ct}^{**}}\right)} \cdot A^{**} \tag{39'}$$

Of course, for $R_W^{**}(\omega_1) = 0.446 B_d^{**}$, the second eq.(4) holds too, and then:

$$\frac{1}{B_d^{**}} = p \cdot \frac{\left(A^{**}/B_{d1}^{**} + ... + A^*/B_{dp}^{**}\right)}{p} \cdot \frac{1}{A^{**}} \tag{40}$$

i.e.,

$$0.446\, B_d^{**} = 0.446 \cdot \frac{1}{p\left(\overline{A^{**}/B_d^{**}}\right)} \cdot A^{**}$$

Using eqs.(38', 39' and 40), eq.(27") gets the form:

$$1 - \frac{1}{\alpha_D^{**}(\omega_1)} = \frac{\left[1/2\left(\overline{A/A_{ct}}\right)\right]A - \left[1/p\left(\overline{A^{**}/A_{ct}^{**}}\right)\right]A^{**}}{0.446\left[1/p\left(\overline{A^{**}/B_d^{**}}\right)\right]A^{**}} \tag{41}$$

Some important conclusions come out from eqs.(27" and 41):

A) The drug $D \in (1^{**})$ *doesn't adsorb and doesn't influence the charge transfer.*

Then:

$$A^{**} = A \quad \text{and} \quad 2\left(\overline{A/A_{ct}}\right) = p\left(\overline{A^{**}/A_{ct}^{**}}\right) \tag{42}$$

and consequently:

$$\alpha_D^{**}(\omega_1) = 1, \text{ i.e., } \omega_{Th,p}\left[\alpha_D^{**}(\omega_1)\right] = 0 \tag{42'}$$

which also means $D \in (1)$

B) The drug $D \in (1^{**})$ *doesn't adsorb, but influences the charge transfer.*

Them:

$$A^{**} = A \qquad \text{and} \qquad 2\left(\overline{A/A_{ct}}\right) \neq p\left(\overline{A^{**}/A_{ct}^{**}}\right) \tag{43}$$

The situation:

$$2\left(\overline{A/A_{ct}}\right) \langle\ p\left(\overline{A^{**}/A_{ct}^{**}}\right) \tag{43'}$$

is impossible, because would lead to the conclusion $1 - \dfrac{1}{\alpha_D^{**}(\omega_1)} > 0$, i.e.,

$\alpha_D^{**}(\omega_1) > 1$ (see eq.(41)). Therefore, the correct conditions of the case B, are:

$$A^{**} = A \qquad \text{and} \qquad 2\left(\overline{A/A_{ct}}\right) \rangle \; p\left(\overline{A^{**}/A_{ct}^{**}}\right) \quad (44)$$

Suppose now that by *increasing* the concentration of the drug D, one passes from $1 - \dfrac{1}{\alpha_D^{**}(\omega_1)} = -k_1$, to $1 - \dfrac{1}{\alpha_D^{**}(\omega_1)} = -k_2$, and $k_2 > k_1$. Then $\omega_{Th,p}\left[\alpha_D^{**}(\omega_1)\right]$ will *increase* from $\sqrt{1 - \dfrac{1}{1+k_1}} \cdot \omega_1$ to $\sqrt{1 - \dfrac{1}{1+k_2}} \cdot \omega_1$. Of course, if $k_2 < k_1$, $\omega_{Th,p}\left[\alpha_D^{**}(\omega_1)\right]$ will *decrease* from $\sqrt{1 - \dfrac{1}{1+k_1}} \cdot \omega_1$ to

$\sqrt{1 - \dfrac{1}{1+k_2}} \cdot \omega_1$. Therefore, if the conditions(44) hold true, *both situations are possible*.

C) The drug D∈ (1**) *adsorbs and influences the charge transfer*.
Then:

$$A^{**} \langle A \; ; \qquad 2\left(\overline{A/A_{ct}}\right) \neq p\left(\overline{A^{**}/A_{ct}^{**}}\right) \qquad (45)$$

and:

$$1 - \frac{1}{\alpha_D^{**}(\omega_1)} = \frac{\left[1/2\left(\overline{A/A_{ct}}\right)\right]\left(A/A^{**}\right) - \left[1/p\left(\overline{A^{**}/A_{ct}^{**}}\right)\right]}{0.446\left[1/p\left(\overline{A^{**}/B_d^{**}}\right)\right]} \qquad (46)$$

Now, the correct conditions are:

$$A^{**} \langle A \text{ and } \left[1/2\left(A/A_{ct}\right)\right]\left(A/A^{**}\right) \langle \left[1/p\left(\overline{A^{**}/A_{ct}^{**}}\right)\right] \qquad (47)$$

and again, *both situations are possible*.

D) The drug D∈ (1**) *adsorbs but doesn't influence the charge transfer*.
Because $A/A^{**} \rangle 0$, and $2\left(\overline{A/A_{ct}}\right) = p\left(\overline{A^{**}/A_{ct}^{**}}\right)$ from eq.(46)

results: $1 - \dfrac{1}{\alpha_D^{**}(\omega_1)} \rangle 0$, which is *impossible*. Thus, *the case D, is not possible*.

This is a correct conclusion, because if there is adsorption, the exchange current densities of the electrode reactions must change their values.

Let's go further, and let's compare two different drugs, D_i and D_j, and let's suppose that these drugs satisfy the *conditions* of the case C), i.e.,

$$[1/2\overline{(A/A_{ct})}](A/\,_iA^{**})\langle\ [1/p_i(\overline{\,_iA^{**}/\,_iA_{ct}^{**}})] \tag{48}$$

$$[1/2\overline{(A/A_{ct})}](A/\,_jA^{**})\langle\ [1/p_j(\overline{\,_jA^{**}/\,_jA_{ct}^{**}})] \tag{48'}$$

respective:

$$1-\frac{1}{\alpha_{D_i}^{**}(\omega_1)} = \frac{[1/2\overline{(A/A_{ct})}]\left(A/\,_iA^{**}\right)-[1/p_i(\overline{\,_iA^{**}/\,_iA_{ct}^{**}})]}{0.446\,[1/p_i\left(\overline{\,_iA^{**}/\,_iB_d^{**}}\right)} \tag{49}$$

$$1-\frac{1}{\alpha_{D_j}^{**}(\omega_1)} = \frac{[1/2\overline{(A/A_{ct})}]\left(A/\,_jA^{**}\right)-\left[1/p_j\left(\overline{\,_jA^{**}/\,_jA_{ct}^{**}}\right)\right]}{0.446[1/p_j\left(\overline{\,_jA^{**}/\,_jB_d^{**}}\right)]} \tag{49'}$$

Then if the second member of eq.(49) is $-k_i$, the *Thomson radial frequencie* will be $\omega_{Th,p}[\alpha_{D_i}^{**}(\omega_1)] = \sqrt{1-\frac{1}{1+k_i}}\cdot\omega_1$. Similarly, if the second member of eq.(49') is $-k_j$, $\omega_{Th,p}[\alpha_{D_j}^{**}(\omega_1)]$ will be $\sqrt{1-\frac{1}{1+k_j}}\cdot\omega_1$.

Depending on the values of k_i and k_j, *there are possible all three situations*, i.e.,

$$\omega_{Th,p}[\alpha_{D_i}^{**}(\omega_1)] \geq \omega_{Th,p}[\alpha_{D_j}^{**}(\omega_1)]$$

and:

$$\omega_{Th,p}[\alpha_{D_i}^{**}(\omega_1)] \langle\ \omega_{Th,p}[\alpha_{D_j}^{**}(\omega_1)]$$

Of course, it is possible to compare a drug D_i with a mixture of Drugs or even to compare two mixtures of drugs. To simplify the matter, we don't indicate the drugs which enter in the compositions of the respective mixtures. In our experiments we have used four drugs $D_i \in (1^{**})$, and two mixtures : M_1^{**} containing the drugs *Am* and *Uh*, and M_2^{**} containing all four drugs: B, Am, Cf and Uh (see Table 2). As for the numbers of electrode reactions in the multielectrodes containing the mixtures M_1^{**}, respective

M_2^{**}, we shall use the notations q_1, respective q_2. Finally, the quantities A^{**}, B_d^{**} in the presence of the mixtures M_1^{**}, respective M_2^{**}, will be denoted $_1A^{**}$, $_1B_d^{**}$, respective $_2A^{**}$, $_2B_d^{**}$. Thus, consider first, the comparison between $D_i \in (1^{**})$, and the mixture M_1^{**}. Then, eq.(49) remains valid, and instead of eq.(49'), appears:

$$1 - \frac{1}{\alpha_{M_1}^{**}(\omega_1)} = \frac{[1/2\overline{(A/A_{ct})}]\left(A/\,_1A^{**}\right) - \left[1/q_1\left(\overline{_1A^{**}/\,_1A_{ct}^{**}}\right)\right]}{0.446\,[1/q_1\left(\overline{_1A^{**}/\,_1B_d^{**}}\right)]} \quad (50)$$

In the case of the comparison between $D_i \in (1^{**})$ and the mixture M_2^{**}, eq.(49) remains still valid, and instead of eq.(50), appears:

$$1 - \frac{1}{\alpha_{M_2}^{**}(\omega_1)} = \frac{[1/2\overline{(A/A_{ct})}]\left(A/\,_2A^{**}\right) - [1/q_2\left(\overline{_2A/\,_2A_{ct}^{**}}\right)]}{0.446\,[1/q_2\left(\overline{_2A^{**}/\,_2B_d^{**}}\right)} \quad (50')$$

What it is important, is the fact that *in both comparisons*, *there are possible all three situation*, i.e.,

$$\omega_{Th,p}[\alpha_{D_i}^{**}(\omega_1)] \,\rangle\, \omega_{Th,p}[\alpha_{M_1}^{**}(\omega_1)$$
$$\omega_{Th,p}[\alpha_{D_i}^{**}(\omega_1)] \,\langle\, \omega_{Th,p}[\alpha_{M_1}^{**}(\omega_1)$$

respective:

$$\omega_{Th,p}[\alpha_{D_i}^{**}(\omega_1)] \,\rangle\, \omega_{Th,p}[\alpha_{M_2}^{**}(\omega_1)$$
$$\omega_{Th,p}[\alpha_{D_i}^{**}(\omega_1)] \,\langle\, \omega_{Th,p}[\alpha_{M_2}^{**}(\omega_1) \quad (51)$$

It is obvious that eqs.(50 and 50') describe the comparison between M_1^{**} and M_2^{**} with the same three possibilities, i.e.,:

$$\omega_{Th,p}[\alpha_{M_1}^{**}(\omega_1)] \,\geq\, \omega_{Th,p}[\alpha_{M_2}^{**}(\omega_1)]$$
$$\omega_{Th,p}[\alpha_{M_1}^{**}(\omega_1)] \,\langle\, \omega_{Th,p}[\alpha_{M_2}^{**}(\omega_1)] \quad (52)$$

CONCLUDING REMARCS

The mean values of the obtained *Thomson radial frequencies* (see Tables 3 and 4) are represented under the form of an *histogram* in Figure2. On the horizontal axis are the investigated drugs, and mixtures, put in the sequence given in Table 3 and 4, and the heights of the vertical segments give the mean values of the corresponding *Thomson radial frequencies* $\omega_{Th,p}[\alpha^{**}(\omega_1)]$. The drugs used in two different concentrations, are indicated by the index numbers 1 and 2.

Because $\omega_{Th,p}[\alpha^{**}(\omega_1)] = \omega_1 \sqrt{1 - \alpha^{**}(\omega_1)}$ and $0 \leq \alpha^{**} \leq 1$, we have divided the class(I**) in four subclasses, which express the degree of efficiency of the investigated drugs and mixtures of drugs. Some important conclusions come out from this histogram:

- all the values $\omega_{Th,p}[\alpha_D^{**}(\omega_1)]$ are less than the *resonance Thomson radial frequency* $\omega_{Th,p}[\alpha_D^{**}(\omega_1) = 0] = \omega_1 = 1.256 \text{s}^{-1}$, showing that all drugs and mixtures investigated belong to the class(1**);

- the *resonance Thomson radial frequency* ω_1 corresponds to the *greatest efficiency* of a drug(or a mixture of drugs). Therefore, the efficiency *increases* if $\omega_{Th,p}[\alpha_D^{**}(\omega_1)]$ *increases* towards ω_1.

- it is obvious that for drugs belonging to the class(1*), $\omega_{Th,s}[\alpha_D^{*}(\omega_1)]$ are *greater* than the *resonance Thomson radial frequency*, which remains ω_1 too, and that their efficiency *increases* if $\omega_{Th,s}[\alpha_D^{*}(\omega_1)]$ *decreases* towards ω_1.

It is easy to verify, by means of equation $\omega_{Th,s}[\alpha_D^{*}(\omega_1)] = \omega_1 / \sqrt{1 - \alpha_D^{*}(\omega_1)}$, that the four subclasses of the class(1*), corresponding to the values $\alpha_D^{*}(\omega_1) = 0; 0.25; 0.50; 0.75$ and 1, will be given by the values $\omega_{Th,s}[\alpha_D^{*}(\omega_1)] = (1.256; 1.450; 1.776; 2.512$ and $\infty) \text{ s}^{-1}$.

In this way, $\omega_{Th,s}[\alpha_D^{*}(\omega_1)]$ and $\omega_{Th,p}[\alpha_D^{**}(\omega_1)]$ represent *two criteria of classifying the drugs in eight subclasses*, namely four subclasses for each general class, i.e., (1*), respective (1**). Indeed, suffice to estimate how far away are the values of the respective *Thomson radial frequencies* from ω_1, i.e., from the *resonance Thomson radial frequency, which expresses the greatest efficiency.*

- finally, the values of the *Thomson radial frequencies* given in figure 3 prove the correctness of eqs.(49), (49') and (50), (50'), by which one may explain the effects of adsorption processes, and of the new charge transfer processes (see "*A way of interpreting the obtained Thomson radial frequencies*").

The great difference between the efficiencies of Cf_1 and Cf_2, indicates that the drug Cf has *an important adsorption*, while the drugs entering in the subclass of *good efficiency*: adsorb and also lead to new charge transfer reactions, or at least, influence the existente reactions. Our future work will try to analyse separately these two kinds of effects.
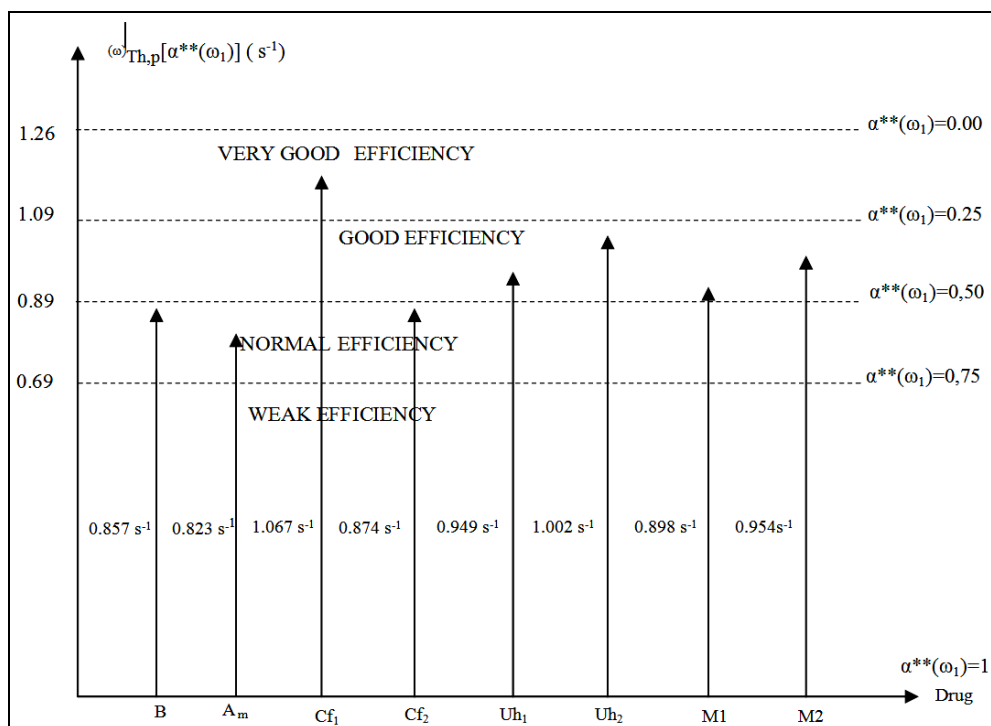

Figure 3. Histogram of the Thomson radial frequencies corresponding to the investigated drugs and mixtures of drugs

REFERENCES

1. N. Bonciocat, S. Borca and St. Moldovan, *Bulg. Acad. Sci. Commun. Depart. Chem.*, **1990**, *23*, 289.
2. Adina Cotarta, Ph.D Thesis, Chemical Research Institute, Bucharest, **1992**.
3. N. Bonciocat, *Electrokhimiya*, **1993**, *29*, 97.
4. N. Bonciocat, *Electrochimie si Aplicatii*, Dacia Europa - Nova, Timisoara, **1996**, chapter 5, 262.
5. N. Bonciocat and A. Cotarta, *Revue Roumaine de Chimie*, **1998**, *43*, 925

6. N. Bonciocat and A. Cotarta, *Revue Roumaine de Chimie*, **1998**, *43*, 1027.

7. N. Bonciocat, "*Alternativa Fredholm in Electrochimie*", Editura MEDIAMIRA, Cluj-Napoca, **2005**, chapter 2.

8. N. Bonciocat, *Electrochimie si Aplicatii*, Dacia Europa-Nova, Timisoara, **1996**, chapter 6, 268-277.

9. N. Bonciocat, *Electrochimie si Aplicatii*, Dacia Europa-Nova, Timisoara, **1996**, chapter 6, 278.

10. Adina Radu(Cotarta), Ph.D. These, Institut National Polytechnique de Grenoble, **1997**.

11. N. Bonciocat and A. Cotarta, "A new approach based on the theory of variational calculus in studying the electrodeposition process of chromium in the system $Cr^0/CrCl_2$, LiCl-KCl", *Contract Copernicus 1177-2* "Utilisation de sels fondus en metallurgie", Final Report of European Community, July **1998**.

12. I.O. Marian, E. Papadopol, S. Borca and N. Bonciocat, *Studia Universitatis Babes-Bolyai, Cluj-Napoca, Ser. Chemia*, **1998**, *43*, 91.

13. N. Bonciocat, *Scientific Bulletin Chemistry Series Politechnica University Timisoara*, **1998**, *43*, 5.

14. N. Bonciocat, "*Alternativa Fredholm in Electrochimie*", Editura MEDIAMIRA, Cluj-Napoca, vol. I, **2005**, chapter 5.

15. N. Bonciocat, E. Papadopol, S. Borca and I.O. Marian, *Revue Roumaine de Chimie*, **2000**, *45*, 981.

16. N. Bonciocat, E.Papadopol, S. Borca and I.O. Marian, *Revue Roumaine de Chimie*, **2000**, *45*, 1057.

17. I.O. Marian, R. Sandulescu and N. Bonciocat, *Journal of Pharmaceutical and Biomedical Analysis*, **2000**, *23*, 227.

18. I.O. Marian, N. Bonciocat, R. Sandulescu and C. Filip, *Journal of Pharmaceutical and Biomedical Analysis*, **2001**, *24*, 1175.

19. N. Bonciocat, A. Cotarta, J. Bouteillon and J.C. Poignet, *Journal of High Temperature Material Processes*, **2002**, *6*, 283.

20. N. Bonciocat, I.O. Marian, R. Sandulescu, C. Filip and S. Lotrean, *Journal of Pharmaceutical and Biomedical Analysis*, **2003**, *32*, 1093.

21. N. Bonciocat, "*Alternativa Fredholm in Electrochimie*", Editura MEDIAMIRA, Cluj-Napoca, vol. II, **2006**, chapter 2, 25.

22. N. Bonciocat and A. Cotarta, *"Spectroscopia de Impedanta Electrochimica in cazul limitarilor de transfer de sarcina si difuziune",* Editura Printech, Bucuresti, **2005**.

23. N. Bonciocat and I.O. Marian, *" Metoda Impedantei Faraday si variantele sale"* Presa Universitara Clujeana, **2006**, chapter 5.

24. N. Bonciocat and A. Cotarta, *Annals of West University of Timisoara, Series Chemistry,* **2006**, *15*, 137.

25. N. Bonciocat and A. Cotarta, *Scientific Bulletin Chemistry Series Politehnica University Timisoara*, **2007**, *52*, 1-2, 90.

26. N. Bonciocat, *Studia Universitatis Babes-Bolyai, Cluj-Napoca, Seria Chemia*, **2008***,* LIII, 1, 31.

27. N. Bonciocat, A. Cotarta, *Scientific Bulletin Chemistry Series Politehnica University Timisoara,* **2009**, in press.

PRELIMINARY STUDY FOR DEGRADATION CHARACTERISTICS OF HYDROXYAPATITE COATINGS ON TITANIUM IN RINGER SOLUTION

DANIEL MARECI[a], GINA UNGUREANU, NECULAI AELENEI, IONEL MARCEL POPA, IGOR CRETESCU

ABSTRACT. The aim of this work was to study the effect of electrochemical and electrophoretic deposition of hydroxyapatite (HA) on commercial pure titanium substrates, regarding the corrosion behaviour of the coated biomaterials during their preservation in physiological media. The coated surfaces were analyzed by X-Ray Diffraction and Scanning Electron Microscopy. The degradation characteristics of HA coated on the Titanium implants was investigated as a function of immersion time in Ringer solution, using the Electrochemical Impedance Spectroscopy (EIS) technique. A double-layer model of the coated film was found; a compact protective inner layer and a porous external layer with open or sealed pores, as a function of immersion period.

Keywords: Coating, Titanium implants, Hydroxyapatite, Electrochemical Impedance Spectroscopy

INTRODUCTION

Metallic materials have found wide application in restorative surgery as basic biomaterials for manufacturing implant prostheses for skeletal replacements and fixtures. In this case, metallic materials, which combine good mechanical characteristics, high corrosion resistance and good compatibility with biological materials, are chosen. Titanium and its alloys have been used extensively in the last several decades as materials for orthopedic implants, dental implants, and medical devices due to their low density, excellent biocompatibility, corrosion resistance and mechanical properties [1-9]. When the prosthesis are placed in the human body, the passive film undergo further transformations, namely thickening of the passivating film and stoichiometric changes, as well as metal dissolution [10, 11]. Both passivation and metal dissolution are electrochemical processes.

[a] *"Gh. Asachi" Technical University of Iaşi, Faculty of Chemical Engineering and Environmental Protection, Mangeron Blvd., no. 71, Iasi, Romania, 700500, danmareci@yahoo.com*

There are few reports describing the electrochemical process on the alloy during the growth of hydroxyapatite (HA). Bioactivity of titanium surfaces is not high enough to induce the direct growth of the bone tissue and good bone fixation takes several months. Modifications of metal surfaces often are employed as a mean of controlling tissue-titanium interactions and shortening the time of bone fixation [12]. The hydroxyapatite coatings on metallic implant devices offer the possibility of combining the strength of the metals with the bioactivity of the ceramics [13-16]. Many different techniques have been used for preparation of HA coatings among them ion sputtering, plasma spraying, sol-gel coating, electrodeposition and a biomimetic deposition [17].

This investigation was aimed to study the effect of electrochemical and electrophoretic deposition of hydroxyapatite on commercial pure titanium substrates, regarding the corrosion behaviour of the coated biomaterials during their preservation in physiological media. In the present work electrochemical impedance spectroscopy (EIS) measurement were carried out in order to understand the structure of the electrochemical deposed layer/substrate interface. EIS spectra were recorded and the data were analysed to evaluate the equivalent circuit (EC) parameters as a function of time storage of the coated metal in Ringer's solution.

RESULTS AND DISCUSSIONS

Samples depositions and characterization

The short deposition time in electrochemical deposition entail just an initiation of the coating process, creating only the centre for ulterior deposition of HA after implantation. The nucleus of deposed phase can be observed on SEM micrographs (Figure 1a).
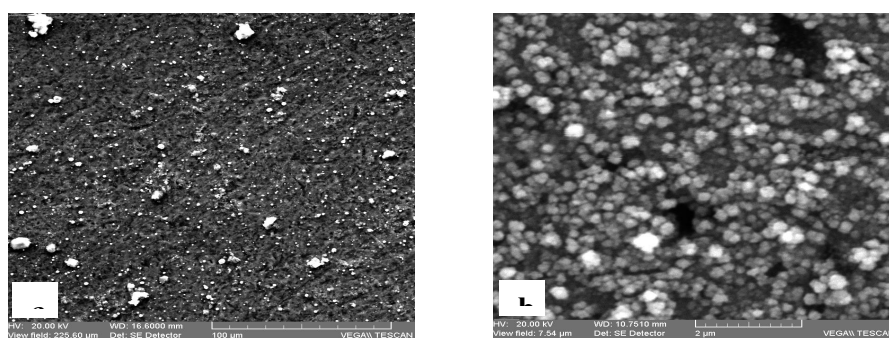

Figure 1. SEM micrographs of the electrochemically coated titanium

The microstructure of these hydroxyapatite islands is presented in Figure1b at a higher magnification. The EDX spectrum for surface presented in Figure 1a indicating the presence both the calcium phosphate compounds and titanium oxides (Figure 2).
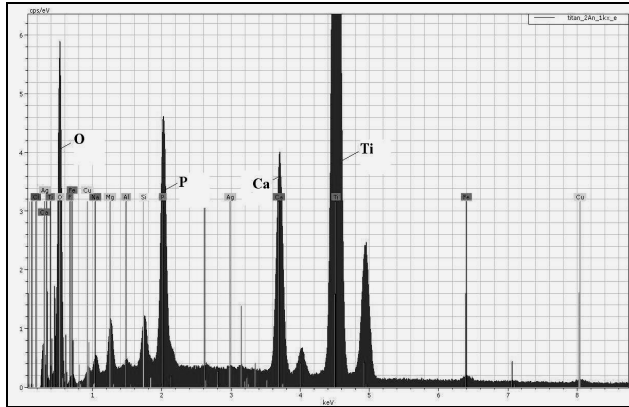
Figure 2. EDX spectrum for electrochemically coated titanium surface

The XRD spectrum after electrochemical deposition of calcium phosphate, presented in Figure 3a, attest the presence of Monetite on titanium surface. Taking into account the reduced intensities of the characteristic peaks one can confirm that the deposed material is in a very small quantity.
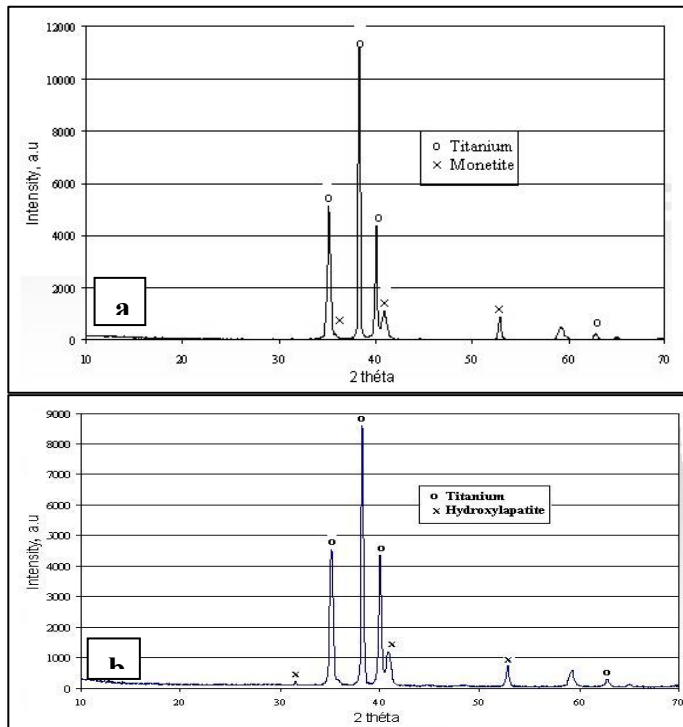

Figure 3. XRD patterns of the coated titanium surface after electrochemical deposition (a) and after monetite→hydroxyapatite conversion (b)

The XRD spectrum registered after monetite→hydroxyapatite conversion (Figure 3b), confirm this transformation by hydroxyapatite peaks occurrence, in the same small quantity.

The surface structure after electrophoretic deposition of hydroxyapatite is presented in Figure 4, before and after annealing process.
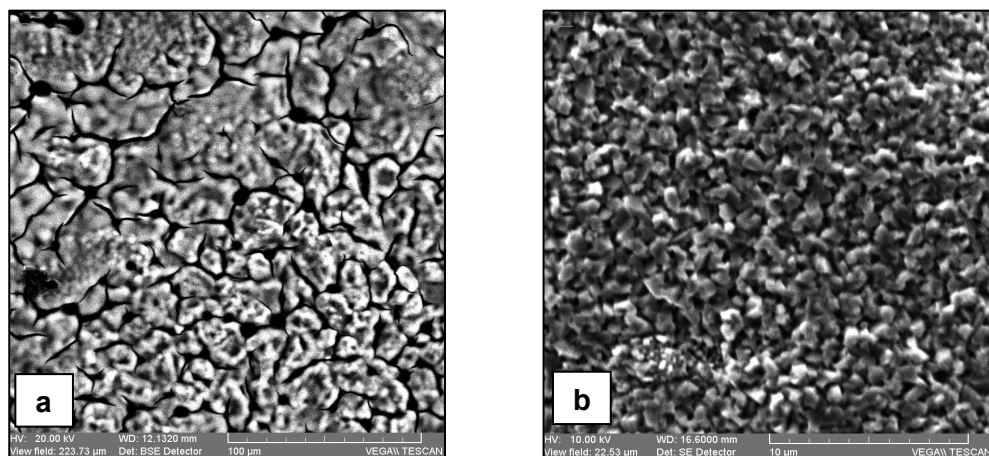
Figure 4. SEM micrograph of the electrophoretically coated hydroxyapatite
(a) after deposition; (b) after calcinations for 2.5 hours at 800°C

One can remark the uniform coating of titanium surface with a compact layer of very well packed HA particles (Figure 4a), and the fine microstructure of the hydroxyapatite crystals (1-1.5 μm) after calcination (Figure 4b).
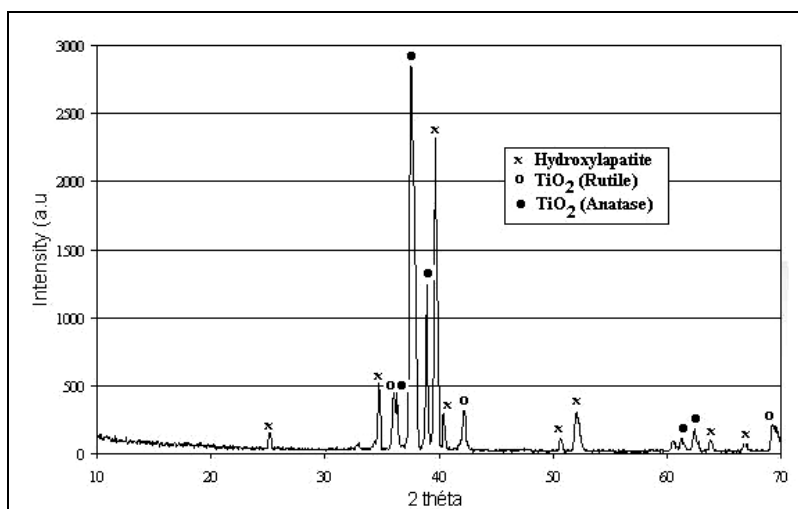
Figure 5. XRD pattern for electrophoretically coated and sintered sample

The XRD pattern obtained for sample coated by electrophoretic method and calcinated (Figure 5) indicate the fact that heating titanium coated with hydroxyapatite at $800^{\circ}C$ a crystalline hydroxyapatite is obtained. On the other hand, by this heating the free surface of titanium plate was oxidized to TiO_2; a mixture of rutile and anatase being identified.

Electrochemical measurements

Electrochemical impedance spectroscopy measurements offer useful information regarding the superficial layer of the coated sample and their time evolution in Ringer solution. EIS measurements were performed at the open circuit potential. Typical impedance spectra obtained for different immersion period in Ringer solution of the electrochemical HA-coated sample are shown in Figure 6. They are presented as Bode diagrams.
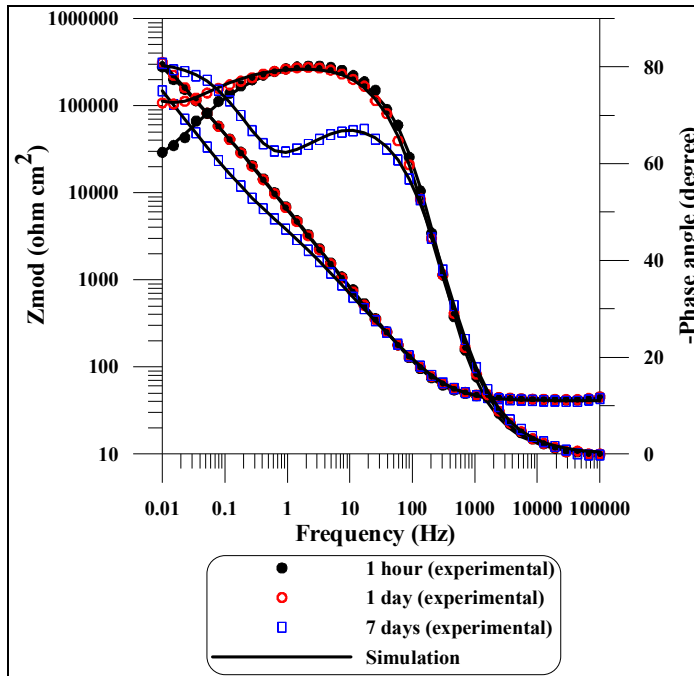
Figure 6. EIS data, for electrochemical HA-coated titanium sample, immersed in Ringer solution for different times, measured at open circuit potential.

Generally, three frequency regions referring to the high, intermediate and low frequency values are distinguished from impedance spectra. The high frequency plateau of the impedance values at frequency higher than 10^4 Hz, with the phase angle approaching to zero, yields the value of the

solution resistance (R_{sol}). The intermediate frequency region (10^3 to 10 Hz) has the maximum phase angle and the logarithm of impedance versus logarithm of the frequency slope approaching to -1. These impedance responses correspond to the capacitive behaviour of the electrode and describe the dielectric properties of the electronically conducting surface film. The low frequency region (under 10 Hz) detects the mass transfer (diffusion or migration) processes, or other relaxation processes taking place at the film-electrolyte interface or within the pores of the surface film.

From Figure 6, the phase angle observed at low frequency for the sample after 1 hour immersion was -60°. However, at intermediate frequency, the phase angle shifted to -80° and remind constant over a wide range of frequency, indicating a capacitive response for the sample. One can observe that the changes of the surface properties are less noticeable after 1 day of immersion. The Bode plots for sample immersed for one day and for one hour are similar. Once with increase of the immersion time to 7 days, two distinct capacitive behaviours can be evidenced and, at low frequencies, the phase angle values are shifted to -80°. The high-frequency region evidences the penetration process of the electrolyte through the porous film and the low-frequency domain evidences the processes taking place at the substrate/ electrolyte interface [18]. Such behaviour is typical for a metallic material covered with a porous film, which is exposed to an electrolytic environment.

It was found that the whole set of experimental data could be satisfactorily fitted with two EC presented in Figure 7. The impedance data of electrochemical HA-coated titanium specimen maintained for one hour and one day in Ringer solution were fitted with the EC presented in Figure 7a, while for the same sample maintained for seven days in solution was better fitted with the EC presented in Figure 7b.

In these equivalent circuits CPE is the constant phase element and "n" the exponent of the constant phase element, described by an empirical impedance function of the type [19]:

$$Z_{CPE} = \frac{1}{Q(j\omega)^n} \qquad (1)$$

where: "Q" is the combination of properties related to both the surfaces and electro-active species independent of frequency; "n" (exponent of the frequency term) is related to the slope of the lg Z_{mod} vs lg Frequency in Bode plots and varies between -1 an $+1$, "ω" - the angular frequency and j is imaginary number ($j^2 = -1$).
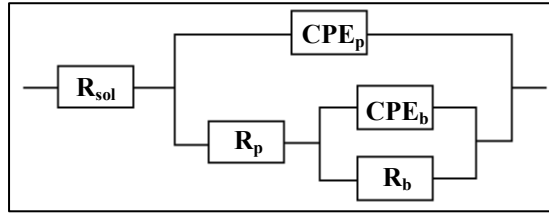
(a)
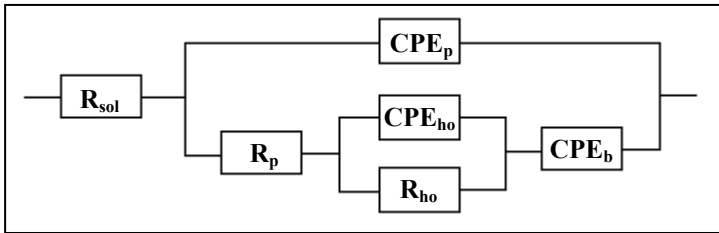
(b)

Figure 7. Equivalent circuit for Two-layer model: a compact inner layer and a porous external layer: (a) with unsealed pores and, (b) with sealed pores.

The EC presented in Figure 7a contains the following elements: solution resistance (R_{sol}), constant phase element (CPE_p) of the intact (non-defective) coating layer, charge transfer resistance associated with the penetration of the electrolyte through the pores or pinholes existing in the coating (R_p), the polarization resistance of the substrate (R_b) as well as the electrical double layer constant phase element at the substrate/electrolyte interface (CPE_b).

The circuit presented in Figure 7b was developed to represent a sealed anodic oxide film [20]. The EC is similar to that proposed by R.M. Souto et al for plasma-sprayed HA-coatings on Ti6Al4V in physiological media [18]. That is, the model represented by circuit presented in Figure 7a modified to take in account the precipitation of some hydrates/precipitates inside the external porous film. In this case, the CPE_{ho} and R_{ho} introduced in circuit represent the constant phase element and resistance of hydrates/precipitates inside the pore of the superficial film.

The quality of fitting was judged by the error distribution vs. frequency, comparing experimental with simulated data for different models. These error distributions indicate the fact that in the case of electrochemically coated sample the "two-layer model of unsealed porous film" can be successfully used to fit the EIS data for short times of immersion (1 day), while the "two-layer model of a sealed porous film", can be used to best fit the EIS data for long time immersions (7 days); in both situations, the errors being of less than 5%.

The values of the circuit elements from equivalent circuits that fit best the experimental data in the case of electrochemical-coated sample are presented in Table 1.

Table 1. Impedance parameters for electrochemical HA-coated titanium sample after different immersion times in Ringer's solution

	CPE_p (S cm^{-2} s^n)	n_p	R_p (Ω cm^2)	CPE_b (S cm^{-2} s^n)	n_b	R_b (Ω cm^2)	R_{ho} (Ω cm^2)	CPE_{ho} (S cm^{-2} s^n)	n_{ho}
1 hour	2.4×10^{-5}	0.90	2×10^5	8.9×10^{-6}	0.81	6×10^5	-	-	-
1 day	3.1×10^{-5}	0.88	1×10^5	9.8×10^{-6}	0.80	5×10^5	-	-	-
7 days	3.5×10^{-5}	0.85	5×10^3	4.7×10^{-5}	0.79	-	1×10^5	2.4×10^{-5}	0.65

The sample maintained 7 days in solution appear to be un-protected at action of solution, from point of view of the charge transfer resistance (R_p) (for highly corrosion resistance materials the values may even reach 1 MΩ cm^2 [21]). However, this effect seems to be compensated by polarization resistance of substrate (R_b) that is sufficiently high. The same value for solution resistance, R_{sol} of the test electrolyte, equals 45 ± 5 Ω, was observed for the specimens, indifferent of the immersion time, and was not inserted in Table 1.

The EIS spectra for the electrophoretically deposition of hydroxyapatite on pure commercially titanium immersed in Ringer solution are shown as Bode plots in Figure 8.
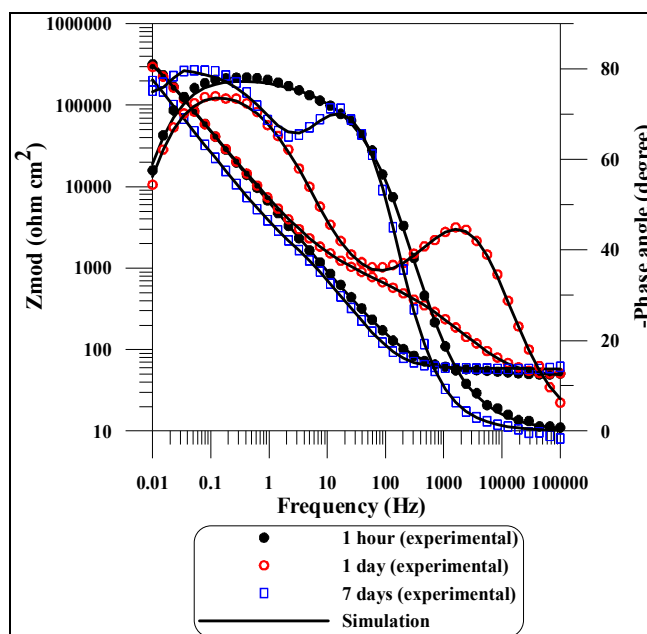

Figure 8. Bode plots for electrophoretical HA-coated titanium sample, recorded at open circuit potential, after different time of immersion in Ringer solution

In Figure 8, the experimental data are shown by individual points, while the theoretical spectra resulting from the fits to a relevant equivalent circuit model are shown by continuous lines. For the electrophoretical HA-coated commercial pure titanium specimen EIS recorded at open circuit potential after 1 hour of immersion in Ringer solution a capacitive behaviour, is indicated from medium to low frequency by phase angle approaching -80°. In this case, noticeable changes after 1 day of immersion were observed. With increase in time to 1 day of immersion the sample exhibited two distinct capacitive behaviours. At 7 days of immersion, the nature of Bode plots was similar to that of 1 day of immersion.

The impedance data for electrophoretical coated sample maintained for 1 hour in Ringer's solution (initial moment) are best fitted with EC presented in Figure 7a, while for sample maintained both one day and 7 days in Ringer solution are best fitted with the EC presented in Figure 7b. The circuit elements values are draw in Table 2.

Table 2. Impedance parameters at different immersion times in Ringer solution for electrophoretical HA-coated titanium sample

	CPE_p (S cm^{-2} s^n)	n_p	R_p (Ω cm^2)	CPE_b (S cm^{-2} s^n)	n_b	R_b (Ω cm^2)	R_{ho} (Ω cm^2)	CPE_{ho} (S cm^{-2} s^n)	n_{ho}
1 hour	3.1×10^{-5}	0.86	2×10^5	9.4×10^{-6}	0.85	6×10^5	-	-	-
1 day	3.5×10^{-5}	0.88	5×10^3	3.7×10^{-5}	0.70	-	5×10^5	3×10^{-5}	0.75
7 days	3.9×10^{-5}	0.90	5×10^3	1.8×10^{-5}	0.70	-	2×10^5	3.5×10^{-5}	0.81

In this case, after only one day of immersion the EIS spectrum reflects that the pores in the coated layer are filled with precipitates. The metal dissolution continues through the coating, because the impedance spectra are below 10^6 Ω cm^2 at all exposure times.

CONCLUSIONS

1. By short time electrochemical coating one can obtain an initiation of the hydroxyapatite deposition on pure titanium surface, whereas by electrophoretic method in the same time period (10 min) a consistent hydroxyapatite layer can be deposed. A previous etching and/or alkaline activation of the metal surface favour these depositions.

2. Through heating at 800°C the partial amorphous deposition is transformed in a crystalline hydroxyapatite.

3. Electrochemical impedance spectroscopy is a useful technique for studying the corrosion behaviour of surgical metallic implants, even when they are coated with a ceramic material such as hydroxyapatite. In the case of electrochemical HA-coated commercial pure titanium specimen after a sufficient time of immersion in Ringer's solution (more than a 1 day)

the electrolyte penetrate in the metal substrate trough the pores of the substrate film (most probable Hydroxyapatite and TiO_2). The nature of the materials which fill the superficial pores was not investigated in this study, but may probably be the result of metal phosphate formation or incorporation of metal ions in the HA structure, correlated with the presence of oxygen from air. In the case of the electrophoretic HA-coated titanium only after one day of immersion in Ringer's solution the Bode plots exhibited two distinct capacitive behaviours. The pores are penetrated much more rapid by electrolyte and after 1 day of immersion the pores of the superficial layer are blocked. Also, one can be remark that after a significant time of exposure (7 days) both coated samples have similar electrochemical behaviour.

4. The EIS spectra are fitted using an equivalent circuit. For coated samples maintained short time in Ringer solution, a two-layer model of an unsealed porous surface film is suitable, while for coated samples maintained long time in Ringer solution, a two-layer model with sealed pores is adequate.

EXPERIMENTAL SECTION

Materials

The pure titanium plates (60x12x5 mm) used as substrate for HA coating were first roughened by acid etching for 60 min at $60^{o}C$, in a mixed acidic solution (18% HCl and 48% H_2SO_4). Then, acid-treated surfaces are ultrasonically cleaned successively with acetone, ethanol and distilled water for 10 min each and dried in air at $120^{o}C$.

The electrolytic deposition of hydroxyapatite was realized via monetite. For this purpose o potential difference of 2V between titanium (cathode) and platinum (anode) was applied for 25 min. The electrolyte medium was a solution rich in Ca^{2+} and PO_4^{3-} ions, whose composition is: 0.5M $Ca(OH)_2$, 0.5M H_3PO_4 and 1M Lactic acid (CH_3CHCO_2HOH). The electrochemical reaction was conducted in an electrochemical cell with three electrodes, the reference being a saturated calomel electrode. The cathodic deposition vas carried out with a VOLTALAB 40 potentiostat (PGZ 301 type – Radiometer Copenhagen). The temperature was controlled in the domain 70 – $75^{o}C$. During the deposition process the current density has been varied between 0.6 and 0.2 $\mu A/cm^2$. After deposition the sample was washed with deionised water and dried at $120^{o}C$. By this process on the titanium surface was formed the monetite, $CaHPO_4$, The conversion of monetite to hydroxyapatite ($Ca_{10}(PO_4)_6(OH)_2$) was realized immersing the covered sample in 0.1M NaOH for 67 hours at ordinary temperature.

For electrophoretic deposition, the roughened sample was firstly activated by an alkaline treatment in 10M NaOH for 4 hours at $75^{o}C$. The electrophoretic coating was realized from a suspension of Hydroxyapatite

powder in an aqueous-organic media (4.2 g HA, 100 mL isopropyl alcohol and 5 mL 0.5N HCl) in a two-electrode cell, with titanium as cathode and platinum as anode. A potential of 63 V was applied for 10 min. After washing, the sample was dried at 120°C and then burn off for 2.5 hours at 800°C.

Samples characterization

The coated surfaces were investigated using a VEGA-TESCAN Scanning Electron Microscope equipped with QUANTAX Bruker AXS Microanalysis system. The XRD patterns were obtained with a Philips Analytical PW3710 XPERT system equipped with a Ni filter and Cu Kα (λ =1.5418 Å) radiation (40 kV, 30 mA) at 0.05° steps at the rate of 10 s per step over the range 10°<2θ<70°.

Electrochemical measurements

The corrosion behaviour and time evolution of the coated surfaces were analyzed by Electrochemical Impedance Spectroscopy (EIS). The measurements were carried out at 25°C in a naturally aerated Ringer's solution (NaCl – 6 g/L, KCl – 0.4 g/L, $CaCl_2$ $2H_2O$ – 0.2 g/L, sodium lactate – 3,05 g/L) at pH=6.5, in a three electrodes cell: the studied sample, a platinum counter-electrode and saturated calomel - as reference electrode (SCE). The measurements were made with a PAR 263 A potentiostat/ galvanostat connected with a PAR 5210 lock-in amplifier, controlled by a computer (Princeton Applied Research). The impedance spectra were acquired in the frequency range of 10^5 Hz to 10^{-2} Hz with a 10 mV amplitude sine wave. Nyquist and Bode plots were registered, at the open circuit potential. The analysis of the EIS data was performed using commercial software package Electrochemistry Power Suite (ZSimpWin).

REFERENCES

1. J. Pan, D. Thierry, C. Leygraf, *Electrochim. Acta*, **1996**, *41*, 1143.
2. J. E. Gonzalez, J. C. Mirza Rosca, *J. Electroanal. Chem*., **1999**, *471*, 109.
3. R. M. Souto, G. T. Burstein, *J. Mater. Sci: Mater. Med*., **1996**, *7*, 337.
4. R. M.Souto, G. T. Burstein, *Mater. Sci. Forum*, **1998**, 799.
5. N. Aelenei, Gh. Nemtoi, D. Mareci, D. Aelenei, C. Chiper, R. Chelariu, *Studia Universitatis Babes-Bolyai, Chemia*, **2001**, *XLVI 1-2*, 105.
6. S. Luiz de Assis, S. Wolynec, I. Costa, *Electrochem. Acta*, **2006**, *51*, 1815.
7. I. Milosev, T. Kosec, H. H. Strehblow, *Electrochim. Acta,* **2008**, *53,* 3547.

8. D. Mareci, R. Chelariu, D. M. Gordin, G. Ungureanu, T. Gloriant, *Acta Biomater*., **2009**, *5*, 3625.

9. E. Vasilescu, P. Drob, D. Raducanu, I. Cinca, D. Mareci, J. M. Calderon Moreno, M. Popa, C. Vasilescu, J. C. Mirza Rosca, *Corr. Sci.*, **2009**, *51*, 2885.

10. K. E. Healy, P. Ducheyne, *J. Biomed. Mater. Res.*, **1992**, *26*, 319.

11. K. E. Healy, P. Ducheyne, *J. Colloid Interf. Sci.*, **1992**, *150*, 404.

12. T. Kokubo, I. L. M. Kim, M. Kawashita, *Biomaterials*, **2003**, *24*, 2161.

13. C. P. A. T. Klein, P. Patka, J.G.C. Wolke, J.M.A. de Blieck-Hogevorst, K. de Groot, *Biomaterials*, **1994**, *15*, 146.

14. A. Moroni, V. L. Caja, C. Sabato, E. L. Egger, F. Gottsauner-Wolf, E. Chao, *J. Mater. Sci.: Mater. Med.*, **1994**, *5*, 411.

15. C. L. Tisdel, V.M. Goldberg, J. A. Parr, J. S. Bensusan, L. S. Staikoff, S. Stevenson, *J. Bone Joint Surg.*, **1994**, *76A*, 169.

16. P. L. Tranquiilli, A. Merolli, O. Palmacci, G. Gabbi, A. Cacchioli, G. Gonizzi, *J. Mater. Sci: Mater. Med.*, **1994**, *5*, 345.

17. E. C. S. Ringo, L. C. Oliveira, L. A. Santos, A. O. Boschi, *Rev. Eng. Biomed.*, **1999**, *15*, 21.

18. R. M. Souto, M. M.Laz, R. L. Reis, *Biomaterials*, **2003**, *24*, 4213.

19. B. A. Boukamp, *Solid State Ionics*, **1986**, *21*, 31.

20. A. Baltat-Bazia, N. Celati, M. Keddam, H. Takenouti, R. Wiart, *Mater. Sci. Forum*, **1992**, *111-112*, 359.

21. F. Mansfeld, *J.Electrochem. Soc.*, **1973**, *120*, 515.

EFFECT OF ALBUMIN PROTEINS ON THE ELECTROCHEMICAL BEHAVIOUR OF Ti6Al7Nb ALLOY IN SIMULATED BODY FLUID

DANIEL MARECI[a], ADRIAN CĂILEAN, GEORGIANA BOLAT, IGOR CREȚESCU, DANIEL SUTIMAN

ABSTRACT. The purpose of this study was to investigate the effect of human albumin proteins on the corrosion behaviour of Ti6Al7Nb alloy in Hank's Balanced Salt Solution (HBSS) using electrochemical polarization and electrochemical impedance spectroscopy techniques. The results showed that the presence of albumin in HBSS had a significant influence on the zero current potential (ZCP), polarization resistance (R_p) and capacitance (C). For the polarization scan, an albumin addition of 37.5 mg/ml to the HBSS significantly moved the ZCP towards a more negative (cathodic) potential and inhibited the cathodic corrosion reaction. The R_p value for Ti6Al7Nb alloy immersed in HBSS are high (order of 5×10^5 Ωcm^2) and increased after albumin addition (order of 10^6 Ωcm^2) with increasing potential from -500 mV to 1000 mV indicative of albumin adsorption. The presence of albumin proteins in HBSS improved the corrosion resistance of Ti6Al7Nb alloy.

Keywords: Ti6Al7Nb alloy, albumin, polarization resistance, impedance, corrosion

INTRODUCTION

Titanium and its alloys are the most preferred metallic materials for orthopaedic implants in the field of medicine due to their good mechanical properties and biocompatibility. In what the use of titanium and its alloys as implant material is concerned extensive and well documented researches have been performed [1-8].

Ever since the pioneer metal alloys have been use as biomaterials, lack of biocompatibility has been extensively reported and research on improved materials with appropriate mechanical behaviour and adequate biocompatibility was developed. The Ti6Al4V alloy was the first titanium alloy registered as implant material in the ASTM standards (F-136-84). Hallab et al., 2005 reported that V is toxic in vitro at concentrations below those in synovial fluids in vivo [9]. The administration of metallic ions, using metallic powders, to fibroblast L929 and osteoblast MC3T3-E1 cells showed that Ti,

---

[a] *"Gh. Asachi" Technical University of Iaşi, Faculty of Chemical Engineering and Environmental Protection, Mangeron Blvd., no. 71, Iaşi, Romania, 700500, danmareci@yahoo.com*

Zr, Sn, Nb and Ta had no effect on their relative growth ratios. However, Al and V ions exhibited cytotoxicity at concentrations ≥ 0.2 ppm [10]. Based on these previous observations, further investigation of titanium alloys is increasingly important for gaining a better understanding of traditionally used alloys, and for helping in the search for new titanium alloys. Because of the possible risks associated with vanadium, Semlitsch, 1987 developed the alternative alloy, Ti6Al7Nb, in which the vanadium was exchanged for niobium [11]. Ti6Al7Nb alloy exhibits a broader passive range than Ti6Al4V alloy in simulated physiological solution [7, 12, 13]. Based on EIS measurements, Metikos-Hukovic et al., 2003 proposed that the corrosion resistance increases due to incorporation of Nb cations into the TiO_2 matrix [13].

Because surgical implants are being used on younger people and the older population is living longer, good long-term durability and corrosion resistance of implants are two important prerequisites for the choice of the specific device [14].

Titanium implants inserted into a human body are usually surrounded with blood-rich tissue, and the serum proteins in blood may also influence the corrosion of the implant materials. It is well known that proteins affect the corrosion behaviour of some metals, and that their presence can either inhibit or accelerate the corrosion phenomena. Proteins are known to behave differently with different metals, since their role in a corrosive environment is governed by many factors such as the surface chemistry of the metal, protein adsorption characteristics, interaction of protein molecules with other ions present in the electrolyte solution to produce organic complexes, and the transport of anionic and cationic charges around and away from the local environment [15-25].

The objective of the study was to determine the effect of the albumin protein on the electrochemical impedance spectrum of a Ti6Al7Nb alloy immersed in a simulated body fluid.

RESULTS AND DISCUSSIONS

The polarization curves of Ti6Al7Nb alloy in simulated physiological Hank's Balanced Salt Solution (HBSS) with and without albumin proteins are presented in figure 1.

Prior to each measurement, the Ti6Al7Nb electrodes were cathodically polarized at –1500 mV in the working solution for 120 s, in order to remove any spontaneously formed surface film.

Due to the fact that HBSS electrolyte used in this experiment is an oxygen-containing solution, the cathodic current recorded in the presented potential region can be attributed to the reduction of oxygen dissolved in the solution [26]. It can be observed that the addition of albumin protein decreased the cathodic current and moved the zero current potential (ZCP) in the negative

(cathodic) direction. It is known that many organic corrosion inhibitors prevent corrosion by forming an adsorbed film and blocking the mass transportation of the corrosion process. It is also well known that proteins have a high affinity for adsorption onto solid surfaces [27-29]. The decreasing cathodic current can be explained due to the presence of adsorbed albumin protein molecules which cover the reaction sites and/or block the transportation of dissolved oxygen to the electrode surface [24].
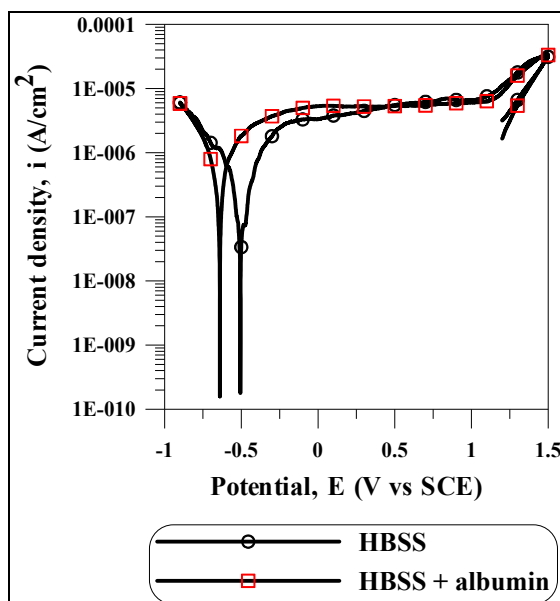

Figure 1. Potentiodynamic polarization curve recorded over the range of −900 mV to 1500 mV and reverse to 1200 mV for Ti6Al7Nb alloy in HBSS with and without albumin proteins, at 25^0C. dE/dt = 0.5mVs^{-1}

The anodic scans indicate that the Ti6Al7Nb alloy in HBSS with and without albumin protein forms the oxide film without the apparition of an active region representative for metal corrosion.

The current density is low and steady in the passive region, which extends over a wide range of potentials for Ti6Al7Nb alloy in HBSS with and without albumin protein, but some slightly differences can be observed when considering the potential dependence of the passive current. The anodic current density increases at potential around 1200 mV, which may be probably related to the changes in the composition of the passive film.

The potential domain for investigation of the electrochemical behaviour by EIS measurements for the Ti6Al7Nb alloy was chosen from above anodic polarisation curve. It was decided to perform these tests at the -500 mV, 0 mV, 500 mV and 1000 mV.

Impedance spectroscopy results for Ti6Al7Nb alloy in HBSS with and without albumin protein at selected potential values are presented as Nyquist diagrams (figures 2 and 3).
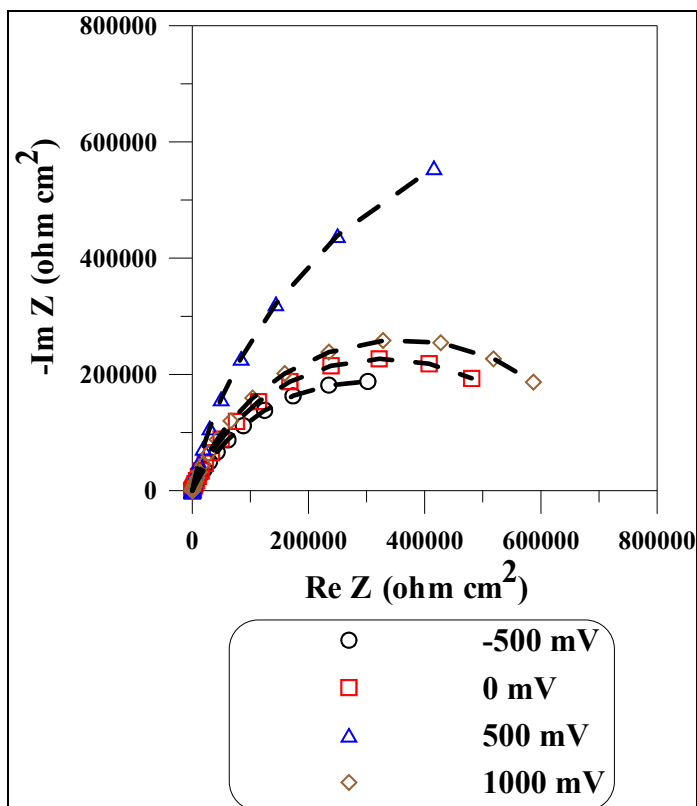

Figure 2. The effect of potential on the Nyquist impedance diagram of HBSS

Ti6Al7Nb alloy in both electrolytes, display a capacitive impedance spectrum with one time constant. The diameters of the semicircles correspond to the polarizing resistance. The Randles equivalent circuit (EC) which comprises only one time constant (figure 4) was used to model the experimental spectra, and good agreement between experimental data and fitted data was obtained.

Studies performed on Ti-based alloys under physiological conditions showed that the Randles equivalent circuit can be used successfully to describe the behaviour of these materials as well [2, 17, 24, 25]. The parameter R_p coupled with Q describes the processes at the electrolyte/oxide film interface. R_p is the polarization resistance related to the rate of corrosion reaction (s) at different potentials, and is inversely proportional to the corrosion current.
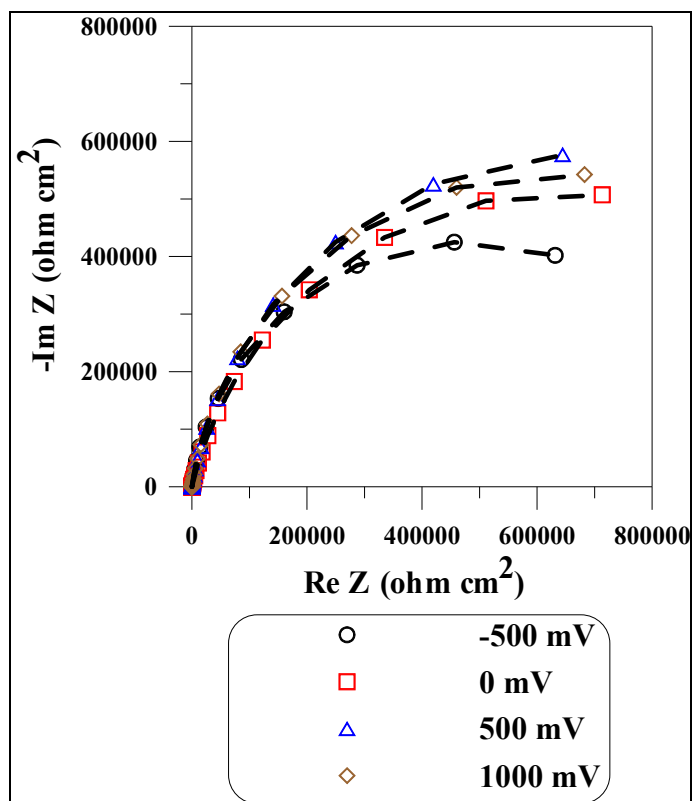
Figure 3. The effect of potential on the Nyquist impedance diagram
of HBSS with albumin

The symbol Q signifies the possibility of a non-ideal capacitance (CPE, constant phase element) with n varying from 0.80 to 0.90 for impedance data at different potential. The impedance of the CPE is given by [30] as shown in equation (1):

$$Q = Z_{CPE} = \frac{1}{C(j\omega)^n} \qquad (1)$$

where for n = 1, the Q element reduces to a capacitor with a capacitance C and, for n = 0, to a simple resistor. Generally, the use of a CPE is required due to a distribution of the relaxation times as a result of inhomogeneities present on the microscopic level under the oxide phase and at the oxide – electrolyte interface.
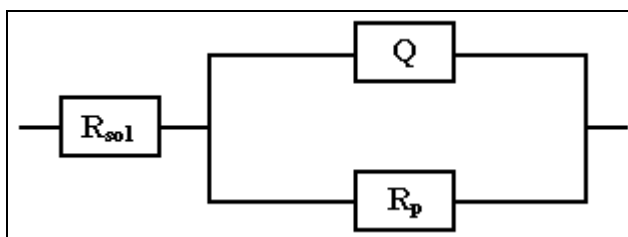
Figure 4. Equivalent circuit (EC) used to fit the impedance data

The values of fitted parameters of the EC and at different potentials are presented in table 1.

Table 1. Values of fitted parameters of the equivalent circuits as a function of applied potential of Ti6Al7Nb alloy in HBSS with and without albumin proteins

Applied potential (mV)	Q ($S\ cm^{-2}\ s^n$)	n	R_p ($\Omega\ cm^2$)
HBSS			
-500	9.6×10^{-6}	0.80	6.1×10^5
0	5.7×10^{-6}	0.80	6.6×10^5
500	4.2×10^{-6}	0.81	9.5×10^5
1000	3.8×10^{-6}	0.81	7.2×10^5
HBSS + 37.5 mg/ml albumin proteins			
-500	7.1×10^{-6}	0.85	1.2×10^6
0	2.7×10^{-6}	0.89	1.4×10^6
500	2.1×10^{-6}	0.90	1.4×10^6
1000	1.7×10^{-6}	0.90	9.8×10^5

R_{sol} is the resistance of the electrolyte between the working (Ti6Al7Nb alloy) and the reference electrode. This parameter has a value around 30 Ωcm^2 in HBSS and 45 Ωcm^2 in HBSS with albumin proteins.

Large values of R_p (order of $6 \times 10^5\ \Omega cm^2$) are obtained at -500 mV, confirming the formation of a passive layer of Tl6Al7Nb alloy in HBSS. As the potential changes from -500 mV to 0 mV and from 0 mV to 500 mV, R_p increases. These results seem to correspond to a slight thickening of the titanium oxide film. As the potential increases from 500 mV to 1000 mV the R_p decreases. The decrease in resistance indicates that the oxide layer may become more defective at large over potential [6, 31, 32]. But, the R_p of Ti6Al7Nb alloy in HBSS was large at 1000 mV as seen in table 2. This indicates that the alloy is still highly resistant to corrosion even at very large over potentials.

The Nyquist plots show that the impedance for Ti6Al7Nb in HBSS with albumin increases in time. The R_p increases with the addition of albumin to the HBSS.

Proteins can influence the corrosion reactions in several ways and thus shift the position of equilibrium. For example, proteins can bind to metal ions and transport them away from the interface thus encouraging further dissolution [22]. Proteins can accelerate the dissolution of metals through their chelation effects [15, 27].

Our data suggest that the albumin proteins are increasing the corrosion resistance of the Ti6All7Nb alloy.

At physiological pH, albumin is negatively charged (isoelectric pH 4.7 – 4.9). It may be possible that under these conditions proteins molecules adsorbed to the surface restrict metal dissolution. The adsorption of organic species may cause the blocking of terminal oxygen atoms at the interface passive film-electrolyte, which, consequently, hinders the charge transfer responsible for the passive film dissolution [17].

In order to compare capacitance values for Ti6Al7Nb alloy at different potentials, they were calculated, using equation [33]:

$$C = \left(R^{1-n}Q\right)^{\frac{1}{n}} \qquad (2)$$

Decrease in capacitance, starting from the -500 mV to 1000 mV (figure 5), can be attributed to thickening of the oxide layer, because:

$$C = \frac{\varepsilon\varepsilon_0 s}{l} \qquad (3)$$

where: s is the effective surface, ε is the dielectric constant for the oxide layer, ε_0 is the permissivity of free space and l is the thickness of oxide layer.

Values of C in HBSS with albumin proteins are smaller than those of C in HBSS at all observed potential (figure 5).

Since the proteins decreased the C, it is possible that the adsorbed proteins formed a compact film.

Serro et al. [34] determined a similar magnitude with a capacitance of 24–32 μFcm^{-2} for Ti immersed in Hank's salt solution containing bovine albumin serum. Contu et al. [17] reported on the interfacial capacitance of Ti6Al4V alloy immersed in bovine serum albumin with aging time. The capacitance of a constant phase element initially started at 27 μFcm^{-2} and stabilized at 11 μFcm^{-2} after 140 hours.

Gileadi [35] reported that the capacitances decrease as the fractional coverage of adsorbing species approaches unity. With further increasing potentials, the capacitance drops because the adsorbed albumin serves as an inhibiting anion or barrier to the aggressive ions on the alloy surface.
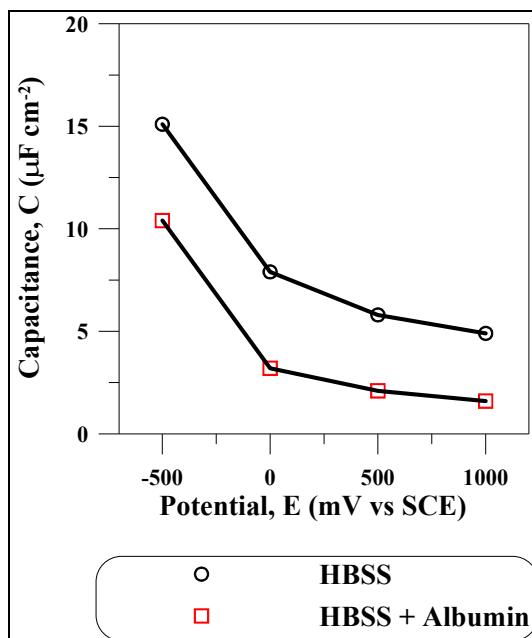
Figure 5. Capacitances (C) deduced from EIS data as a function of applied potential on Ti6Al7Nb alloy in HBSS with and without albumin proteins, at 25°C

CONCLUSIONS

The electrochemical behaviour of Ti6Al7Nb alloy in HBSS with and without albumin protein was studied using electrochemical polarization and electrochemical impedance spectroscopy techniques. The potentiodynamic polarization curves of Ti6Al7Nb alloy in HBSS, with and without albumin proteins addition, exhibited a passive behaviour. The albumin proteins shifted the zero corrosion potential in the negative direction and inhibited the cathodic corrosion reaction. The EIS simulated with a single time-constant representing a resistance–capacitance equivalent circuit elucidated an interaction between the albumin and the passive film. The charge transfer reactions, simulated by the polarizing resistance, indicate that albumin protein increases the corrosion resistance of Ti6Al7Nb alloy.

EXPERIMENTAL SECTION

The Ti6Al7Nb alloy used in present investigation was acquired in form of a road from National Institute of Research & Development for Non-ferrous and Rare Metals, Bucharest, Romania. The Ti6Al7Nb alloy was submitted to a semi-quantitative chemical analysis by plasma optical emission spectrometry technique and its results are given in table 2.

Table 2. Chemical composition of Ti6Al7Nb alloy determined by plasma optical emission spectrometry technique

Element	Ti	Al	Nb	Fe	Si	O_2	N_2	C
Weight %	balance	6.21	7.08	0.13	0.088	0.11	0.032	0.082

The microstructure of Ti6Al7Nb alloy is shown in figure 6. The alloy had a ($α + β$) duplex microstructure which consists in a globular and short lamellar $α$-phase into $β$-phase matrix.
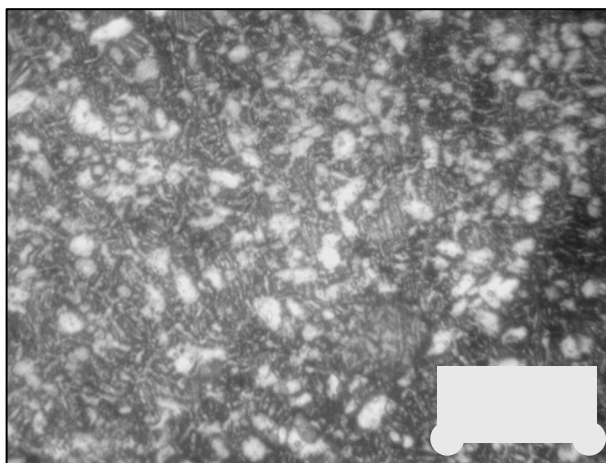

Figure 6. Optical photographs for Ti6Al7Nb microstructure.
The sample was etched using 10%HF + 5%HNO$_3$ solution at 25°C

The working electrodes were cut into 0.2 cm^2 sizes and brass nut was attached to sample using conductive paint to ensure electrical conductivity. The assembly was then embedded into an epoxy resin disk. Then the samples were ground with SiC abrasive paper up to 1000 grit, final polishing was done with 1 μm alumina suspension. The samples were degreased with ethyl alcohol followed by ultrasonic cleaning with deionised water and dried under a hot air stream.

The electrolytes used included:

1. Simulated physiological Hank's Balanced Salt Solution (HBSS) consisting of (g/l): 8 NaCl, 0.4 KCl, 0.35 NaHCO$_3$, 0.25 NaH$_2$PO$_4$×H$_2$O, 0.06 Na$_2$HPO$_4$×2H$_2$O, 0.19 CaCl$_2$×2H$_2$O, 0.19 MgCl$_2$, 0.06 MgSO$_4$×7H$_2$O, 1 glucose, at pH=6.9.

2. Simulated physiological Hank's Balanced Salt Solution (HBSS) + 37.5 mg/ml human albumin protein (KEDRION S. p. A., Italy). Peters [36] reports that the average albumin content of 42 mg/ml occurs in human blood with a

range of 35–50 mg/ml, for males requiring nursing care, the albumin level ranges 35–40 mg/ml or ages of 40–96 years. As a consequence, an albumin content of 37.5 mg/ml was selected for the electrolyte to approximate the midrange albumin content representing patients requiring medical attention (e.g., surgical implants).

Electrochemical measurements were carried out in aerated solution at 25°C using a Princeton Applied Research potentiostate (Model 263 A) connected with a Princeton Applied Research 5210 lock-in amplifier controlled by a personal computer and a specific software package called Electrochemistry Power Suite (Princeton Applied Research). A glass corrosion cell kit with a platinum counter-electrode and a saturated calomel reference electrode (SCE) were used to perform the electrochemical measurements. All potentials referred to in this article are with respect to SCE. Polarization diagrams were obtained for Ti6Al7Nb alloy immersed in HBSS with and without albumin protein, at a scanning rate of 0.5 mV/s.

Electrochemical impedance spectroscopy (EIS) measurements were performed in HBSS with and without albumin protein at different potentials at 25°C. EIS results at different potentials were obtained 30 minutes after the overpotential has been applied. The EIS spectra were recorded in the 10^{-2} Hz to 10^{5} Hz frequency range. The applied alternating potential signal had amplitude of 10 mV. In order to supply quantitative support for discussions of these experimental EIS results, an appropriate model (ZsimpWin-PAR, USA) for equivalent circuit (EC) quantification has also been used.

ACKNOWLEDGEMENTS

REFERENCES

1. J. Pan, D. Thierry, C. Leygraf, *Electrochimica Acta*, **1996**, *41*, 1143.
2. J. E. G. González, J. C. Mirza Rosca, *Journal of Electroanalytical Chemistry*, **1999**, *471*, 109.
3. I. Milosev, M. Metikos-Hukovic, H. -H. Strehblow, *Biomaterials*, **2000**, *21*, 2103.
4. E. B. Taddei, V. A. R. Henríquez, C. R. M. Silva, C. A. A. Cairo, *Materials Science Engineering*, **2004**, *24C*, 683.
5. H. S. Kim, S. H. Lim, I. D. Yeo, W. Y. Kim, *Materials Science Engineering,* **2007**, *451A*, 322.
6. S. L. Assis, S. Wolynec, I. Costa, *Electrochimica Acta*, **2006**, *51*, 1815.

7. S. Tamilselvi, R. Murugaraj, N. Rajendran, *Materials Corrosion*, **2007**, *58*, 113.
8. D. Mareci, C. Bocanu, Gh. Nemtoi, D. Aelenei, *Journal of the Serbian Chemical Society*, **2005**, *70*, 891.
9. N. J. Hallab, S. Anderson, M. Caicedo, A. Brasher, K. Mikecz, J. J. Jacobs, *Journal of Biomedical Materials Research*, **2005**, *74A*, 124.
10. Y. Okazaki, S. Rao, Y. Ito, T. Tateisji, *Biomaterials*, **1998**, *19*, 1197.
11. M. Semlitsch, *Clinical Materials*., **1987**, *2*, 1.
12. D. Mareci, G. Ungureanu, D. Aelenei, J. C. Mirza Rosca, *Materials Corrosion*, **2007**, *58*, 848.
13. M. Metikos-Hukovic, A. Kwokal, J. Piljac, *Biomaterials*, **2003**, *24*, 3765.
14. A. C. Fraker, "Corrosion of metallic implants and prosthetic devices. Metals handbook", Metals Park, OH: American Society for Metals, **1989**, 9th ed., vol. 13.
15. G. C. F. Clark, D. F. Williams, *Journal of Biomedical Materials Research*, **1982**, *16*, 125.
16. D. F. Williams, *Critical Reviews in Biocompaibility*, **1985**, *1*, 1.
17. F. Contu, B. Elsener, H. Bohni, *Journal of Biomedical Materials Research*, **2002**, *62*, 412.
18. F. Contu, B. Elsener, H. Bohni, *Journal of Biomedical Materials Research*, **2003**, *67*, 246.
19. Y. Okazaki, T. Tateishi, Y. Ito, *Materials Transaction*, **1997**, *38*, 78.
20. J. Lima, S. R. Sousa, A. Ferreira, M. A. Barbosa, *Journal of Biomedical Materials Research*, **2001**, *5*5, 45.
21. S. R. Sousa, M. A. Barbosa, *Clinical Materials*, **1993**, *14*, 287.
22. M. A. Khan, R. L. Williams, D. F. Williams, *Biomaterials,* **1999**, *20*, 63.
23. M. A. Khan, R. L. Williams, D. F. Williams, *Biomaterials*, **1999**, *20*, 765.
24. X. Cheng, S. G. Roscoe, *Biomaterials*, **2005**, *26*, 7350.
25. N. Padilla, A. Bronson, *Journal of Biomedical Materials Research*, **2007**, *81*, 531.
26. H. N. McMurray, D. A. Worsley, B. P. Wilson, *Chemical Communications*, **1998**, *8*, 887.
27. S. Omanovic, S. G. Roscoe, *Langmuir,* **1999**, *15*, 8315.
28. S. Omanovic, S. G. Roscoe, *Journal of Colloid and Interface Science*, **2000**, *227*, 452.
29. D. R. Jackson, S. Omanovic, S. G. Roscoe, *Langmuir*, **2000**, *16*, 5549.
30. I. D. Raistrick, J. R. MacDonald, D. R. Francschetti, in: J. R. MacDonald (Ed.), "Impedance Spectroscopy Emphasizing Solid Materials and Systems", John Wiley& Sons, New York, **1987**.
31. I. C. Lavos-Valereto, S. Wolynec, I. Ramires, A. C. Guastaldi, I. Costa, Journal of Materials Science: Materialss in Medicine, **2004**, *15*, 55.
32. A. Cremasco, W. R. Osorio, C. M. A. Freire, A. García, R. Caram, *Electrochimica Acta*, **2008**, *53*, 4867.
33. Milosev, T. Kosec, H.-H. Strehblow, *Electrochimica Acta*, **2008,** *53*, 3547.
34. I. P. Serró, A. C. Fernández, B. Saramago, J. Lima, M. A. Barbosa, *Biomaterials*, **1997**, *18*, 963.
35. E. Gileadi, "Electrode Kinetics for Chemists", VCH Publishers, New York, **1993**.
36. T. Peters, "All About Albumin: Biochemistry, Genetics and Medical Applications", Academic Press, New York, **1996**.

ELECTROCHEMICAL METALS RECOVERY FROM ELECTRONIC WASTES. PART. I. COPPER RECOVERY FROM SYNTHETIC SOLUTIONS

FLORICA IMRE-LUCACI[a], SORIN-AUREL DORNEANU, PETRU ILEA

ABSTRACT. This work presents the results concerning the copper recovery by electrodeposition from a synthetic solution simulating the dissolution of metallic part of electronic wastes in H_2SO_4. Batch electrolyses were carried out on graphite rotation disc electrode, at cathodic potentials between -100 and -300 mV vs. Ag/AgCl reference electrode and rotation rate from 100 to 700 rpm. The purity of cathodic deposit was evaluated by ICP-MS spectroscopy. The copper recovery efficiency from the synthetic solutions depends on applied cathodic potential. At more negative values (-300 mV), the electrodeposition rate increases, but the current efficiency and the deposit quality decrease. The electrodeposition tests confirm the possibility of copper recovery from a synthetic solution simulating the dissolution of the metallic part of electronic wastes in H_2SO_4, and the purity of the copper deposits are greater than 99 % in all of the tests.

Keywords: materials recycling; copper recovery, electronic wastes

INTRODUCTION

The number of electronic equipments discarded increases globally every year. The recycling of this type of wastes is still quite limited due to the heterogeneity of used materials [1]. This waste contains approximately 30% metals and 70% nonmetals and the presence of metals, such as Cu, Sn and precious metals encourage recycling studies [2]. Moreover, the presence of heavy metals, as Pb and Cd, turns these residues into dangerous ones, reclaiming further researches concerning the recycling of these wastes [3]. In this context, the recycling/removal of heavy metals by electrodeposition presents many advantages: metal recovery in pure form, low operating costs and no sludge disposal problems. The studies for recovering copper, lead and tin from scrap printed circuit boards (PCBs) and electronic components (EC) has been carried out using a combination of leaching and electrodeposition [1-11].

Starting from previous studies [12 - 14], in this work we present the results concerning the electrochemical copper recovery from a synthetic solution simulating the dissolution of metallic part of electronic wastes in H_2SO_4 [3], using

---

[a] *Department of Physical Chemistry, "Babes-Bolyai" University, 11 Arany Janos, 400028 Cluj-Napoca, Romania; fimre@chem.ubbcluj.ro*

a graphite rotation disc electrode (RDE). Batch electrolyses were carried out at cathodic potentials (E) between -100 and -300 mV vs. Ag/AgCl/KCl$_{SAT}$ reference electrode (RE) and rotation rate (ω) from 100 to 700 rpm. The purity of the copper deposits was evaluated by ICP-MS spectroscopy.

RESULTS AND DISCUSSION

Hydrodynamic voltammetry studies

In order to evaluate the possibilities of the Cu electroextraction, preliminary measurements were completed by hydrodynamic voltammetry (HV) in mono-element (5 g/L Cu in 2M H_2SO_4) and mixed solutions. The synthetic mixed solution, simulating the dissolution of metallic part of electronic wastes in H_2SO_4 contains 5 g/L Cu, 0.056 g/L Al, 0.045 g/L Fe, 0.041 g/L Ni, 0.05 g/L Zn, 0.061 g/L Pb, 1.91 g/L Sn and 2M H_2SO_4. The measurements were performed at a scan rate of 10 mV/s, for different values of ω (from 100 to 1600 rpm), the corresponding voltamograms being presented in Figure 1.

(A)　　　　　　　　　　　**(B)**
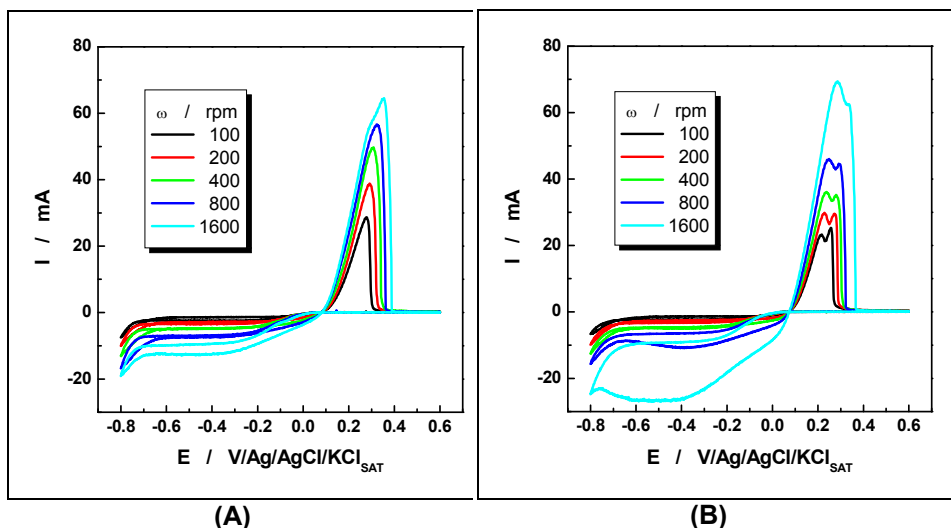
Figure 1. Hydrodynamic voltamograms recorded on Pt RDE for different rotation rates, in the mono-element solution contain 5 g/L Cu (A) and the mixed solution (B).

In the mono-element solution (Fig. 1 A), the anodic scan on the studied potential domain emphasizes a single peak around 0.3 V/RE, characteristic to the oxidation of the Cu electrodeposited during the cathodic scan. For the mixed solution (Fig. 1 B), two distinct oxidation peaks can be observed, corresponding to the successive anodic dissolutions of Sn and Cu. Moreover, the corresponding cathodic currents increase due to the simultaneous electrodeposition of Cu and Sn.

106

Electrorecovery studies

The studies concerning the copper electrodeposition from the mixed synthetic solution were performed using 250 mL of fresh electrolyte for each experiment.

During the electroextraction of copper from the mixed solution, the current (I) evolution was recorded and the purity of the Cu deposit was evaluated by ICP-MS at the end of each experiment. The measurements were performed at different values of the cathodic polarization potential and electrode rotation rate.

The influence of cathodic potential on Cu electrorecovery

The measurements' results concerning the influence of the cathodic potential on the current evolution are presented in Figure 2.
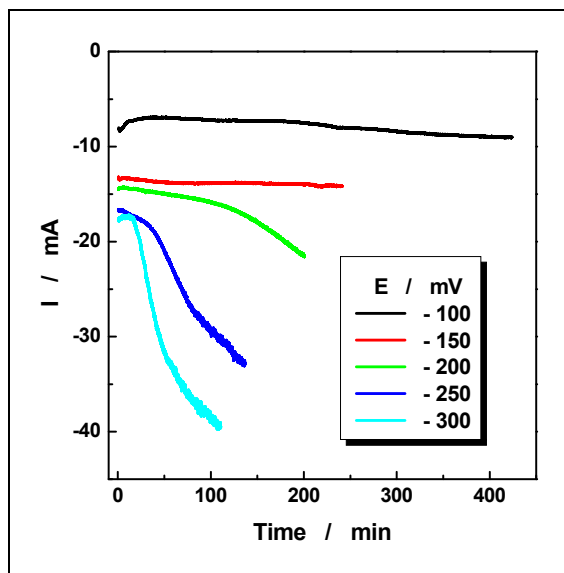
Figure 2. The evolution of the recorded currents for different values of the cathodic polarization. Experimental conditions: mixed solution; graphite - RDE; ω = 200 rpm.

For working electrode potentials of −100 mV/RE and −150 mV/RE, the formation of a compact cathodic deposit of Cu maintains a quasi constant electrode surface and the current don't increases significantly. The increase of the cathodic polarization potential from −200 mV/RE to − 300 mV/RE increases the available electroactive surface due to dendrites growth. This fact allows an increase of the recorded currents and, consequently, the decrease of the time required for the electrodeposition of the same amount of Cu.

After each experiment, the obtained deposit was dissolved in *aqua regia* and the metal impurities concentrations were evaluated by ICP-MS spectroscopy. The influence of the cathodic potential on the purity of the copper deposits is presented in Table 1.

Table 1. The influence of the cathodic potential on the purity of the copper deposits (ω = 200 rpm).

Impurities	Electrode potential, mV/RE				
	-100	**-150**	**-200**	**-250**	**-300**
Al, %	0.0018	-	0.0066	0.0001	0.0035
Zn, %	0.0015	0.0007	0.0027	0.0039	0.0039
Sn, %	0.0018	0.0022	0.0040	0.1516	0.6795
Total, %	0.0051	0.0029	0.0133	0.1556	0.6869

The ICP-MS analyses show that, in the Cu deposit, Fe, Ni and Pb are under detection limit (under 0.0001 %) and Al and Zn can be found in very low concentrations. Contrarily, the increase of the cathodic polarization potential to more negative values induces a significant increase of the Sn contents. Anyway, the purity of Cu deposits was always above 99% and the current efficiency is near 100% in all of the tests. In these conditions, a polarization potential of -200 mV/RE was considered at the best compromise between the electrodeposition rate and deposit purity (>99.9%).

The influence of rotation rate on Cu electrorecovery

The influence of the electrode rotation rate on Cu electrodeposition was evaluated in mixed solution, at a polarization potential of -200 mV/RE. The current evolution for different values of ω is presented in Figure 3 and the influence of the rotation rate on the purity of the copper deposits is presented in Table 2.

At the minimum investigated value of ω (100 rpm), the mass transport is insufficient to assure a constant concentration of the electrolyte on the electrode surface, favouring, as it can see in Table 2, the co-deposition of Sn in the Cu deposit. For greater ω values (ω > 100 rpm), the mass transport becomes sufficient to assure a quasi-constant concentration of Cu on the electrode surface, allowing the purity's increase of the Cu deposit. Due to the increase of ω, the recorded currents also increase, inducing a decrease of the electrorecovery time for the same quantity of charge (200 A s).

At the polarisation potential of – 200 mV/RE, for all investigated values of ω, the contents of Fe, Ni and Pb in the Cu deposit are under detection limit (under 0.0001 %) and Al and Zn can be found in very low concentrations.
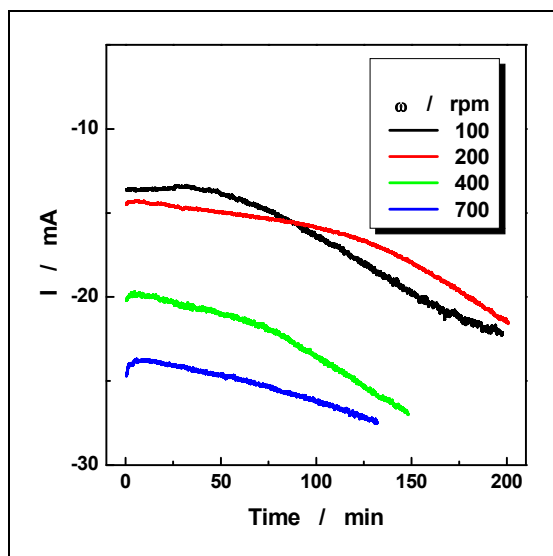
Figure 3. The evolution of the electrode current for different values
of the rotation rate (E = -200 mV/RE).

Table 2. The influence of the rotation rate on the purity
of the copper deposits (E = - 200 mV/RE).

Impurities	Rotation rate, rpm			
	100	200	400	700
Al, %	0.0017	0.0066	0.0050	-
Zn, %	0.0032	0.0027	0.0044	0.0022
Sn, %	0.0120	0.0040	0.0045	0.0040
Total, %	0.0169	0.0133	0.0139	0.0062

CONCLUSIONS

The results of our researches concerning the electrodeposition of copper from complex solutions, simulating the dissolution of the metallic part of electronic wastes in H_2SO_4, confirm the possibility of copper recovery.

The preliminary HV tests show that, at polarisation potentials more negative that -200 mV/RE, the Cu electrodeposition becomes mass transport controlled. The HV measurements completed in mixed solutions confirm that, on the studied potential domain, a Cu - Sn co-deposits can be obtained.

The experiments concerning the Cu electrorecovery in potentiostatic mode, at constant electrode rotation rate (200 rpm), showed that a polarization potential of -200 mV/RE represents the best compromise between the electrodeposition rate and deposit purity (>99.9%).

109

The measurements completed at different electrode rotation rate and a constant polarization potential (-200 mV/RE) establish that the increase of ω induce the enhancement of Cu deposit purity simultaneously with the augmentation of the electrodeposition rate.

The analyses by ICP-MS of the obtained Cu deposits show that, for all experiments, the contents of Fe, Ni, Pb have insignificant values and Al, Zn can be found in very low concentrations. Also, the purity of the obtained copper deposits is greater than 99 % in all condition.

Comparing our results with the bibliographic information [3], we can conclude that, using the potentiostatic mode and an improved mass transport, the purity of the Cu deposit can be significantly increased (around 10 times).

EXPERIMENTAL SECTION

Reagents

The electrolytes used for experiments were prepared using solid salts (analytical grade) of the corresponding metals ($CuSO_4$, $Al_2(SO_4)_3$, $FeSO_4$, $NiSO_4$, $ZnSO_4$, $PbSO_4$, $SnSO_4$) and 98 % H_2SO_4, dissolved in double distillate water. The composition of the synthetic mixed solution, including 2 M H_2SO_4 as supporting electrolyte, is presented in the Table 3 [3]. The obtained Cu deposits were dissolved in *aqua regia* (33 % v/v of 36 % HCl + 67 % v/v of 65 % HNO_3).

Table 3. The composition of the synthetic mixed solution.

Element	Cu	Al	Fe	Ni	Zn	Pb	Sn
Conc., g/L	5.0	0.056	0.045	0.041	0.050	0.061	1.91

Experimental setups

For HV tests, a glass electrochemical cell, a RDE from Pt (ϕ = 4 mm) as cathode and a Pt wire (ϕ = 0.8 mm, L = 15 mm) as anode were used. Saturated Ag/AgCl/KCl electrodes were used as reference electrodes for all experiments, including the electrorecovery test.

For electrodeposition tests, a glass electrochemical reactor (electrolyte volume of 250 cm^3) was used. The cathode was a graphite RDE, (ϕ = 10 mm, area of 0.785 cm^2) and a graphite rod (ϕ = 12 mm, L = 30 mm) was used as anode.

A PC equipped with a PCI 6024 E data acquisition board (National Instruments, USA) were used to drive a HP72 potentiostat (Wenking, Germany). The LabView 6.1 software (National Instruments, USA) was used for the process control and data acquisition.

The measurements concerning the heavy metals concentration in the obtained Cu deposit were performed with an ICP-TOF-MS Spectrometer Optimas-9500 (GBC, Australia).

REFERENCES

1. C-H. Lee, S-L. Chang, K-M. Wang, L-C. Wen, *J. Hazard. Mater*., **2000**, *73*, 209

2. J. Cui, E. Fotsserberg, *J. Hazard. Mater.*, **2003**, *99*, 243.

3. H.M. Veit, A.M. Bernardes, J.Z. Ferreira, J.A.S. Tenorio, C.F. Malfatti, *J. Hazard. Mater.*, **2006**, *B137*, 1704.

4. A. Mecucci, K. Scott, *Energy and Electrochemical Processes for a Cleaner Environment*, **2001**, 293.

5. N.P. Brandon, G.H. Kelsall, T. Muller, R. Olijve, M. Schmidt, Q. Yin, *Energy and Electrochemical Processes for a Cleaner Environment*, **2001**, 323.

6. K. Huang, J. Guo, Z. Xu, *J. Hazard. Mater*., **2009**, *164*, 399.

7. Y. Zheng, Z. Shen, S. Ma, C.Cai, X. Zhao, Y. Xing, *J. Hazard. Mater.*, **2009**, *170*, 978.

8. J. Cui, L. Zhang, *J. Hazard. Mater*., **2008**, *158*, 228.

9. J. Li, H. Lu, J. Guo, Z. Xu, Y. Zhou, *Environ. Sci. Technol.*, **2007**, *41*, 1995.

10. L. Barbieri, R. Giovanardi, I. Lancellotti, M. Michelazzi, *Environ. Chem.Lett.*, **2009**, *7,* 1610.

11. I. Masavetas, A. Moutsatsou, E. Nikolaou, S. Spanou, A. Zoikis-Karathanasis, E. A. Pavlatou, N. Spyrellis, Global NEST Journal, **2009**, in press.

12. C.G. Ilea, S.A. Dorneanu, A. Imre, P. Ilea, *Studia Universitatis Babes-Bolyai*, *Seria Chemia*, **2005**, *L,* 1, 3.

13. S.A. Dorneanu, F.L. Beke, P. Ilea, *Studia Universitatis Babes-Bolyai*, *Seria Chemia*, **2008**, *LIII,* 1, 97

14. F. Imre-Lucaci, S.A. Dorneanu, P. Ilea, *Studia Universitatis Babes-Bolyai*, *Seria Chemia*, **2009**, *LIV,* 3, 97.

ELECTROCHEMICAL IMPEDANCE CHARACTERIZATION OF POLY{N,N′-ETHYLENEBIS[N-[(3-(PYRROLE-1-YL)PROPYL) CARBAMOYL)METHYL]-GLYCINE]} MODIFIED ELECTRODES

GEORGE-OCTAVIAN BUICĂ[a], IOANA MAIOR[a], ELEONORA-MIHAELA UNGUREANU[a], DĂNUŢ-IONEL VĂIREANU[a], CHRISTOPHE BUCHER[b], ERIC SAINT-AMAN[b]

ABSTRACT. Glassy carbon disk electrodes modified with film of poly N,N′-ethylenebis[N-[(3-(pyrrole-1-yl)propyl)carbamoyl)methyl]-glycine] (polyL) have been studied by electrochemical impedance spectroscopy (EIS) in order to get a better understanding of their complexing properties towards metal ions. Investigation of the EIS equivalent circuit clearly demonstrated that the morphological structure of the polyL depends on the film thickness and of the complexing species (ions of Hg^{2+}, Cu^{2+} or Pb^{2+}) and their oxidation state as well.

Keywords: Poly(N,N′-ethylenebis[N-[(3-(pyrrole-1-yl)propyl) carbamoyl)methyl]-glycine]) films; Modified electrodes; Electrochemical Impedance Spectroscopy.

INTRODUCTION

There are numerous health problems associated with exposure to high levels of metal ions such as Cd^{2+}, Pb^{2+}, Hg^{2+}, $As^{3+/5+}$ because of their tendency to accumulate in the body, their toxicity and their low rate of clearance. For instance, the biological half-life of cadmium is 10–30 years, while that of lead in bones is more than 20 years [1]. The Environmental Protection Agency (US EPA) estimates that nearly 20 % of human exposure to lead occurs through contaminated drinking water [2]. It is therefore critical for humans to experience minimal exposure to these contaminants and to develop reliable tools allowing fast and accurate quality monitoring. Also, the great concern in recent years regarding the toxicity of mercury has contributed to the motivation for developing new electrode materials without mercury for electroanalytical applications. Such materials include various forms of carbon, widely applied as electrodes and as electrode substrates [1]. Glassy carbon has particularly played an important role in voltammetric studies due to

[a] *Faculty of Applied Chemistry and Material Sciences, University "Politehnica" of Bucharest, Gheorghe Polizu 1-7, 011031 Bucharest, Romania, em_ungureanu2000@yahoo.com*
[b] *Université Joseph Fourier Grenoble 1, Département de Chimie Moléculaire, UMR CNRS-5250, Institut de Chimie Moléculaire de Grenoble, FR CNRS-2607, BP 53, 38041, Grenoble Cedex 9, France*

its low permeability to gases, low porosity, hardness, good electrical conductivity and large accessible potential range. Carbon film electrodes, obtained by coating a substrate with a thin pyrolytic carbon layer, have recently emerged as a promising alternative form of carbon electrode. Carbon film electrodes usually exhibit large potential windows after electrochemical surface pre-treatment [3] and have been successfully applied to the development of sensors [4–10] and biosensors [11–14].

Electrochemical impedance spectroscopy (EIS) is a reliable and accurate technique perfectly suited to investigate the properties of polymeric materials [4, 5, 15, 16]. Such analyses used in connection to model circuit simulations lead to essential information concerning the ohmic resistance of the electrolyte solution, the charge transfer resistance at the solid polymer matrix / solution interface, the double layer capacitance and redox capacitance of the film and also on diffusion characteristics (diffusion coefficients of electronic and ionic charge carriers) [16].

There are two principal approaches to model the impedance of electronically conducting polymers; one describes the system as a uniform homogenous solid, while the other refers to a porous polymer membrane. In both approaches, electronic and ionic fluxes are regarded as separable participants in the whole conduction phenomena of this material. For the compact model, with a diffuse transport polarons and counter ions in the polymer layer, the charge transfer process take place at the polymer / solution interface only. This process leads to a finite diffusion low-frequency limit of the impedance, where the thickness and density of the membrane limit the diffusion rate of ions. However, the charge transfer and the interfacial charge are related to the coupled fluxes of electrons and ions [17-19]. Bard *et al.* have applied this technique to polypyrrole materials for the first time [5]. Although polypyrrole films exhibit porous structures, the authors have shown that electron transfer reactions may also occur at the polymer surface.

The synthesis of an original EDTA-like pyrrole-containing dendronic ligand, the ethylenediamine tetra-N-(3-pyrrole-1-yl)propylacetamide **L**, and the sensing properties of poly**L** coated carbon electrodes towards Hg(II) and Cu(II) cations, using the open circuit preconcentration-anodic stripping technique have been previously reported [20]. The purpose of the present work was to characterize the poly**L** glassy carbon modified electrodes by EIS.

RESULTS AND DISCUSSION

The poly**L** films have been deposited as previously shown [20], using a specific electropolymerization charge Q, and they have been investigated using EIS technique. The complex plane impedance (Nyquist diagram) and Bode plots have been recorded for the poly**L** modified glassy carbon electrodes (C/Poly**L**) of various film thicknesses, after pre-treatment in 0.1M acetate buffer solution, pH = 4.5. The electrochemical parameters have been

evaluated from the circular regression of electrochemical impedance (EI) spectra. An equivalent circuit that fits the experimental data has been proposed and the elements of the circuits have been evaluated and discussed.

a) Influence of the PolyL film thickness

The complex plane impedance (Nyquist diagram) and Bode plots for poly**L** modified glassy carbon electrodes of various film thicknesses are presented in Figures 1 and 2. From these dependencies the electrochemical parameters were evaluated by circular regression and then they were used as entry values for the fitting step.

Analyzing the Nyquist diagrams for the various film thicknesses, it can be observed that, at high frequencies, capacitive loops are obtained. The depressed semicircles are followed by diffusives regions at medium and low frequencies. This aspect shows a typical slope for Warburg impedance due to the mass transfer effects that can be interpreted as a result of the diffusion process adjacent to the electrode interface [16].

The real impedance axes intercept at high frequency agrees with the uncompensated resistance of the bulk solution (R_S) for all the data presented.

From Figure 1 it can be observed that with the increase of the electropolymerization charge Q the capacitive loop becomes wider and higher; therefore the charge transfer resistance has higher values, meaning that the composite film is thicker and more adherent.
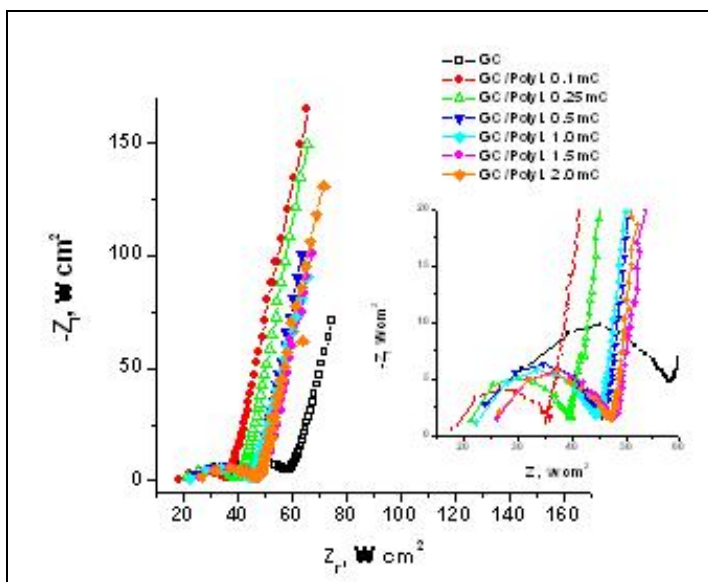
Figure 1. Complex plane impedance plots for glassy carbon and poly**L** modified glassy carbon electrodes of various film thicknesses, in 0.1 M acetate buffer solution, pH = 4.5. Inset: detail of the high frequency region.
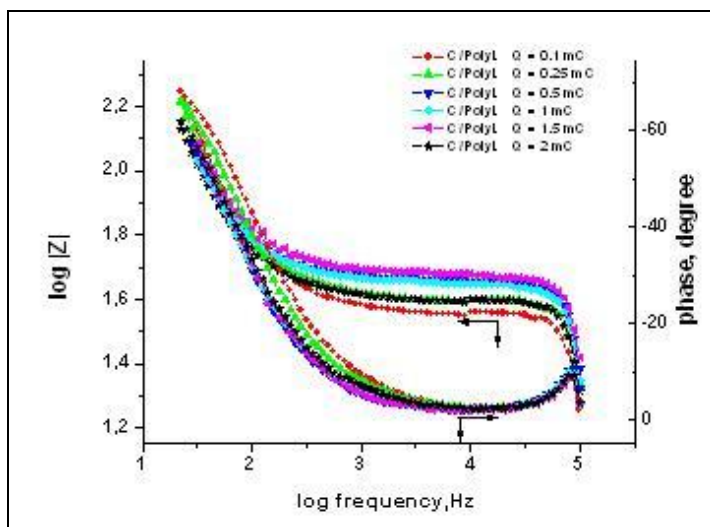
Figure 2. Bode plots for glassy carbon and poly**L** modified glassy carbon
electrodes of various film thicknesses, in 0.1 M acetate buffer solution, pH = 4.5.

The Bode diagrams from Figure 2 confirm these results. As one can notice from this figure, on the dependence of phase angle versus frequency logarithm, one maximum tends to be reached. It corresponds to a single relaxation time constant. Thus, for obtained composite films, the relaxation time constant corresponds to a phase angle between 60 and 70°, which means a capacitive behavior with slight diffusive tendency.

Capacitance values decrease when the film thickness increases (from 99 nF cm^{-2} at 0.1mC to 77.7 nF cm^{-2} at 0.5mC) reaching a minimum value for Q = 0.5mC. Beyond this minimum value, the capacitance remains constant regardless the film thickness (applied electrical charge of polymerization).
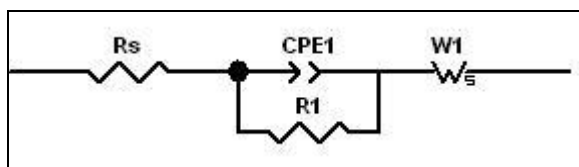
Figure 3. Equivalent circuit used to fit the impedance results: R_S – uncompensated ohmic solution resistance between working electrode and reference electrode; R_1 – charge transfer resistance of the polymer | electrolyte interface; CPE_1 - constant phase element of the polymer | electrolyte interface; W_1 – Warburg element as the diffusional control element for the polymer | electrode interface.

The equivalent circuit that fits the experimental data is shown in Figure 3. This circuit was used to fit the impedance spectra and extract the values of electrical parameters. It contains an uncompensated ohmic resistance of the electrolyte solution R_S, a sub-circuit related to the poly**L** | electrolyte interface and a Warburg element related to the GC | poly**L** interface, respectively. This circuit is inspired by the one proposed by Waller and Compton [18], but in this case we added a Warburg element that is responsible for the diffusional part of the impedance spectra of the thicker films (diffusion of ions from the bulk of the electrolyte to the interface). The constant phase CPE1 element is associated to the double layer capacitance at the polymer | electrolyte interface. CPE1 is a constant phase element with a roughness factor α_1 (where the value of 1 represents a perfectly smooth surface); this element is related to the charge capacitance or to the counter-ion accumulation at the polymer | electrolyte interface. R_1 is related to an electronic charge transfer resistance during the electrochemical process or to an ionic charge transfer resistance associated to the redox process of the polymer.

The use of CPE instead of capacitor in case of micro-heterogeneous surfaces (rough or porous) is necessary to compensate the geometrical in-homogeneity of the electrode surface. The fractional exponent α takes values between 0 and 1; for $\alpha = 0$, CPE describes an ideal resistor and for $\alpha = 1$ it describes an ideal capacitor; for $\alpha = 0.5$ it represents homogenous semi-infinite diffusion. CPE also describes the distribution of relaxation times of the process occurring in the in-homogeneous polymer film.

The results obtained by fitting the data supplied by the EI spectra into Zview modelling software containing the above proposed equivalent circuit (Figure 3) for poly**L** modified glassy carbon electrodes of various film thicknesses are shown in Table 1.

Table 1. Calculated data obtained by fitting the supplied EI spectra into a ZView modeling software analysis for C/poly**L** modified glassy carbon electrodes with various film thicknesses obtained by using different polymerization charges Q (mC).

Circuit elements \ Q, mC	0*	0.1	0.25	0.5	1	1.5	2
R_S, $\Omega \cdot cm^2$	52.7	33.25	36.82	42.6	42.95	44.25	44.45
CPE_1, $\mu F \cdot cm^{-2}$	14.51	54.8	56.54	66.72	57.65	52.20	62.18
α_1	0.93	0.95	0.96	0.97	0.97	0.99	0.97
R_1, $\Omega \cdot cm^2$	5483	1975	1761	1257	1250	808	1165
W_1-R, F	14.58	7.21	8.38	8.00	8.59	9.26	7.41
W_1-T$\cdot 10^3$, s$\cdot$rad^{-1}	0.258	0.517	0.655	0.793	0.708	0.732	0.672
W_1-P, Ω s$^{-1/2}$	0.435	0.444	0.447	0.446	0.438	0.443	0.446

*bare glassy carbon electrode

The charge transfer resistance R1 for C/poly**L** modified electrodes is lower than for bare glassy carbon. This implies that the charge transfer process is relatively fast compared to the bare glassy carbon.

The film morphology affects the impedance responses due to the interactions between specific interfaces (polymer | electrolyte interface and electrode | polymer interface) when the polymer is in its oxidized or reduced form. In the case of low porosity (high values for α_1), the charge transfer resistance (R1) is higher and can control the impedance response. If the film is very porous (roughness factor α_1 is near 0), the surface of the electrode | electrolyte interface is larger relatively to the electrode | polymer interface, and the charge transfer between the metal and the electrolyte is favoured in appropriate conditions. From Table 1 it can be seen that the values of α_1 characteristics of the polymer | electrolyte interface are essentially unchanged by the film thickness. Meanwhile, in the full range of measured frequencies, the impedance phase and module values are dependent on the films morphology, being controlled by the electrical charge of synthesis. Thus, the diffusional phenomena are visible in all the recorded spectra due to the Warburg impedance that remains constant whatever the film thickness.

b) Influence of the metal ion nature

The influence of the complexing ions nature absorption during the accumulation stage was investigated for poly**L**–coated film glassy carbon electrodes which were complexed with Hg^{2+}, Cu^{2+} or Pb^{2+} ions to see if they exhibit any alterations of the electrochemical impedance parameters. Before the electrochemical impedance measurements, the modified electrode (obtained using 0.5mC polymerization charge) was soaked for 20 minutes under stirring in 10^{-5}M Hg^{2+}, Cu^{2+} or Pb^{2+} ions acetate buffer solution, then the EI spectra were recorded at open circuit potential (OCP).

The impedance spectra (Nyquist and Bode plots) are shown in Figures 4 and 5 and the analysis of the experimental results is given in Table 2 using the equivalent circuit shown in Figure 3.

After recording these EI spectra, the poly**L** modified electrodes containing Hg^{2+}, Cu^{2+} or Pb^{2+} ions were submitted to controlled potential electrolysis (CPE) for 3 minutes in order to reduce the metallic ions. The reductions of metal ions were performed at -1.8; -1.4 and -0.9V for Hg, Pb and Cu, respectively. After reduction the EI spectra (Figures 6 and 7) were recorded at OCP. The analysis of the results is given in Table 2 using the same equivalent circuit as for the modified electrodes in absence of metal ions (Figure 3).

Comparison of the EI spectra from Figure 4 shows that, although the impedance is greater in the presence of Hg^{2+}, Cu^{2+} or Pb^{2+} ions than in their absence, the shape of the spectra is not altered by the presence of

metal ions in the polymer film. The larger impedance values in the presence of metal ions than in their absence reflects a higher charge transfer resistance (due to the partial blocking of the polymer film near the electrode surface by the metal) and a lower value of the capacitance C ($C_{polyL-M}^{z+} < C_{polyL}$). This feature could be attributed to the formation of a more stable passive layer, which is the complexed film.
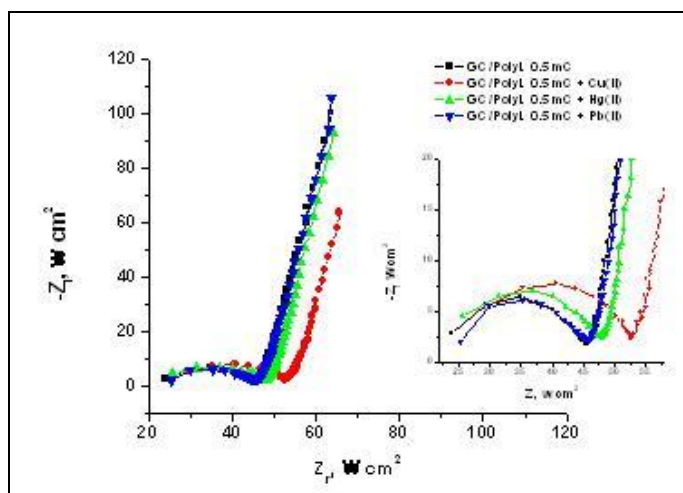

Figure 4. Complex plane impedance plots for C/poly**L** modified electrodes after complexation with 10^{-5} M Hg^{2+}, Cu^{2+} and Pb^{2+} in 0.1 M acetate buffer solution (pH = 4.5). Inset: detail of the high frequency region.
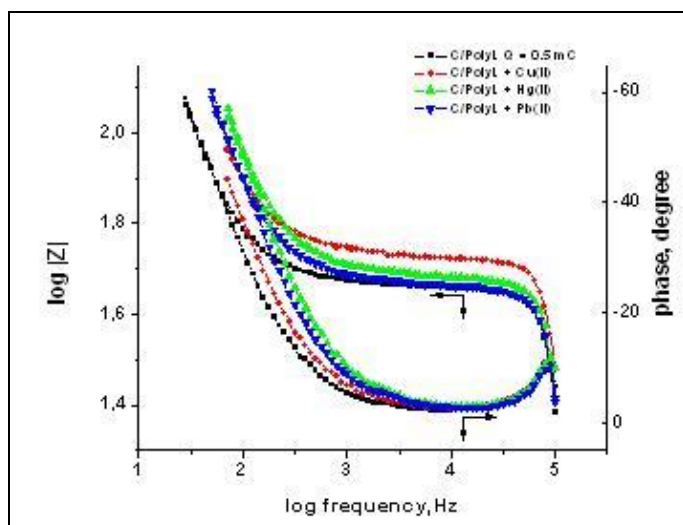
Figure 5. Bode plots for C/poly**L** modified electrodes after complexation with 10^{-5} M Hg^{2+}, Cu^{2+} and Pb^{2+} in 0.1 M acetate buffer solution (pH = 4.5).

119

From Table 2, one can also notice that the capacitance is irreversibly decreased after metal ion insertion. Variations in double layer capacitance CPE1 and α_1 values with addition of metal ions confirms the changing of the morphology of the modified electrode surface due to the polymer / metal ions interactions. The lowest value of double layer capacitance CPE1 in case of C/poly**L** – Hg^{2+} modified electrode confirms the formation of a more stable passive layer by addition of this complexing ion, than in the case of Cu^{2+} and Pb^{2+}. This behavior is in agreement with the better complexation properties of the poly**L** film toward Hg^{2+} which were found by other methods [21].
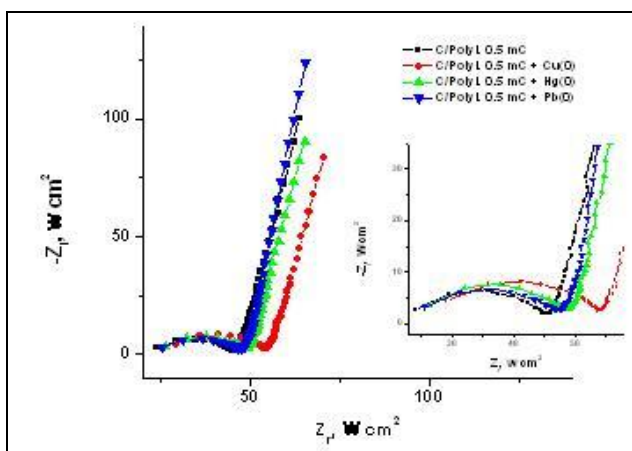
Figure 6. Complex plane impedance plots for C/poly**L** modified electrodes after complexation and reduction of Hg(II), Cu(II) and Pb(II) ions. Inset: detail of the high frequency region
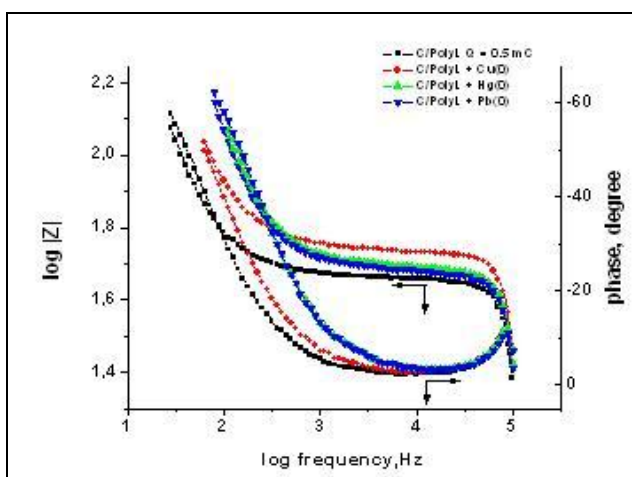
Figure 7. Bode plots for C/poly**L** modified electrodes after complexation with Hg^{2+}, Cu^{2+} and Pb^{2+} and reduction of the ions

Table 2. Calculated data obtained by fitting the supplied EI spectra into a ZView modeling software analysis for 0.5 mC C/poly**L** modified glassy carbon electrodes after complexation with Hg^{2+}, Cu^{2+} and Pb^{2+} and reduction

Complexed species\ Circuit elements	None	Cu^{2+}	Cu^0	Hg^{2+}	Hg^0	Pb^{2+}	Pb^0
R_S, Ω cm^2	42.6	49.42	50.41	44.63	45.17	42.83	44.35
CPE_1, μF cm^{-2}	66.72	55.48	44.36	38.65	23.99	44.51	25.89
α_1	0.97	0.93	0.94	0.93	0.93	0.94	0.94
R_1, Ω cm^2	1257	5855	4817	9009	8736	5153	4223
W_1-R, F	8.00	8.76	9.23	7.47	7.87	7.72	7.23
W_1-T$\cdot 10^3$, s rad^{-1}	0.793	0.654	0.576	0.441	0.320	0.508	0.337
W_1-P, Ω s$^{-1/2}$	0.446	0.442	0.444	0.449	0.451	0.448	0.461

After the metal ion reductions, the charge transfer resistance R_{ct} remains higher than the initial value of the modified electrodes before the metal ion insertion (Table 2). The observed increase of the charge transfer resistance R_{ct} after ions reduction may suggest that the modified electrodes in contact with heavy metals have increased values of the conductivity.

In Figures 8 and 9 are given, as example, the Nyquist and Bode plots for modified electrodes with poly**L** films before and after complexation with Hg^{2+}, and also after reduction of Hg^{2+} to Hg^0. They reflect the influence of Hg^{2+}/Hg^0 on the EI parameters of C/poly**L** modified electrodes.
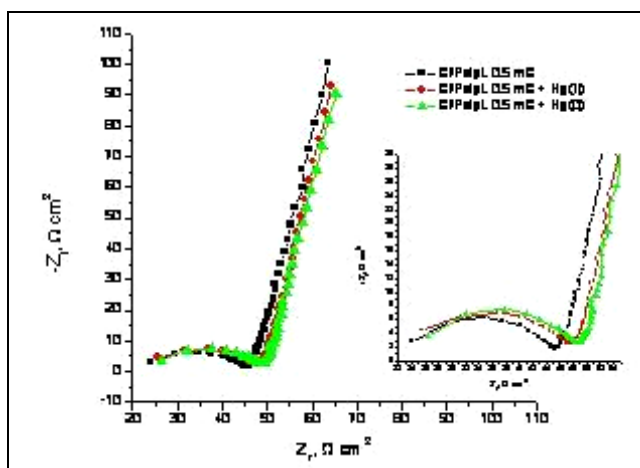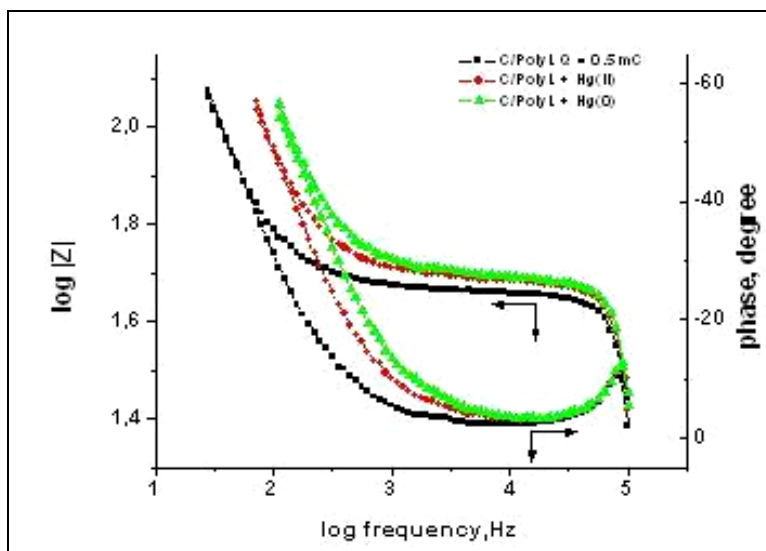

Figure 8. Complex plane impedance plots for C/poly**L** modified electrode (0.5mC) in 0.1 M acetate buffer solution (*p*H = 4.5) (■), after complexation in 10^{-5} M Hg^{2+} (●), and after the reduction of the Hg(II) ions (▲).
Inset: detail of the high frequency region

Figure 9. Bode plots for C/poly**L** modified electrode (0.5mC) in 0.1 M acetate
buffer solution (*p*H = 4.5) (■), after complexation in 10^{-5} M Hg^{2+} (●),
and after the reduction of the Hg(II) ions (▲)

CONCLUSIONS

The poly**L** glassy carbon modified electrodes (C/poly**L**) were characterized
by electrochemical impedance spectroscopy (EIS). The modifications of the
glassy carbon electrode by various electropolymerization charges lead to the
formation of polymer films with different morphologies on the electrode surface
depending on their thicknesses. The bulk of the material also contribute to the
increase of the total impedance due to the presence of a diffusional control of
the ions through the polymer matrix (characterized by the Warburg element at
lower frequencies) and to the charge accumulation at very low frequencies
(characterized by the limiting capacitance of the film).

The EIS behavior was also investigated for the complexed C/poly**L**
electrodes obtained by immersion of C/poly**L** in Hg^{2+}, Cu^{2+} and Pb^{2+} solutions.
Their EIS parameters are different in comparison with the non-complexed
C/poly**L** electrodes. Electrochemical impedance spectroscopy has shown that
the complexation with heavy metal ions does not affect the shape of the
Nyquist plots, but it influences the electrochemical parameters. A selective
behavior of the C/poly**L** modified electrodes for Hg^{2+} ions against other heavy
metal ions (Cu^{2+}, Pb^{2+}) was found. The Hg^{2+} metal ions determine a high
modification of the charge transfer resistance and a decrease of the double
layer capacitance.

EXPERIMENTAL SECTION

1. Reagents and Materials

The synthesis of (N,N'-ethylenebis[N-[(3-pyrrole-1-yl) propyl)carbamoyl) methyl]-glycine) (**L**) was performed according to a previously reported procedure [20]. Acetonitrile (Rathburn, HPLC grade S) was used as received. Tetra-n-butylammonium perchlorate (TBAP, Fluka puriss) was dried under vacuum at 80°C for 3 days. Suprapur grade sodium acetate and acetic acid (Merck) were used to prepare 0.1 mol L^{-1} acetate buffers. Copper(II) acetate - $Cu(CH_3CO_2)_2,H_2O$, lead(II) nitrate - $Pb(NO_2)_2$, mercury(II) acetate - $Hg(CH_3CO_2)_2$ were used as source of metal ions. Copper(II) acetate and lead(II) nitrate were from Prolabo. Mercury(II) acetate was purchased from Strem. All reagents were used without further purification. Perchloric acid was obtained from Merck. Distilled water was obtained from an Elgastat water purification system (5 MΩ cm).

2. Electrochemical Equipment

The experiments were performed with a PG STAT 12 Autolab potentiostat, using a conventional three-electrode system. The working electrode was a modified carbon disk (3 mm diameter, from CH Instruments). The counter electrode was a platinum wire. The reference electrode used for electropolymerizations was an Ag/10 mM $AgNO_3$, 0.1 M TBAP, CH_3CN while that used for electroanalytical and EIS experiments was a conventional Ag/AgCl electrode. Electrochemical impedance spectroscopy (EIS) measurements were carried out using a VoltaLab 40 – PGZ 301 Potentiostat controlled with a VoltaMaster v 4.0 software. A Denver-Instrument Model 220 pH-conductivity meter was used to measure pH.

3. Preparation of the Modified Electrodes

Prior to electropolymerization, glassy carbon disk working electrodes were polished with 0.2 µm diamond paste. Electropolymerization was performed by controlled potential electrolysis (CPE) at a potential of +0.9 V/(Ag/Ag$^+$) until reaching the desired charge. Poly**L** films were grown on glassy carbon disk electrodes in solution of **L** (10^{-3}M) in 0.1mol L^{-1} TBAP, acetonitrile containing two-molar equivalents of $HClO_4$, using the previously described procedure [20]. Films with Γ_L values between 8×10^{-10} and 2×10^{-9}mol cm^{-2} were typically obtained using polymerization charges of 0.3 to 1mC. Apparent surface coverages in complexing sites Γ_L (mol cm^{-2}) were determined from the charge recorded under the polypyrrole oxidation wave measured by cyclic voltammetry (CV) at the scan rate of 2mV/s, taking into account that one ethylenediaminotetracetamide group is attached to 2 pyrrole rings and assuming that one in three pyrrole units is oxidized [22].

Modified polypyrrole films usually exhibit high background currents leading to major limitations of the electrochemical window and thereby making metal detection difficult [23]. A straightforward solution to this problem was to overoxidize polypyrrole [24-26]. Before each analytical experiment, the pyrrole-based electroactivity was therefore destroyed upon cycling the electrode potential (5 cycles) between -0.2 V and +1.2 V in a buffer acetate (pH = 4.5). This treatment leads to C/poly**L** modified electrodes covered with non-conducting polymer which were used for the electrochemical investigation.

4. Accumulation and Voltammetric Procedures

Accumulation of metal ions into poly**L** films was carried out at open circuit upon dipping C/poly**L** modified electrodes for a given time into 5 mL of a stirred buffer solution at pH = 4.5 containing a given metal salt. The electrodes were then removed from the accumulation cell and thoroughly washed with purified water to remove uncomplexed ions from the modified electrode surface. After transferring the latter into an electroanalytical cell containing 0.1M acetate buffer solution, the accumulated metal ions were subjected to electrochemical impedance spectra (EIS). The EI spectra were also recorded after 3 minutes reduction of the complexed modified electrodes at specific potential for each complexed cation (-1.8; -1.4 and -0.9V for Hg, Pb and Cu, respectively).

5. Electrochemical Impedance Measurements

EIS measurements with C/poly**L** modified electrodes were carried out in a three electrode cell configuration. The working electrode was the poly**L** modified glassy carbon disk electrode (3 mm diameter), the counter electrode was a platinum wire and the reference electrode was Ag/AgCl. EIS measurements were performed in the frequency range from 100 kHz to 500 MHz with an amplitude perturbation of 30 mV at OCP.

REFERENCES

1. R. A. Goyer, "Toxicology, The Basic Science of Poisons fifth ed.," McGraw-Hill, New York, **1996**.

2. http://www.epa.gov/safewater/lead/leadfacts.

3. C. M. A. Brett, L. Angnes, H. D. Liess, *Electroanalysis*, **2001**, *13*, 765.

4. O. M. S. Filipe, C. M. A. Brett, *Electroanalysis*, **2004**, *16*, 994.

5. C. Gouveia-Caridade, C. M. A. Brett, *Electroanalysis*, **2005**, *17*, 549.

6. O. M. S. Filipe, C. M. A. Brett, *Talanta*, **2003**, *61*, 643.

7. R. Pauliukaite, C. M. A. Brett, *Electroanalysis*, **2005**, *17*, 1354.

8. R. Pauliukaite, M. Florescu, C.M.A. Brett, *Journal of Solid State Electrochemistry*, **2005**, *9*, 354.

9. R. Pauliukaite, M. E. Ghica, C. M. A. Brett, *Analytical and Bioanalytical Chemistry*, **2005**, *381*, 972.

10. C. Gouveia-Caridade, C. M. A. Brett, *Journal of Electroanalytical Chemistry*, **2006**, *192*, 113.

11. M. E. Ghica, C. M. A. Brett, *Analytical Letters*, **2005**, *38*, 907.

12. M. Florescu, C. M. A. Brett, *Talanta*, **2005**, *65*, 306.

13. R. Pauliukaite, A. M. Chiorcea-Paquim, A. M. Oliveira-Brett, C. M. A. Brett, *Electrochimica Acta*, **2006**, *52*, 1.

14. M. E. Ghica, C. M. A. Brett, *Electroanalysis*, **2006**, *18*, 748.

15. T. Zalewska, A. Lisowska-Oleksiak, S. Biallozor, V. Jasulaitiene, *Electrochimica Acta*, **2000**, *45*, 4031.

16. M. Martinia, T. Matenciob, N. Alonso-Vantec, M. A. De Paoli, *Journal of the Brazilian Chemical Society*, **2000**, *11(1)*, 50.

17. R. A. Bull, F. R. F. Fan, A. J. Bard, *Journal of the Electrochemical Society*, **1982**, *129(5)*, 1009.

18. A. M. Waller, R. G. Compton, *Journal of the Electrochemical Society (Faraday Transactions)*, **1989**, *85(4)*, 977.

19. A. Sezai Sarac, M. Ates, B. Kilic, *International Journal of the Electrochemical Science*, **2008**, *3*, 777.

20. M. Heitzmann, C. Bucher, J.-C. Moutet, E. Pereira, B.-L. Rivas, G. Royal, E. Saint-Aman, *Electrochimica Acta*, **2007**, *52*, 3082.

21. G.-O. Buica, *PhD Thesis,* University Politehnica of Bucharest, **2009**.

22. G. K. Chandler, D. Pletcher, "Electrochemistry, Specialist Periodical Reports", Royal Society of Chemistry, London, 1986, 117 – 150.

23. A. Wanekaya, O. A. Sadik, *Journal of Electroanalytical Chemistry*, **2002**, *537*, 135.

24. D. W. M. Arrigan, D. S. Gray, *Analytica Chimica Acta*, **1999**, *402*, 157.

25. H. Shiigi, H. Yakabe, M. Kishimoto, D. Kijima, Y. Zhang, U. Sree, B. A. Deore, T. Nagaoka, *Microchimica Acta*, **2003**, *143*, 155.

26. H. Shiigi, D. Kijima, Y. Ikenaga, K. Hori, S. Fukazawa, T. Nagaoka, *Journal of the Electrochemical Society*, **2005**, *152*, 129.

DETECTION OF ELECTROACTIVE PRODUCTS RESULTED FROM ELECTROCHEMICAL NITRATE REDUCTION IN ALKALINE MEDIA

FLORINA MARIA BĂLAJ[a], FLORICA IMRE-LUCACI, SORIN AUREL DORNEANU, PETRU ILEA

ABSTRACT. Nowadays, the damage of the environment quality has reached alarming levels requiring severe measures for stopping this process. In order to harmonise with the maximum admitted concentrations of nitrate in the discharged effluents, the electrochemical procedures represent a clean, flexible and efficient alternative of decontamination. Electrochemical reduction of nitrate/nitrite (ERNN) can be advantageously applied to the treatment of industrial waste water, whereby this species can be transformed into harmless products. In this context, the present paper describes the results of our researches concerning the design of an original technique for on-line detection of electroactive products resulted from ERNN in alkaline media. The obtained results shows that, using an adequate pH value, at least three electroactive species generated from the NO_3^- reduction (NO_2^-, NH_2-OH and NH_4^+) could be electrochemically detected at different applied potentials on the Pt-ring electrode.

Keywords: nitrate, nitrite, waste waters, electroactive products detection

INTRODUCTION

The interest for the nitrate/nitrite removal results from the high concentration of this ions in the surface and subterranean water streams and the need to reduce this dangerous pollution [1]. The main source of this pollution are industrial wastewater and, in some areas, the intensive agriculture. The problem of nuclear waste treatment represents another aspect of NO_3^- removal because this ion significantly increases the volume of waste and has a negative impact on the waste cohesion after solidification [2].

The maximum contaminant level (MCL) of nitrate in the potable water is 45 mg/L in the United States, while the European Union legislation admits a maximum level of 50 mg/L for drinking water [2, 3]. Various methods such as biological, physicochemical, etc. have been proposed for the removal of nitrate from potable water and wastewaters. Even the biological denitrification represent the most used method, it has several disadvantages e.g. it is slow,

---

[a] *Department of Physical Chemistry, "Babes-Bolyai" University, 11 Arany Janos, 400028 Cluj-Napoca, Romania, florinabalaj@chem.ubbcluj.ro*

difficult to control, produces organic residues and requires intensive maintenance and a constant supply of the organic substrate [4]. The physicochemical processes such as ion exchange [5], reverse osmosis [6] and electrodialysis [7] produce secondary brine wastes, because the nitrates are merely separated but not destroyed. The reduction of the nitrate/nitrite is another mean for removing these ions from polluted waters.

The electrochemical reduction of nitrate/nitrite represents an attractive and promising solution due to its convenience, environmental friendliness, and low cost effectiveness [8]. Nitrate electroreduction leads to the coexistence of several more or less stable intermediate products like nitrite, hydrazine, hydroxylamine, ammonia, nitrogen and other oxygen-containing nitrogen species [9]. From a practical and an environmental point of view, it is highly desirable that the electrochemical process transform nitrate efficiently and selectively into the harmless N_2 gas.

Using the electrochemical reduction of nitrate/nitrite (ERNN), the final compounds composition depends mainly on the electrolyte pH, the applied potential and the used cathode material. On the other hand, electrochemistry provides promising solutions when it is combined with ion exchange, the last one being capable of NO_3^- selective removal from the treated water.

The nitrate reduction using a copper electrode, in alkaline media, represents an interesting option because this system is less liable to produce oxides of nitrogen as by-products [10, 11, 12, 13], but, in this case, ammonia represents the main product. The use of other electrode materials (Cu-Sn alloys [14], Rh [15], Sn [16], Pd-Cu alloys [17]) allows the selectively reduction of nitrate/nitrite ions into the harmless N_2 gas. Nevertheless, the ERNN process requires fast and easy monitoring method of generated species.

In this context, in our work, we evaluate the possibility of on-line detection of electroactive products resulted from ERNN in alkaline media: NH_3, NO_2^- and NH_2-OH.

The electrochemical measurements were carried out in unconventional conditions, combining the cyclic voltammetry at relative high scan rate (500 mV/s) with the controlled hydrodynamic mass transport using a Pt/Pt or Pt/Cu rotating ring-disk electrode (RRDE). This original technique will be named cyclic hydrodynamic voltammetry (CHV).

RESULTS AND DISCUSSION

Detection of electroactive species in mono-component solutions

In order to evaluate the possibility of electrochemical detection of electroactive products resulted from ERNN in alkaline media, we perform preliminary studies in mono-component solution.

The CHV measurements were completed using the Pt ring as working electrode, at a scan rate of 500 mV/s and a rotation speed of 1000 rpm. In order to assure the desorption of adsorbed species on the electrode surface, the electrode potential was scanned between – 1.5 and +2.0 V/RE. For each studied species, the electrochemical cell was firstly filled with 100 mL of 1 M Na_2SO_4 as supporting electrolyte after that different amounts of NO_2^-, NH_2-OH and NH_4^+ concentrated solutions were added successively (resulting concentration of 0.1, 0.5, 1.0, 2.0 g/L). Before each experiment, the pH value of the prepared solutions was adjusted at 11 using 1 M NaOH solution.

The details including the anodic and cathodic peaks corresponding to the voltammograms recorded in the presence of different concentrations of NO_2^- and NH_2-OH are presented in Figure 1 and Figure 2.
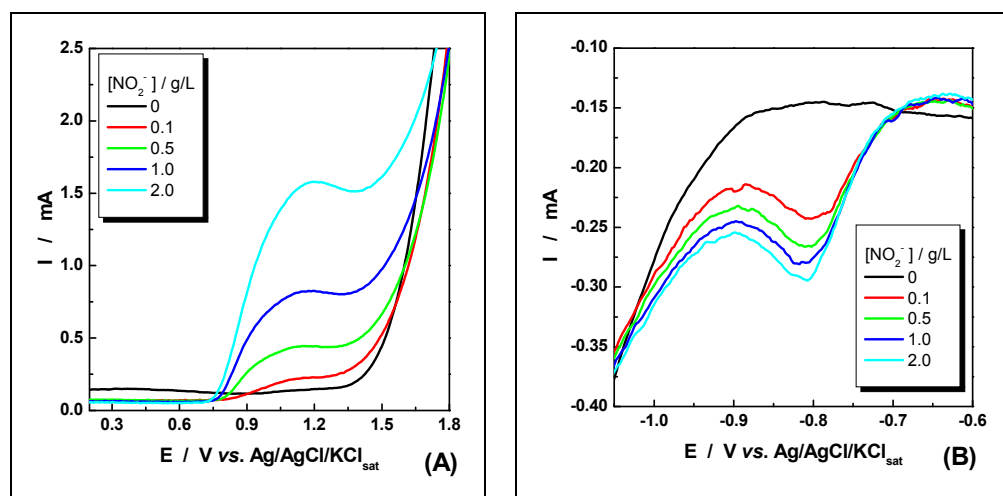
Figure 1. Influence of NO_2^- concentrations on the corresponding anodic (A) and cathodic (B) peak currents recorded by CHV. (Disk electrode disconnected).

As it can be seen from Figure 1, in monocomponent solutions, nitrite presents oxidation peaks close to + 1.2 V/RE and cathodic peaks at – 0.8 V/RE. The corresponding peak currents are proportional with the nitrite concentrations.

Similarly, hydroxylamine (see Figure 2), in monocomponent solutions, presents oxidation peaks near + 1.3 V/RE and cathodic peaks around – 0.9 V/RE. Also, the corresponding peak currents are proportional with the hydroxylamine concentrations.

Comparing Figure 1 and 2, it can be observed that both species present similar oxidation and reduction peaks' potentials, causing difficulties for individual ion detection. From another point of view, for the same concentration, the peak current values corresponding to the hydroxylamine oxidation and reduction are 4, respectively, 8 times higher than the corresponding peak currents recorded for nitrite.
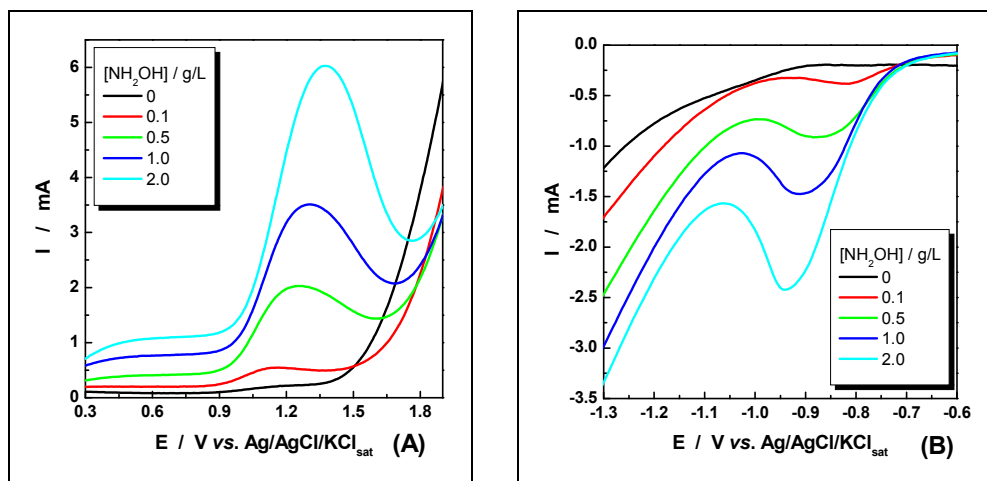
Figure 2. Influence of NH_2-OH concentrations on the corresponding anodic (A) and cathodic (B) peak currents recorded by CHV. (Disk electrode disconnected).

The details including the anodic peaks related to the voltammograms recorded in the presence of different concentrations of ammonium are presented in Figure 3.
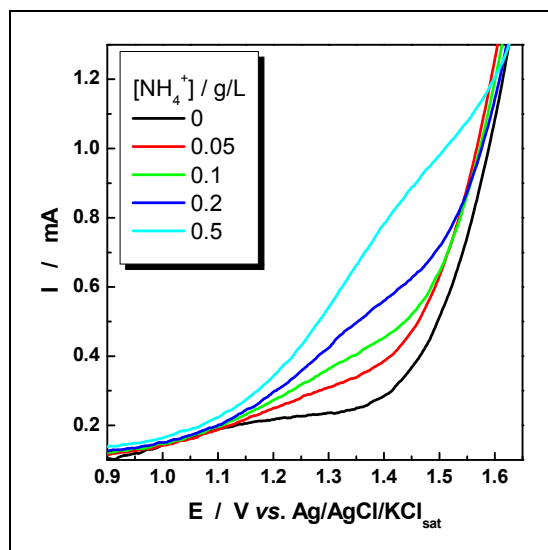

Figure 3. Influence of NH_4^+ concentrations on the anodic peak currents recorded by CHV. (Disk electrode disconnected).

As it can be seen from Figure 3, due to the fact that, at pH= 11, the ratio between NH_3:NH_4^+ is 40:1, ammonium can be electrochemically detected by ammonia oxidation at potentials over + 1.4 V/RE.

Starting from the presented results, we tray to perform similar measurements in mixed solutions, containing different concentrations of NO_2^-, NH_2-OH and NH_4^+. The obtained results (not shown in this paper) demonstrated that the invoked species interact among themselves, making very difficult their individual detection.

Detection of electroactive species generated by nitrate reduction

In order to evaluate the possibility of electrochemical detection of electroactive products resulted from ERNN in alkaline media by CHV, a consecrated working disk electrode of Cu was used. This choice was based on the fact that, on this material, depending on the applied potential, a wide variety of species can be generated. For a real and accurate comparison, before each set of CHV measurements, the surface of the Pt rotating disk electrode was covered with a thin layer (0.5 μm) of freshly electrodeposited cooper. A 45 g/L $CuSO_4$ solution in 177 g/L H_2SO_4 was used for Cu electrodeposition and also for the complete removing of the previous Cu layer by anodic dissolution. The amount of copper on the surface of the Pt rotating disk electrode was controlled by the charge quantity used for electrodeposition.

For each set of measurements, the working disk electrode (Pt covered with Cu) was polarised at a constant potential value, fixed between -0.7 and -1.8 V/RE, with 0.1 V increment. The potential applied to the Pt ring electrode was cycled between -1.5 and +2.0 V/RE at a scan rate of 500 mV/s, recording 8 successively cycles without Cu layer refreshing. The measurements were performed in a 2 g/L NO_3^- solution containing 1 M Na_2SO_4 as supporting electrolyte (pH = 11), at a rotation speed of 1000 rpm.

In order to evaluate the electrocatalytic stability of Cu layer towards ERNN, we compare the anodic currents recorded on the Pt ring electrode, corresponding to the oxidation of the disk generated species. For example, Figure 4 presents details of the currents recorded on the Pt ring electrode during the anodic scans, for 3 different disk polarisation potentials. In order to assure a better visibility, only the anodic portions from the 1st, 2nd, 4th and 8th cycles are presented. It can be observed that, for all presented potentials, every first cycle indicates a maximum electrocatalitic activity of the freshly copper disk electrode, which decreases rapidly for the following recorded voltamograms. The decrease of the copper electrode electroactivity upon the first seconds (one complete cyclic scan take 14 s) may be related to the adsorption of hydrogen and nitrate reduction products [18]. We can conclude that the Cu disk electrode surface can be rapidly poisoned by the reduced products and presents a poor stability, requiring a periodic surface refreshing.
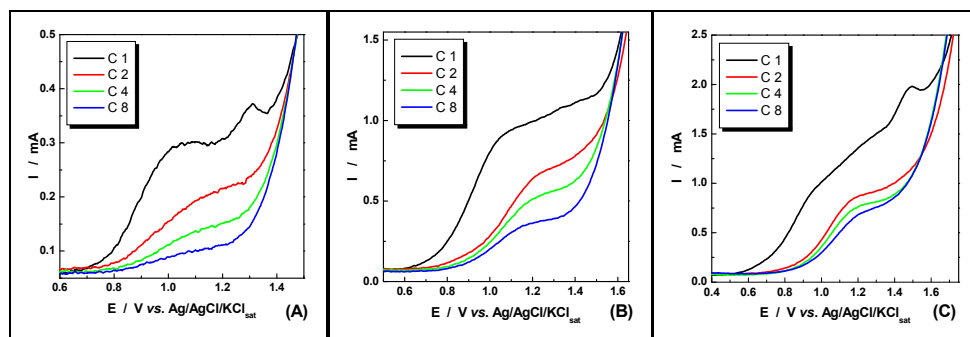
131

Figure 4. Influence of progressive poisoning of Cu disk surface on the oxidation currents recorded by repeated CHV on the Pt ring, at different disk polarisation potentials: (A) -0.9 V, (B) - 1.2 V. and (C) – 1.4 V.

Based on previous obtained information, we start a detailed study concerning the influence of the polarization potentials of the Cu disk electrode on the ERNN product composition. The anodic current of the voltamograms, corresponding for every first cycle recorded at different values of the applied potential on the Cu disk electrode, are presented in Figure 5.
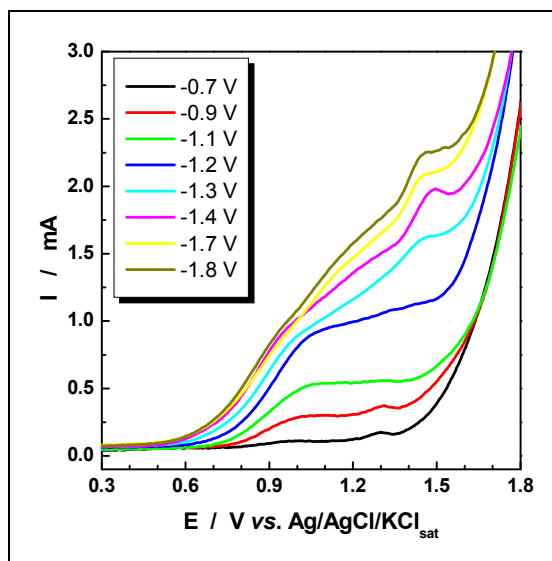
Figure 5. Influence of the polarization potential of Cu disk electrode on the oxidation currents recorded by CHV on the Pt ring electrode. The figure presents only the first anodic scan after the disk surface renewing by Cu electroplating

As expected, the nitrate reduction rate and the ratio between the amounts of the resulted species strongly depend of the applied potential. The decrease of disk applied potential to more negative values determines the increase of the ring currents corresponding to the detection of the generated species on the Cu electrode.

It is worth to note that, depending on the disk applied potential, different electroactive species can be detected at specific ring polarization potentials. For example, at potential values applied on the disk electrode more positive than -1.1 V/RE, two oxidation peaks can be observed, corresponding to nitrite and hydroxylamine oxidation. If the applied potential on the Cu electrode ranges among -1.1 and -1.3 V/RE, the interaction between the electrogenerated species makes complicated the detection of these compounds. For disk potentials more negative than -1.3 V/RE (corresponding to "hydrogen domain"), a net peak corresponding to ammonia oxidation can be observed at ring potentials around +1.5 V.

CONCLUSIONS

The results of our researches concerning the on-line detection of electroactive products resulted from ERNN in alkaline media allow us to formulate the following conclusions:

- The measurements performed in monocomponent solutions proved that, combining cyclic voltammetry at high scan rates with hydrodynamic techniques and using an adequate pH value, at least three electroactive species generated from the NO_3^- reduction (NO_2^-, NH_2-OH and NH_4^+) could be electrochemically detected at different applied potentials on the Pt-ring electrode.
- The designed technique was tested using a Cu disk electrode (one of the most used electrode material for ERNN), demonstrating the ability of *on-line* detection of the invoked species.
- The voltammograms, recorded successively without Cu layer refreshing, demonstrated that the electrocatalytic activity of this electrode material decreases very fast (in few seconds), requiring additional studies concerning the synthesis of new electrode materials with increased stability and/or the periodic reactivations of the electrode surface.

EXPERIMENTAL SECTION

Reagents

The solutions were prepared using analytical grade solid reagents ($NaNO_3$, $NaNO_2$, $(NH_3OH)_2SO_4$, $(NH_4)_2SO_4$ and Na_2SO_4) and double-distilled water. 1 M Na_2SO_4 was used as supporting electrolyte for all measurements.

Before each experiment, the pH value of the prepared solutions was adjusted at 11 using 1 M NaOH solution. All measurements were made at room temperature (298±1 K).

Experimental setups

Electrochemical measurements were carried out in controlled hydrodynamic conditions using a Pt/Pt and Pt/Cu rotating ring-disk electrode (Radiometer, France; ring: ID = 4.2 mm, OD = 4.8 mm; disk: ϕ = 4 mm). The CE was a Pt wire (ϕ = 0.8 mm, L = 15 mm) and an Ag/AgCl/KCl$_{sat}$ system was used as reference electrode (RE). A fully computer controlled home-made bipotentiostat and applications elaborated with the Labview 8.5 software were used for experimental parameter's control and data acquisition.

ACKNOWLEDGEMENTS

REFERENCES

1. The Nitrate Directive of European Council 91/676/EHS.
2. J.O'M. Bockris and J. Kim, *Journal of Applied Electrochemistry,* **1997**, *27*, 623
3. N. F. Gray, „Drinking Water Quality: Problems and Solutions", J. Wiley & Sons Ltd. Chichester, **1994**, 21.
4. M. I. M. Soares, *Water, Air and Soil Pollution*, **2000**, *123*, 183.
5. **W**orld **H**ealth **O**rganization (WHO), Rolling Revision of the WHO Guidelines for Drinking-Waters Quality, Nitrates and Nitrites in Drinking-Waters, WHO Ed., **2004**.
6. J. J. Shoeman and A. Steyn, *Desalination*, **2003**, *155*, 15.
7. K. M. Hiscock, J. V. Lloyd and D. N. Lemer, *Water. Research*, **1991**, *25*, 1099.
8. L. Panyor and C. Fabiani, *Desalination,* **1996**, *104*, 165.
9. K. N. Mani, *Journal of Membrane Science,* **1991**, *38*, 117.
10. M. Paidar, I. Rouar and K. Bouzek, *Journal of Applied Electrochemistry*, **1999**, *29*, 611.
11. S. Cattarin, *Journal of Applied Electrochemistry*, **1992**, *22*, 1077.
12. C. Polatides and G. Kyriacou, *Journal of Applied Electrochemistry*, **2005**, *35*, 421.
13. G. E. Badea, *Electrochimica Acta*, **2009**, *54*, 996.
14. Z. Mácová, K. Bouzek, J. Šerák, *Journal of Applied Electrochemistry*, **2007**, *37*, 557.
15. P. M. Tucker, M. J. Waite, B. E. Hayden, *Journal of Applied Electrochemistry*, **2004**, *34*, 781.
16. I. Katsounaros, G. Kyriacou, *Electrochimica Acta*, **2007**, *52*, 6412-6420.
17. A.C.A. de Vooys, R.A. van Santen, J.A.R. van Veen, *Journal of Molecular Catalysis A*, **2000**, *154*, 203.
18. G. Denuault, C. Milhano, D. Pletcher, *Physical Chemistry Chemical Physics*, **2005**, *7*, 3545.

STUDY OF HYDROGEN PEROXIDE ELECTROSYNTHESIS ON ELECTROCHEMICALY MODIFIED GRAPHITE USING A WJRDE

CODRUȚA VLAIC[a], SORIN AUREL DORNEANU[a], PETRU ILEA[a]

ABSTRACT. The hydrogen peroxide electrosynthesis by partial reduction of oxygen represents an attractive alternative to the anthraquinone process. The result presented in this paper show that the two steps electro-activation of a graphite electrode, consisting in the oxidizing of the surface followed by the partial reduction of the active sites generated upon oxidation, induces an improvement of hydrogen peroxide electrosynthesis efficiency. Because the stability of the generated active sites is limited, a special programmable cyclic multi-step technique was used and the experimental parameters were optimized for a rectangular shape applied potential. In order to understand the electrosynthesis mechanism and to optimize the electro-activation potentials, cyclic hydrodynamic voltammetry studies were performed. For all the measurements, a wall-jet ring disk electrode was used.

Keywords: oxygen reduction, hydrogen peroxide electrosynthesis, electrochemical activation, graphite.

INTRODUCTION

The hydrogen peroxide (HP) is an environmental friendly oxidizing agent with many applications in the pulp industry, organic and inorganic synthesis and waste water treatment [1, 2, 3, 4, 5]. It is worth to note the exceptional ability of HP for pollution control due to the fact that it is transformed into noncontaminant products such as water and oxygen. For example, HP can reduce the environmental impact caused by chlorine based oxidants. In wastewater treatment, HP can oxidize organic pollutants to CO_2, offering, in comparison to traditional biodegradation methods, several advantages in terms of treatment rate, cost and availability [3].

Presently, HP is produced mainly by the "anthraquinone process" (AqP). The electrochemical methods based on the two-electron reduction of oxygen offer some important advantages over the AqP, including higher purity, greater safety and also less separation steps, unwanted by-products and environmental concerns [2]. Considering this, the Hydrogen Peroxide Electrosynthesis by Partial Reduction of Oxygen (HPEPRO) has received increased attention during the last two decades as an alternative to the AqP process.

[a] "Babes-Bolyai" University, Faculty of Chemistry and Chemical Engineering, 11 Arany Janos Street, RO-400028 Cluj-Napoca, Romania, e-mail: cvlaic@chem.ubbcluj.ro

The electrochemical reduction of oxygen on bulk carbon electrodes has been intensively studied because this material is electrocatalytically active for O_2 reduction in alkaline media [6,7,8]. Modified and unmodified carbonaceous materials are widely used for HPEPRO, a special attention being accorded to the graphite [7,8]. The native ability of carbonaceous materials to electrocatalyse the peroxide formation in alkaline solution was related to the high concentration of active centers on the surface of this electrode material. The chemical nature of active sites on graphite surfaces and how these affect electron transfer reactions have been the subject of many studies and suppositions [9,10,11,12,13].

In order to obtain increased electrocatalytical properties for HPERDO, the graphite surface can be modified through an electrochemical activation [11]. Unfortunately, this modification of the graphite surface also catalyzes the unwanted reaction corresponding to the subsequent reduction of the peroxide. This unwanted reaction lowers the selectivity of the graphite electrode for HPERDO and the efficiency of the electrosynthesis process.

In this work, the effect of graphite surface electroactivation upon HPEPRO efficiency was studied. In order to overcome the drawback of the electrochemical activation, a special programmable multi-step technique was elaborated.

RESULTS AND DISCUSSION

Based on our previous researches [8], a similar experimental setup based on a wall-jet ring-disk electrode (WJRDE) was used, the main difference consisting of the replacement of the inox ring electrode with a Pt one. The evaluation of the hydrodynamic parameters of the new WJRDE (collection factor and the type of flow regime) was performed using a 2 mM $K_3[Fe(CN)_6]$ in 1 M KCl as supporting electrolyte. During all other measurements, for the detection of the generated H_2O_2, the ring was polarized at +0.5 V/RE.

In order to evaluate the effect of graphite surface electroactivation upon HPEPRO efficiency, a special programmable multi-step technique was elaborate. It consists of a cyclic three potential steps program. In the first step, in order to generate new activated sites, the graphite surface was oxidized at potentials between +1.0 and +1.5 V/RE. During the second step, the active centers formed in the first step were partially reduced at disk potentials between -0.6 and -0.8 V/RE. In the final step, the HPEPRO efficiency was evaluated at disk potentials between -0.2 and -0.3 V/RE. An example of the applied potential on the disk electrode and the corresponding currents recorded on disk and ring electrodes for 5 repeated experiments is presented in Figure 1.
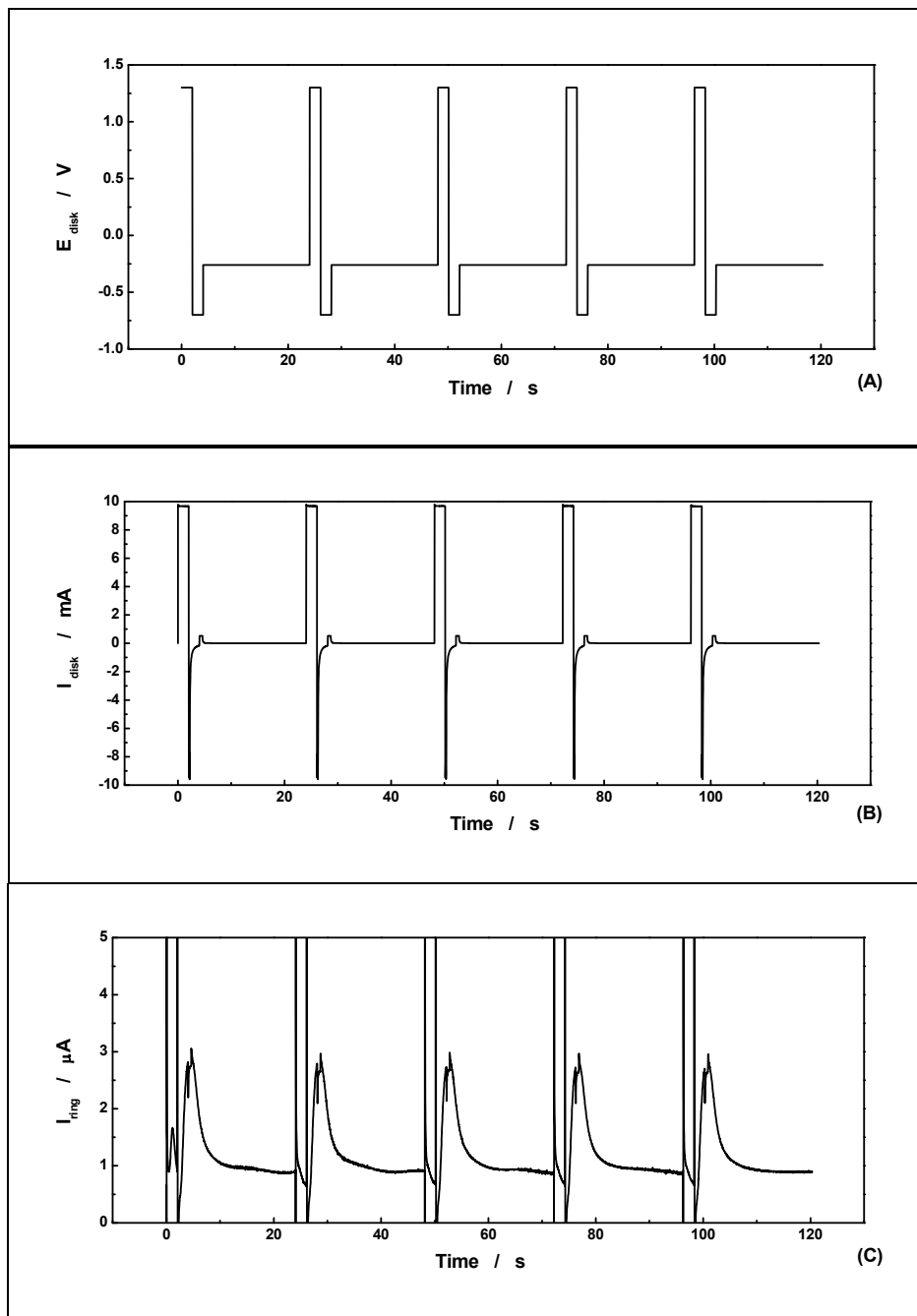
Figure 1. Applied potential on the disk (A) and the recorded currents on disk (B) and ring (C) for graphite oxidation at +1.3 V for 2 s, reduction at -0.7 V for 2 s and hydrogen peroxide generation at -0.26 V for 20 s (5 repeated experiments).

137

In the first step, activated sites are generated on the graphite surface, but they are in an oxidized form, incapable to electrocatalyse HPEPRO. We observed that the partial reduction of these active sites during the second step induces a significant improvement of hydrogen peroxide production.

The oxidative pre-treatment of the electrode surface, followed by partial reduction of the active sites allows the shift of the HPEPRO towards more positive values, which is an argument for the increase of the electrocatalytic properties of the modified graphite surface. We observed that the active sites in their partially reduced form, obtained by this original technique, are capable to generate hydrogen peroxide also through a pure chemical path. These active sites are, most probably, oxygen containing functional groups in their partially reduced form, very similar to the native functional groups of the graphite surface, considered responsible for the electrocatalytic properties of this material in the HPEPRO.

Based on the recorded currents on the ring electrode (see Figure 1.C), we concluded that the stability of the generated active sites is limited, requiring a periodic reactivation of the surface. For this reason, a special programmable multi-step technique was elaborated and employed. This technique allows the periodic reactivation of the graphite by cyclically repeating, in a programmed manner, the three potential steps described above.

The Figure 1.B and 1.C shows that the above described pre-treatment produces a net growth of the hydrogen peroxide yield during the third step, but the energy consumption during the first two steps is very large. This huge energy consumption is due to the large currents involved in (i) the oxidation and partial reduction of the graphite surface, (ii) the charge/discharge of the double layer capacitance, (iii) the adsorption / desorption of the reagents and products and also (iv) in the oxidation / reduction of the adsorbed electroactive species. From another point of view, the period of the three described steps plays also an important role in the energy consumption and the HPEPRO efficiency. Based on these information, a preliminary optimization study was performed using the described rectangular shape of the applied disk potential. The best result was obtained at the experimental parameters described in Figure 1.

In order to understand better the HPEPRO mechanism and to establish the optimum electro-activation potentials for the active sites' generation, we performed cyclic hydrodynamic voltammetry (CHV) studies, monitoring the produced HP on the ring electrode.

For the optimization of the oxidation potential (corresponding to the first step), the CHV measurements were performed starting from -0.8 V/RE and using different return potentials, the obtained results being presented in Figure 2.
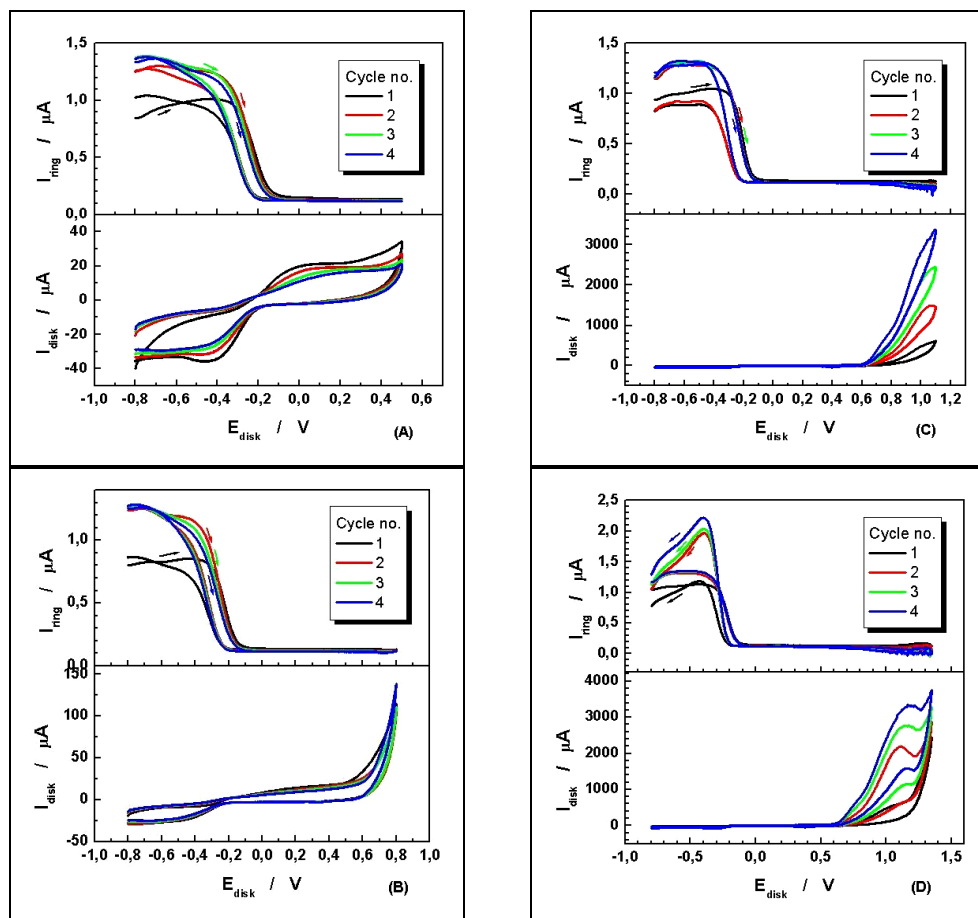
Figure 2. Influence of the oxidation potential upon HPERDO for cyclic hydrodynamic voltametry between - 0.8 V and + 0.5 V (A), + 0.8 V (B),+1.1 V (C), +1.35 V (D)

As it can be seen from Figure 2, the best results are obtained when the disk is oxidized at potential values between +0.5 and +0.8 V/RE. At higher oxidizing potentials (see Figure 2.C and 2.D), HPERDO is still improved, but the currents recorded on the disk are very large due to the oxygen evolution. This thing makes insignificant the obtained positive result (increased HP productivity) due to the high energy consumption.

In order to optimize the potential for the partial reduction of the active sites (corresponding to the second step), the CHV measurements were performed using the same return potential (+0.8 V/RE) and different starting potential values between -0.4 and -1.1 V/RE, the obtained results are presented in Figure 3.

139
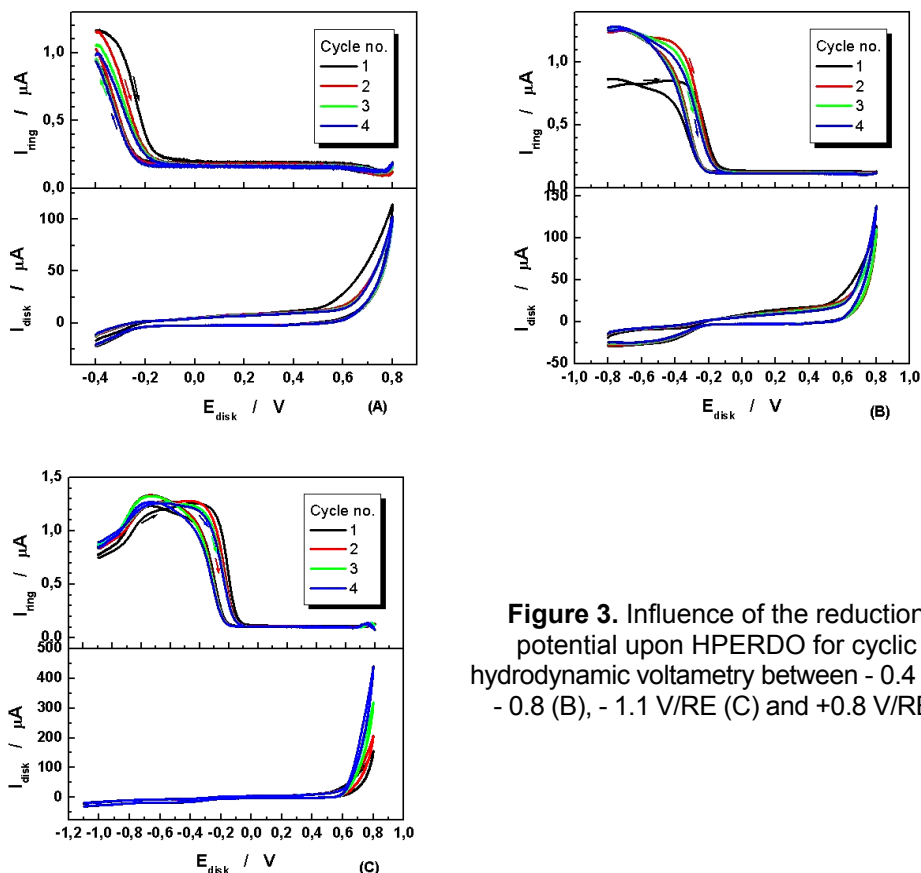
Figure 3. Influence of the reduction potential upon HPERDO for cyclic hydrodynamic voltametry between - 0.4 (A), - 0.8 (B), - 1.1 V/RE (C) and +0.8 V/RE.

Figure 3 shows that the applied potential for the partial reduction of the active sites generated by graphite surface oxidation is a key step for HPERDO and the optimum value is around -0.8 V/RE. For more positive potentials no effect can be observed and, for more negative potentials, the active centers are probably destroyed.

CONCLUSIONS

Contrary to some previous results presented in the literature [11], our results show that the electrocatalytic activity of the graphite towards HPEPRO can be increased by electrochemical pre-treatment. The proposed electro-activation of the graphite electrode consists of two steps, involving the oxidation of the surface followed by the partial reduction of the species generated upon oxidation.

Due to the fact that the stability of the generated active sites is limited, a special programmable cyclic multi-step technique was designed and used. The experimental parameters were optimized for a rectangular shape applied potential, but the recorded energy consumption remains still high.

The promising results obtained require that further investigations should take place in order to minimize the energy consumption of the first two steps.

EXPERIMENTAL SECTION

The electrochemical measurements were carried out in controlled hydrodynamic conditions, using a wall-jet ring-disc electrode (WJRDE). A disc ($\varnothing$ = 2.5 mm) of spectral graphite (Ringsdorff-Werke GmbH, Germany) was used as working electrode and the ring electrode (I.D. = 3 mm, O.D. = 3.5 mm) was made of Pt. The CE was a Pt wire and an Ag/AgCl/1M KCl system was used as reference electrode (RE). A peristaltic pump (Reglo Digital, Ismatec, Switzerland), a home-made wall-jet cell (WJC) [8] and a fully computer controlled home-made bipotentiostat were also used. Applications elaborated with the Labview 8.5 software were used to control the experimental parameters and data acquisition. The distance between the injector and disc electrode was fixed at 1 mm. The hydrodynamic regime - planar parallel flow was established using the method described in our previous paper [8]. The collecting efficiency (N) were evaluated using a 2 mM $K_3[Fe(CN)_6]$ solution in 1 M KCl as supporting electrolyte. For HPEPRO experiments, an air saturated ($[O_2] \sim 8$ ppm) aqueous electrolyte, containing 1 M NaOH as supporting electrolyte, was pumped in the WJC at a volume flow rate of 1.42 mL/min.

ACKNOWLEDGMENTS

REFERENCES

1. J. González-García, C. E. Banks, B. Šljukić, R. G. Compton, *Ultrasonics Sonochemistry,* **2007**, *14,* 405.

2. N. Guillet, L. Roue, S. Marcotte, D. Villers, J.P. Dodelet, N. Chhim, S. Trévin, *Journal of Applied Electrochemistry,* **2006**, *36,* 863.

3. J. C. Forti, C. E. Venâncio, M. R. V. Lanza, R, Bertazzoli, *Journal of Brazilian Chemical Society,* **2008**, *Vol. 19, No. 4*, 643.

4. E. Lobyntseva, T. Kallio, N. Alexeyeva, K. Tammeveski, K. Kontturi, *Electrochimica Acta,* **2007**, *52,* 7262.

5. E. Brillas, F. Alcaide, P.L. Cabot, *Electrochimica Acta,* **2002**, *48,* 331.

6. K. Tammeveski, K. Kontturi, R. J. Nichols, R. J. Potter, D. J. Schiffrin, *Journal of Electroanalytical Chemistry,* **2001**, *515,* 101.

7. N. Alexeyeva, T. Laaksonen, K. Kontturi, F. Mirkhalaf, D. J. Schiffrin, K. Tammeveski, *Electrochemistry Communication,* **2006**, *8,* 1475.

8. P. Ilea, S. Dorneanu, I.C. Popescu, Journal of Applied Electrochemistry, **2000**, *30*, 187.

9. R. C. Engstrom, *Analytical Chemistry,* **1982**, *54,* 2310.

10. R. C. Engstrom, V. A. Strasser, *Analytical Chemistry,* **1984**, *56,* 136.

11. C. Paliteiro, A. Hamnet, J.B. Goodenough, *Journal of Electroanalytical Chemistry,* **1987**, *233,* 147.

12. Tsutomu Nagaoka, Takashi Yoshino, *Analytical Chemistry,* **1984**, *58,* 1037.

13. Tsutomu Nagaoka, Toshiaki Sakai, Kotaro Ogura, Takashi Yoshino, *Analytical Chemistry,* **1984**, *58,* 1953.

ELECTROCHEMICAL STUDIES ON 5,10,15,20-TETRAKIS (4-PYRIDYL)-21H,23H-PORPHINE AND ITS ZN(II) COMPLEX

GHEORGHE FĂGĂDAR-COSMA[a], EUGENIA FĂGĂDAR-COSMA[b]

ABSTRACT. The electrochemical characterization of 5,10,15,20-tetrakis(4-pyridyl)-21H,23H-porphine (TPyP) and of Zn(II)5,10,15,20-tetrapyridylporphyrin (ZnPyP) is presented. Voltammetric and corrosion studies were carried out in order to investigate the electroactivity of TPYP and ZnPyP. Cyclic voltammograms obtained on Pt electrode, in H_2SO_4 0.1N or a mixture (1:1 vol.) of H_2SO_4 0.1N and AcCN, present two peaks for oxidation and one for reduction in case of TPyP and two oxidation and two reduction peaks for ZnPyP. The corrosion inhibiting abilities of TPyP and ZnPyP were illustrated by potentiodynamic curves obtained on carbon steel in 1N H_2SO_4, indicating a decrease of the current in the active region of the anodic polarization curves. Corrosion tests monitoring the mass loss of steel were also carried out.

Keywords: 5,10,15,20-tetrakis(4-pyridyl)-21H,23H-porphine, cyclic voltammetry, corrosion inhibition

INTRODUCTION

Porphyrins are capable to develop supramolecular structures. The molecules of porphyrins can change their properties by reconfiguring the electron distribution of the aromatic ring, thus allowing the accomplishment of some major objectives. Some applications of these compounds are in the fields of fundamental sciences (physics and chemistry), nanotechnologies [1-3], highly strategically technology domains (photovoltaic cells [4]), safety and durability for building engineering (corrosion inhibition [5]), monitoring the quality of the environment (electrochemical sensors [6-8]) and competitive health treatments (PDT therapy of cancer) [9].

The electrochemical behavior of porphyrins was well studied in nonaqueous systems [10]. Porphyrins are electrochemically active substrates and are supposed to be mixed corrosion inhibitors [11].

Porphyrins form highly stable metallic complexes having a great potential as corrosion inhibitors [12, 13]. Their planar molecules containing four pyrrole subunits present bonding sites for complexes formation at the

---

[a] *"Politehnica" University of Timisoara, 2 T. Lalescu Street, 300223-Timisoara, Romania, e-mail: gfagadar@yahoo.com*
[b] *Institute of Chemistry Timisoara of Romanian Academy, 24 M. Viteazul Ave, 300223-Timisoara, Romania*

nitrogen atoms. The whole molecule structure shows conjugated double bonds due to the –CH= bridging groups and thus, a very mobile electronic system. These properties are very important in the adsorption process of these compounds on diverse metals surfaces.

The present paper presents the voltammetric studies regarding the electrode reactions of 5,10,15,20-tetrakis(4-pyridyl)-21H,23H-porphine (TPyP) and Zn(II)5,10,15,20-tetrapyridylporphyrin (ZnPyP), with the corresponding structures presented in Scheme 1, and their corrosion inhibition effect.
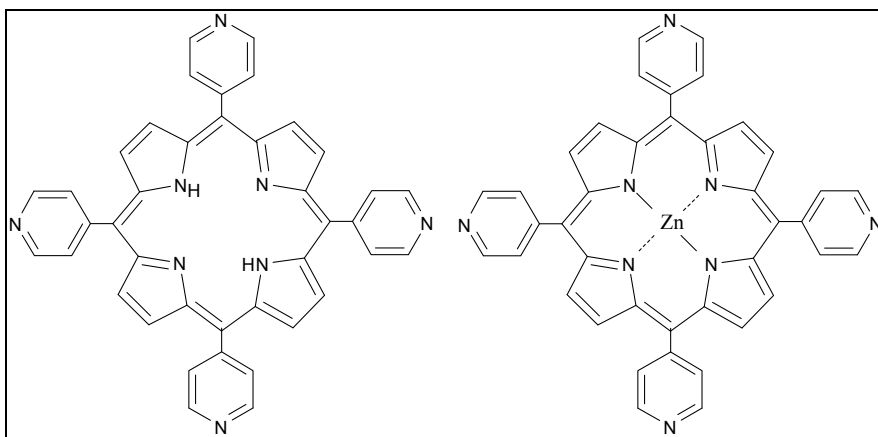
Scheme 1

The adsorption of TPyP and ZnPyP on the metal surface occurs as a result of electrostatic forces between the electric charge on the metal and the high polarizability of the organic substrate molecules. The interaction of TPyP and ZnPyP with the metal interface, covered with oxides and water molecules, is even more favored by the presence of the four pyridyl *meso*-substituents.

When iron is immersed in an aqueous phase, water molecules adsorb on its surface. Porphyrin molecules are adsorbed in their turn, by replacing the water molecules, this being considered the first step of metal-porphyrin interaction (Scheme 2):

$$[PORPHYRIN]_{soln} + [nH_2O]_{adsorbed} \rightleftharpoons [PORPHYRIN]_{adsorbed} + [nH_2O]_{soln}$$
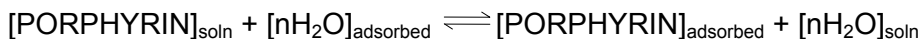
Scheme 2

In a second step, the porphyrinic compound, in its adsorbed state, can form a Fe(II) coordination complex with the Fe^{2+} ions located on the metal surface, these compounds having a corrosion inhibitor activity given by both their high stability and low solubility in the solution.

144

RESULTS AND DISCUSSION

The voltammetric investigations on TPyP, Figure 1, and on ZnTPyP, Figure 2, revealed the existence of the following oxidation and reduction potentials (V/SCE): TPyP: ε_{pa1} = 0.0 and ε_{pc1} = - 0.1 ($\varepsilon_{1/2}$ = - 0.05) and ε_{pa2} = 1.37 (irrev.); ZnTPyP: ε_{pa1} = 1.1, ε_{pc1} = 0.45 ($\varepsilon_{1/2}$ = 0.77) and ε_{pa2} = 1.49, ε_{pc2} = 1.05 ($\varepsilon_{1/2}$ = 1.27).

By using a mixture of aqueous H_2SO_4 and AcCN, the electrode reaction peaks are the same, as can be seen in Figure 3, the organic co-solvent having no influence on the reaction mechanism.

The corrosion inhibition of porphyrin-base TPyP and metalloporphyrin ZnPyP was investigated on carbon steel in H_2SO_4. The results are presented in Figure 4 and demonstrate that both compounds present an important inhibition effect on the corrosion process of carbon steel. The decrease of the critical current density for passivation (in the active region) is significant, but there is also some influence as inhibitor in the transpassive region (the oxygen evolution) and on the cathodic hydrogen evolution reaction. It is also notable that the onset potential for the active region is the same in every solution. However the potential corresponding to the peak as well as the onset of passivation (i.e. Flade potential) is decreased by the inhibitor.
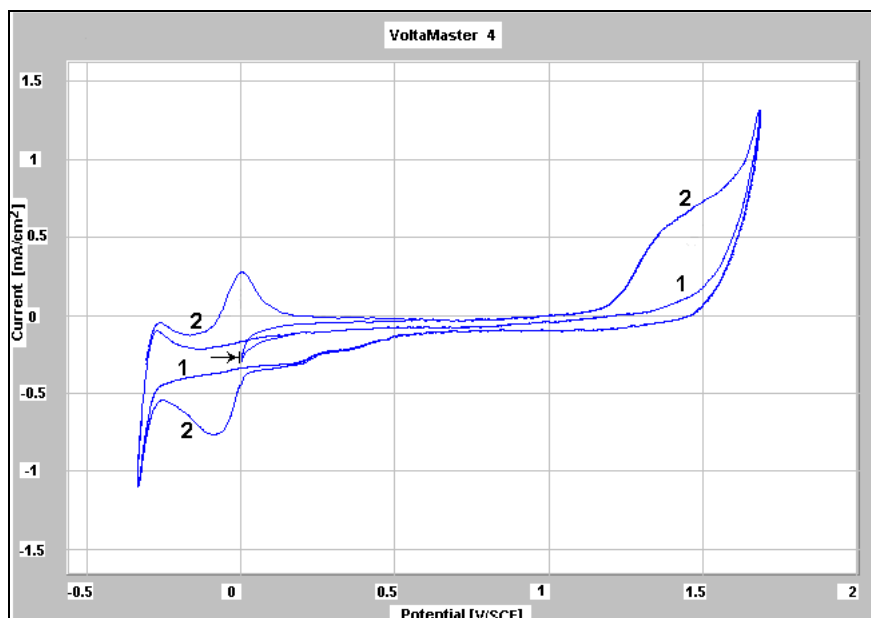

Figure 1. Cyclic voltammograms of TPyP (Pt electrodes, scan rate 50 mV/s, ref. SCE, 25°C); curve 1: H_2SO_4 0.1N, curve 2: H_2SO_4 0.1N + TPyP 1.5 mM
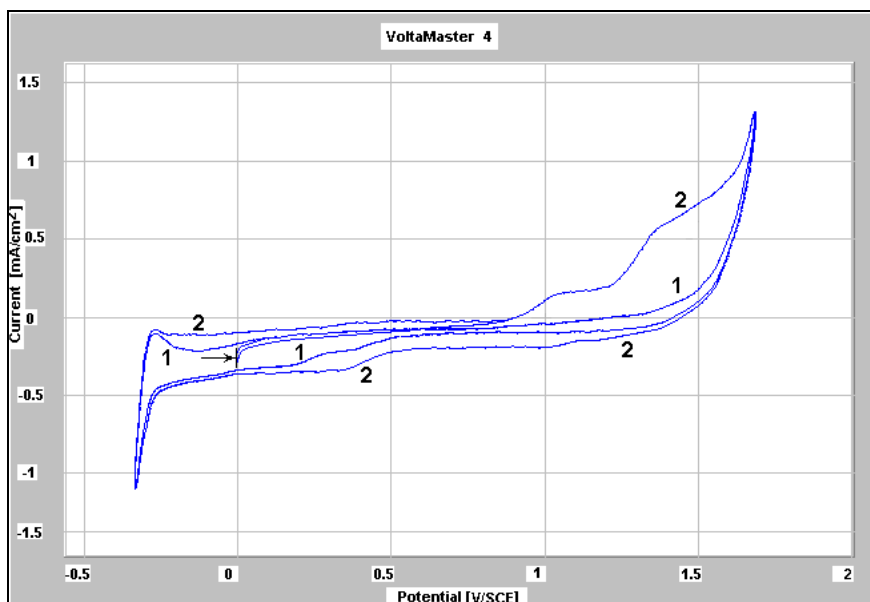
Figure 2. Cyclic voltammograms of ZnPyP (Pt electrodes, scan rate 50 mV/s, ref. SCE, 25°C); curve 1: H_2SO_4 0.1N, curve 2: H_2SO_4 0.1N + ZnPyP 1.0mM
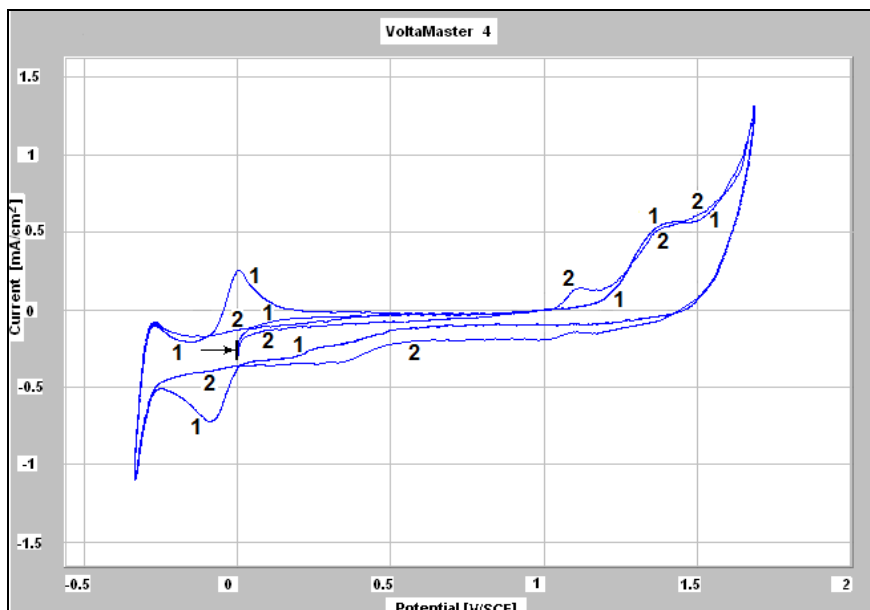

Figure 3. Cyclic voltammograms of TPyP and ZnPyP (Pt electrodes, scan rate 50 mV/s, ref. SCE, 25°C); curve 1: H_2SO_4 0.1N + AcCN (1:1 vol.) + TPyP 1.5 mM, curve 2: H_2SO_4 0.1N + AcCN (1:1 vol.) + ZnPyP 1.0mM
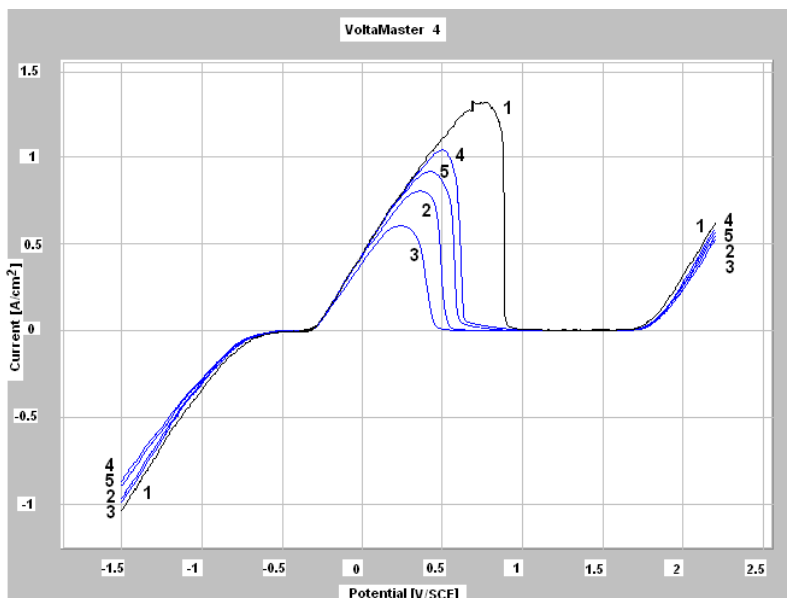
Figure 4. Potentiodynamic curves obtained on carbon steel in H_2SO_4 1N, scan rate 100 mV/s, 25°C. Porphyrin conc., mM: without porphyrin (curve 1), 0.08 TPyP (2), 1.3 TPyP (3), 0.37 ZnPyP (4) and 0.75 ZnPyP (5).

Corrosion tests monitoring the mass loss of steel were also carried out. Measuring the mass loss of steel during the corrosion process the results presented in Table 1 were obtained. The testing method consisted in measurement of the volume of hydrogen evolved during the corrosion process. The inhibiting efficiency is in the range of 30-50% for this very aggressive medium, depending on the inhibitor concentration and the temperature.

Table 1. The effect of TPyP concentration on the corrosion rate of carbon steel in H_2SO_4 5%, at 25°C, after 1.5 hours.

TPyP concentration, mM	Mass loss, g/(m²day)	P, mm/year	Inhibition efficiency, %
0	109.68	5.1	-
0.05	84.00	3.9	23
0.1	75.36	3.5	31
0.2	64.56	3.0	41
0.5	60.24	2.8	45
1.0	58.08	2.7	47

CONCLUSIONS

TPyP and ZnPyP present electrochemical activity. They are oxidized/ reduced on platinum electrode, in aqueous H_2SO_4 medium. From the influence of these compounds on the passivation curve of carbon steel in H_2SO_4, and from mass loss measurements, an important corrosion inhibition activity is to be noticed.

EXPERIMENTAL SECTION

Voltammetric studies were made using a three-electrode cell and a potentiostat VOLTALAB PGZ 301 Dynamic – ETS Voltammetry – Radiometer Copenhagen with a VoltaMaster 4 program, at room temperature. The working electrodes were carbon steel (for corrosion inhibition studies) and platinum (for cyclic voltammetry). Counter electrode and reference electrode were always platinum and SCE. Other experimental specifications are given at the proper locations.

Carbon steel C55 specimens, produced by MECHEL Campia Turzii, in the form of fibres for concrete reinforcing, containing: 0.53-0.61% C, 0.44-0.45% Mn, 0.23-0.25% Si, max 0.01% S, max 0.01% P, max 0.03% Al, max 0.06% Cu, max 0.03% Cr, max 0.06% Ni, max 0.09% Mo, the remainder Fe were used.

Porphyrins were obtained according to previous published literature data [14].

The mass loss of the steel during the corrosion process was calculated from the volume of the evolved hydrogen, and confirmed by weight measurements.

ACKNOWLEDGMENTS

REFERENCES

1. E. Fagadar-Cosma, C. Enache, I. Armeanu, D. Dascalu, G. Fagadar-Cosma, M. Vasile, I. Grozescu, *Materials Research Bulletin*, **2009**, *44*, 426.
2. E. Fagadar-Cosma, C. Enache, D. Vlascici, G. Fagadar-Cosma, M. Vasile, G. Bazylak, *Materials Research Bulletin*, **2009**, *44*, 2186.

3. E. Fagadar-Cosma, M. Mirica, I. Balcu, C. Bucovicean, C. Cretu, I. Armeanu, G. Fagadar-Cosma, *Molecules*, **2009**, *14*, 1370.

4. G. Mihailescu, L. Olenic, S. Garabagiu, G. Blanita, E. Fagadar-Cosma, A. S. Biris, *Journal of Nanoscience and Nanotechnology*, 2009, 9, *in press*.

5. G. Făgădar-Cosma, E. Făgădar-Cosma, I. Popa, I. Tăranu, *Chemistry Bulletin of "POLITEHNICA" University (Timisoara),* **2007**, *52*, 109.

6. G. Fagadar-Cosma, D. Vlascici, E. Fagadar-Cosma, *Journal of Biological Inorganic Chemistry*, **2007**,*12*, 218.

7. D. Vlascici, E. Fagadar-Cosma, O. Bizerea-Spiridon, *Sensors*, **2006**, *6*, 892.

8. D. Vlascici, E. Fagadar-Cosma, E. M. Pica, V. Cosma, O. Bizerea, G. Mihailescu, L. Olenic, *Sensors,* **2008**, *8*, 4995.

9. E. Fagadar-Cosma, L. Cseh, V. Badea, G. Fagadar-Cosma, D. Vlascici, *Combinatorial Chemistry & High Throughput Screening*, **2007**, *10*, 466.

10. E. Făgădar-Cosma, D. Vlascici, G. Făgădar-Cosma, "Porfirinele de la sinteza la aplicatii", Editura Eurostampa, Timisoara, **2008**, chapter 7.

11. V.S. Sastri, "Corrosion Inhibitors. Principles and Applications", John Wiley & Sons Ed., Chichester, **1998**, pp. 599-603.

12. Y. Feng, S. Chen, W. Guo, Y. Zhang, G. Liu, *Journal of Electroanalytical Chemistry*, **2007**, *602*, 115.

13. Y. Feng, S. Chen, W. Guo, G. Liu, H. Ma, L. Wu, *Applied Surface Science*, **2007**, *253*, 8734.

14**.** E. Fagadar-Cosma**,** C. Enache, I. Armeanu, G. Fagadar-Cosma, *Digest Journal of Nanomaterials and Biostructures*, **2007**, *2*, 175.

ELECTROCHEMICAL REDUCTION-ADSORPTION PROCEDURE FOR THE REMOVAL OF NITROPHENOL CONTAMINANTS FROM AQUEOUS MEDIA

MIHAELA-CLAUDIA TERTIS[a], MARIA JITARU[a], VIRGINIA COMAN[b], MIUTA FILIP[b], DANIEL A. LOWY[c]

ABSTRACT. Work reported here was performed with the goal of reducing the concentration of 4-nitrophenol (4-NP) and 2,6-dinitrophenol (2,6-DNP), present in synthetic solutions to values below 0.5 mg L^{-1}, the maximum concentration level tolerated by international environmental regulations [1, 2]. In the electrochemical reduction of 4-NP the final product was 4-aminophenol, as assessed by HPLC. Three methods were used for decreasing 4-NP and 2,6-DNP concentrations: electrochemical reduction, adsorption on active carbon, and the combined electrochemical reduction-adsorption. Best results were obtained by applying the combined procedure, which employed as the cathode granular activated carbon in fluidized bed. In these experiments 95-97% removal of 4-NP and 2,6-DNP from solutions occurred within the first 20 min.

Keywords: nitrophenol removal, electrochemical reduction, removal by adsorption, activated carbon, fluidized bed cathode.

INTRODUCTION

Nitrophenols (NPs) are important and versatile organic compounds used in industrial, agricultural, and defense applications. They serve frequently as intermediates in the manufacturing of explosives, pharmaceuticals, pesticides, pigments, dyes, and rubber chemicals [3]. Because they are very toxic to humans and animals, their monitoring is essential in environmental pollution control. In order to avoid environmental water pollution, the European Council Directive "Dangerous Substances Directive 67/548/EEC" of 2006 [2] enforces low concentrations of nitrophenols (below 0.5 mg L^{-1}).

A variety of treatment technologies are being explored or already used for the removal of nitrophenols from wastewater. These methods belong to several types, such as *physical procedures*, such as adsorption on solid

---

[a] *Research Center LAF-INT-ECOL, Faculty of Chemistry and Chemical Engineering, "Babes-Bolyai" University, 11 Arany Janos Street, 400028; e-mail mjitaru@chem.ubbcluj.ro*

[b] *Chemical Research Center (ICCRR), "Babes-Bolyai" University, 30 Fantanele Street, Cluj-Napoca, Romania, e-mail v.coman@iccrr.ro*

[c] *Davia Corporation, 13255 Revilo Loop, Woodbridge, VA 22191, USA, e-mail: daniellowy@davia.biz*

adsorbents, including non-porous carbon blacks [4], granular activated carbon and hyper-cross-linked polymer resins [5, 6], methacrylate based adsorbents [7], anion-cation modified palygorskites [8], or natural linear polysaccharides, e.g., alginate extracted from marine brown algae [9]. As of today, activated carbon is the most widely used adsorbent in wastewater treatment [10, 11]. Given that it is an expensive material for large-scale application, search is directed toward identifying low-cost and widely available adsorbents, such as zeolites, biosorbents, and clays [12-16]. Next one has c*atalytic* and *photocatalytic* procedures, ranging from photocatalytic ozonation, ozonation, and catalytic ozonation to photocatalysis and photolysis, all conducted on TiO_2 in the presence of visible/UV light [17]. Photocatalytic degradation of NPs yielded improved results on TiO_2 modified with a thin layer of molecular imprinted polymer, where the polymer provides molecular recognition ability toward the template molecules [18], a process, which has been shown to occur via a charge-transfer-complex-mediated pathway [19]. A group of *biological* methods typically consist in biodegradations conducted in an aerobic sequencing batch reactor [20, 21], while *electrical* techniques showed useful upon applying various types of pulsed electrical discharges, the most efficient being the pulsed corona discharge in humid air above the water [22]. Several electrochemical methods belong to oxidations and reductions, which can be driven as a direct or mediated process. Examples include, but are not limited to electro-oxidation of nitrophenols on tantalum substrate born-doped diamond electrode [23, 24-26], degradation by electrochemical oxidation on lead oxide/ titanium modified anodes [27]. Electrochemical treatment is promising for waste waters containing organics that are not biodegradable, where, in most cases, total mineralization of the organic compounds can be accomplished [26, 28]. For example, by the electrochemical reduction of NP, the aromatic nitro group undergoes conversion to aromatic biodegradable amines [29]. Finally, reported in the literature is a limited number of *combined procedures*, which exploit the synergic effect of applying two procedures in an integrated device; for example oxidation and adsorption were utilized simultaneously in a device performing ozonation and adsorption on activated carbon [30].

Owing to its high surface area, low specificity, and fast adsorption kinetics, activated carbon remains the most effective adsorbent for organic contaminants [31]. Therefore, when designing our combined procedure, we built on the favorable properties of activated carbon, exploiting not only its adsorptive capacity, but also its good electric conductivity, which enables its use as an electrode in an electrochemical cell. When activated carbon is introduced in an electrochemical reactor, operated in the fluidized mode, the reactor becomes a fluidized electrochemical reactor in which electrochemical conversions (reduction or oxidation) and adsorption are integrated in one combined procedure.

There are only a few reports in the literature on the treatment by combined electrochemical and adsorption methods of biorefractory nitrophenol derivatives. Papers published so far refer exclusively to the combined treatment

of 4-nitrophenol, a procedure, which consists of adsorption associated with electrochemical oxidation [32-34].

Work described here discloses preliminary results obtained in the removal of nitrophenols from solutions, by utilizing the combined procedure of adsorption-electrochemical reduction (Ads+ER) on activated carbon. The goal of the research was to reduce 4-NP and 2,6-DNP concentrations in synthetic solutions to the low values enforced by environmental legislation. Also, we assessed the advantages of using the combined procedure as compared to the individual techniques of electrochemical reduction (ER) or adsorption on active carbon (Ads).

RESULTS AND DISCUSSION

1. Preliminary determinations

1.1. UV-Visible spectrophotommetry

We determined spectral and calibration data for treated nitrophenol derivatives in water by UV-visible spectrophotometry. Results were reported in a previous paper [35]. Optimal ranges of nitrophenols concentrations for UV-vis spectrophotometry are:

0.15 ÷ 15 mg L^{-1} for 4-NP (maximum accepted level 0.33 mg L^{-1});
0.2 ÷ 20 mg L^{-1} for 2,6-DNP (maximum accepted level 0.5 mg L^{-1}).

1.2. Cyclic voltammetry

Voltammetric properties and calibration data of treated nitrophenols were determined by cyclic voltammetry (CV). The supporting electrolyte was 1 mol L^{-1} aqueous sodium phosphate buffer (pH 4). For 4-nitrophenol we found a linear relationship between I_p and concentration, in the range from 0.001 to 1.5 mg L^{-1}, with the regression coefficient 0.9935. Statistical treatment of ten CV scans yielded standard deviations of 3.20% and a relative error of 3.05%. In the case of 2,6-dinitrophenol, we found a linear relationship of I_P vs. concentration for both peaks; the linear range encompassed 0.002 ÷ 2 mg L^{-1}, with excellent regression coefficients (0.976 respective 0.9912). The relative standard deviation calculated for ten scans was 2.8%, while the relative error was 1.85%.

The electrochemical reduction of both nitro group in the case of 2,6-DNP takes place easier ($E_{P,1}$ = -0.37 V vs. Ag/AgCl,KCl; $E_{P,2}$ = -0.55 V vs. Ag/AgCl,KCl) comparing to 4-NP (E_P = -0.65 V vs. Ag/AgCl,KCl).

1.3. High performance liquid chromatography (HPLC)

HPLC determinations are important, as they allow for determining the final composition of the solutions yielded by the electrochemical process. The HPLC diagram of 4-NP and the corresponding amine is shown in Figure 1, while Figure 2 displays the HPLC diagram of 2,6-DNP. Retention times indicate that

the mixture components are well resolved; we found 2.503 min for 4-aminophenol, 3.670 min for 2,6-DNPI; 11.89 min for 4-NP. Consequently, HPLC can be used for determining the composition of solutions obtained in the electrochemical treatment of nitrophenol derivatives.
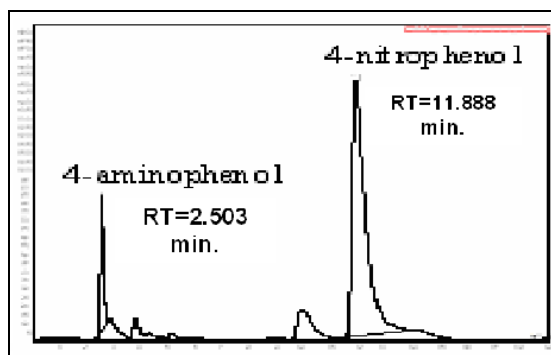

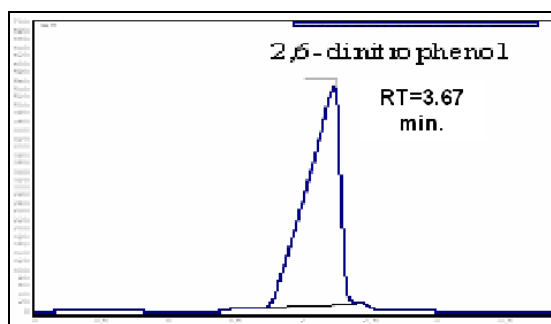**Figure 1.** HPLC of the mixture of 4-aminophenol and 4-nitrophenol (1:1, v/v)

Figure 2. HPLC of 2,6-DNP (0.25 mg mL^{-1}).

2. Electrochemical reduction experiments

Electrochemical reduction experiments of nitrophenols were performed in 3 different electrochemical reactors, under various hydrodynamic conditions, and in dissimilar supporting electrolytes. Most results were discussed in detail in our previous publications [36-38]. Results are summarized in Figure 3.

Best results for electrochemical reduction of 4-NP were obtained in an electrochemical micro-flow cell (experimental setup A), on nickel cathode (98% of 4-NP removal). In the case of 2,6-DNP satisfactory results were obtained at low concentrations only (experimental setup C; 99% of 2,6-DNP removal). The experimental setups characteristics are presented in experimental section.
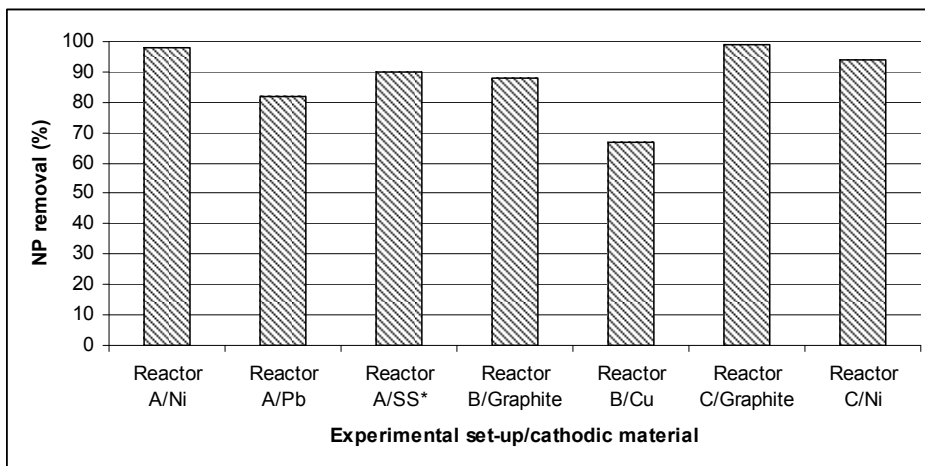
Figure 3. Synoptic presentation of nitrophenols (NP) removal experiments by the mean of electrochemical reduction in different electrochemical reactors.
* SS – stainless steel.

3. Combined procedure for the removal of nitrophenols

3.1. Batch tests

In order to evaluate the advantages of supplementing activated carbon to the electrochemical reactor, we used the same reactor for comparing the removal of nitrophenol derivatives by (i) adsorption, (ii) electrochemical reduction, and (iii) their combined process, respectively.

In Figure 4 the efficiency (η) of nitrophenol removal expressed in %, is plotted versus time. When utilizing the combined process, η reaches high values within significantly shorter time than in the individual processes. Thus, in the combined procedure, after 30 min 95% of 4-NP is removed from the solution, as compared to only 43% in adsorption and 21% in electrochemical reduction (see Figure 4a). The efficiency of removal for 2,6-DNP is of 97% in combined procedure, as compared to only 66% in adsorption and 27% in electrochemical reduction (Figure 4b).

Total organic carbon (TOC) determinations supported the results of spectrophometric measurements. Variation of TOC values over time is displayed in Figure 5, for 4-NP, Figure 5 (a), and 2,6-DNP, Figure 5 (b). In both cases we compare removal processes by simple adsorption on active carbon, by electrochemical reduction on graphite cathode, and by the combined (Ads + ER) procedure.
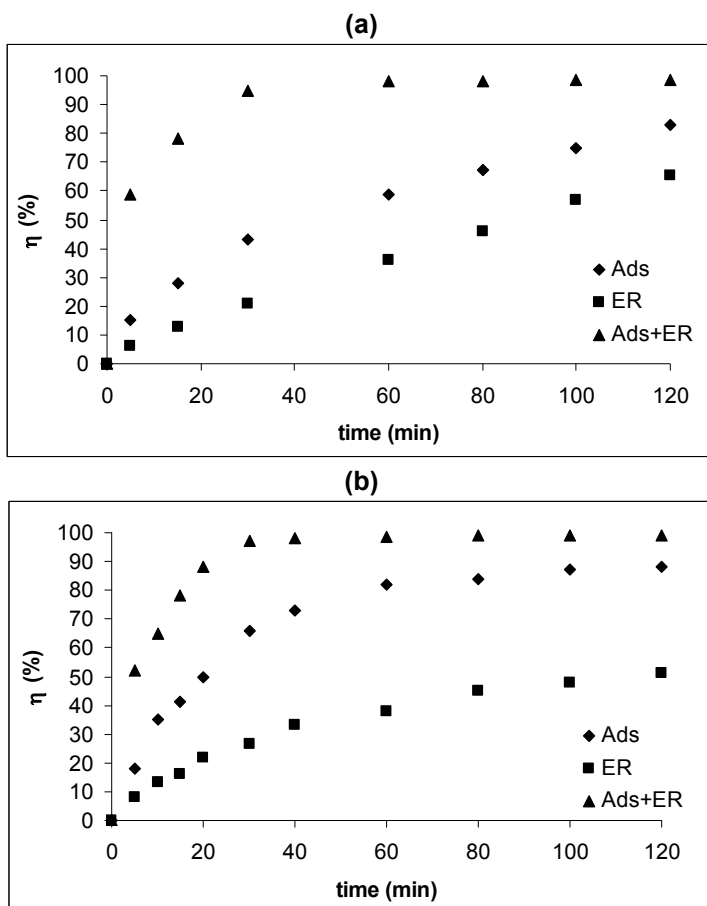
(a)

(b)

Figure 4. Comparison of the removal efficiency, η, by adsorption (Ads), electrochemical reduction (ER), and their combined process (Ads + ER) for (a) 4-NP and (b) 2,6-DNP

3.2. Electrochemical removal of nitrophenol on cathodes of activated carbon in fixed bed

After the batch tests, experiments were performed using electrochemical reactor type B, with fixed bed of activated carbon type NORIT ROW 0.8 mm pellets, employed as the cathode, while Ti plates were used as the anode.

Figure 6 (a) and 6 (b) present the variation of absorbance over time in 4-NP and 2,6-DNP removal, respectively. Results were obtained with the combined (Ads + ER) procedure. Removal of nitrophenols from the solutions was completed very fast. Hence, within the initial 20 min 94% of 4-NP 92% and of 2,6-DNP, respectively, were removed.
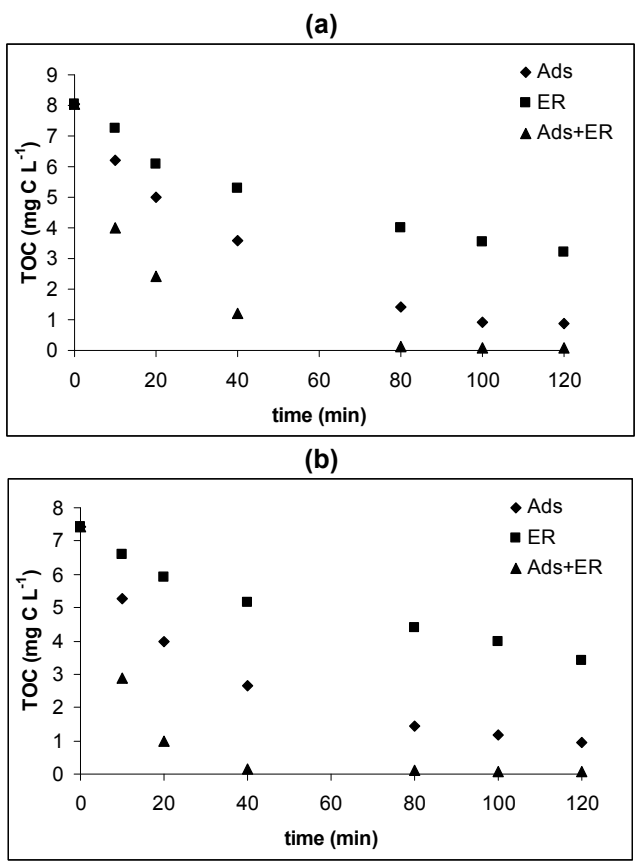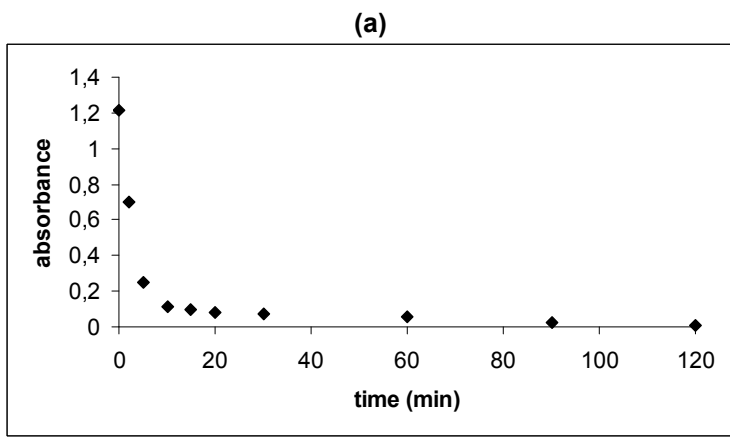
(a)

(b)

Figure 5. Comparison of TOC variation over time for: (a) 4-NP and (b) 2,6-DNP removal by adsorption, electrochemical reduction, and their combined process.
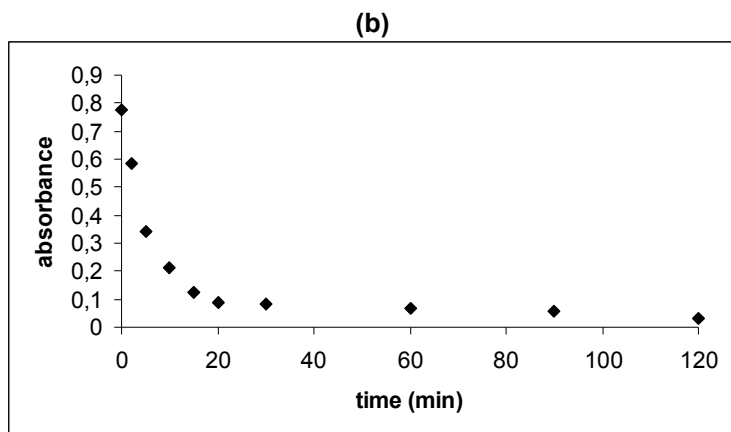
(a)

157

(b)

Figure 6. Absorbance variation over time for the removal of (a) 4-NP (λ = 317nm) and (b) 2,6-DNP (λ = 417nm) by the combined procedure of adsorption + electrochemical reduction on activated carbon fixed bed cathode.

CONCLUSIONS

Work reported in this paper attempted reducing the concentration of 4-nitrophenol and 2,6-dinitrophenol present in synthetic solutions below 0.5 mg L^{-1}, which is the maximum concentration tolerated by international environmental regulations. UV-vis spectrophotometry, cyclic voltammetry, total organic carbon (TOC) determination, and HPLC were useful techniques for monitoring the removal of nitrophenols from aqueous solutions. In the electrochemical reduction of 4-NP the final product was 4-aminophenol. In HPLC, 4-aminophenol and 4-nitrophenol were well separated, yielding symmetrical peaks; hence this method is efficient for determining the two compounds in mixture, 4-aminophenol being the final product in the electrochemical reduction of 4-NP. Also, HPLC enables for detection limits of less than 3 ng L^{-1}.

Three avenues were explored toward decreasing the concentration of nitrophenols: electrochemical reduction, adsorption on active carbon, and the combined electrochemical reduction-adsorption. Best results were obtained by applying the combined procedure, which employed as the cathode granular activated carbon in fluidized bed. Experiments performed by this combined technique secured 95-97% removal of 4-nitrophenol and 2,6-dinitrophenol from solutions within the first 20 min.

EXPERIMENTAL SECTION

Reagents and solutions preparation

4-Nitrophenol (purity >98%, Merck, Germany) and 2, 6-DNP (purity >95%, calculated based on dry substance, moistened with 20% H$_2$O, Aldrich, Switzerland) were used to prepare the solutions of desired concentration.

158

Distilled water was used to prepare the aqueous solutions. All other reagents were analytical grade, and used without further purification.

Two adsorbents were used: granular activated carbon type NORIT GAC 1240W, (Netherlands) with the following characteristics: micropores volume: 0.38 cm^3 g^{-1}; specific area: 1062 m^2 g^{-1}; mesopores volume: 0.45 cm^3 g^{-1}; apparent density: 495 kg m^{-3}; and steam activated NORIT ROW 0.8 mm pellets. Prior to use, activated carbon was washed several times with deionized water, dried for 24 h to constant weight at 105 ^{o}C, and kept in a desiccator until it cooled to room temperature, so that re-adsorption of moisture before use was prevented.

Experimental setups

Electrochemical reduction experiments were carried out by means of three different experimental setups.

Experimental setup (**A**) consisted of a commercially available electrochemical filter press cell (Electrocell AB, Sweden). It was used as a micro-flow cell, being equipped with a DSA-O₂ anode (20 cm^2 area) and a cathode made of nickel, copper, lead, or stainless steel (20 cm^2 area). The compartments of the electrochemical cell were separated with a Nafion 117 Millipore proton-exchange membrane. This filter press cell was inserted into a hydraulic circuit, which comprised a GILSON MINIPULS 3 peristaltic pump for circulating the electrolyte in the compartments of the cell, at flow rates in the range from 1 x 10^{-6} to 3.3 x 10^{-3} L min^{-1}. In addition, experimental setup (**A**) had two glass reservoirs for the anolyte and catholyte, respectively.

Experimental set-up (**B**) was an undivided electrochemical reactor, with a volume of 1500 cm^3, equipped with a pump, which operated at the flow rate of 1.2 L min^{-1}. Two stainless steel anodes (212.3 cm^2 projected geometric surface area) and a graphite or copper cathode (185.7 cm^2) served for electrodes.

Experimental set-up (**C**) was an electrochemical reactor made of glass, and equipped with Ti/Pt-Ir anode and graphite or nickel cathode, each having a projected geometric surface area of 100 cm^2. A Nafion 117 Millipore cation exchange membrane was inserted between the half-cells. A WATSON MARLOW Mod.313 F/D peristaltic pump with two heads operated under conditions of full recycle, at flow rates in the range from 0.090 to 1.4 L min^{-1}. In all performed experiments Setups (**A**-**C**) described above were operated under galvanostatic conditions. Further details on the experimental equipment were reported in previous work [36].

The combined electrochemical reduction-adsorption procedure on activated carbon was first performed in a batch reactor, described in other work [37]. This reactor comprised a glass container (1 L volume), a titanium anode with oxide coating (grid; active surface: 47 mm x 65 mm) and a graphite

cathode (active surface 47 mm x 65 mm). A known mass of activated carbon was introduced into the reactor before start up, and a magnetic stirrer allowed for maintaining the activated carbon in suspension (350 rpm). In each experiment we treated a volume of 0.5 L synthetic wastewater, containing 10^{-4} mol L^{-1} 4-NP or 2,6-DNP in sodium phosphate buffer solution, adjusted with H_3PO_4 to pH 4. Experiments were performed under galvanostatic conditions, at the current density of 20 mA cm^{-2}. Minor adjustments of the applied voltage (cell voltage was around 5 V) were needed for keeping the current density constant over the duration of experiment. At appropriate time, 3 mL of sample was taken for analysis. The stirring was stopped for 5 s during the sampling, and after measurements the sample was reintroduced into the batch reactor. All experiments were performed at constant temperature (20 ± 2 ^{o}C).

After completing preliminary batch experiments, the combined procedure was performed in experimental set-up (**B**), described above, but in this case the cathode was a fixed bed of activated carbon, type NORIT ROW 0.8 mm pellets.

Electrolysis efficiency was monitored by sampling the electrolyte over time, and analyzing the concentration of residual reagents by voltammetry, spectrophotometry, as well as by TOC and HPLC measurements.

Methods

Spectrophotometric measurement was carried out with a Unicam Helyos B spectrophotometer, with VISION 32 software, and a quartz vat of 2 mL, an optical path length of 1 cm, and a Direct Reading Spectrophotometer type DR/2800 HACH-LANGE with a quartz vat of 2 mL and an optical path length of 1 cm.

TOC determinations performed with a TOC-DR2800 HACH-LANGE spectrophotometer, using Lange TOC cuvette test type LCK 385 (in the concentration range from 0 to 30 mg L^{-1}) and LCK 386 (in the concentration range from 30 to 300 mg L^{-1}).

HPLC separations were accomplished with a JASCO 980 chromatograph equipped with Intelligent UV-VIS Detector JASCO UV-980-975, with specific software CHROMPASS; stationary phase: NUCLEOSIL 120C18 (5 μm, 25 x 0.46 cm) column; mobile phase: MeOH–H_2O–H_3PO_4 (30:70 $\pm$ 0.1, v/v); flow: 1 mL min^{-1}; detection at λ = 280 nm; the column temperature 21 °C.

Voltammetry was recorded with a Model 630C potentiostat-galvanostat system (CH Instruments, Austin, Texas), and data processed with the software of the instrument. Experiments were conducted in 3-electrode geometry, with glassy carbon working electrode (active surface of 0.0125 cm^{2}), a platinum plate auxiliary electrode, and Ag/AgCl, 3 M KCl electrode reference. All measurements were carried out in a glass cell, containing 5.0 mL of solution, without stirring. The supporting electrolyte was aqueous sodium phosphate buffer, adjusted to pH 4. Prior to each measurement the electrolyte was

degassed with nitrogen for 15 min and the scans were recorded under N_2 blanket. The optimized parameters in cyclic voltammetry were found to be: scan rate of 0.1 V s^{-1} in the potential range from 0 and -1 V vs. Ag/AgCl, 3 M KCl.

REFERENCES

1. A. Santos, P. Yustos, S. Rodriguez, F. Garcia-Ochoa, *Applied Catalysis B: Environmental,* **2006**, *65 (3-4)*, 269.

2. European Council Directive "Dangerous Substances Directive 67/548/EEC", amended by Directive 121/EEC of the European Parliament and of the Council, December 18, **2006**.

3. D-P. Zang, W-L. Wu, H-Y. Long, Y-C. Liu, Z-S. Yang, *International Journal of Molecular Science*, **2008**, *9*, 316.

4. P.J.M. Carrott, M.M.L. Ribeiro Carrott, T.S.C. Vale, L. Marques, J.M.V. Nabais, P.A.M. Mourao, Suhas. *Adsorption Science & Technology*, **2008**, *26* (10), 827.

5. C.H. Hong, W.M. Zhang, B.C. Pan, L. Lv, Y.Z. Han, Q.X. Zhang, *Journal of Hazardous Materials*, **2009**, *168* (2-3), 1217.

6. J.H. Huang, C. Yan, K.L. Huang, *Journal of Colloid and Interface Science*, **2009**, *332* (1), 60.

7. M. Erdem, E. Yuksel, T. Tay, Y. Cimen, H. Turk, *Journal of Colloid and Interface Science*, **2009**, *333* (1), 40.

8. Y. Chang, X.Q. Lv, F. Zha, Y.G. Wang, Z.Q. Lei, *Journal of Hazardous Materials*, **2009**, *168* (2-3), 826.

9. S. Peretz, O. Cinteza, A. Peretz, *Revista de Chimie (Bucuresti),* **2007**, *58 (11),* 1129.

10. L.R. Radovic, C. Moreno Castilla, J. Rivera Utrilla, *Chemistry and Physics of Carbon*, **2000**, *27 (1),* 227.

11. P.C. Chiang, E.E. Chang, J.S. Wu, *Water Science and Technology*, **1997**, *35 (7),* 279.

12. B. Koumanova, P. Peeva-Antova, *Journal of Hazardous Materials*, **2002**, *90 (3)*, 229.

13. S.H. Lin, M.J. Cheng, *Waste Management*, **2002**, *22 (6),* 595.

14. N. Calace, E. Nardo, B.M. Petronio, M. Pietroletti, *Environmental Pollution*, **2002**, *118 (3),* 315.

15. Z. Kircheva, G. Oltean, D. Covaciu, B. Koumanova, M. Jitaru, *Journal of the University of Chemical Technology and Metallurgy (Sofia)*, **2004**, *39 (3),* 343.

16. A. Li, Q. Zhang, G. Zhang, J. Chen, Z. Fei, F. Liu, *Chemosphere,* **2002**, *47 (9),* 981.

17. F.J. Beltran, F.J. Rivas, O. Gimeno, *Journal of Chemical Technology and Biotechnology*, **2005**, *80* (9), 973.

18. X.T. Shen, L.H. Zhu, G.X. Liu, H.W. Yu, H.Q. Tang, *Environmental Science & Technology*, **2008**, *42* (5), 1687.

19. N. Wang, L.H. Zhu, Y.P. Huang, Y.B. She, Y.M. Yu, H.Q. Tang, *Journal of Catalysis,* **2009**, *266* (2), 199.

20. M. Martin-Hernandez, J. Carrera, J. Perez, M.E. Suarez-Ojeda, *Water Research*, **2009**, *43* (15), 3871.

21. C.P. Goh, C.E. Seng, A.N.A. Sujari, P.E. Lim, *Environmental Technology*, **2009**, *30* (7), 725.

22. T.H. Dang, A. Denat, O. Lesaint, G. Teissedre, *European Physical Journal-Applied Physics*, **2009**, *47* (2) Article Number: 22818.

23. C.Y. Gao, M. Chang, *Acta Physico-Chimica Sinica*, **2008**, *24* (11), 1988.

24. A. Dabrovski, P. Podkoscielny, K. Hubcky, M. Barczak, *Chemosphere*, **2005**, *58 (8)*, 1049.

25. S. Espugas, J. Jimenez, S. Contreras, E. Pascual, M. Rodriguez, *Water Research*, **2002**, *36 (4),* 1034.

26. P. Canizares, C. Saez, J. Lobato, M.A. Rodrigo, *Industrial and Engineering Chemistry Research*, **2004**, *43 (9)*, 1944.

27. F.R. Zaggout, N. Abu Ghalwa, *Journal of Environmental Management*, **2008**, *86* (1), 291.

28. M. Marcu, C. Pirvu, A. Banu, E. Vulpasu, *Revista de Chimie (Bucuresti)*, **2008**, *59 (8),* 867.

29. M. Jitaru, L.R. Mandoc, C. Mihai, O. Tudoran, *Studia Universitatis Babes-Bolyai Chemia*, **2005**, *50*, 137.

30. L. Gu, X.W. Zhang, L.C. Lei, Y. Zhang, *Microporous and Mesoporous Materials*, **2009**, *119* (1-3), 237.

31. E. Sabio, E. Gonzalez, J.F. Gonzalez, C.M. Gonzalez-Garcia, A.J. Ramiro, *Carbon*, **2004**, *42 (11),* 2285.

32. M. Zhou, Q. Dai, L. Lei, D. Wang, *Journal of Zhejiang University of Science*, **2004**, *5 (12),* 1512.

33. M. Zhou, L. Lei, *Chemosphere*, **2006**, *65 (7),* 1197.

34. M. Jitaru, B. Koumanova, *Studia Universitatis Babes-Bolyai Chemia*, **2006**, *51 (2)*, 113.

35. M-C. Tertis, M. Jitaru, F. Ionescu, *Studia Universitatis Babes-Bolyai Chemia,* **2009** (*in press*).

36. M-C. Tertis, M. Jitaru, M. Toma, *Scientific Study and Research*, **2008**, *9 (3),* 281.

37. M-C. Tertis, M. Jitaru, *Revista de Chimie (Bucuresti),* **2009** (*in press*).

38. M-C. Tertis, M. Jitaru, *Studia Universitatis Babes-Bolyai Chemia,* **2007**, *52 (4),* 153.

ORGANOCLAYS AND INORGANIC-ORGANIC PILLARED CLAYS. PREPARATION, CHARACTERIZATION AND POTENTIAL USE AS ELECTRODE MODIFIER

VICTOR K. TCHIEDA[a,c], IGNAS K. TONLE[b], MIHAELA-CLAUDIA TERTIŞ[c], EMMANUEL NGAMENI[a], MARIA JITARU[c*], DANIEL A. LOWY[d]

ABSTRACT. We report on the synthesis of organoclays and inorganic-organic clays obtained by inserting in natural clay hexadecylpyridinium (HDPB) bromide and HDPB plus hydroxy-aluminium, respectively. The effect of synthesis conditions on the physical, chemical, and structural properties of the products was examined by total organic carbon determination, specific surface and porosity measurement, and performing SEM and FT-IR of the surface. Glassy carbon electrodes were modified by a film of the organoclays, and utilized as the working electrode in ion-exchange voltammetry. Multistep cyclic voltammetry revealed a time dependence accumulation of anions in the clay layer, by adsorption from the supporting electrolyte. Thereby, the modified clays have been shown to be useful in analytical applications that involve high affinity ion capturing. Recorded adsorption isotherms show that these modified clays are promising materials for environmental application as adsorbents of organic pollutants such as 2,4- and 2,6-dinitrophenols.

Keywords: modified clays, organoclays, organic-inorganic clays, ions exchange voltammetry, and dinitrophenols.

INTRODUCTION

Most industrial waste waters contain hydrophobic organic compounds, e.g., nitrophenol derivatives, along with oxyanions, such as chromate ions. Even when present at trace levels, these contaminants are toxic to animals and to microorganisms in the soil [1], or may act as possible mutagens and carcinogens [2]. Recovery or total immobilization of these pollutants from residual waters is a major concern, which triggers research toward developing new and more efficient adsorbents [1, 3-7].

[a] *Laboratory of Analytical Chemistry, Faculty of Science, University of Yaoundé 1, PO Box 812 Yaoundé, Cameroon; email: engameni@yahoo.fr*
[b] *Department of Chemistry, Faculty of Science, University of Dschang; PO Box 67 Dschang, Cameroon; email: itonle@yahoo.com*
[c] *Research Center LAF-INT-ECOL, Faculty of Chemistry and Chemical Engineering, "Babes-Bolyai" University, 11 Arany Janos Street, 400028 Cluj-Napoca, Romania, e-mail: mjitaru@chem.ubbcluj.ro*
[d] *Davia Corporation, 13255 Revilo Loop, Woodbridge, VA 22191, USA, e-mail: daniellowy@davia.biz*

Smectite clay minerals are readily available crystalline materials, which can be used as less expensive adsorbents. They possess a lamellar structure, which comprises overlaid sheets, where each tetrahedral sheet is bound to the octahedral sheet. Clays possess permanent negative charges, and the presence of cations renders them electrically neutral. These interlayer Na^+, Ca^{2+}, and K^+ cations are exchangeable: they can be substituted by organic cations or by hydroxylmetal cations. By exchanging the original interlayer cations for organocations, one could obtain organically modified materials, known as *organoclays* [8,9]; while clays treated with inorganic ions are referred to as *pillared clays* [10, 11].

In both cases, the surface properties of the obtained materials undergo a dramatic change. As a result of the treatment, the surface of clays become organophilic, as it accommodates covalently linked organic moieties. The lamellar structure of the organoclay remains, however, analogous to the parent phyllosilicate. Owing to their great affinity for hydrophobic organic compounds, they manifest excellent adsorptive properties toward them [12]. On their turn, pillared clays are efficient adsorbents of heavy metals and oxyanions [13, 14]. Consequently, clays with an intercalated organic surfactant and a hydroxyl-metal cation, termed as *organic-inorganic clay* [15] should adsorb from aqueous solutions organic compounds and oxyanions, simultaneously.

Four procedures are described for the synthesis of organic-inorganic clays (abbreviated as IO clays) [15] termed alternatively as inorganic clay–organic cation complexes [16]. Typically, the synthetic procedure involves a controlled hydrolysis reaction, which may proceed either in solution or in the interlayer galleries of the clay. When the hydrolysis takes place in solution, the yielded amount of polycation is determined by the identity of reactants and their initial concentrations, the degree of hydrolysis, temperature, the rate at which the reactants are added, and the overall duration of the reaction [17]. Zhu and co-workers [18] demonstrated that cetyltrimethylammonium bromide (CTAB) surfactant and Al could not be both inserted in the interlayer gallery of bentonite, when added at the same time, or when CTAB was first incorporated. Conversely, when Al_{13} was added first, the aluminum cations "blocked" the interlayer space, hence, the eventual insertion of CTAB becomes extremely difficult.

In this work, we synthesized an organoclay and an inorganic-organic clay via insertion of hexadecylpyridinium bromide (HDPB), and HDPB plus hydroxy-aluminium, respectively. The effect of synthesis conditions on the physical, chemical, and structural properties of the products was examined by (i) total organic carbon determination, (ii) specific surface and porosity measurements, (iii) FT-IR, and (iv) ion-exchange voltammetry. Batch adsorption experiments show that these modified clays are promising materials for environmental application, as adsorbents of hazardous 2,4- and 2,6-dinitrophenols.

RESULTS AND DISCUSSION

Clay modification

Modified smectites were obtained according to procedures described in the Experimental part. Sample codes and sample descriptions are listed in Table 1.

Table 1. Samples code and description of the natural and modified clays

Sample	Description
Sa01	Natural clay
Sa01-Na	Natural clay converted in homo-ionic form
O- Sa01(a)	Sa01-Na clay modified with organic substance, 0.5 time CEC
O- Sa01(b)	Sa01-Na clay modified with organic substance, 1 time CEC
O- Sa01(c)	Sa01-Na clay modified with organic substance, 2 time CEC
I- Sa01	Clay modified with inorganic substance, Al_{13} (10 mmol/g of clay)
OI- Sa01(a)	Clay modified with organic substance, 0.5 time CEC and Al_{13} (10 mmol /g of clay)
OI- Sa01(b)	Clay modified with organic substance, 1 time CEC and Al_{13} (10 mmol/g of clay)

CEC: Cation-exchange capacity
Organic substance: hexadecylpyridinium bromide (HDPB)
Inorganic substance: hydroxy-aluminum with the formula $[Al_{13}O_4(OH)_{24}(H_2O)_{12}]^{7+}$, abbreviated as Al_{13}

Materials characterization

TOC values obtained for the investigated samples are listed in Table 2.

Table 2. COT values determined for different samples

Sample	TOC (mg C /g clay)	Carbon (%wt)
Sa01	0.87	0.087
O-Sa01(b)	84.0	8.40
OI-Sa01(b)	54.0	5.40

Data in Table 2 reveal that natural clay contains a very low quantity of carbon, which originates from the organic impurities present in the sample. The high carbon proportion determined in the other two samples originates from HDPB. The lower carbon percentage of the hybrid (OI-Sa01(b)) as compared to the organoclay (O-Sa01(b)) is a result of utilizing Al_{13} in the second step of the sample treatment. This aluminum complex replaces in part HDPB present in the interlayer space, decreasing the overall carbon content of the resulting modified clay [19].

Overlaid IR spectra of samples Sa01, O-Sa01(b) and OI-Sa01(b) are shown in Figure 1. The very strong absorption band, present in the three samples around 3635 cm^{-1} can be assigned to the internal OH group linked to Al or Mg in the montmorillonite sheets [20-21]. Upon examining these spectra one can notice three major changes in the two modified clays, as compared to the starting material.
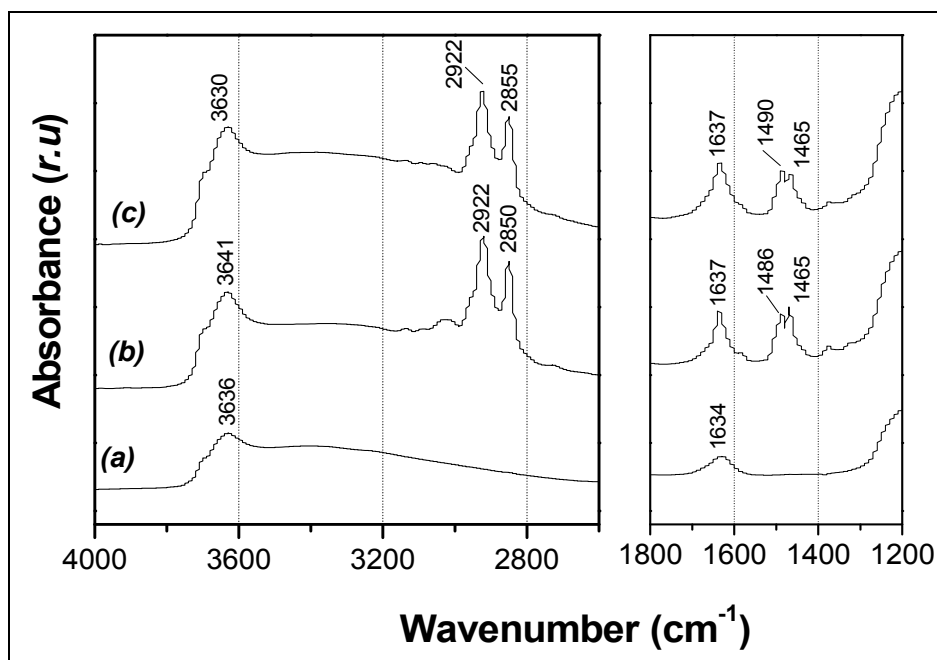

Figure 1. IR spectra (recorded in the range from 4000 to 1200 cm^{-1}) of (a): Sa01, (b): O-Sa01(b) and (c): OI-Sa01(b) materials.

Absorptions bands between at 3000 and 2800 cm^{-1} present in modified materials correspond to the vibrations and symmetrical deformations of -CH$_2$-groups. Furthermore, the absorption bands around 1490 and 1465 cm,$^{-1}$ which are not present on the spectra of the unmodified clay, can be assigned to the in-plane deformation of the C-H bond. The changes arising with the clay modification support the idea of intercalation of the organic molecules between the clay sheets.

Microphotographs recorded by SEM for samples modified and unmodified clays (Figure 2) reveal that the unmodified material, i.e., the native clay has a uniform surface with even pore distribution. These findings confirm the results of specific surface and porosity measurements, Table 3.
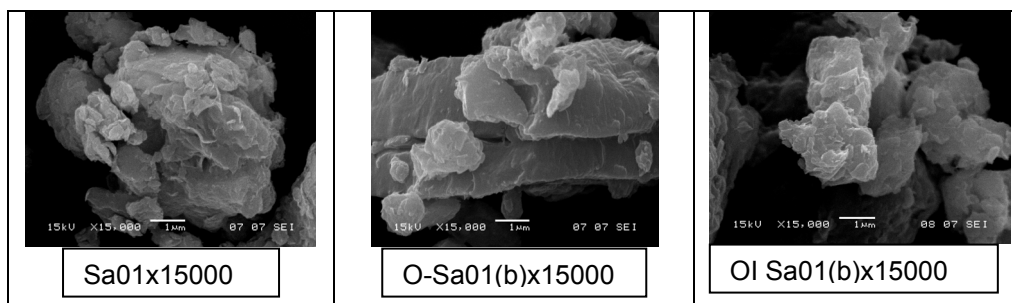
Figure 2. SEMs of Sa01, O-Sa01(b) and OI-Sa01(b) materials.

Table 3. Specific surface and pores distribution of some clays.

Sample	Surface Area		Pore volume (t-plot)	Mezo- and Macropores (BJH-desorbtion)		
	Single point m² g⁻¹	BET m² g⁻¹	Cumulative volume of pores, cm³ g⁻¹	Total area m² g⁻¹	Total volume cm³ g⁻¹	Average pore diameter nm
O-Sa01(b)	1.4954	1.6652	-	1.6216	0.015936	3.9309
Ol-Sa01(b)	3.1324	3.3639	-	5.6173	0.030170	2.1484
Sa01	59.7219	60.6172	0.00748	58.5195	0.109799	0.7505

Comparing with unmodified smectite, the specific surface of O-Sa01 and OI-Sa01 decrease and the average pore diameter increase after modification, Table 3. Thereby, the modified clays could be able to absorb the big anions such ferricyanide, chromates, etc. from the surrounding solution.

Characterization of materials by ion-exchange voltammetry

As we intend to use the organoclays in high affinity analytical ion capturing, it was necessary to study the behaviour of a solid electrode substrate covered by these materials. Thus, some electrochemical experiments were performed through a glassy carbon (GC) electrode modified by dip-coating using a 2 %wt (organo)clay suspension (O-Sa01), and drying the film in air at room temperature. Such electrodes were scanned in the classical ferricyanide/ferrocyanide system.

As revealed by Figure 3(A), the magnitude of peak current recorded with OI clay-modified GC electrode is more than two fold greater than the signal obtained with a bare GC electrode. The greater signal, however, needs to be developed over time (see Figure 3(B)).
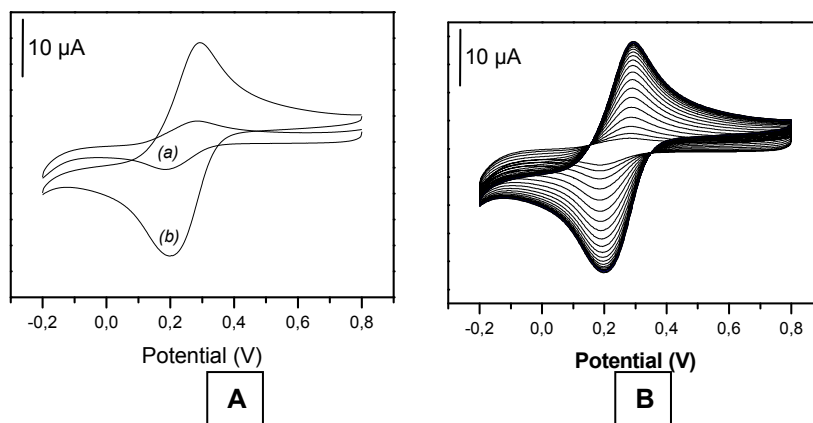
Figure 3. (A) Cyclic voltammetry of 10^{-3} M $[Fe(CN)_6]^{3-}$ in 0.1 M KCl performed with (**a**) unmodified glassy carbon (GC) electrode and (**b**) GC modified with an organic-inorganic clay film. (Scan rate: 50 mV s^{-1})
(B) Successive scans (20 scans) of 10^{-3} M $[Fe(CN)_6]^{3-}$ in 0.1 M KCl performed with GC electrode modified with an organic-inorganic clay film. (Scan rate: 50 mV s^{-1})

Shown in Figure 3(B) is the increase of peak currents with the number of successive scans. Very scarce Faradaic activity is noticed in the first cycle, as if the supporting electrolyte were not electroactive. This observation is a consequence of the blocking properties of the clay film located on the electrode surface. Over the next scans however, peak currents increase progressively, owing to the incorporation of electroactive species in the film. Redox species are continuously accumulated in the clay film via the replacement of counter ions of the weekly bound surfactant. By this, ion pairs are formed between the HDP$^+$ cations and the $[Fe(CN)_6]^{3-}$ anions [22]. After about 15 cycles, the peak currents stabilize at constant values, indicating that the system has reached the steady state. This observation indicates that the electrode coating enables the fixation of anions from solution. The explanation of the phenomenon is that several smectites, though negatively charged prior to being applied as a coating layer onto the GC surface, are able to absorb the anions from the supporting electrolyte, and store them in its pores, or even on the sides of the clay surface, which interact strongly with the anions [23,24].

Another possible reason for $[Fe(CN)_6]^{3-}$ build-up in the clay film is the following: during the synthesis a large number of surfactant cations (HDP$^+$) substituted by Al polycations are retained by the clay via hydrophobic interactions with their long carbon chain [25]. As a consequence, the overall positive charge of the clay increases, which is a driving force for absorbing additional ferricyanide anions from the surrounding solution.
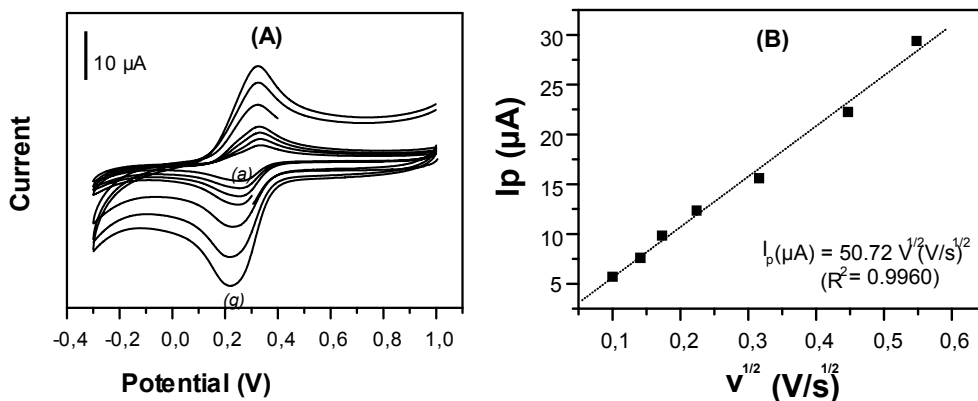
168

Figure 4. (**A**) Cyclic voltammetry performed in 10^{-3} M $[Fe(CN)_6]^{3-}$ in 0.1 M KCl with a GC modified with a film of OI clay, at scan rates of 10 (a), 20, 30, 50 , 100, 200 and 300 (g) mV s^{-1}. (**B**) Variation of peak current with the square root of scan rate.

Figure 4(A) displays the cyclic voltammograms, recorded at increasing potential scan rates from 10 to 300 mV s^{-1}. As one can notice, the the peak potential separation was not really affected with scan rate; however, the peak currents correlate linearly with the square root (Figure 4(B)) of the potential scan rate (R^2 =0.9971).

Adsorption properties of the modified clays

In order to investigate the potential of our modified clays as adsorbents of environmental contaminants, we investigated the extent to which they retain model compounds. Because of their environmental impact we have chosen 2,4-dinitrophenol (2,4-DNP) and 2,6-dinitrophenol (2,6-DNP) The sorption isotherms were presented in Figure 5. The values of 1/n were obtained from the application of the Freundlich model and Langmuir [7]. Further, the slope 1/n between 0 and 1 is a measure of adsorption intensity or surface heterogeneity, with the surface becoming more heterogeneous, when the value is closer to 0 [26]. As 1/n is less than 0.40, the materials have a heterogeneous surface. The 2,4-DNP adsorption capacities for O-Sa01 and IO-Sa01 calculated according to Langmuir isotherm are 53.48 and 54.05 mg g^{-1}, respectively, and 43.10 and 43.67 mg g^{-1} for 2,6-DNP adsorption on O-Sa01 and IO-Sa01, respectively [27], comparable to the adsorption capacity (q_{max} = 41.15mg.g^{-1}) of 2,6-dinitrophenol on activated carbon, obtained by Tertis and co-workers [28].
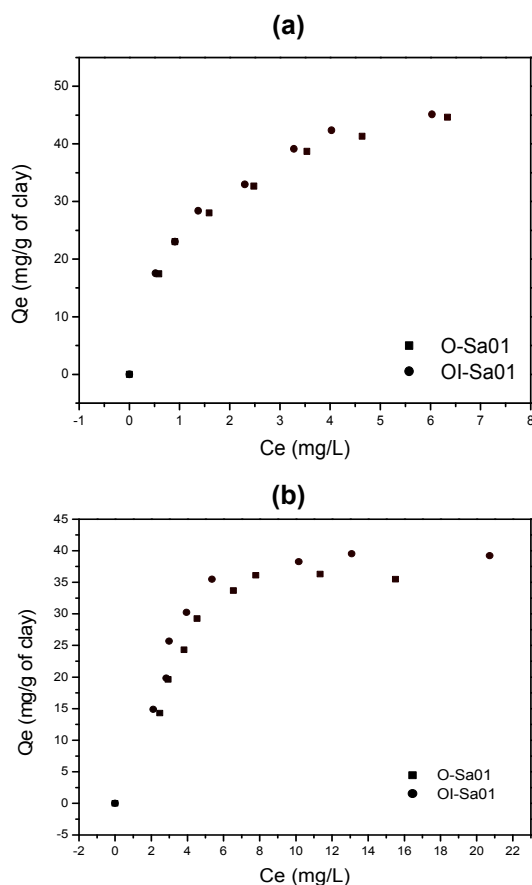
(a)

(b)

Figure 5. Sorption isotherms of 2.4-DNP (a) and of 2,6-DNP (b) on O-Sa01 and OI-Sa01.

No significant difference is observed on the maximum amount of adsorption during the adsorption of these derivatives between nitrophenols on O-Sa01 and IO-Sa01; however, the latter has the advantage to adsorb simultaneously hydrophobic organic compounds and inorganic substances from aqueous solution [18, 25].

CONCLUSIONS

New organoclays (O-Sa) and inorganic-organic (OI-Sa) clays were synthesized by insertion of (HDPB) and (HDPB) plus $[Al_{13}O_4(OH)_{24}(H_2O)_{12}]^{7+}$, respectively. These modified smectites were characterized (SEM, FT-IR, TOC, specific surface, porosity) and were used to modify glassy carbon electrode with a clay film (GCE-CF). The (GCE-CF) was working electrode in ion-exchange voltammetry for a model ferri/ferro cyanide system.

The main conclusions are:

- Clay modification was confirmed by FT-IR, SEM and TOC determination;
- The specific surface of O-clay and OI-clay decrease and the average pore diameter increase after modification, Table 3. Thereby, the modified clay are able to absorb the anions, such ferricyanide.
- Modified clays reported here show promising properties as adsorbents of environmental pollutants, such as 2,4- and 2,6-dinitrophenols (q_{max} = 53.48-54.05 mg g^{-1})

As we intend to use the organoclays in high affinity analytical ion capturing, future experiments will be done to confirm the adsorption capability of modified clay for other anions.

EXPERIMENTAL SECTION

Materials and methods

2,4-DNP with 0.5 mL H_2O/g (Merck, Germany), and 2,6-DNP with purity Greater than 95% (wt.% calculated based on dry substance), moistened with 20% H_2O (Aldrich, Switzerland) were used for preparing solutions with concentrations needed for our experiments. Aqueous solutions were prepared with distilled water. All reagents were analytical grade, and used without further purification.

The clay utilized in this work originates from Sabga, a locality of the North-West Region of Cameroon. Its characterization and chemical composition correspond to smectite, as reported in previous work [27]. Details on the synthesis and characterization of organo-clays and inorganic-organic pillared clays are being published elsewhere [29].

Clay modification

First, the clay is cleaned, and dried in air, and then crushed, and sifted through a sieve of 90 μm diameter mesh. Raw clay is enriched in clay minerals by sedimentation, followed by the collection of the fine fraction (particles with diameter less than 2 μm).

Conversion into homo-ionic form

An amount of 5 g of fine clay fraction are dispersed in 200 mL of 1M NaCl in distilled water, and stirred for 24 h. This operation is repeated three times to ensure that the clay is fully converted in the homo-ionic form. Then, the solid is collected by centrifugation, and washed with distilled water, until its silver nitrate test becomes negative.

Intercalation of the organic surfactant

The solution of hexadecylpyridinium bromide is mixed with homo-ionic clay; the mixture is stirred for 5 h, centrifuged, washed several times with distilled water, and then the solid is dried in air, at ambient temperature.

This clay is referred to O-Sa01(a), a referring to the amount of surfactant in relation with the CEC of the clay (see Table 1).

Modification with hydroxy-aluminum, $[Al_{13}O_4(OH)_{24}(H_2O)_{12}]^{7+}$

The title process is performed by adding a solution of hydroxy aluminum to a 2% suspension of O-Sa01 in distilled water, such that the Al/clay ratio is 10 mmol g^{-1}. Addition takes place at 60 °C, and then the mixture is stirred for 2 h at the same temperature. Again, the solid is washed with distilled water, until negative to chloride test, and then dried at 60 °C for 24 h. This modified clay is referred to under the code name IO-Sa01.

Materials characterization

(i) *Structural characterization* was performed by S_{spec}, pores volume and distribution measurement (Micrometrics TriStar II 3020 V1.01), SEM (JEOL JSM 5510 LV) and FT-IR (Brucker VERTEX 70).

Porosity measurements were performed by adsoptiob/desorption of nitrogen. Prior to the measurements the materiel was degassed for eliminating the water molecules retained by physical adsoption or condensation in the pores of the clay. In work reported here we degassed the clay at 65 ^{0}C for 24 h, which prevented decomposition of the hexadecylpyridinium bromide surfactant molecules (with a fusion temperature in the range of 79-82 ^{0}C). Control samples, which did not contain organic surfactants, were degassed at 150 ^{0}C, providing similar results.

(ii) Organic carbon content of organic modified clays (TOC determination)
The measurement was carried out by means of a Model LCK 385 TOC-DR 2800 Hach Lange for water quality instrument comprised of a digestion container, equipped with a TOC-5 stirrer, a thermostat, and a photometer. TOC determination involved two steps:

(a) *Sample preparation* by the elimination of total inorganic carbon, as follows: 2 mL of sample suspension were placed in the digestion container, and then the stirrer was inserted.

(b) *TOC determination*: the digestion container is heated in the thermostat at 95°C for 2 h, and then allowed to cool to ambient temperature. Then, the outer wall of the container is wiped, and inserted in the photometer for performing the measurements.

(iii) Batch adsorption experiments
Adsorption experiments were carried out by using the conventional batch technique. Nitrophenol solutions were prepared by dissolving required amounts of solid NP in distilled water. The initial concentrations of NP compounds was between 11.4 and 29.4 mg L^{-1}, for 2,4-DNP, and from 11.4 to 36.8 mg L^{-1}, for 2,6-DNP. The amount of clay (0.03 g) added to 0.05 L of NP solution and the temperature (25 $\pm$ 2) ^{0}C were kept constant during the adsorption experiments. The concentration of adsorbed NP was determined from absorbance data [27, 28].

172

ACKNOWLEDGMENTS

REFERENCES

1. P.X. Wu, Z.W. Liao, H.F. Zhang, J.G. Guo, *Environment International*, **2001**, *26*, 401.
2. F.M.M. Paschoal, M.A. Anderson, M.V.B. Zanoni, *Journal of Hazardous Materials*, **2009**, *166*, 531.
3. C. Volzone, L.B. Garrido, *Journal of Environmental Management*, **2008**, *88*, 1640.
4. L. Zeng, X. Li, J. Liu, *Water Research*, **2004**, *38*, 1318.
5. H.-D. Choi, W.-S. Jung, J.-M. Cho, B.-G. Ryu, J.-S. Yang, K. Beak, *Journal of Hazardous Materials*, **2009**, *166*, 642.
6. S. Arfaoui, N. Frini-Srasra, E. Srasra, *Desalination*, **2008**, *222*, 474.
7. I.A.W. Tan, A.L. Ahmad, B.H. Hameed, *Journal of Hazardous Materials*, **2009**, *164*, 473.
8. R.K. Kukkadapu, S.A. Boyd, *Clays and Clay Minerals*, **1995**, *43* (3), 318.
9. H. He, R.L. Frost, T. Bostrom, P. Yuan, L. Duong, D. Yang, Y. Xi, J.T. Kloprogge, *Applied Clay Science*, **2006**, *31*, 262.
10. P. Yuan, H. He, F. Bergaya, D. Wu, Q. Zhou, J. Zhu, *Microporous and Mesoporous Materials*, **2006**, *88*, 8.
11. P. Yuan, X. Yin, H. He, D. Yang, L. Wang, J. Zhu, *Microporous and Mesoporous Materials*, **2006**, *93*, 240.
12. L. Zhu, X. Ruan, B. Chen, R. Zhu, *Chemosphere*, **2008**, *70*, 1987.
13. J.Z. He, A.D. Cristofaro, A. Violante, *Clays and Clay Minerals*, **1999**, *479*, 226.
14. T. Kasama, Y. Watanabe, H. Yamada, *Applied Clay Science*, **2004**, *25*, 167.
15. H. Khalaf, O. Bouras, V. Perrichon, *Microporous Materials*, **1997**, *8*, 141.
16. T. Wanga, M. Wang, Z. Zhanga, X. Gea, Y. Fanga, *Materials Letters*, **2007**, *61* (17), 3723.
17. J.Q. Jiang, N.J.D. Graham, *Journal of Chemical Technology and Biotechnology*, **1998**, *73*, 351.
18. R. Zhu, T. Wang, F. Ge, W. Chen, Z. You, *Journal of Colloid and Interface Science*, **2009**, doi: 10.1016/j.jcis.2009.03.033.
19. Z. Navrátilová, P. Kula, *Fresenius Journal of Analytical Chemistry*, **2000**, *367*, 369.

20. H. Zhao, Z.F. Jaynes, G.F. Vance, *Chemosphere*, **1996**, *33*, 2089.

21. B.S. Krishna, D.S.R. Murty, B.S.J. Prakash, *Journal of Colloid and Interface Science,* **2000**, *229*, 230.

22. E. Ngameni, I.K. Tonlé, J.T. Apohkeng, R.G.B. Bouwé, A.T. Jieumboué, A. Walcarius, *Electroanalysis*, **2006**, *18*, 2243.

23. P. Kula, Z. Navrátilová, P. Kulová and M. Kotoucek, *Analytica Chimica Acta*, **1999**, *385,* 91.

24. Z. Navrátilová, P. Kula*, Journal of Solid State Electrochemistry*, **2000**, *4*, 342.

25. R. Zhu, L. Zhu, J. Zhu, F. Ge, T. Wang*, Journal of Hazardous Materials*, **2009**, doi:10.1016/j.jhazmat.2009.03.057.

26. F. Haghseresht, G. Lu, *Energy Fuels*, **1998**, *12*, 1100.

27. V.K. Tchieda, I.K. Tonle, M. Jitaru, M. C. Tertis, E. Ngameni (*manuscript sended to Environmental Engineering and Management Jourmal*).

28. M-C. Tertiş, M. Jitaru, F. Ionescu, *Studia Universitatis Babes-Bolyai Chemia*, **2009**, *in press*.

29. I. Tonle, E. Ngameni, D. Njopwouo, C. Carteret, A. Walcarius, *Physical Chemistry Chemical Physics*, **2003**, *5 (21)*, 4951.

ELECTRODEPOSITION OF BISMUTH, TELLURIUM AND ANTIMONY FROM IONIC LIQUIDS BASED ON CHOLINE CHLORIDE AND UREA AS THERMOELECTRIC FILMS

FLORENTINA GOLGOVICI[a], ANCA COJOCARU[a], CAMELIA AGAPESCU[b], YITENG JIN[c], MARIN NEDELCU[a], WEI WANG[c], TEODOR VISAN[a]

ABSTRACT. The aim of this work was to study the electrodeposition of Bi, Sb and Te as singular components of thermoelectric films using an ionic liquid medium (choline chloride + urea; 1:2 molar mixture). Ionic complex species ($BiCl_4^-$, $SbCl_4^-$ and $TeCl_6^{2-}$) were supposed as participant species at the cathodic process, and were prepared by dissolving BiO_2, $SnCl_3$ and TeO_2 in 0.5 - 10 mM concentrations. Cyclic voltammograms on Pt exhibited a single couple of reduction/ oxidation peaks at all scan rates (2 – 200 mVs^{-1}) and temperatures (40 – 85 ^0C). Values of diffusion coefficients and activation energy for diffusion were also estimated. Nyquist and Bode spectra, obtained from electrochemical impedance measurements, proved the diffusion control. By fitting the experimental data with an equivalent electrical circuit of modified Randles type the differences in double layer capacitances and also in charge transfer resistances for the three cathodic processes of Bi, Sb or Te ions were evidenced.

Keywords: electrodeposition, bismuth, antimony, tellurium, cyclic voltammetry, electrochemical impedance spectroscopy

INTRODUCTION

Bi and Sb are elements of Vth group with relatively good electrical properties and a superposition of valence and conduction bands; tellurium is a semiconductor belonging to VIth group. All these elements are involved in preparation of binary or ternary thermoelectric materials. The increase of Sb content in BiSb solid solution leads to enlargement of band gap and to diminution of thermal conduction, thus improving its thermoelectric behavior. BiSb alloys are very attractive materials for thermoelectric refrigeration at low temperature (below 200K). Bismuth and antimony telluride-based materials are of great interest for thermoelectric applications in the temperature range of 200-400 K, whereas BiSbTe ternary compound (written sometimes as Bi_2Te_3-Sb_2Te_3 mixture) is the best for both thermoelectric refrigeration and thermoelectric power generation [1-3].

[a] *Politehnica University of Bucharest, Department of Applied Physical Chemistry & Electrochemistry, Calea Grivitei 132, 010737 Bucharest, Romania, floregov@yahoo.com*
[b] *Remed Prodimpex Company, Bd Basarabia 208A Bucharest, Romania*
[c] *Department of Applied Chemistry, School of Chemical Engineering and Technology,Tianjin University, Tianjin 300072, China*

In addition to bulk thermoelectric materials, which are processed by solidification methods or powder metallurgy, films varying from sub-micron to several microns thick have been studied, because of their potential applications in miniature thermoelectric devices and thermobatteries. In general, the thermoelectric films are fabricated by chemical or physical vapor deposition. Compared to these techniques, the electrodeposition may offer some advantages, including it cost-effectiveness, rapid deposition rates, and relative ease in controlling film thickness.

In last years ionic liquids were increasingly applied for electrochemical deposition of numerous metals on various substrates [4], replacing the traditional baths of aqueous solutions. An ionic liquid as solvent in the electrodeposition bath shows a good electric conductivity, a large potential window as well as a high thermal stability. From literature examination, we noticed that experiments with electrodeposition of tellurium, bismuth or antimony as pure metals or their compounds using ionic liquid media are relatively seldom reported. Historically, most of such electrochemical studies employed imidazolium salts [5,6] or molten chloroaluminates [7] as electrolytes.

Recently, we reported [8] results on film codeposition of Te with Bi and Sb (as binary compounds) using a bath consisting in the eutectic of choline chloride (**ChCl**) and urea as supporting electrolyte, with additions of Bi oxide or Sb chloride, respectively. To our best knowledge such processes in ChCl containing ionic liquids have not been yet reported. The choice of ChCl-urea system was related to the works of Abbott *et al*. who showed [8] that an ionic liquid can be formed by mixing choline chloride (2 hydroxy-ethyl-trimethyl-ammonium) with a hydrogen bond donor species such as an amide (urea).

The electrochemical procedure of thermoelectric material deposition reported here is environmentally friendly compared with the conventional methods of deposition using aqueous baths and also compared with other ionic liquids used as deposition baths. We found out that Bi, Sb and Te precursors (in our experiments BiO_2, $SbCl_3$, TeO_2, respectively) dissolve relatively easy in ChCl-urea eutectic and we performed electrolysis experiments at 40 - 85^0C using this electrolyte. Cyclic voltammetry (CV) and electrochemical impedance spectroscopy (EIS) were chosen as electrochemical techniques in order to evidence processes of deposition/ dissolution of Bi, Sb and Te.

RESULTS AND DISCUSSION

Regarding the relatively high solubility of bismuth, antimony and tellurium compounds in ChCl-urea (1:2) ionic liquid in such amounts to have a significant electrochemical response for Bi(III), Sb(III) and Te(IV) ions, an explanation may be the presence of chloride anion Cl^- as ligand forming complexes. For instance, by dissolution of bismuth oxide and antimony chloride precursors in the electrolyte

we suppose the formation of $BiCl_4^-$ and $SbCl_4^-$ complex ions in ChCl-urea eutectic, leading to a low diffusive ionic species [8]; correspondingly, tellurite TeO_2 should be converted in tellurium chloride and incorporated in ionic liquid as $[TeCl_{4+x}]^{x-}$ ions with low diffusion coefficients, too [6]. Similar situation was suggested for zinc chloride dissolved in quaternary ammonium halides [10] which forms complex chlorozincate anions, $ZnCl_3^-$, $Zn_2Cl_5^-$ and $Zn_3Cl_7^-$. The existence of $BiCl_4^-$ and $SbCl_4^-$ ions in very concentrated aqueous chloride electrolytes (6M HCl or 5M NaCl + 1M HCl solutions) was supposed in our previous work [11].

Cyclic voltammetry measurements were carried out, within 40 - 85^{0}C temperature range, in order to investigate the electrochemical reversibility of electrode process and the appropriate potential range for electrodeposition/ dissolution of single metal films. Typical cyclic voltammograms of the separately investigated ions recorded on Pt electrode in the absence of solution stirring are presented in Figures 1-3. We selected the CV curves at various scan rates which were obtained by sweeping the potential from stationary potential in cathodic direction (until -0.8 V limit) and returning to anodic region (a limit of maximum 0 V) and back. The CVs with enlarged potential range did not show any supplementary electrode process except the cathodic and anodic processes of background electrolyte.
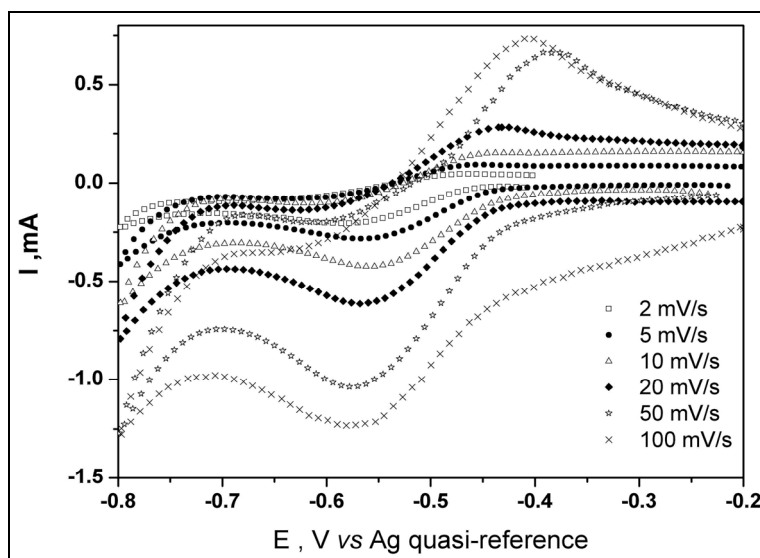

Figure 1. Cyclic voltammograms of Bi(III) ions on Pt electrode in ChCl – urea eutectic; Bi(III) concentration: 10 mM; temperature 80 ^{0}C.

During the examination of the electrochemical behavior of Bi ionic species (Fig. 1) only a couple of reduction/oxidation peaks can be observed at all scan rates. At lowest scan rate and 80^0C temperature the cathodic peak and the anodic peak are located at potentials -0.53 V and -0.43 V *vs.* Ag quasi-reference electrode, respectively. With higher scan rates the peak separation for this couple, ΔE_p, increases from 100 mV to *cca.* 200 mV. Similar results were also found in the CVs recorded in Sb(III) and Te(IV) containing solutions (Figs. 2 and 3). As Fig. 2 shows, for Sb(III) containing ionic liquid and 80 ^{0}C temperature the reduction/oxidation peaks are located at potentials -0.6 V and -0.53 V, respectively, and the corresponding peak separation, ΔE_p, recorded for various scan rates ranged in a larger potential interval, 70 - 300 mV. For either Bi ions or Sb ions the metallic film formation may take place as:
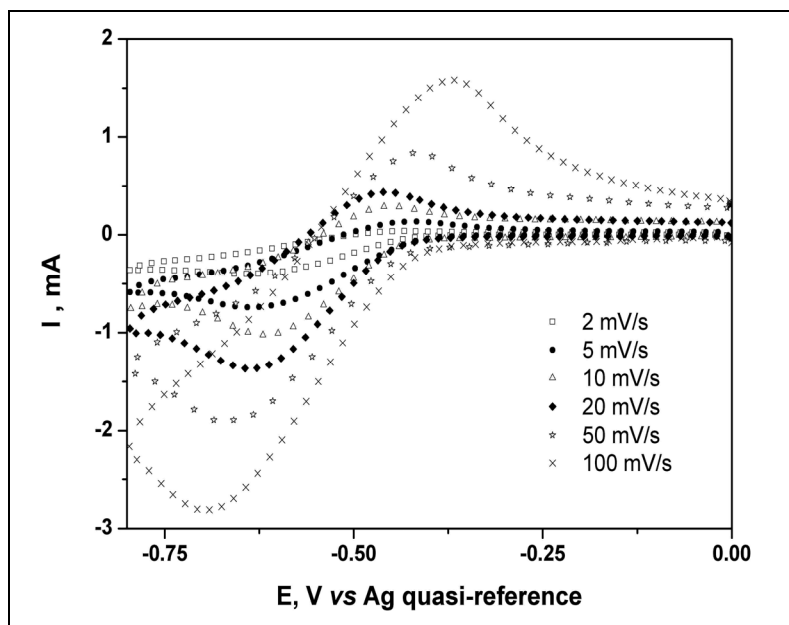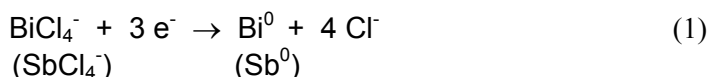
$$BiCl_4^- + 3\ e^- \rightarrow Bi^0 + 4\ Cl^- \tag{1}$$
$$(SbCl_4^-) \qquad\qquad (Sb^0)$$

Figure 2. Cyclic voltammograms of Sb(III) ions on Pt electrode in ChCl – urea eutectic; Sb(III) concentration: 10 mM; temperature 80 ^{0}C.

In the example illustrated by Fig. 3, the voltammetric curves at 70 ^{0}C temperature for Te ion reduction on Pt show a single reduction peak (*e.g.* at potential about -0.6 V for 10 mVs^{-1} scan rate) attributed to deposition of tellurium film; also a single anodic peak (*e.g.* about -0.38 V for 10 mVs^{-1} scan

rate), corresponding to the stripping of deposit, was recorded. So, a direct discharge of $[TeCl_{4+x}]^{x-}$ ions, written $TeCl_6^{2-}$ as the most probable anion [6], is expected in the cathodic process:

$$TeCl_6^{2-} \; + \; 4\,e^- \; \rightarrow \; Te \; + \; 6\,Cl^- \tag{2}$$
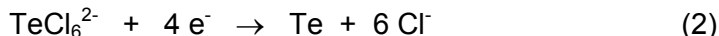
The increase of scan rate gives rise to a peak separation values for Te(IV)/Te couple within 200 - 280mV potential interval.
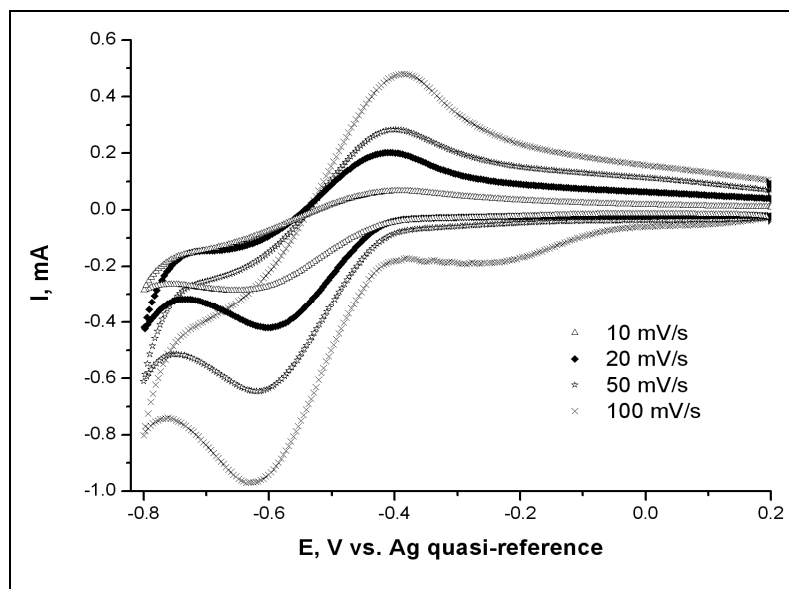
Figure 3. Cyclic voltammograms of Te(IV) ions on Pt electrode in ChCl – urea eutectic; Te(IV) concentration: 5.5 mM, temperature 70 ^{0}C

The above observations of CV shapes are valid at all investigated ion concentrations and working temperature. The cathodic peaks representing the formation of Bi^0, Sb^0 and Te^0 have a shape with a relatively large diffusion current if the applied potential was more negatively. The oxidation peaks on the anodic branches of voltammograms correspond to redissolution of freshly deposited metallic layer. The peak potential separation and peak shapes reveal that the reduction/oxidation processes of Bi(III), Sb(III) and Te(IV) on Pt surface are all quite irreversible (from electrochemically point of view). However, we consider that these electrode processes are actually moderately irreversible, due to a quite large contribution in the potential peak separation of a non-compensated ohmic drop inside the ionic liquid.

It may be observed from reactions (1) and (2) that four or six chloride ions are supplementary produced, thus enriching the ionic liquid medium with complexing agent. This fact is important in alloy electrodeposition, because complexation brings the reduction potentials of bismuth, antimony and tellurium ions close to each other, favouring their co-deposition. In the investigated ionic liquid the underpotential deposition (UPD) of Bi, Sb or Te was rarely noticed. Also, the shape and the potential region for both cathodic and anodic peaks are different from these reported for Bi, Sb and Te ions in aqueous (nitrate or chloride) acid solutions [11]. The main reason for this disagreement could be the difference in chemical nature of electrolytes, aqueous or ionic liquid.
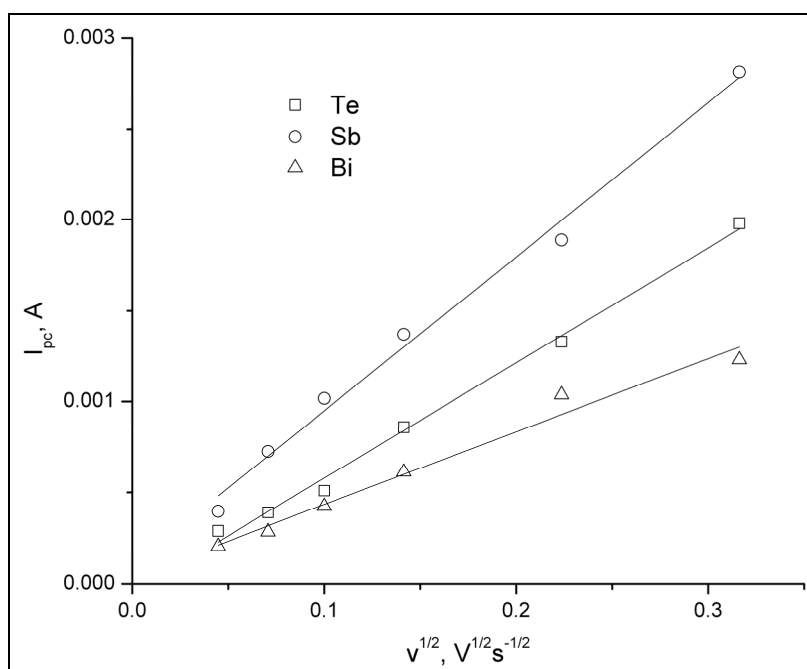

Figure 4. I_{PC} *vs.* $v^{1/2}$ dependence for Bi, Sb, Te electrodeposition on Pt in ChCl – urea eutectic at 80^0 C; the same 10 mM concentration for all three ions: Bi(III), Sb(III) and Te(IV) ions.

In a quantitative analysis of CVs, it can see that both cathodic and anodic peak currents increase with the potential scan rate and temperature. As Figure 4 shows, linearly dependences of cathodic current (I_{pc}) with square root of scan rate ($v^{1/2}$) are obtained in all three cases, proving a diffusion-controlled deposition process. This fact allowed calculation of the diffusion coefficients of Bi(III), Sb(III) or Te(IV) ionic species, using the well-known Randles-Sevcik equation for a metal deposition [14]:

$$I_{pc} = 0.6401\,nFAc\sqrt{\frac{nF}{RT}\,v\,D} \qquad (3)$$

In Eq.(3), n is the number of electrons changed in electrode process; F, R and T are the Faraday number, ideal gas constant and absolute temperature, respectively; A – the surface area of electrode; v – the scan rate; D – the diffusion coefficient of ionic species. Using the above equation reliable results for diffusion coefficient may be obtained by performing a series of CV experiments with various ion concentrations and scan rates under a severe control of temperature. From our preliminary investigations we obtained D values for Bi, Sb or Te ionic species of the order of 10^{-7} - 10^{-5} cm^{2}s^{-1}. For instance, we found at 353 K a diffusion coefficient D = 1.75×10^{-7} cm^{2}s^{-1} for Te(IV) species, taking number of transferred electrons n = 4 [8]; similarly, D values of the order of 10^{-6} cm^{2}s^{-1} were obtained for Bi(III) or Sb(III) species, with higher D values for antimony species. However, this order of magnitude for diffusion coefficient at 353 K is generally much lower than in aqueous solutions (D about 10^{-5} cm^{2}s^{-1}), a fact which is expected for diffusion in such ionic liquid media having higher viscosity and density than aqueous media.
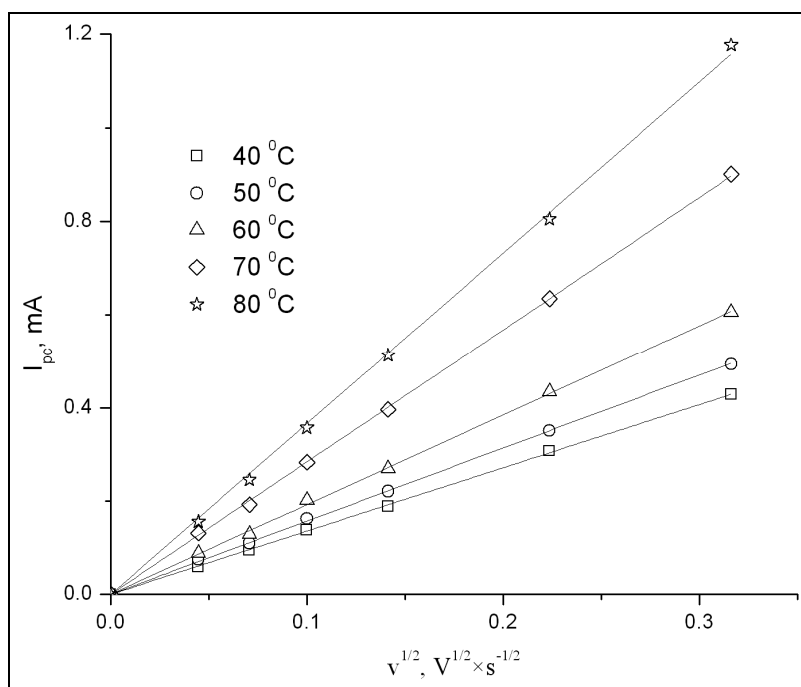

Figure 5. I_{PC} *vs.* $v^{1/2}$ for Sb deposition on Pt in ChCl – urea eutectic at various temperatures; Sb(III) concentration = 5 mM

Regarding the influence of temperature upon the diffusion coefficient an Arrhenius exponential dependence was found, from which the activation energy for diffusion was estimated. As examples, Figs. 5 and 6 present I_{PC} vs. $v^{1/2}$ straightlines as well as ln D vs. 1/T Arrhenius dependence for Sb deposition at various temperatures, using a constant Sb(III) ion concentration in ChCl-urea eutectic. Similar behavior was noticed for all three investigated ions in the same ionic liquid. In general, the obtained values of $E_{activation}$ ranged within 50 - 100 kJ/mole interval, with higher value for Te ions, this being probable due to the differences in ionic radius.

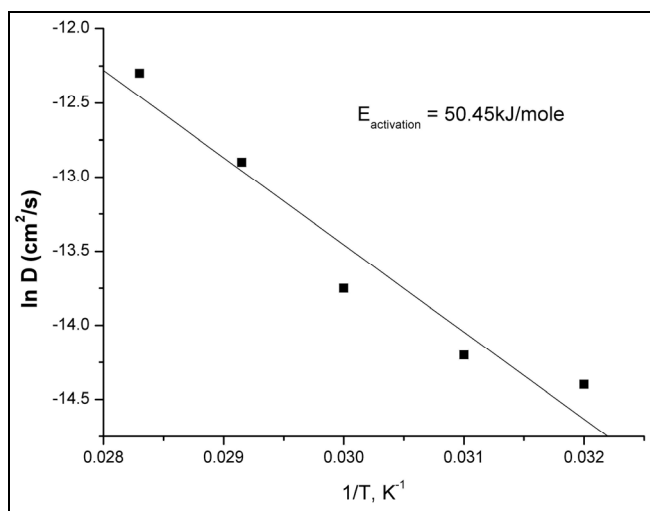**Figure 6.** Arrhenius dependence of diffusion coefficient for Sb(III) ion, in *In D vs. 1/T* coordinates; Sb(III) concentration = 5.5 mM

The differences in Bi, Sb and Te behavior during cathodic deposition on Pt using ChCl-urea ionic liquid are also revealed on the electrochemical impedance (EIS) spectra that can give us information about the cathodic process and properties of films. Figures 7 - 9 show Nyquist and Bode diagrams obtained at various electrode potentials, the temperature being 80 ^{0}C. During the experimental procedure, the potential of the cathode was consecutively maintained at increasingly negative values: first at potentials where the reduction process does not start (-0.3 ÷ -0.35 V), then in the region of beginning the process, reaching the maximum cathodic current (-0.4 ÷ -0.5 V) and, finally, in the area of massive metal deposition (-0.6 ÷ -0.7 V).

The Nyquist spectra show clearly capacitive semi-circles in the region of high frequencies, followed by a linear dependence of imaginary part of impedance against the real part. The shape of depressed semi-circles may be attributed to the non-uniformity of platinum electrode surface used as

cathode, especially when the first nuclei of electrocrystallized metal occur forming a monolayer, which is then thickened. The large linear portions for more negatively polarized samples are correlated with the thickening of film onto platinum electrode. The gradually decrease of the semi-circle diameter (diminution of the charge transfer resistance), if the electrode potential is more negative, indicates the increase of electrodeposition current.
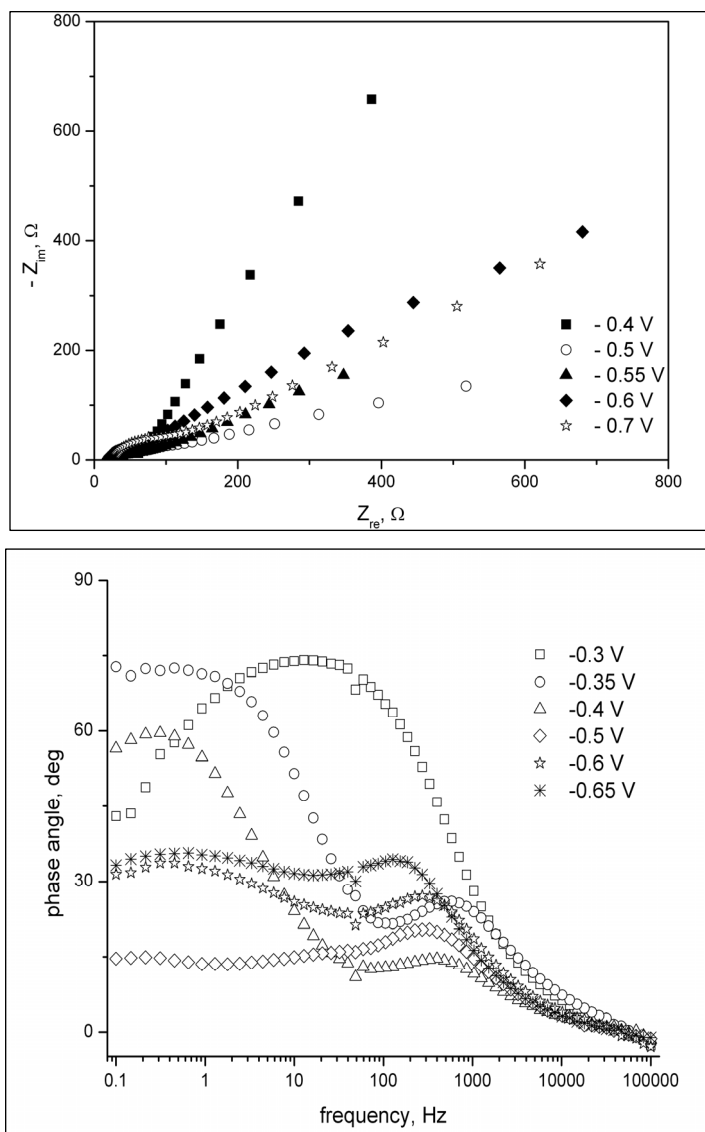

Figure 7. Nyquist and Bode spectra obtained at various potentials on Pt (0.5 cm^2) in ChCl-urea eutectic + 10 mM Bi$_2$O$_3$; 80 ^{0}C
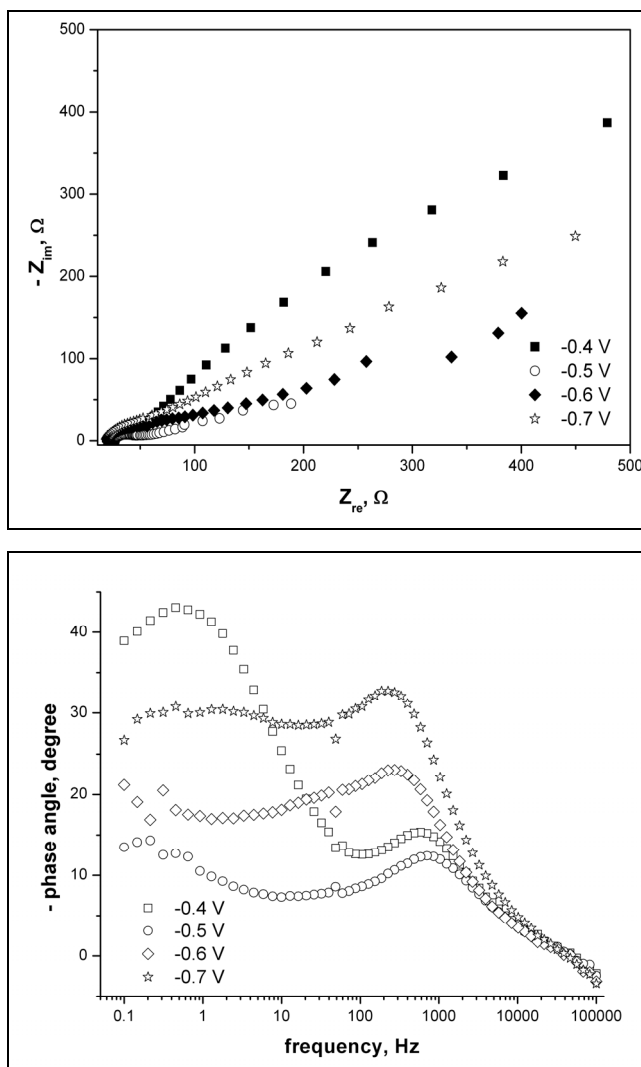
Figure 8. Nyquist and Bode spectra obtained at various potentials;
Pt/ ChCl-urea eutectic + 10 mM SbCl$_3$; 80 ^{0}C

The same behavior by polarizing Pt electrode at various electrode potentials is evidenced in Bode diagrams (we selected the phase angle *vs*. frequency dependence, only). In Fig. 7 the phase angle at -0.3 V shows a single maximum around -75^0, meaning a significant capacitive behavior when Bi deposition does not start. For more negative potentials, this maximum shifts toward higher frequencies and diminishes drastically together with occurrence of a new maximum located at low frequencies that may be attributed to Bi film

formation. Phase angle of -60^0 means an intermediate behavior between capacitive and diffusion response, whereas the values of -20^0 and less illustrate the massive deposition. Bode spectra for Sb and Te ions show the same characteristics; however, the variation of phase angle in Fig. 9 indicates a Te deposition already at -0.4 V and a less electrical conductive deposit.
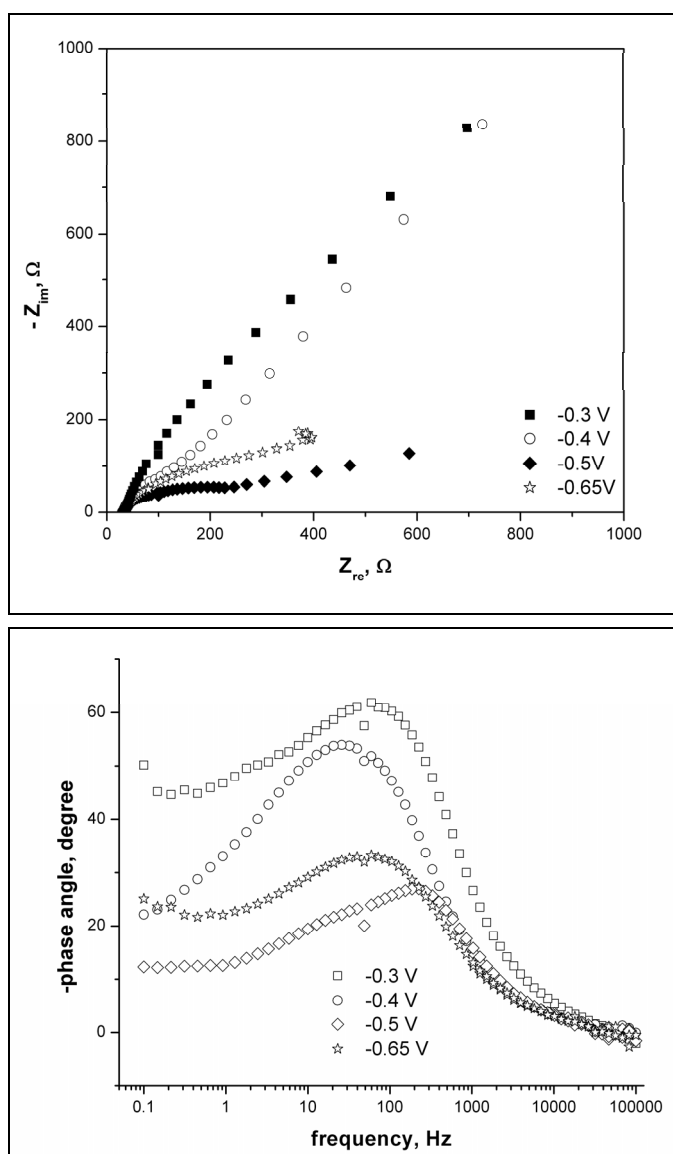
Figure 9. Nyquist and Bode spectra obtained at various potentials; Pt/ ChCl-urea eutectic + 10 mM TeO_2; 80 ^{0}C

The obtained Nyquist and Bode spectra were interpreted on the basis of an equivalent electrical circuit as electrochemical model of the interface, using a specialized fitting software Zview 2.90c (Scribner Assoc.).

Figure 10 exhibits the proposed equivalent circuit used for fitting the experimental data. The elements of this Randles modified circuit are: R_s -ohmic resistance of electrolyte solution; C_1 -film capacitance in a parallel combination with the film resistance (R_1) and a second parallel combination consisted in a constant phase element (CPE_2) and charge transfer resistance (R_2). The constant phase element CPE_2 takes into account the deviation of electrochemical double layer from pure capacitive behavior and has the expression:

$$CPE_2 = \frac{1}{T(j\omega)^P} \qquad (4)$$

where T is the capacity element of CPE, ω – the angular frequency, j – the imaginary vector unit ($j=\sqrt{-1}$) and P – the CPE exponent. CPE acts as a pure capacitor when the exponent is unity, P = 1, and shows a pure diffusion behaviour when P=0.5.
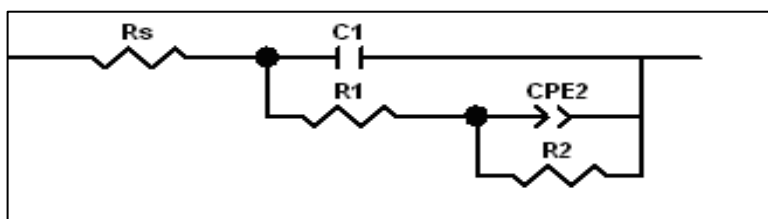

Figure 10. Schematic representation of the electrical equivalent circuit diagram; the used symbols are presented in text

Table 1 contains the values of the equivalent circuit elements for the best fitting of experimental data. As can be seen from this Table, the ohmic resistance of ionic liquid has, as expected, a constant value for a given temperature (80 ^{0}C). Values of the same order of magnitude were recorded for film/ionic liquid capacitances and film resistances in various polarization states. Values of P in a narrow range (P= 0.43 - 0.65) show the diffusion control of cathodic process. However, there are differences in behavior of electrochemical double layer of Bi, Sb or Te interfaces (CPE-T values), explained by different semiconductor properties after massive deposition of films. Also, it is obvious that in all three cases the charge transfer resistance (R_2) decreases by shifting the electrode potential towards negative direction until the voltammetric peak is recorded; the subsequent increase of R_2 occurs at potentials corresponding to the diffusion limiting current zone. Therefore, the EIS behavior is in good agreement with CV curves.

Table 1. Values of the circuit parameters for Pt electrode (0.5 cm^2) polarized at various electrode potentials (E); temperature 80 ^{0}C

Ion	Values of electrical circuit elements						
	E, V	Rs, Ω	C1, µF	R1, Ω	CPE-T, µF	CPE-P	R2, Ω
Bi	-0.3	14.9	9.34	8	50	0.79	23720
	-0.35	14.6	12.61	28	300	0.88	8760
	-0.4	30.8	14.96	30	820	0.80	6340
	-0.5	26.3	14.07	20	2800	0.43	570
	-0.6	19.3	16.86	27	1600	0.54	1960
	-0.65	23.8	18.65	40	1000	0.52	3950
Sb	-0.3	17.0	15.09	61	247	0.88	25530
	-0.4	23.7	13.11	18	1775	0.64	1600
	-0.5	26.9	12.73	16	6200	0.48	253
	-0.6	20.9	15.13	15	1980	0.38	57
	-0.7	14.5	16.34	16	1940	0.44	2280
Te	-0.3	15.8	10.65	4	100	0.66	26770
	-0.4	31.5	11.39	90	300	0.65	37960
	-0.65	34.5	12.42	62	500	0.51	554

CONCLUSIONS

The cyclic voltammograms and electrochemical impedance spectra showed that the cathodic process during the single deposition of Bi, Sb or Te films in an ionic liquid medium (choline chloride + urea, 1:2 molar mixture) is mainly controlled by diffusion. Only a couple of reduction/oxidation peaks was observed at all scan rates and temperatures, involving ionic complex species ($BiCl_4^-$, $SbCl_4^-$ and $TeCl_6^{2-}$) as participants. The diffusion coefficients have values of 10^{-7}-10^{-5} cm^{2}s^{-1} and activation energies for diffusion are of the order of tens kJ/mole. The results of electrochemical impedance measurements showed that Bi, Sb or Te films have almost similar semiconductor characteristics with a faster process for Sb deposition.

EXPERIMENTAL SECTION

The preparation of choline chloride+urea ionic medium, cell and electrochemical procedures were described elsewhere [8,12,13]. The supporting electrolyte was prepared by mixing choline chloride (Aldrich) with urea (Aldrich) in 1:2 molar proportions at above 90^{0}C for 30 min. The working solutions were made by dissolution of bismuth oxide, antimony chloride and tellurium dioxide (all reagents purchased from Alfa Aesar) as precursors of Bi(III), Sb(III) or Te(IV) ionic species. Concentrations in molarities were found in 0.5 to 11 mM range by using density values for ChCl-urea eutectic

of 1.131-1.134 gcm^{-3}, determined in our laboratory within working temperature range (40 – 85 ^0C). The working electrode was a Pt sheet (0.5 cm^2), the auxiliary electrode was a cylindrical gauze of Pt, whereas the quasi-reference electrode was a Ag wire immersed in the same electrolyte. Cyclic voltammetry and electrochemical impedance spectroscopy investigations were controlled by a Zahner Elektrik IM6e potentiostat provided with a frequency analyzer (FRA). The scan rates in recorded voltammograms were in 2 - 100 mVs^{-1} range and in the impedance study a.c. voltage has frequencies between 10^5 and 10^{-2} Hz with amplitude of ± 10 mV.

REFERENCES

1. R. Venkatasubramanian, E. Siivola, T. Colpitts, B. O'Quinn, *Nature,* **2001**, *413,* 597.
2. J.P. Fleurial *et al.*, Proc. 18th Int. Conf. on Thermoelectrics (IEEE catalog 99th 8407), A.C. Ehrlich Ed., **1999**, 294.
3. M. Nedelcu, M. Apostol, Reversibile power supply–cooling machine, US Provisional Patent Application No. 61/032,329, Febr. 28 **2008** (United States Patent & Trademark Office).
4. F. Endres, A.P. Abbott, D.R. MacFarlane, Electrodeposition of metals using ionic liquids, Wiley-VCH, Weinheim, **2008**; A.P. Abbott, J.C. Barron, K.S. Ryder, D. Wilson, *Chem. Eur. J.,* **2007**, *13,* 6495.
5. M.H. Yang, I.W. Sun, *Journal of Applied Electrochemistry*, **2003**, *33*, 1077.
6. S.I. Hsiu, I.W. Sun, *Journal of Applied Electrochemistry,* **2004**, *34*, 1057.
7. H. Ebe, M. Ueda, T. Ohtsuka, *Electrochimica Acta*, **2007**, *53*, 100.
8. F. Golgovici, A. Cojocaru, M. Nedelcu, T. Visan, *Chalcogenide Letters*, **2009**, *6* (8), 323.
9. A.P. Abbott et al., US Patent 7, 196, 221, March 27, **2007.**
10 A.P. Abbott, G. Capper, D.L. Davies, H. Munro, R.K. Rasheed, *Inorganic Chemistry*, **2004**, *43,* 3447.
11. M. Nedelcu, A.C. Manea, A. Cojocaru, B. Savu, S. Stanciu, T. Visan, in vol.: 1st Regional Symp. on Electrochemistry of South-East Europe, RSE-SEE, 4-8 May **2008**, Rovinj, Croatia, **2008**, 117.
12. L. Anicai, A. Cojocaru, A. Florea, T. Visan, *Studia Universitatis Babes-Bolyai, Chemia,* **2008**, *53,* 119.
13. T. Visan, A. Cojocaru, A. Florea, L. Anicai, vol.: *Int. Conf. "Ionic Liquids for Electrochemical Devices – ILED 2008*", Rome, Italy, June 9-11, **2008**, 63-65.
14. D. J. Schiffrin, *Journal of Electroanalytical Chemistry*, **1986**, *201,* 199.